

**Measuring and Modelling the Primary
Production of a Sea Lough in Northern
Ireland**

Elisa Capuzzo

A thesis submitted in partial fulfilment of
the requirements of Edinburgh Napier
University, for the award of Doctor of
Philosophy

April 2011

*Misura ciò che è misurabile, e
rendi misurabile ciò che non lo è.*

Galileo Galilei

[Measure what is measurable and
make measurable what is not]

Acknowledgements

According to the Cambridge dictionary, a ‘scientist’ is *an expert who studies or works in one of the sciences*. I feel extremely lucky because in the last 5 years I have been given the chance to be supervised, directed, taught and supported by 3 scientists who I admire. I am extremely grateful to Dr. Richard Gowen, Prof. Paul Tett and Dr. Linda Gilpin for the trust they put in me and my work, and for the effort and time they spent providing feedback, comments and constructive criticisms to this work. Their inspiring examples have given me the basis to become an enthusiastic and proficient scientist.

I am thankful to the Northern Ireland Lough Agency for funding this PhD and to the Agri-Food and Bioscience Institute (AFBI) for providing all the facilities and equipment needed. I am particularly grateful to Dr. Adam Mellor, William Clarke, Ann Marie Crooks, Andrew McDougall and all the staff of the Aquatic Branch of AFBI for helping during sampling events and for assisting me with broken instruments. I am grateful to Brian Stewart, Raymond Gilmore and Claire Smyth for carrying out the analysis of chlorophyll and dissolved nutrients concentrations, and for the assistance in the laboratory. I am also grateful to Dr. Bob Foy and Harry Nicholson (AFBI) for providing the hourly solar irradiance data measured by the AFBI weather station in Hillsborough. A special thank to Dr. Heather Moore for her friendship and being trusting enough to sit in a car with me when I was still not sure on which side of the road to drive.

The sampling events will not have been possible without the help of the crew of the *FPV Mytilus*, and the fishing vessels of Brian Cunningham and Oliver Finnegan. I am thankful to Ciaran McGonigle for providing estimates of SPM concentration for the sampling activity in 2006. I would like also to thank Dr. Grahame Savidge of Queen’s University Belfast for providing part of the equipment for the experiments.

A special acknowledgment to my current employer CEFAS for giving me the opportunity to take time off from work for finishing this research project. I am also thankful to my colleagues and friends in Lowestoft for giving me motivation in concluding this study.

During the last 5 years I have been on a journey that has led my knowledge and understanding of the marine ecosystem to get stronger year after year. It was also a 'physical' journey that took me from Italy to Northern Ireland, Scotland and England, where I meet lots of friends. Some of them crossed my path temporarily; others are still walking along side with me. Nevertheless I am very grateful to all of them. I would like to thank in particular all the occupiers of the postgraduate room G30 in AFBI, and the occupiers of the room D8 in Edinburgh Napier University, for sharing with me hard work as well as a good laugh over a nice cup of coffee. I am particularly grateful to Dr. Enrique Portilla for transposing a script from Matlab into R syntax, which formed an integral part of the PhD research. A special thank to the guys of 25 University Avenue in Belfast, for their friendship and support during my first 2 years away from home; my spoken English would not be so good without them! I am very grateful to Dolan and his lovely family for sharing some of my happiest memories in Northern Ireland and for made me feel like a member of the family.

I am thankful to all the speakers and lecturers I listened to during conferences, workshops, symposia and university lectures for fuelling my interest and love for the marine environment.

This journey would have not been possible without the support and precious friendship of my dear friends 'little Cordula', Daniela and Chiara; the distance made our friendship even stronger. A special thank to my 'tango partner' for leading me through some up and downs of my life.

All my gratitude goes to my family for being there in every moment; they kept me going with their love, long international phone calls and emergency parcels of Italian goodies. My last acknowledgement is for David, who 'effortlessly' makes my life so beautiful.

Table of content

Abstract	9
Outline of the thesis	11
Acronym list	13
CHAPTER 1	15
1.1 Introduction	16
1.2 Aim and testable hypotheses	18
1.3 Sampling site: Carlingford Lough.....	19
1.4 Definition of primary production and its importance	22
1.5 History of primary production measurements.....	22
1.6 Physiology and biochemistry of photosynthesis	24
1.7 Respiration	25
CHAPTER 2	27
2.1 Introduction to Carlingford Lough.....	28
2.2 Methods.....	35
2.2.1 Sampling	35
2.2.2 CTD calibrations	36
2.2.3 Phytoplankton	37
2.2.4 Nutrients.....	39
2.2.5 Chlorophyll and calculation of chlorophyll standing stock	40
2.2.6 Suspended Particulate Matter (SPM).....	41
2.2.7 Data analysis	42
2.3 Results.....	44
2.3.1 Physical variables.....	44
2.3.2 Nutrients.....	48
2.3.3 Chlorophyll and Suspended Particulate Matters	54
2.3.4 Phytoplankton population	57
2.4 Discussion	72
2.4.1 Physical and chemical variables	72
2.4.2 Biological variables.....	76

2.5 Conclusions	81
CHAPTER 3	82
3.1 Introduction	83
3.1.1 The electromagnetic spectrum	83
3.1.2 Inherent optical properties	84
3.1.3 Vertical attenuation coefficient (apparent optical properties).....	86
3.1.4 Measurements of the underwater light field.....	91
3.1.5 How to derive K_d	93
3.2 Methods.....	97
3.2.1 <i>In situ</i> measurements of the underwater light field.....	97
3.2.2 Estimates of K_d	98
3.2.3 Calculation of surface incident PAR and daily surface mixed layer irradiance.....	102
3.2.4 Data analysis	102
3.3 Results	104
3.3.1 Seasonal trends of surface irradiance, Secchi depth, OACs and K_d	104
3.3.2 Empirical relationships for deriving K_d	108
3.3.3 Seasonal variability of modelled K_d and relationship with OACs.....	111
3.4 Discussion	114
3.4.1 K_{dI} and K_{dR}	114
3.4.2 A model for predicting K_d	115
3.4.3 Seasonal variability of K_d	116
3.4.4 Timing of the start of the phytoplankton spring bloom	117
3.5 Conclusions	120
CHAPTER 4	121
4.1 Introduction	122
4.1.1 Primary production measurements.....	122
4.1.2 The ^{14}C technique.....	126
4.2 Standard operating procedure for primary production incubations	130
4.2.1 Sampling	130
4.2.2 Light gradient incubators (photosynthetrons).....	130
4.2.3 ^{14}C incubations	133

4.2.4 Acidification problem	138
4.3 Conclusions	144
CHAPTER 5	145
5.1 Introduction	146
5.1.1 Photosynthetic parameters	146
5.1.2 Variability of the photosynthetic parameters	149
5.1.3 Estimates of α^B and P_{max}^B and models of the photosynthesis/irradiance relationship	150
5.2 Methods	153
5.2.1 Estimates of photosynthetic parameters using ' <i>Plcurvefit4.R</i> '	153
5.2.2 Initial values of α^B and P_{max}^B	156
5.2.3 Identification of outliers	158
5.2.4 Data analysis	161
5.3 Results	162
5.3.1 Comparison of the models	162
5.3.2 Variability in estimates of α^B and P_{max}^B (JasPlatt model)	173
5.4 Discussion	178
5.4.1 Comparison of P/E models	178
5.4.2 Variability of the photosynthetic parameters (JassPlat model) and investigations on the estimates of E_k	180
5.4.3 Environmental control on the photosynthetic parameters	188
5.5 Conclusions	193
CHAPTER 6	194
6.1 Introduction	195
6.1.1. Classification of primary production models	197
6.1.2 The Behrenfeld and Falkowski classification	198
6.1.3. The Sathyendranath, Platt and Forget classifications	199
6.2 Methods	203
6.2.1 Calculation of daily column production	203
6.2.2. Relationships between gross daily column production and other environmental variables	206
6.2.3 Background information on ' <i>HPLF2d.M</i> '	206

6.2.4. Estimates of annual production (<i>HPLF2d.M</i>).....	208
6.2.5. Microplankton community respiration and net community production	215
6.3 Results.....	217
6.3.1 A comparison of estimates of daily primary production derived with different light-saturation models	217
6.3.2 Seasonal variability in production and respiration.....	223
6.3.3 Relationships between gross production, microplankton community respiration and environmental variables	225
6.3.4 Estimates of gross annual production using the TFS	228
6.3.5 Estimates of annual MCR using the TFS	234
6.4 Discussion	238
6.4.1 A critical evaluation of the method used to derive daily and annual column production	238
6.4.2 A comparison of estimates of gross production between Carlingford Lough and other water bodies	241
6.4.3 Relationships between daily column production and other environmental variables	246
6.4.4 Respiration and net production	250
6.5 Conclusions	254
CHAPTER 7	255
7.1 General conclusions and further considerations	256
REFERENCES	264
APPENDIX 1	286
APPENDIX 2	290

Abstract

The aim of this study was to develop a simple and robust methodology for the routine estimation of primary production in coastal water bodies, such as the sea loughs of Northern Ireland. Primary production estimates are a key element in assessing the trophic status of a water body as well as in defining its carrying capacity. The traditional methods for deriving production, although sensitive and reliable, are time consuming and not suitable for routine monitoring programme. To achieve the aim of this study, high frequency sampling was carried out for two years (April 2006 - March 2008) in Carlingford Lough (NI), to characterise the main environmental properties of the Lough, and to run incubations to derive primary production and microplankton community respiration.

From the observations and analyses carried out, it is evident that run off from the River Clanrye strongly influenced the physical, chemical and biological characteristics of the Lough. Phytoplankton biomass showed the typical seasonal cycle observed in temperate coastal waters. Microalgal growth was light limited during winter, and potentially nutrient limited (silicate and nitrogen), during spring and summer respectively. Diatoms dominated the phytoplankton population during the year, due to the high nutrient concentration in the Lough and mixed/stratified water column conditions. The sub-surface light climate was considered to be the main factor controlling the timing of the phytoplankton spring bloom, and suspended solids were the optically active constituent that explained the higher proportion of variability in K_d (30%).

The ^{14}C technique was chosen for estimating primary production due to its high sensitivity. A standard operating procedure was developed for deriving estimates of production of the Lough that involved the use of a photosynthetron and short term incubations. The photosynthesis-irradiance curves derived from incubations were fitted by light-saturation models and the hyperbolic tangent of Jassby and Platt (1976) consistently produced a good fit to the data sets. α^B and P_{\max}^B showed seasonal variability and significant relationships with some environmental variables (e.g. ammonium, incubation temperature). Single daily values of chlorophyll concentration, K_d and photosynthetic parameters were used to derive daily column production for a given sampling event. The range of estimates of daily

gross column production of Carlingford Lough ($3.2 - 1210 \text{ mgC m}^{-2} \text{ d}^{-1}$) was comparable to the ranges derived for other temperate estuaries and coastal areas. The seasonal trend in gross production in Carlingford Lough showed 2 main peaks (one in spring and one at the end of the summer). Chlorophyll standing stock explained 71% of the variability in daily production. This increased to 89% when irradiance during the sampling and K_d were included in the relationship.

A model to implement a truncated Fourier series (TFS) was applied to daily estimates of production to derive annual production that was estimated as $116 \text{ gC m}^{-2} \text{ y}^{-1}$ with 90% confidence interval of 98-141 $\text{gC m}^{-2} \text{ y}^{-1}$. Annual microplankton community respiration was estimated as $117 \text{ gC m}^{-2} \text{ y}^{-1}$ (90% confidence interval 105-134 $\text{gC m}^{-2} \text{ y}^{-1}$). It was concluded that within the Lough there were periods of net production but these episodes were not cyclical and that on an annual balance, Carlingford Lough was a heterotrophic system.

This study confirmed that chlorophyll standing stock can be used to derive estimates of daily gross production. The TFS analysis also appears to be a useful method for estimating annual production and quantifying the associated error to provide confidence intervals that could be used to assess long-term change. A preliminary test using Belfast Lough data suggests that the relationship chlorophyll stock/production and the TFS can be used in other Northern Ireland sea loughs. The empirical relationship with chlorophyll standing stock, together with the TFS analysis, shows promise as a method for estimating annual production in estuarine and coastal waters, and merits further validation and testing.

Outline of the thesis

Chapter 1

This chapter sets the scene of this research study and the framework for the next chapters. It highlights the aim of the study, and the hypothesis tested, provides background information of the study site, of the importance of studying primary production, and of the history of primary production studies. A brief description of the physiology of photosynthesis, and its reverse process respiration, is also given in this section.

Chapter 2

The second chapter provides background information of the sampling site and of Carlingford Lough, followed by a description of the methods used to collect and to analyse samples of the main environmental variables such as temperature, salinity, nutrients, chlorophyll, phytoplankton, particulate suspended matter (SPM), and river flow. Descriptive analyses of these variables are shown together with plots depicting their annual trends. Discussion highlights the physical and chemical characteristics of the sampling site, the phytoplankton population, and which nutrients are more likely to limit microalgal growth.

Chapter 3

This chapter is a complement of Chapter 2 providing information on the underwater light field and water column transparency measurements. It starts with an introduction to the underwater light optics, and follows with details of the methods adopted to estimate diffuse light attenuation coefficient for downward irradiance (K_d) in Carlingford Lough. The optical compounds of the water medium influencing the variability of K_d are identified in this chapter, together with a discussion of the influence of the underwater light field on the timing of the phytoplankton spring bloom.

Chapter 4

The fourth chapter presents a review of the main techniques used for measuring primary production with particular focus on the ^{14}C technique.

Advantages and disadvantage of the latter technique are described. The standard operating procedure developed during the primary production experiments with samples from Carlingford Lough and the problems encountered in the setting up of the method are also reported in this chapter.

Chapter 5

The fifth chapter of the thesis focuses on the photosynthetic parameters, α^B and P_{\max}^B (derived from photosynthesis-irradiance curves) and on their variability. The photosynthesis/irradiance curves were fitted by 9 light-saturation models and the ability of the models to fit the curves is also discussed in this section. Estimates of α^B and P_{\max}^B for Carlingford Lough were regressed versus the main physical, chemical and biological variables (e.g. temperature, nutrient concentration) for identifying which environmental variables are related to changes in the photosynthetic parameters.

Chapter 6

This chapter provides an overview of models adopted for measuring production, and focuses on two models (*day_colum_prod4.M* and *HPLF2d.M*) used to calculate gross daily and annual column production in this study. Estimates and seasonal trends of gross daily and annual production, as well as microplankton community respiration, were compared to estimates and trends derived for other coastal water bodies. Relationships of gross production and respiration with other environmental variables were discussed in this chapter, together with considerations about the trophic status (autotrophic or heterotrophic) of Carlingford Lough.

Chapter 7

The final chapter of this thesis provides general conclusions and further considerations of this study. It also gives an example of the application of the model *HPLF2d.M* for estimates of gross daily production derived from Belfast Lough.

Acronym list

AFBI	Agri-Food and Bioscience Institute
ACC	Average phytoplankton Chlorophyll Content
ACV	Average phytoplankton Cell Volume
ADP	Adenosine DiPhosphate
APM	Annual Production Model
ASSI	Area of Special Scientific Interest
ATP	Adenosine TriPhosphate
BEQUALM	Biological Effects Quality Assurance in Monitoring programmes
CDOM	Coloured Dissolved Organic Material
CEFAS	Centre for Environment, Fisheries and Aquaculture Science
CLNBuoy	Carlingford Lough North Buoy
CTD	Conductivity Temperature Density profilers
Cyt b/f	Cytochrome b ₆ /f
DARDNI	Department of Agriculture and Rural Development of Northern Ireland
DCNP	Daily Column Net Production
DF	Degree of Freedom
DIC	Dissolved Inorganic Carbon
DIM	Depth Integrated Model
DIN	Dissolved Inorganic Nitrogen
DPM	Disintegrations Per Minute
ETRs	Electron Transport Rates
FRRf	Fast Repetition Rate fluorometry
GACP	Gross Annual Column Production
GDCP	Gross Daily Column Production
GPP	Gross Primary Production
HAB	Harmful Algal Bloom
IMAR	Institute of Marine Research
IOCCG	International Ocean Colour Coordination Group
IS incubations	<i>In situ</i> incubations
IS	Irish Sea
MCR	Microplankton Community Respiration
MIMS	Mass Inlet Membrane Spectrometry
MSFD	Marine Strategy Framework Directive (2008/56/EC)
NADPH or NADP ⁺ or NADP	Nicotinamide Adenine Dinucleotide Phosphate
NAO	North Atlantic Oscillation
NI	Northern Ireland
NIOZ	Nederlands Instituut voor Onderzoek der Zee
NMP	Net Microplankton Production
NPP	Net Primary Production
NS	North Sea
OACs	Optically Active Components
OSIL	Ocean Scientific International Limited
P/E	Photosynthesis/irradiance (curves)

PAM	Pulse Amplitude Modulated (fluorometry)
PAR	Photosynthetically Available Radiation
PCI	Phytoplankton Community Index
PET	Photosynthetic Electron Transfer
PP	Primary Production
PSI	Photosystem I
PSII	Photosystem II
PSU	PhotoSynthetic Units
RQ	Respiratory Quotient
RRE	Region of Restricted Exchange
RSS	Residual Sum of Squares
RUBISCO	RibUlose – 1,5 – Biphosphate Carboxylase-Oxygenase
SIS	Simulated <i>in situ</i>
SMILE	Sustainable Mariculture in Northern Irish Lough Ecosystems
SML	Surface Mixed Layer
SPA	Special Protection Area
SPM	Suspended Particulate Matter
SRP	Soluble Reactive Phosphorus
STW _s	Sewage Treatment Works
SYKE	Finnish Environmental Institute
TA	Total activity
TFS	Truncated Fourier Series
TIM	Time Integrated Model
TSS	Total Sum of Squares
TSS	Total Suspended Solids
UK	United Kingdom
UV	UltraViolet
WFD	Water Framework Directive (2000/60/EC)
WIM	Wavelength Integrated Model
WRM	Wavelength Resolved Model

CHAPTER 1

General introduction

1.1 Introduction

The sea loughs of Northern Ireland are characterized by sheltered conditions and restricted water exchange. These coastal water bodies are also influenced by a wide range of human activities such as commercial freight and leisure, with urbanization along the shoreline, and different land use within the catchment (e.g. pasture, natural grasslands). These activities can result in introduction of anthropogenic nutrients into the sea loughs.

Inputs of nitrogen and phosphorus can stimulate algal production and in some circumstances lead to eutrophication, which is perceived to be an international problem (Duarte 2009; Nixon 2009). Nixon (1995) defined eutrophication as '*an increase in the rate of supply of organic matter to an ecosystem*', and suggested classifying a marine system as eutrophic when its supply of organic carbon is between 301 and 500 gC m⁻² y⁻¹. Nixon definition of eutrophication implies that the increase of organic matter in a marine system can be caused by supply of organic matter within the system (autochthonous carbon) or from outside the marine system (allochthonous carbon); furthermore according to the definition of Nixon, nutrient enrichment is one of the factors causing increased supply of organic matter (Nixon 1995). Tett *et al.* (2010) proposed an improved definition of eutrophication as '*an enrichment of a water body by nutrients leading to increased growth, primary production and biomass of algae, as well as changes in the balance of organisms and water quality degradation*'.

Assessment of the quality status of water bodies is a requirement of the EU Water Framework Directive (WFD; Directive 2000/60/EC for inland and coastal waters), and the Marine Strategy Framework Directive (MSFD; Directive 2008/56/EC for marine waters). According to the WFD all inland and coastal waters should achieved at least 'good' water quality status by 2015, where 'good' refers to a low distortion of the biological quality elements due to anthropogenic activity.

A healthy ecosystem is able to resist to a pressure or recover from a disturbance, and has a balanced organization (biodiversity; Costanza 1992). Tett *et al.* (2007) identified 5 groups of indicators that can be used to assess changes in ecosystem health. These are: bulk indicators (phytoplankton biomass as chlorophyll concentration), frequency statistics (e.g. Harmful Algal Bloom events), flux measurements (e.g. annual primary production), structural indicators (e.g.

Phytoplankton Community Indices, PCIs) and indicator species (e.g. *Phaeocystis* spp.).

The sea loughs of Northern Ireland are also used for the cultivation of bivalve molluscs and in recent years there has been a major expansion of this industry. In particular, the annual production of mussels and Pacific oysters cultivated in Northern Ireland (NI) is around 28,000 tons and 603 tons respectively (Ferreira *et al.* 2007). The total global production for the sector is valued at approximately 8 million pounds per annum (Ferreira *et al.* 2007).

Sustainable bivalve cultivation is dependent on good water quality and should not exceed the carrying capacity of the system. In the context of shellfish cultivation, carrying capacity refers to the maximum stocking density that can be supported by a given ecosystem for a given time (Ferreira *et al.* 2008; see review by Smaal *et al.* 1998). The carrying capacity of an ecosystem, such as a sea lough, should be assessed prior the establishment of large-scale shellfish farming, to ensure adequate availability of food for the shellfish. If, for example, shellfish are overstocked their production declines (Heral 1993), and there may be adverse effects on the ecosystem (Ferreira *et al.* 2008). Carrying capacity differs from assimilative capacity that is defined as ‘*a property of the environment and its ability to accommodate a particular activity or rate of an activity ... without unacceptable impacts*’ (GESAMP 2001). In the context of shellfish cultivation, assimilative capacity measures the resilience of an area impacted by shellfish farming, taking into account the amount of ‘wastes’ produced by the farm that the area can assimilate. In fact potential impacts can arise from marine aquaculture such as organic and nutrient enrichment, chemical release, spreading of diseases, escapees and interaction with other activities in the area (Fernandes *et al.* 2001). Phytoplankton primary production is one of the key factors to take into account when defining the carrying capacity of a water body used for bivalve cultivation (Smaal *et al.* 1998; Nunes *et al.* 2003).

It is clear that sustainable bivalve cultivation and maintenance of healthy sea lough ecosystems requires good water quality. Primary production is considered a useful tool for supporting the assessment of coastal eutrophication (Andersen *et al.* 2006; Tett *et al.* 2007) and in quantifying the carrying capacity for shellfish cultivation (Ferreira, Duarte and Ball 1998). The primary production of a Northern Irish sea lough was the subject of the study presented here.

1.2 Aim and testable hypotheses

Although the importance of primary production measurements in the context of eutrophication assessment is well recognised (e.g. Andersen et al. 2006; Tett *et al.* 2007; Nixon 2009; Tett *et al.* 2010), measurements of primary production are not mandatory in monitoring programmes for the European WFD. This could be explained considering that the traditional methods of estimating production (e.g. ^{14}C and oxygen methods) are time consuming, require specialist training and equipment and are generally inappropriate for routine monitoring programmes.

Therefore, the current project aimed to develop a simple and robust methodology for the routine estimation of primary planktonic production in coastal water bodies, such as the sea loughs of Northern Ireland. The methodology combined two approaches for obtaining estimates of annual primary production. The first was an empirical approach that derived gross daily water column production from equations that relate daily estimates of production to other environmental variables (e.g. chlorophyll standing stock, irradiance during the sampling). The second approach used a truncated Fourier series (TFS) for interpolating daily estimates of primary production. A Monte Carlo method, employing the TFS and residual error, was then used to estimate annual primary production and its 90% confidence interval. The data used for estimating annual primary production were derived from measurements of carbon assimilation carried out from April 2006 until March 2008, in Carlingford Lough.

Joint and Pomroy (1993) and Gowen and Bloomfield (1996) used chlorophyll standing stock (log-transformed) to derive daily primary production of the North Sea and the Irish Sea respectively; the regressions between phytoplankton production and chlorophyll standing stock gave an R^2 of 0.698 and 0.710 respectively.

Based on these studies a hypothesis was developed and tested during this research project:

- chlorophyll standing stock explains 70% of the variability in daily primary production for Carlingford Lough.

Gowen and Bloomfield (1996) suggested that part of the variability in primary production not related to chlorophyll standing stock could be explained by considering other factors closely related with the photosynthetic process, such as light availability and the photosynthetic parameters (α^B and P_{\max}^B). The latter are not

constant but variable on a daily and seasonal scale (Côté and Platt 1983). Daily variability in the photosynthetic parameters can be described with maximum photosynthetic activity around noon and minimum at dawn and dusk and during the night (Mac Caull and Platt 1977; Lizon *et al.* 1995; Yoshikawa and Furuya 2006), and can be minimized by sampling at the same time of the day (Jouenne *et al.* 2005). Seasonal variability is more complex and requires regular sampling over a year, and according to Côté and Platt (1983) is driven mainly by temperature, nutrient concentrations, light availability and phytoplankton community (species composition, species diversity and cell volume).

From these considerations a further hypothesis was developed and tested:

- temperature, nutrient concentrations, light availability and phytoplankton community show statistically significant correlations with the photosynthetic parameters of Carlingford Lough.

1.3 Sampling site: Carlingford Lough

Following the Northern Ireland coast line from north to south, it is possible to identify five sea loughs: Lough Foyle, Larne Lough, Belfast Lough, Strangford Lough and Carlingford Lough (Figure 1.1). Carlingford Lough, the most southern, is located on the border between Northern Ireland (County Down and County Armagh) and the Republic of Ireland (County Louth). The Lough extends in a northwest-southeast direction and opens into the Irish Sea.

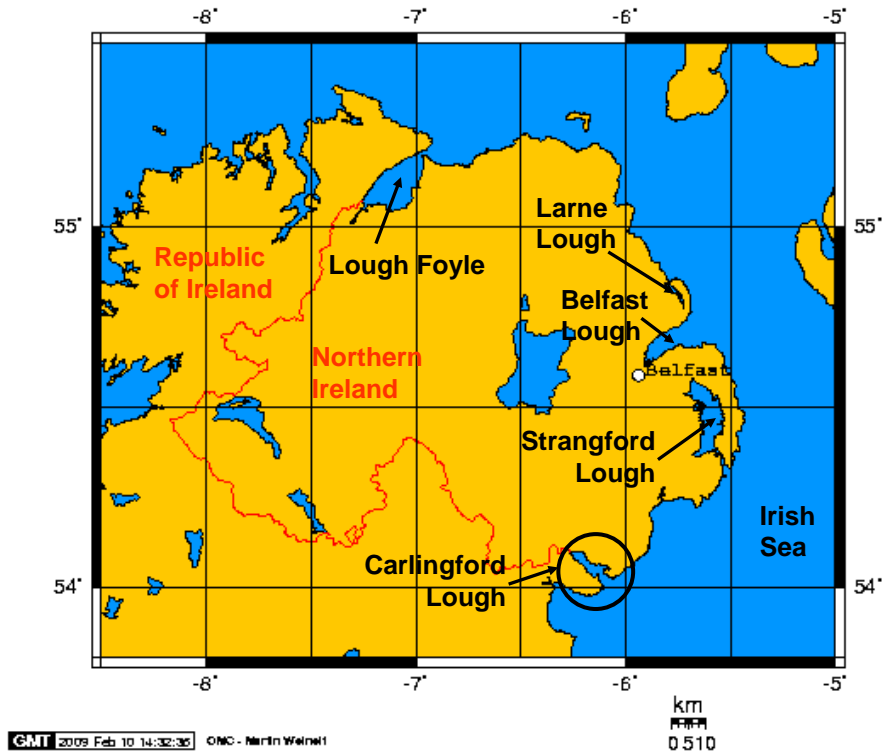


Figure 1.1. A map of Northern Ireland indicating the location of the 5 sea loughs, and in particular Carlingford Lough (black circle). [Map created using the website www.aquarius.ifm-geomar.de, visited 10/02/2009]

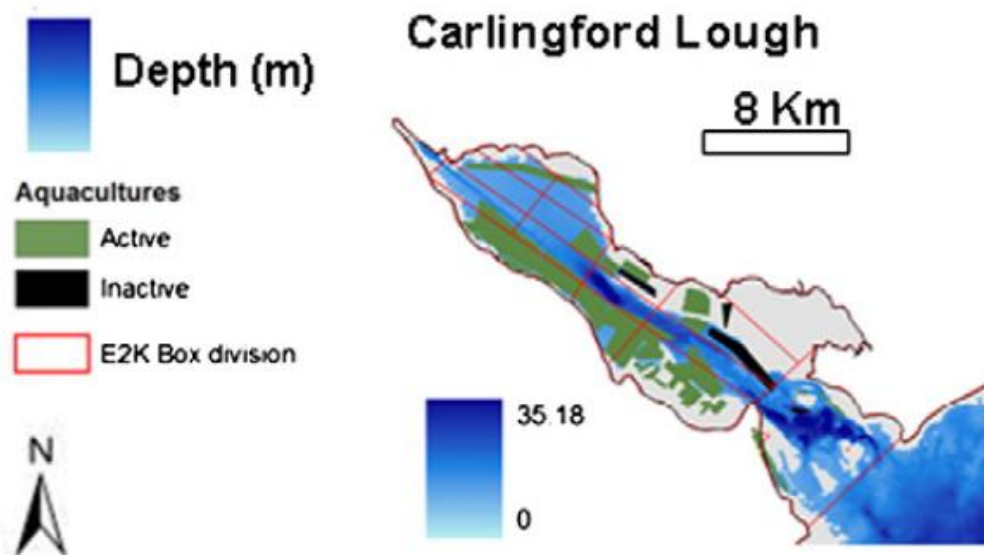


Figure 1.2 Map of Carlingford Lough showing the extension of the active (green) and inactive (black) aquaculture sites (from Ferreira *et al.* 2008).

Overall, the Lough supports a wide variety of aquaculture and fishing interests (Figure 1.2). The main shellfish cultivated in Carlingford Lough are Pacific oysters (*Crassostrea gigas*) and blue mussels (*Mytilus edulis*). The most recent production figures (Ferreira *et al.* 2007) show a production of Pacific oysters of 320 tons y^{-1} , and a production of mussels of 2500 tons y^{-1} . Some cultivation of Manila clams (*Tapes semidecussata*) and scallops (*Pecten maximus*) also occurs (Taylor, Charlesworth and Service 1999). There is also extensive crab (*Cancer pagarus*) and lobster (*Homarus gammarus*) potting throughout the sea lough (DARDNI 2010).

Carlingford Lough is also used for a variety of water sports and recreation fishing. It was designated an Area of Special Scientific Interest (ASSI) in 1996, a Ramsar site for protection of migratory birds and a Special Protection Area (SPA) in 1998 (Ferreira *et al.* 2007).

Land in the vicinity of the Lough supports different types of forest, belts of pasture, natural grassland, moors, heath lands and agricultural areas (AFBI 2010). Industrial activity is minimal along the Lough coastline but there are commercial freight ports in Warrenpoint and Greenore.

Traditionally, local flat oysters (*Ostrea edulis*) and herrings were the main fisheries but overfishing caused the collapse of the herring fishery and oyster industry in the early 19th Century (Douglas 1992). An attempt to restart the oyster industry was made during the first decade of the 1900s, but again overfishing caused a collapse in 1914. During some experimental growth trials with Pacific oyster (*Crassostrea gigas*) in 1973-74, the Lough was demonstrated to provide excellent growth condition for this species. The Pacific oyster was more resistant to endemic disease (e.g. *Bonamia*) than the local flat oyster and showed a faster growth rate. In 1976, the Pacific oyster production in Carlingford Lough increasing to 6 tonnes, was 124 tonnes in 1983 and over 300 tonnes in 1992 (Douglas 1992).

In 2007, the area of the Lough dedicated to aquaculture was 11 km², representing 22% of the total area of the Lough (Figure 1.2); this classifies Carlingford Lough as the Northern Irish sea lough with the greatest proportion of licensed sites (Ferreira *et al.* 2007).

Considering the past history of overexploitation of the resources of the Lough (e.g. oysters) and also considering how mariculture is becoming relevant to the local and regional economy, it is important to regulate this activity in a sustainable way for the environment of the Lough, respecting its carrying capacity.

1.4 Definition of primary production and its importance

All living organisms need organic material to maintain their metabolic activity, growth processes and reproduction cycle. The main carbon source for organic material production is ultimately carbon dioxide. The basic process that converts inorganic carbon into organic carbon using light energy from the sun is the photosynthetic process (Kremer 1981).

The mass of fixed carbon per unit area and time (e.g. $\text{mg C m}^{-2} \text{ h}^{-1}$) of a plant community available for other trophic levels is called net primary production or NPP (Falkowski, Barber and Smetacek 1998). Gross primary production (GPP) is defined as NPP plus plant community respiration.

Primary production is a critical part of the carbon cycle (Falkowski, Barber and Smetacek 1998) and the net global flux of carbon assimilated annually by primary producers is estimated as 105 to 117 Pg C, where $1 \text{ Pg} = 10^{15} \text{ g}$ (Beardall and Raven 2004; Behrenfeld *et al.* 2001; Falkowski *et al.* 2004; Field *et al.* 1998).

In the aquatic environment algae are the dominant fixers of CO_2 (Raven 1997). In particular, phytoplankton is responsible for 46% (48.5 Pg C) to 50% (59 Pg C) of global NPP (Beardall and Raven 2004; Behrenfeld *et al.* 2001; Falkowski *et al.* 2004; Field *et al.* 1998). Although these microscopic algae represent less than 1% (around 1 Pg C) of the photosynthetic biomass of the Earth (Falkowski *et al.* 2004; Falkowski, Barber and Smetacek 1998; Field *et al.* 1998), they occupy a key position in defining global climate, and oceanic and atmospheric chemical composition (Tett 1990).

Furthermore, phytoplankton production is the base of the food web in marine ecosystems, and it influences the nature of marine food webs and abundance of marine organisms (Tett 1990).

The importance of primary production for assessing ecosystem health and for estimating the carrying capacity of a water body has been highlighted in section 1.2 of this chapter.

1.5 History of primary production measurements

The concept of primary production was introduced for the first time at the end of the eighteenth century when an accurate description of photosynthesis and its

stoichiometry was developed, as depicted in the review by Barber and Hilting (2002). After 1850, the new concept of production was applied to the aquatic (fresh water) environment, and algal production was estimated by *in situ* incubation of water samples in light and dark glass bottles, measuring the variation in oxygen and carbon dioxide concentrations in the bottles (see review by Barber and Hilting 2002).

The study of primary production was extended to marine ecosystems in the early 1900s with the main purpose of understanding fishery resources, since a reduction of fishery yields had been observed. As summarised by Barber and Hilting (2002), up to the 1940s there were two principal ways to measure production:

1. measuring changes in oxygen concentration using the Winkler method, in light and dark bottles;
2. measuring carbon dioxide uptake by determining pH changes.

The light and dark bottle oxygen method was the most widely used. In coastal areas, with high algal biomass, the method gave reproducible results with short incubation (e.g. for the light portion of the day; Ryther 1956). For the open ocean, low phytoplankton biomass required several day (e.g. 3) incubations to detect changes in oxygen concentration and this gave misleading results because of bacterial growth and protozoan grazing in the dark bottles (see Barber and Hilting 2002 review).

The first studies that used ^{14}C for measuring production were developed after 1940 when ^{14}C was produced for the first time (by bombarding graphite in a cyclotron), and the Geiger-Müller counter (capable of counting ^{14}C efficiently), was developed in 1949 (see review by Barber and Hilting 2002). With this new instrument and a source of ^{14}C , Steemann Nielsen established a new method for measuring primary production in 1952 (Steemann Nielsen 1952). This method allowed the measurement of primary production to be standardised. By the 1970s the ^{14}C method had been used in most oceanic regions of the world.

Chapter 4 presents a review of the main techniques used to measure primary production and provides a detailed description of the method adopted in this study.

1.6 Physiology and biochemistry of photosynthesis

Photosynthesis occurs in eukaryotic cells in organelles called chloroplasts and involves three processes (Falkowski and Raven 1997). These are: 1. light absorption by pigments; 2. synthesis of NADPH and ATP (intermediate energy-conserving compounds); 3. CO₂ fixation in the Calvin cycle.

Chlorophyll *a* (or divinyl chlorophyll *a*) is the only pigment present in all phytoplankton organisms and is essential for photosynthesis. In addition to chlorophyll *a*, phytoplankton organisms contain accessory chlorophylls (e.g. b, c, d), carotenoids and/or phycobilins that help in the process of absorption of light (Geider and MacIntyre 2002).

During photosynthesis, two types of reactions can be identified: light reactions and light-independent reactions (Falkowski and Raven 1997). The first type of reactions takes place in the thylakoid (membranes within the chloroplasts), and involves:

- photon absorption in light-harvesting antennae;
- migration of excitation energy of absorbed photons to reaction centres;
- electron transfer from H₂O to NADP⁺;
- generation of ATP by a trans-thylakoid pH gradient (set up as a consequence of electron transfer).

According to Falkowski and Raven (1997), the photosynthetic electron transfer (PET) that links O₂ evolution to NADPH production is catalyzed by three major complexes and small molecules: Photosystem II (PSII), cytochrome b₆/f complex (cyt b/f) and Photosystem I (PSI).

The light-independent reactions that occur in the stroma of chloroplasts, involves a cycle of reactions named the photosynthetic carbon reduction cycle or Calvin cycle. A description of this can be found in the review by Geider and MacIntyre (2002). During this cycle, CO₂ is fixed in carbohydrate ((CH₂O)_n) and phosphates are produced. This process requires energy in the form of ATP and reduction of NADPH to NADP. The most important enzyme catalyzing the Calvin cycle is called RUBISCO (RibUlose – 1,5 – Biphosphate Carboxylase-Oxygenase).

According to Geider and MacIntyre (2002), the rate with which carbon is fixed depends on the:

- amount of RUBISCO in the cell;

- RUBISCO maximum catalytic activity;
- intracellular concentration of CO₂ at the active site of RUBISCO.

RUBISCO is also involved in another important process, photorespiration, which is described in more detail in section 1.7.

1.7 Respiration

Respiration is a major process in which the carbon fixed by photosynthesis is consumed (Iriarte *et al.* 1991); therefore it has to be considered carefully when estimating primary production.

Depending on whether the process takes part in the light or in the dark, two types of respiration can be distinguished: photorespiration and dark respiration. Photorespiration is a specific sequence of reactions taking place in the light and including glycolate oxidation and concomitantly O₂ consumption and CO₂ release (Peterson 1980). In some conditions, such as high irradiance (Peterson 1980), glycolate can be excreted from the cell. As a consequence, if photorespiration occurs at a significant rate, the gross and net CO₂ fixation and its relationship with the assimilation of ¹⁴C have to be defined with care (Geider and MacIntyre 2002). In particular, during incubations with ¹⁴C, photorespiration may be associated with a decline in particulate ¹⁴C assimilation and with increased dissolved organic ¹⁴C production (Fogg 1977).

Dark respiration has two important roles. First, it is the source of energy for cell maintenance and biosynthesis during the dark phase (e.g. supply the NADPH and ATP; Raven and Beardall 1981). Second, it provides carbon units for biosynthetic processes (Geider and Osborne 1989). Dark respiration can also occur in the light, providing energy (NADPH and ATP) for photosynthesis (Geider and Osborne 1989; Raven and Beardall 1981).

The light processes of respiration are less well understood than the dark processes and they are more difficult to estimate. In general, dark respiration increases with growth rates (Geider and Osborne 1989). Iriarte *et al.* (1991) observed that chlorophyll concentration and respiration rates were significantly correlated. Fourqurean *et al.* (1997) also found a positive correlation with temperature and a negative correlation with dissolved inorganic nitrogen (DIN). In contrast, Roberts

and Howarth (2006) observed that phytoplankton respiration increased with increasing nutrient availability.

Other studies have shown the contribution of the heterotrophic component to community respiration. Iriarte *et al.* (1991) suggested that at low to moderate chlorophyll concentrations microheterotrophs are the main contributor to community respiration rates, while at high phytoplankton biomass, autotrophic dark respiration is dominant. Microbial (e.g. bacteria and microflagellates) respiration can account for a substantial fraction of plankton respiration in coastal waters (Williams 1981). The bacterial contribution to community respiration can vary from 10% to 90%, reaching the highest value in oligotrophic water (Roberts and Howarth 2006).

The common method used to estimate respiration measures the dissolved oxygen concentration in water samples incubated in the dark for a definite time (e.g. 24 hours), using the Winkler titration technique (Gaarder and Gran 1927) or oxygen electrochemical sensors (Langdon 1984). As the incubation takes place in the dark, this method cannot measure photorespiration (Peterson 1980). For samples collected in the field, containing natural plankton populations, the method cannot distinguish between phytoplankton and microheterotroph respiration. Therefore the method measures ‘microplankton community respiration’ rather than ‘phytoplankton respiration’.

CHAPTER 2

Sampling site: Carlingford Lough

This chapter aims to provide background information for the sampling site in Carlingford Lough, showing annual trends and ranges of variability of the main environmental variables, such as temperature, salinity, nutrients, chlorophyll, phytoplankton community, particulate suspended matter (SPM), and river flow. Chapter 2 also aims to investigate whether environmental variables, in particular nutrient concentrations, are more likely to limit microalgal growth.

2.1 Introduction to Carlingford Lough

Carlingford, or Cairling fjord, took its name from the Vikings, who arrived in Ireland in 800 A.D. (Douglas 1992). Cairling ('Cathair Linn') can be literally translated as "Stone ringfort of the pool", referring to the sheltered waters that characterised the inner part of the Lough (Carlingford Lough 2010).

The Lough is the result of the expansion of the Carlingford glacier in an eastward direction, during the later stage of the last Ice Age (70,000 – 10,000 years b. p.). The glacier was compressed between the Mourne Mountains, on the north side, and the Carlingford Mountains, on the south side (Figure 2.1). A sill (rock bar) left across the mouth of the Lough and the moraine deposits along the northern and southern side of the Lough provide evidence for the presence of this ancient glacier (Douglas 1992).

The main towns along the Lough coastline are Newry, Warrenpoint, Rostrevor and Greencastle, on the north shore, and Greenore, Carlingford and Omeath on the south shore. Newry is the biggest town with approximately 27.4×10^3 inhabitants in 2001 (Bambridge/Newry and Mourne Area Plan 2015, 2010). The towns discharge their sewage into the Lough, after primary (or in some cases secondary) treatments, but small untreated effluents are also discharged into the Lough.

The mean physical characteristics of Carlingford Lough (according to Ball, Raine and Douglas 1997; Taylor, Charlesworth and Service 1999; Ferreira *et al.* 2007) are reported in Table 2.1.

The depth range is between 2 and 36 m (25 m in the navigable channel). Approximately 30% of the total area of the Lough is intertidal and it is mainly located from Killowen to Greencastle (Figure 2.1). The greatest tidal movements

occur along the channel and the tidal range is approximately 3 m. The volume of the tidal prism is $126 \times 10^6 \text{ m}^3$, which is approximately 27% of the total volume of the Lough (Table 2.1). The maximum current speed near the entrance is 0.87 m s^{-1} , while in the vicinity of Rostrevor Narrows is 0.35 m s^{-1} (Ball, Raine and Douglas 1997). Based on the residence time of the water, Carlingford Lough can be divided into three zones: an inner zone with a residence time > 20 days; a middle zone with a residence time between 8-20 days; an outer zone with a residence time of less than 8 days (Ferreira *et al.* 2007). The sea-bed of the upper Lough is dominated by fine muddy sand, while at the mouth the substratum is mostly boulder and cobble, mixed with patches of bedrock. The sediments in the middle part are a mix of the two previous types (Taylor, Charlesworth and Service 1999).

Table 2.1. Physical characteristics of Carlingford Lough (Ferreira *et al.* 2007).

Total area	49-51 km ²
Intertidal area	15 km ²
Length	16.5 km
Maximum width	5.5 km
Coastline	63.4 km
Volume	$460 \times 10^6 \text{ m}^3$
Low water volume	$146 \times 10^6 \text{ m}^3$
Tidal prism volume	$126 \times 10^6 \text{ m}^3$
Clanrye river flow	$1-9 \text{ m}^3 \text{ s}^{-1}$
Flushing time	8-26 days

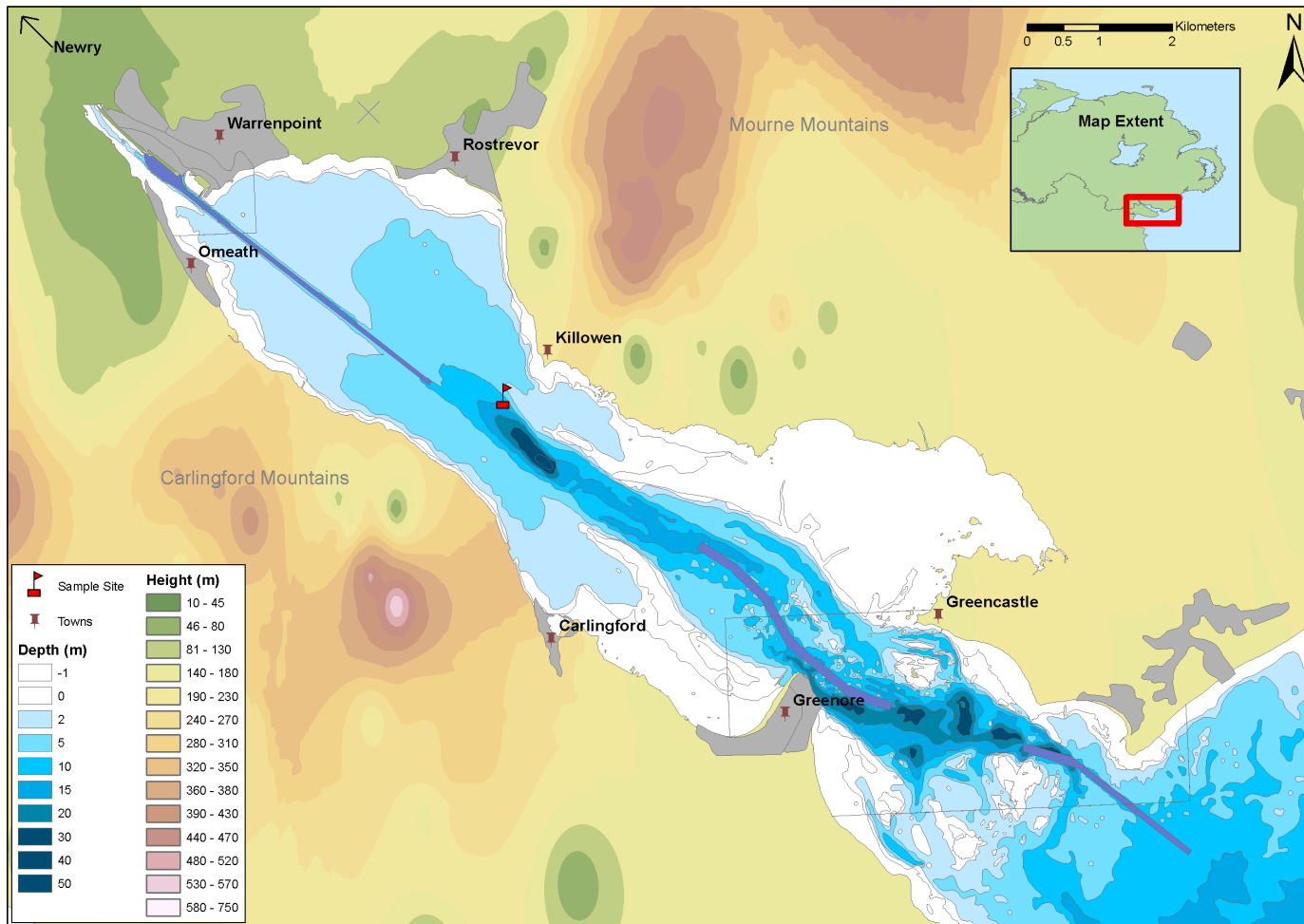


Figure 2.1. A map of Carlingford Lough, showing its bathymetry, the surrounding topography, main towns, and the sampling site CLNBuoy.

The Carlingford Lough drainage basin covers an area of 475 km² and Newry is the largest town in the catchment. The Clanrye (Newry) River is the main freshwater source and is responsible for approximately 70% of the total freshwater, with an average daily volume flow of 471 m³ (Taylor, Charlesworth and Service 1999). The means and ranges of the Lough temperature, salinity and nutrient concentrations measured in previous studies of the Lough are shown in Table 2.2.

Table 2.2. Mean and range of some environmental variables of Carlingford Lough measured in previous studies. The superscript letters and symbols refer to the source of the data and if the data were specific of a station or average of the Lough. In particular: ^a = Douglas (1992), years 1990-91; ^b = Ball, Raine and Douglas (1997), for the year 1992; ^c = Taylor, Charlesworth and Service (1999), for the year 1997; and ^d = Ferreira *et al.* (2007), for the years 1994-2000 unless otherwise specified; * = average of whole Lough; + = station close to CLNBUoy.

Variable	Mean	Range
Salinity	29.08 ^{a+}	25-34 ^{a+}
	---	25-32 ^{b*}
	33.28 ^{c+}	31.55-34.36 ^{c+}
	32.5 ^{d*}	---
Temperature (°C)	12.5 ^{a+}	2.3-17.5 ^{a+}
	11.8 ^{c+}	5.8-18.1 ^{c+}
	---	3-20 ^{d*}
Nitrate (µM)	---	max 19 ^{a*}
	---	<0.6-36 ^{b*}
Ammonium (µM)	---	1.6-11.2 ^{c*}
Soluble Reactive Phosphorus (µM)	---	<0.5-2.6 ^{a*}
	---	<2-3.3 ^{b*}
	---	<1-4.9 ^{c*}
	1.31 ^{d*} (1994-2000)	---
	0.61 ^{d*} (2004-2006)	---
Silicate (µM)	---	<1-43 ^{b*}
	---	<1-38 ^{c*}
Nitrate Clanrye river (µM)	---	37-57 ^b
SRP Clanrye River (µM)	---	5.5-19 ^b

Salinity in Carlingford Lough is related to the freshwater input and the tidal exchange with the Irish Sea. The salinity range in the Lough is narrow compare with other Northern Irish sea loughs, and reflects the small volume (and hence influence)

of the Newry River compared with the tidal prism (Taylor, Charlesworth and Service 1999). The water temperature is influenced by solar heating and the mixing between fresh and sea water, and it shows little variations between the inner and outer Lough (Taylor, Charlesworth and Service 1999). The highest water temperatures are recorded during summer and the lowest during winter.

The dissolved nutrients in the Lough (ammonium, nitrate, nitrite, phosphorus and silica) decrease sharply from the inner Lough to the mouth, and they show maximum concentration in winter and minimum in summer (Ball, Raine and Douglas 1997; Taylor, Charlesworth and Service 1999). In 1997, the total annual loading of dissolved inorganic nitrogen (nitrate + ammonium, of which > 98% was nitrate) to Carlingford Lough was calculated as 1311 tonnes, of which: 77% originated from the Newry River, 11% from other rivers, 7% from Sewage Treatment Works (STWs) and the remaining 5% from atmospheric sources (Taylor, Charlesworth and Service 1999). The main sources of ammonium were STWs, the atmosphere and the Newry River (Taylor, Charlesworth and Service 1999). The same calculation was also made for Soluble Reactive Phosphorus (SRP) and the total annual load was estimated as approximately 57 tonnes, of which: 57% was from the Newry River, 38% from STWs, 4% from other rivers and 1% from atmosphere sources. In particular, during winter the River is the main source of phosphorus while during the rest of the year STWs are the main source (Taylor, Charlesworth and Service 1999). Silicate concentration is closely related to salinity (Ball, Raine and Douglas 1997), and its distribution reflects freshwater input and diatom utilization (Taylor, Charlesworth and Service 1999).

Inputs of nutrient from the sea were not considered in any of the previous studies. However, considering the large tidal exchange (tidal prism volume of $126 \times 10^6 \text{ m}^3$ versus a low tide volume of $146 \times 10^6 \text{ m}^3$, Table 2.1), and the lower nutrient concentration of the Irish sea (e.g. nitrate concentration at station outside Carlingford Lough varied between 0.0-10 μM , Gowen *et al.* 1995), it is likely that there is a net export of nutrient from the Lough to the sea (Taylor, Charlesworth and Service 1999).

Suspended Particulate Matter (SPM) in the Lough was measured by Ball, Raine and Douglas (1997) and by Taylor, Charlesworth and Service (1999), and varied between 5 to 66 g m^{-3} (for the whole Lough) and between 18.29 and 47.20 mg L^{-1} (for a station near CLNBuoy) respectively. The SPM concentration decreased

moving from the inner part to the outer part of the Lough. The higher concentration in the inner part of the Lough could be explained by the loadings from the Newry River, and by resuspension of sediments in the shallower regions. Higher levels of SPM were measured during winter while low levels were recorded during summer (Taylor, Charlesworth and Service 1999).

Chlorophyll concentration decreases from the inner part of the Lough to the outer region (Taylor, Charlesworth and Service 1999), and waters along the south shore of the Lough support higher concentrations than the north shore (Douglas 1992). Considering temporal trends, chlorophyll concentration peaked in early May in 1990 and 1991 (19.44 mg m^{-3} ; Douglas 1992), April in 1992 ($6-9 \text{ mg m}^{-3}$; Ball, Raine and Douglas 1997), and at the end of March in 1997 (10 mg m^{-3} ; Taylor, Charlesworth and Service 1999). During summer, chlorophyll ranged between 3 and 8 mg m^{-3} reaching a maximum at the end of August (12 mg m^{-3} ; Ball, Raine and Douglas 1997). From September the concentration decreased until the winter minimum of $< 2 \text{ mg m}^{-3}$ was reached (Ball, Raine and Douglas 1997). Douglas (1997) observed a small peak in mid/late autumn. The highest chlorophyll concentration measured by Douglas (1992) was 47.8 mg m^{-3} (at a station in front of the Warrenpoint sewage outfall) while the highest concentration measured by Taylor, Charlesworth and Service (1999) was 12.4 mg m^{-3} .

The phytoplankton community in Carlingford Lough was investigated by three previous studies (Douglas 1992; Ball, Raine and Douglas 1997; Taylor, Charlesworth and Service 1999), and the main taxa identified are summarised in Table 2.3. In general diatoms were dominant throughout the year (Taylor, Charlesworth and Service 1999), and the most common microalgae were *Thalassiosira*, *Chaetoceros*, *Leptocylindrus* and *Rhizosolenia*. Dinoflagellate species never accounted for more than 5% of the total biomass (Ball, Raine and Douglas 1997). *Gyrodinium* spp. and *Protoperidinium* spp. were abundant between March and August, in particular in June-July (Taylor, Charlesworth and Service 1999). Ball, Raine and Douglas (1997) also observed *Scropsiella* sp. and *Prorocentrum micans* in low number during summer. Microflagellates were observed throughout the year; in particular, Taylor, Charlesworth and Service (1999) reported the highest abundance of microflagellates in late spring and early summer ($25 \times 10^3 \text{ cells L}^{-1}$), while Ball, Raine and Douglas (1997) in autumn and winter.

Table 2.3. Summary of the main phytoplankton taxa in Carlingford Lough identified in previous studies, during the different seasons (spring = March – May; summer = June – August; autumn = September – November; winter = December – February).

	Douglas (1992)	Ball, Raine and Douglas (1997)	Taylor, Charlesworth and Service (1999)
Spring	<i>Thalassiosira</i> spp., <i>Pleurosigma</i> spp., <i>Asterionella</i> sp.	<i>Thalassiosira</i> <i>rotula/gravida</i> , <i>nordenskioldii</i> , <i>Guinardia flaccida</i>	<i>Chaetoceros</i> spp., <i>T. Peridinium</i> spp., microflagellates
Summer	<i>Rhizosolenia</i> spp., <i>Chaetoceros</i> spp., <i>Asterionella</i> sp.	<i>Leptocylindrus</i> <i>danicus</i> , <i>Asterionellopsis</i> <i>japonica</i> , <i>Rhizosolenia hebetata</i>	<i>Chaetoceros</i> spp., <i>Leptocylindrus</i> spp., <i>Nitzschia</i> spp., <i>Cerataulina pelagica</i> , <i>Thalassiosira</i> spp., <i>Gyrodinium</i> spp., <i>Peridinium</i> spp., microflagellates
Autumn	<i>Chaetoceros</i> spp.	<i>Thalassionema</i> <i>nitzschioides</i> , microflagellates	<i>Chaetoceros</i> spp. <i>Asterionella</i> sp.
Winter	<i>Pleurosigma</i> spp., <i>Coscinodiscus</i> sp.	Microflagellates	---

2.2 Methods

2.2.1 Sampling

The sampling site (CLNBuoy in Figure 2.1) was located next to a permanent instrumented mooring (latitude 054° 04.223 N, longitude 006° 11.506 W; Figure 2.1). Sampling was approximately weekly from March/April to September, and monthly for the other months. Data collection started on the 4th April 2006 and ended on the 13th March 2008, with 48 sampling trips carried out.

Sampling was undertaken mainly onboard the Northern Ireland Loughs Agency boat “*FPV Mytilus*”, and occasionally from an AFBI (Agri-Food and Biosciences Institute) RIB (rigid inflatable boat) or a commercial fishing boat. Sampling usually took place between 9 and 11 a.m. to avoid variation in the photosynthetic parameters related to their circadian cycle (see Chapter 5). On each sampling occasion, temperature and salinity profiles were recorded with a Seabird CTD. Four CTDs were used on different occasions (Seabird 19, Seabird 19 Plus, Cefas Seabird 19 with Li-Cor, and Seabird 19 with 2 light sensors). The Seabird 19 with Li-Cor and the Seabird 19 with 2 light sensors also recorded the underwater light field, details of which are given in Chapter 3.

Water samples were collected with a non-metallic 5 L Kemmerer sampler (by WILDCO) from one meter below the surface, at 4 m and occasionally at 6 or 7 m (if sampling was carried out at high tide). From each depth, water samples for the determination of nutrients, chlorophyll and Suspended Particulate Matter (SPM) concentrations were taken, together with samples for the estimation of phytoplankton abundance, biomass and species composition. Water samples from 4 m depth were also used to estimate phytoplankton carbon assimilation. In particular, details on the method to measure carbon assimilation are reported in Chapter 4.

After collection, water samples for phytoplankton analyses were stored in dark glass bottles of ~250 mL and fixed with 7 mL of 4% formalin. Phytoplankton samples were kept in the dark in a laboratory at AFBI minimising any movement of the bottles, samples were analysed using an inverted microscope between 1 to 12 months after collection. Water samples for dissolved inorganic nutrients (ammonium, nitrite, nitrate, soluble reactive phosphorus – SRP – and silicate) were filtered (Whatman GF/F) on site and stored in ~20 mL Polycon® tubes, until return to the laboratory within 2-3 hours. Water samples for chlorophyll extraction were stored in black plastic bottles until they were filtered in the laboratory on the same day of

sampling. Samples for the estimation of SPM concentration were stored in 2 L plastic bottles, until analysed within a few hours after collection. In the rare event the samples could not be processed on the same day of collection, they were kept in a fridge until the following day.

Before sampling and measurements were conducted, cloud cover (expressed on a scale from 0% = clear sky to 100% = completely overcast) and the state of the sea (according to the Beaufort Scale) were recorded, together with information on wind direction. Clanrye River flow data were provided by the Northern Ireland River Agency.

2.2.2 CTD calibrations

From April 2006 until the start of June 2007, a Seabird 19, a Seabird 19 Plus, and a Seabird 19 with Li-Cor (borrowed from Cefas, Lowestoft) were used on different occasions. On some sampling events, simultaneous CTDs profiles (Seabird 19 Plus and Seabird 19; Seabird 19 Plus and Cefas Seabird 19 with Li-Cor) were collected for comparison of temperature and salinity values. The Seabird 19 Plus was the most recently calibrated CTD (January 2006) and it was used as a reference for the other two CTDs. For each simultaneous profile, temperature and salinity at each depth measured with the Seabird 19 Plus were subtracted from the corresponding temperature and salinity of the Seabird 19 at the same depth. The average differences measured for temperature and salinity between the two CTDs were calculated and used to correct the Seabird 19 measurements. The same process was used to correct the Cefas Seabird 19 (with Li-Cor) measurements. The calibration equations for the Seabird 19 (Equations 2.1 and 2.2) and for the Cefas Seabird 19 with Li-Cor (Equations 2.3 and 2.4) are reported below. From mid June 2007, a Seabird 19 with 2 light meters was used; this CTD was calibrated in March 2007 by the manufacturer Seabird Electronics.

$$\text{Temperature}_{\text{corrected}} = \text{Temperature}_{\text{Seabird19}} - 0.012 \quad (2.1)$$

$$\text{Salinity}_{\text{corrected}} = \text{Salinity}_{\text{Seabird19}} + 0.045 \quad (2.2)$$

$$\text{Temperature}_{\text{corrected}} = \text{Temperature}_{\text{CefasSeabird19}} - 0.025 \quad (2.3)$$

$$\text{Salinity}_{\text{corrected}} = \text{Salinity}_{\text{CefasSeabird19}} - 0.020 \quad (2.4)$$

2.2.3 Phytoplankton

Phytoplankton in the water samples was identified and enumerated using a Nikon phase contrast inverted microscope and a sedimentation method as described by Utermöhl (1958).

The sample was gently mixed turning the bottle upside down for approximately 100 times. Aliquots of 25 or 50 mL of each sample were sedimented and counted. The sedimentation chambers were placed on a horizontal surface to allow the cells to sediment homogeneously on the bottom of the chamber.

Phytoplankton cells along the central strip of the chamber were identified and counted (see Figure 2.2 a) with an objective of magnification x40, and with an ocular of x10, for a total magnification of x400. If less than 200 cells were counted in the central strip, the chamber was rotated 45° or 90° and the count repeated on the new strip. This action was repeated until at least 200 cells were counted, and according to Edler (1979) a count of at least 200 cells should give a maximum error of $\pm 20\%$ on the estimated phytoplankton abundance. The upper or the lower part of the sedimentation chamber was then observed with a magnification of x200, for identification and enumeration of taxa not identified in the central strip (Figure 2.2 b).

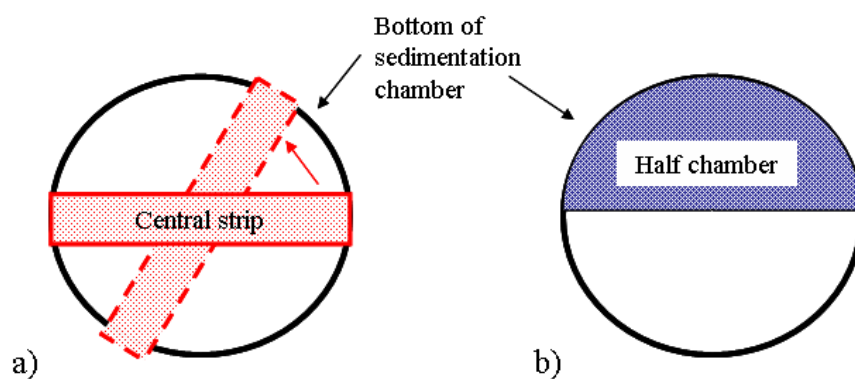


Figure 2.2. View of the investigated areas of the bottom of the sedimentation chamber with a) x400 and b) x200.

Cell abundance was calculated using the following equations:

1. for cells counted in the central strip:

$$\text{abundance (cell L}^{-1}\text{)} = \frac{n \times A_c}{n_s \times A_{cs}} \times 20 \text{ or } 40 \quad (2.5)$$

where n is the number of cells counted in the central strip; A_c is the area of the chamber; n_s is the number of transect counted; A_{cs} is the area of the central strip; 20 is used with 50 mL sedimentation chamber and 40 with 25 mL chambers;

2. for cells counted on half the chamber bottom:

$$\text{abundance (cell L}^{-1}\text{)} = n \times 2 \times 20 \text{ or } 40 \quad (2.6)$$

where n is the number of cells counted in the half chamber; the rest as above.

Phytoplankton abundance of each sample was calculated as the sum of the abundance 1 and 2.

The area of each chamber bottom and the central strip, together with the volume of each chamber were measured annually.

The main reference for species names and aid to identification of phytoplankton species was Tomas (1996). Identification and enumeration skills were tested with internal and external intercomparison test. I took part in the BEQUALM (Biological Effects Quality Assurance in Monitoring Programmes) 2008 intercomparison, in Galway (Ireland). The intercomparison exercise included enumeration and identification sections. My estimates of phytoplankton abundance were ≤ 1 standard deviation from the mean and I scored 97% in phytoplankton identification.

Phytoplankton biomass ($\mu\text{gC L}^{-1}$) was calculated in three steps: 1. phytoplankton cell measurements; 2. calculation of cell volume; 3. estimate of carbon content. During microscopic analysis, measurements of phytoplankton cells were taken with a micrometer. For each sample, each taxon was measured at least once. Using the measurements collected from all of the samples, average measurements of each taxon were calculated. The average cell volume (μm^3) of each taxon was determined using geometric formulas given by Edler (1979). Hillebrand *et al.* (1999) compared the cell volumes of some phytoplankton taxa calculated using different geometric formulas, including those of Edler (1979). They observed that different geometric formulas gave the same results for simple centric diatoms, while the calculated cell volumes were different for taxa with more complex shape such as some benthic pennate diatoms (e.g. *Lichmophora* and *Cymbella*), some centric

diatoms (e.g. *Ditylum*) and some dinoflagellates. In consideration of the findings of Hillebrand *et al.* (1999), phytoplankton cell volumes in this study were calculated using Edler's (1979) equations except for the genus *Ditylum* and *Ceratium* (Appendix 1). *Ditylum* cell volume was calculated according to Hillebrand *et al.* (1999) and *Ceratium* volume according to Thomsen (1992; Appendix 1). Pennate diatoms belonging to the genus *Lichmophora*, *Cymbella*, *Amphora* and *Gomphonema* represented on average 0.4% of the phytoplankton abundance so the error derived from using Edler's simpler equations was considered small.

To convert cell volume to carbon (pg C) the equations of Menden-Deuer and Lessard (2000) were used:

$$\text{for diatoms: carbon content} = 0.288 \times \text{cell volume}^{0.811} \quad (2.7)$$

for all the other phytoplankton:

$$\text{carbon content} = 0.216 \times \text{cell volume}^{0.939} \quad (2.8)$$

The phytoplankton biomass in each sample was obtained by multiplying the carbon content of each taxon by its abundance and summing the biomass of all the taxa. This calculation was made using a simple Matlab (7.1) script named '*biomassa.M*' (Listing 2.1 in the Appendix 2).

For each sample, the abundance of microheterotrophs, ciliates and tintinnids were also determined, counting the organisms on the whole chamber base with x200 magnification.

2.2.4 Nutrients

On return to the laboratory, the water samples that had been filtered for nutrient analysis were preserved with 200 μL of mercuric chloride (2 g L^{-1}) and subsequently frozen ($< -10^\circ\text{C}$) until analysis.

Nutrients (ammoniacal nitrogen NH_4 , nitrate NO_3^- , nitrite NO_2^- , soluble reactive phosphorus PO_4^{3-} , and soluble silica $\text{Si}(\text{OH})_4$) were determined by the AFBI laboratory technicians with an automated colorimetric method (Bran and Luebbe 1991a; Bran and Luebbe 1991b; Bran and Luebbe 1991c; Bran and Luebbe 1991d; Bran and Luebbe 1992), using a Bran and Luebbe segmented continuous-flow analyzer (TRAACS). Three replicates of each sample were analysed, and standardisation of the measurements were performed with nutrient standards by

Ocean Scientific International Limited (OSIL). Detailed information of the different steps of the analysis are reported in Table 2.4, together with the instrument detection limits.

Table 2.4. Description of the chemical analysis of the nutrients and the instrument detection limits.

Nutrient	Analysis
Ammoniacal nitrogen (NH ₄)	Ammonia reacts with a moderately alkaline hypochlorite solution to form monochloramine, which, in the presence of phenol, produces indophenol blue. The intensity of the blue dye is determined colorimetrically at 630 nm. Detection limit: 0.18 µM (Stewart 2008a).
Nitrate (NO ₃ ⁻)	Nitrate is reduced to nitrite with the use of a copper/cadmium reductor coil. The total nitrite (reduced nitrate + nitrite) is coupled with sulphanilamide hydrochloride and N-1-naphthylethyl-enediamine dihydrochloride to form an azo dye. The intensity of the pink dye is determined colorimetrically at 550 nm (Stewart 2008b). Nitrate is calculated by subtracting the nitrite concentration from the total nitrite. Detection limit: 0.06 µM.
Nitrite (NO ₂ ⁻)	Nitrite is coupled with sulphanilamide hydrochloride and N-1-naphthylethyl-enediamine dihydrochloride to form an azo dye. The intensity of the pink dye is determined colorimetrically at 550 nm. Detection limit: 0.02 µM (Stewart 2008c).
Soluble Reactive Phosphate (PO ₄ ³⁻)	Orthophosphate and other labile phosphate react with acidic molybdate to form a yellow complex, which is reduced with ascorbic acid to molybdenum blue. The intensity of the blue dye is determined colorimetrically at 880 nm. Detection limit: 0.06 µM (Stewart 2008d).
Soluble silica (Si(OH) ₄)	Silica reacts with acidic molybdate to form a yellow complex, which is then reduced to an intensely blue coloured complex. The intensity of the blue dye is determined colorimetrically at 880 nm. Interference from phosphate is avoided by the addition of oxalic acid. Detection limit: 0.31 µM (Stewart 2008e).

2.2.5 Chlorophyll and calculation of chlorophyll standing stock

Chlorophyll was determined according to Tett (1987). Three replicate water samples (100 mL in spring and summer and 150 mL for the rest of the year) were filtered through Whatman GF/F filters which were placed into individual tubes (alpha polypropylene). To extract algal pigments, 8 mL of 90% acetone were added to each tube. The tubes with filters and acetone were left for 24 h at 4 °C in the dark

to allow extraction of the pigments. After centrifugation for 5 minutes at 2000 rpm, samples were analysed with a Turner Design Model 10 filter fluorometer. To distinguish between phaeopigments and chlorophyll pigments, measurements were repeated after acidification of each sample with two drops of 8% HCl. Chlorophyll and phaeopigment concentrations (mg m^{-3}) were determined by:

$$[\text{Chl}] = k \times (F_0 - F_a) \times \frac{E}{V} \quad (2.9)$$

$$[\text{Phaeo}] = k \times (H \times F_a - F_0) \times \frac{E}{V} \quad (2.10)$$

Where: F_0 and F_a are fluorometer readings before and after acidification; E is the extract volume in mL; V is the sample volume in litres; k is the calibration coefficient for each instrument range setting (high, medium or low); H is the ratio between the fluorescence coefficients of chlorophyll (F_{ca}) and phaeopigments (F_{pa}), calculated using a standard solution of 1 mg Chl L^{-1} .

Chlorophyll standing stock, expressed as mg Chl m^{-2} , is the quantity of chlorophyll in the water column at the time of the sampling and was estimated using the Matlab (7.1) script named '*interpolatore2.M*' (Listing 2.2 in the Appendix 2). The script (Listing 2.2) calculates the chlorophyll concentration (mg Chl m^{-3}) every 0.5 m by linearly interpolating the chlorophyll data available. The chlorophyll values were then multiplied by 0.5 m (to obtain mg Chl m^{-2}). The sum of the chlorophyll concentrations gives the chlorophyll standing stock in mg Chl m^{-2} . The sampling activity took part at different phases of the tide, therefore to compare chlorophyll standing stocks at different times of the year an average water column of 5.5 m depth was used.

2.2.6 Suspended Particulate Matter (SPM)

SPM data for 2006 were kindly provided by Ciaran McGonigle (NI Loughs Agency) who was undertaking an independent study in Carlingford Lough. From 2007, SPM samples were routinely collected together with chlorophyll, nutrient and phytoplankton samples and analysed in the laboratory at AFBI in Belfast. All the samples (including the data provided by Mr. McGonigle) were analysed following the same procedure, as describe below.

Details of the procedure are reported in Hilton *et al.* (1986). Known volumes of water were filtered on ashed ($450 \text{ }^\circ\text{C}$ in a muffle furnace for > 4 hours) and pre

weighted GF/F filters. After filtration, filters were rinsed with 0.5 M ammonium formate (31.5 g L^{-1}) to remove salt and placed in an oven to dry at $60 \text{ }^\circ\text{C}$ for 2 days (or $100 \text{ }^\circ\text{C}$ for 1 day). The difference in filter weight before (W_0) and after (W_1) filtration gives the total SPM (mg L^{-1}). To quantify the organic and inorganic fraction of SPM, the filter was ashed at $500 \text{ }^\circ\text{C}$ for 4 hours and weighed (W_2). The difference between W_1 and W_2 gives the amount of organic SPM. Inorganic SPM was then derived from the difference between total SPM and organic SPM.

Two litres of the filtered water were collected, filtered a second time, and the filter processed and weighed, as describe above. The amount of inorganic matter measured in this filter provided a measure of the salt not removed by the ammonium formate (W_s) and was usually subtracted from the total SPM. When this measurement was not possible (e.g. less than 2 L of filtrated water available) an average W_s from previous experiments was used.

2.2.7 Data analysis

Descriptive statistics of the data were performed using Microsoft Office Excel 2003, as well as the plots depicting the temporal trend of the main physical, chemical and biological variables. Correlation and regression analyses between the main variables, and paired and two-sample T-test were carried out using Minitab 15.1.1.0, after testing the normal distribution of the variables according to Barnes (1952). The paired T-test was used to check if concentrations of sub-surface (1 m) variable (e.g. nutrient, SPM, chlorophyll) were significantly different from the concentrations at 4 m depth.

Some of the environmental variables (such as phytoplankton taxa abundance) were log transformed before being plotted or used in analysis. The log transformation was applied when the standard deviation of the variates was approximately proportional to their mean, as suggested by Barnes (1952).

To identify the presence of a surface mixed layer, Talling (1971), as cited by Gowen *et al.* (1995), calculated the difference between the temperature at 2 m depth and the temperature at depth z (ΔTemp_{2-z}). He defined the boundary of the surface mixed layer where $\Delta\text{Temp}_{2-z} < 0.5 \text{ }^\circ\text{C}$. In this study of Carlingford Lough the difference in temperature between 1 m and 4 m depth (ΔTemp_{1-4}) was calculated. Gowen *et al.* (1995) also considered the influence of the salinity and suggested that

$\Delta\text{Sal}_{2-z} = 1$ had the same effect on density as $\Delta\text{Temp}_{2-z} = 5$ °C. Therefore, as for the temperature, in this study the difference in salinity between 1 m and 4 m depth (ΔSal_{1-4}) was calculated. The ΔTemp_{1-4} and ΔSal_{1-4} were then combined to give an overall $\Delta(\text{T+S})$. Considering that the average water column depth at station CLNBuoy was 5.5 m, it was assumed that $\Delta(\text{T+S}) < 0.5$ °C indicated a vertical mixed water column while $\Delta(\text{T+S}) \geq 0.5$ °C indicated vertical stratification.

Temporal pattern plots of the biomass of some phytoplankton groups and taxa were created using a Matlab (7.1) script called '*HPLP3A_Elisa.M*' (Listing 2.3 in the Appendix 2). The script plots phytoplankton biomass of a particular species, genus, class (e.g. diatoms) or lifeform (pennate/centric diatoms), for a standard year, using data from a range of years, stations and depths. The script uses a '*switch*' function with 4 cases (species, genus, class or lifeform), and the same commands are repeated in every case. As an example, Listing 2.3 in the Appendix 2 shows the commands for case 0 (species case).

2.3 Results

Descriptive statistics of the environmental variables analysed during this study are reported in Table 2.5.

2.3.1 Physical variables

Temperature varied between 6.02 and 16.55 °C, with an average of 12.11 °C over the studied period (Table 2.5), and exhibited the same pattern in both years. The minimum temperature occurred between December and February and the maximum in summer, from July to September (Figure 2.3 a). The average difference in temperature between 1 m and 4 m depth (ΔTemp_{1-4}) was 0.2 °C but $\Delta\text{Temp}_{1-4} \geq 0.5$ °C was only measured on 4 (9th May 2006, 8th June 2006, 23rd April 2007 and 1st June 2007; Figure 2.4 a) out of 43 occasions, equivalent to 9% of the sampling events.

Salinity ranged between 29.54 and 34.02 with an average for the two years of 32.50 (Table 2.5), and showed a less regular pattern in both years compared to temperature (Figure 2.3 b). In general, lower salinity was observed during winter from December to January, with the exception of May 2006 (Figure 2.3 b). The 3 lowest salinity (< 30) events coincided with high Clanrye River outflow; in particular on the 23rd March 2008 the river outflow was 4.1 m³ s⁻¹, on the 6th December 2006, 12.6 m³ s⁻¹, and on the 17th January 2008, 6.6 m³ s⁻¹ (Figure 2.5). The average ΔSal_{1-4} was 0.23 and exceeded the value of 0.1 in 23 out of 43 sampling events, equal to 54% of the events (Figure 2.4 b). The overall $\Delta(T+S)$ was > 0.5 °C on the 65% of the sampling events (28 out of 43; see Figure 2.4 c).

The average Clanrye River outflow for the period from January 2006 to March 2008 (Figure 2.5) was 2.14 m³ s⁻¹ (Table 2.5). The outflow was variable during the two years studied (range from 0.27 to 21.70 m³ s⁻¹) with the highest peaks during winter (from December to February). March and April 2006 and 2007 were also characterised by high river outflow, while summer (from June to August) 2006 and summer 2007 showed different patterns. The summer of 2006 was generally dry and the average river outflow was 0.67 m³ s⁻¹, while summer 2007 had higher precipitation and the average river outflow was 1.92 m³ s⁻¹ with a peak > 10 m³ s⁻¹ at the end of August.

Table 2.5. Unit of measure and descriptive statistics (number, mean, standard deviation, median, minimum, and maximum) of data from 1 m and 4 m depth, at station CLNBuoy in Carlingford Lough, between April 2006 and March 2008, for the following variables: temperature (Temp), salinity (Sal), river flow (R. flow), Dissolved Inorganic Nitrogen (DIN = NH_4^+ + NO_2^- + NO_3^-), ammonium (NH_4^+), nitrite (NO_2^-), nitrate (NO_3^-), soluble reactive phosphorus (SRP), silicate (Si), SPM total – organic and inorganic (SPM_{tot}), organic SPM (SPM_{or}), inorganic SPM (SPM_{in}), chlorophyll (Chl), chlorophyll standing stock (Chl stock), phaeopigments (Phaeo), chlorophyll/phaeopigments ratio (Phaeo/Chl), phytoplankton abundance (Phyto_{ab}), phytoplankton biomass (Phyto_{bi}), phytoplankton biovolume (Biovol), average phytoplankton cell volume (ACV), average phytoplankton chlorophyll content (ACC), and chlorophyll/carbon ratio (Chl:C).

	Unit	n	Mean	SD	Median	Min	Max
Temp	°C	96	12.11	3.39	12.79	6.02	16.55
Sal	---	96	32.50	1.05	32.76	29.54	34.02
R. flow	$\text{m}^3 \text{s}^{-1}$	821	2.14	2.44	1.34	0.27	21.70
DIN	μM	100	7.80	11.57	2.20	0.34	54.15
NH_4^+	μM	100	1.60	1.06	1.31	0.32	5.39
NO_2^-	μM	100	0.17	0.23	0.04	<0.02	0.92
NO_3^-	μM	100	6.03	10.58	0.74	<0.06	47.85
SRP	μM	100	0.42	0.31	0.35	<0.06	1.27
Si	μM	100	5.16	7.24	1.83	0.02	33.60
SPM_{tot}	mg l^{-1}	72	7.08	3.54	6.17	2.08	18.14
SPM_{or}	mg L^{-1}	66	3.60	1.63	3.25	1.25	8.60
SPM_{in}	mg L^{-1}	66	3.60	2.75	2.58	0.13	14.77
Chl	mg m^{-3}	100	4.47	3.76	3.38	0.28	21.37
Chl stock	mg m^{-2}	47	26.91	22.49	20.61	1.72	125.10
Phaeo	mg m^{-3}	100	1.53	0.69	1.38	0.00	3.06
Phaeo/Chl	ratio	100	0.58	0.56	0.36	0.00	2.77
Phyto_{ab}	$\times 10^3 \text{ cell L}^{-1}$	69	809.1	597.0	637.2	20.4	2,612.0
Phyto_{bi}	$\mu\text{gC L}^{-1}$	69	96.8	70.4	93.6	3.3	310.4
Biovol	$\times 10^9 \mu\text{m}^3 \text{L}^{-1}$	69	1.60	1.27	1.25	0.06	6.00
ACV	$\times 10^3 \mu\text{m}^3 \text{cell}^{-1}$	69	2.34	1.86	1.58	0.47	11.07
ACC	$\times 10^{-9} \mu\text{g} \mu\text{m}^{-3}$	69	3.83	2.35	2.94	0.96	13.44
Chl:C	ratio	69	0.06	0.03	0.05	0.02	0.19

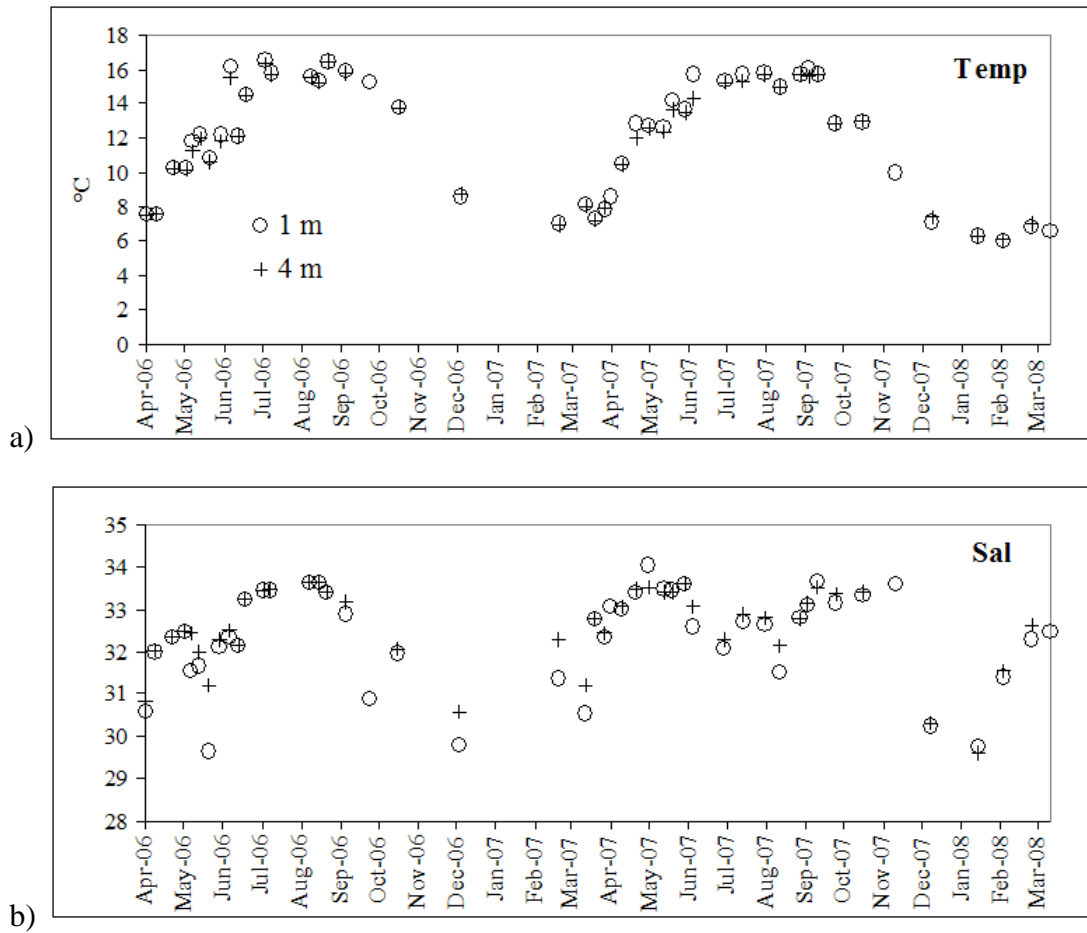


Figure 2.3. The temporal patterns of: a) temperature – Temp (°C) and b) salinity – Sal at 1 m (o) and 4 m (+) depth, at station CLNBuoy in Carlingford Lough, between April 2006 and March 2008.

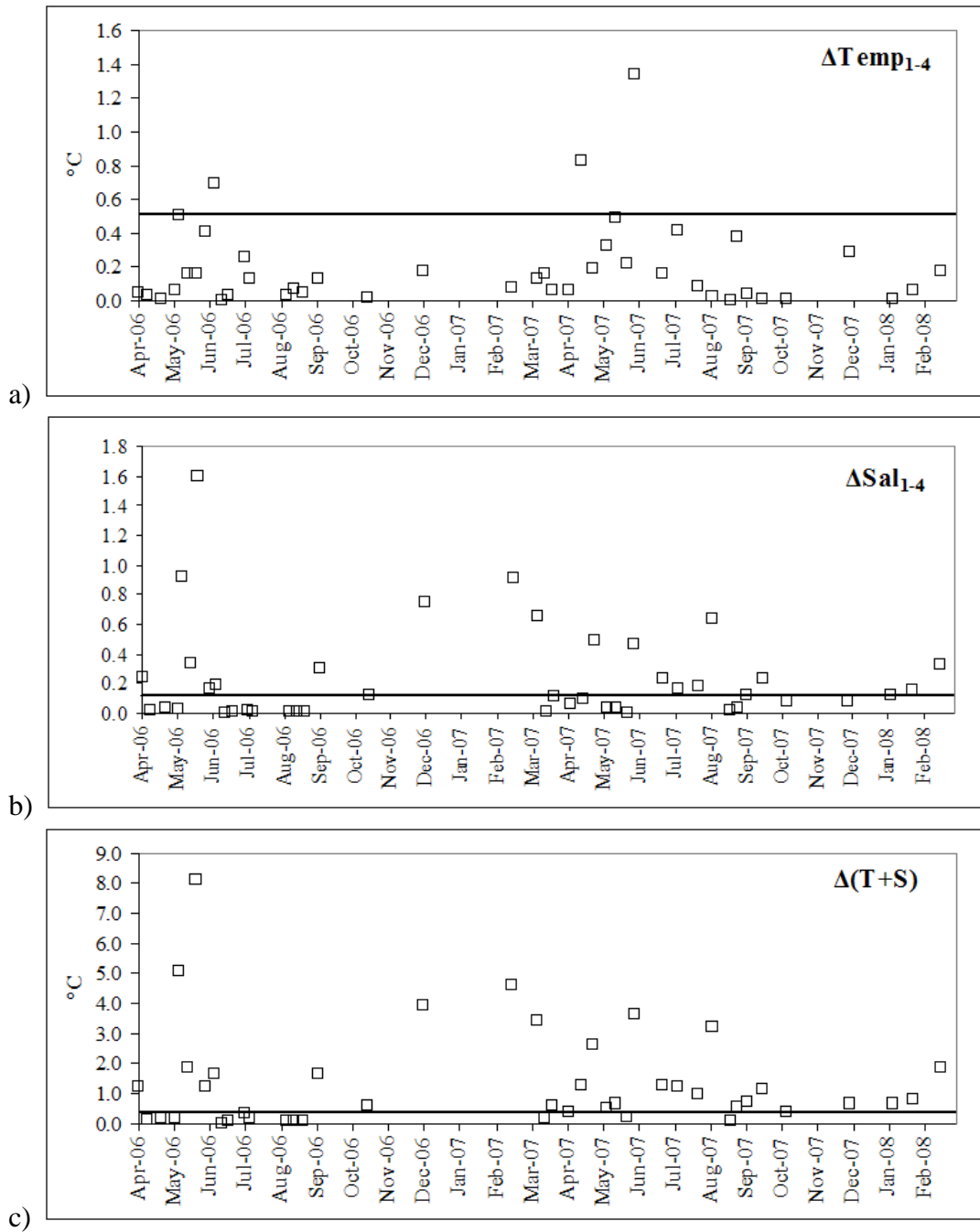


Figure 2.4. The temporal patterns of: a) $\Delta T_{emp_{1-4}}$ (°C), b) ΔSal_{1-4} , and c) $\Delta(T+S)$ (°C) at station CLN buoy in Carlingford Lough, between April 2006 and March 2008. The $\Delta T_{emp_{1-4}} = 0.50$ °C, $\Delta Sal_{1-4} = 0.10$ and $\Delta(T+S) = 0.50$ °C are also drawn as solid line.

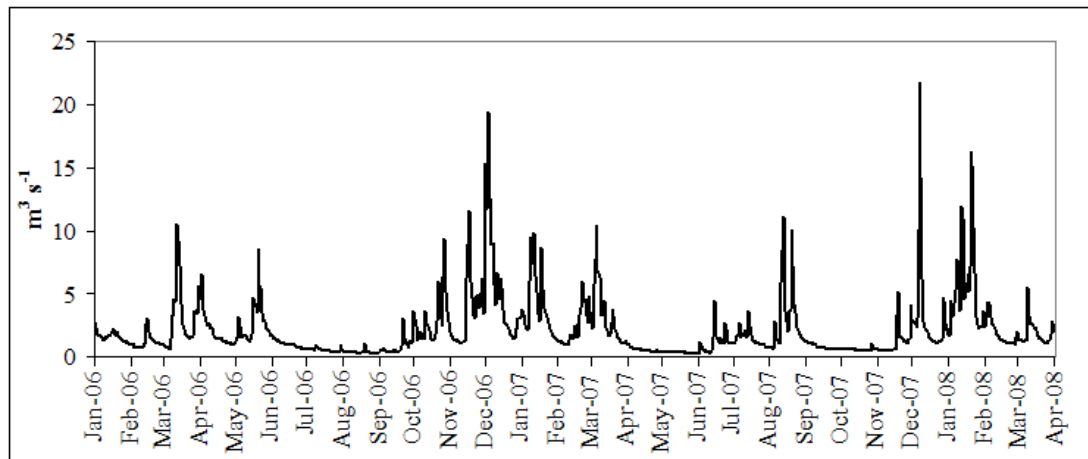


Figure 2.5. The temporal pattern of Clanrye River outflow ($\text{m}^3 \text{s}^{-1}$), measured daily at 00.00 am between January 2006 and March 2008, at station Mountmill Bridge. Data from the Northern Ireland River Agency.

2.3.2 Nutrients

Nutrients (nitrogen compounds, SRP and silicate) exhibited the same temporal pattern, with maximum concentrations in December and January (6th December 2006 and 17th January 2008), and minimum concentrations from April to September (Figure 2.6 and 2.8). Subsurface samples had significantly higher nutrient concentrations than the 4 m depth samples (paired T-test results).

Considering the different nitrogen compounds, ammonium (NH_4^+) varied between 0.32 and 5.39 μM with an average concentration over the study period of 1.60 μM . In relation to its temporal pattern (Figure 2.6 b), spring and summer (from April to August) 2006 exhibited statistically significant (two-sample T-test, T-value = 11.94, DF = 49, and p-value < 0.05) higher NH_4^+ concentration (mean 1.52 μM) compared to the same period in 2007 (mean 0.59 μM). Nitrite (NO_2^-) concentration never exceeded 1.00 μM , and the average concentration was 0.17 μM . In particular, from April to September nitrite concentration was on average < 0.05 μM , and occasionally below the limit of detection (e.g. during June 2006, see Figure 2.6 c). The maximum concentration of nitrate (NO_3^-) measured on the 6th December 2006 was 47.85 μM (Figure 2.6 d), while the average concentration was 6.03 μM (Table 2.5). From April to September of both years, nitrate concentration was low (average 0.47 μM) with the exception of a pulse on the 23rd May 2006 (approximately 7 μM).

On some occasions (e.g. 12th and 23rd April 2007 and 22nd May 2007) NO₃⁻ concentration was below the limit of detection.

Dissolved Inorganic Nitrogen (DIN) was calculated as the sum of nitrate, nitrite and ammonium. The temporal distribution of DIN (Figure 2.6 a) followed the same pattern described for the other nutrients with winter maximum and a spring-summer minimum. Considering the temporal variation in DIN (average of 1 m and 4 m concentrations; see Figure 2.7), ammonium was the dominant nitrogen form from April to August-September, replaced by nitrate for the other months. Ammonium represented on average 58.6% of the DIN with a range from 3.3% (15th March 2007) to 100% (12th April 2007) of the DIN. Nitrate was on average 39.2% of the DIN and varied between 0.0% (12th April 2007) and 95.1% (15th March 2007). Nitrite never represented more than 8% of the DIN and on average only 2.2%.

Soluble Reactive Phosphorus (SRP) varied from below the level of detection to 1.27 µM, with an average concentration over the two years of 0.42 µM (Table 2.5). The temporal pattern (Figure 2.8 a) showed that the minimum concentration was reached in March and April, and from June the concentration started to increase. However in 2007, the SRP concentration remained approximately constant (0.33 µM) during summer (June to August) and started to increase from September.

Silicate ranged between 0.02 and 33.60 µM, with an average concentration of 5.16 µM. Low concentrations (average 1.13 µM) were measured from April to the end of August in 2006 and 2007, with the exception of a small peak (approximately 9 µM) on 23rd May 2006 (Figure 2.8 b).

The temporal pattern of the DIN:SRP ratio is shown in Figure 2.9, and varied between 1.4 (22nd May 2007) and 140.3 (5th May 2006), with an average during the study period of 20.3.

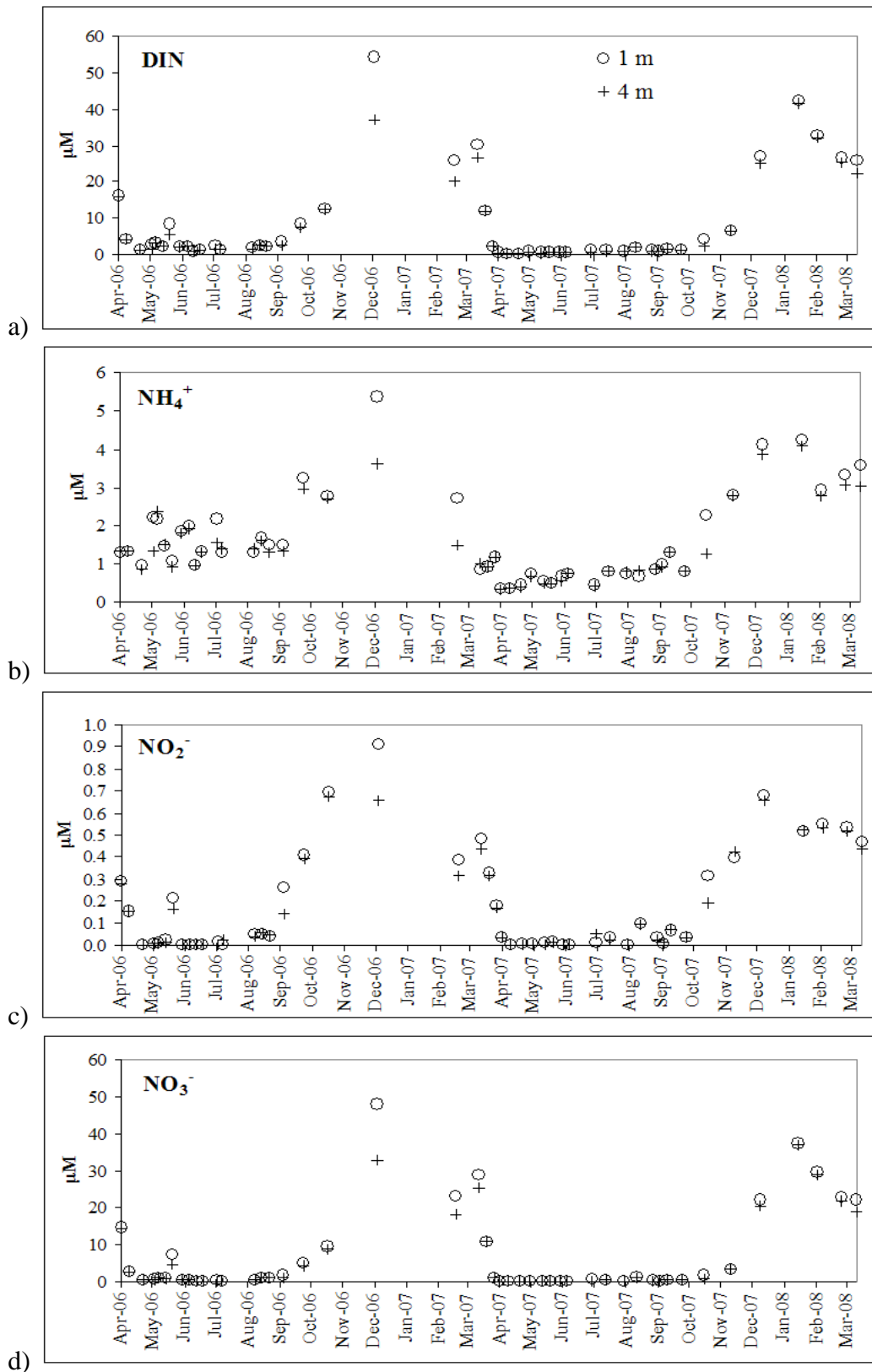


Figure 2.6. The temporal pattern of: a) dissolved inorganic nitrogen - DIN (μM), b) ammonium – NH_4^+ (μM), c) nitrite – NO_2^- (μM), and d) nitrate – NO_3^- (μM), at 1 m (o) and 4 m (+) depth, at station CLN buoy in Carlingford Lough, between April 2006 and March 2008.

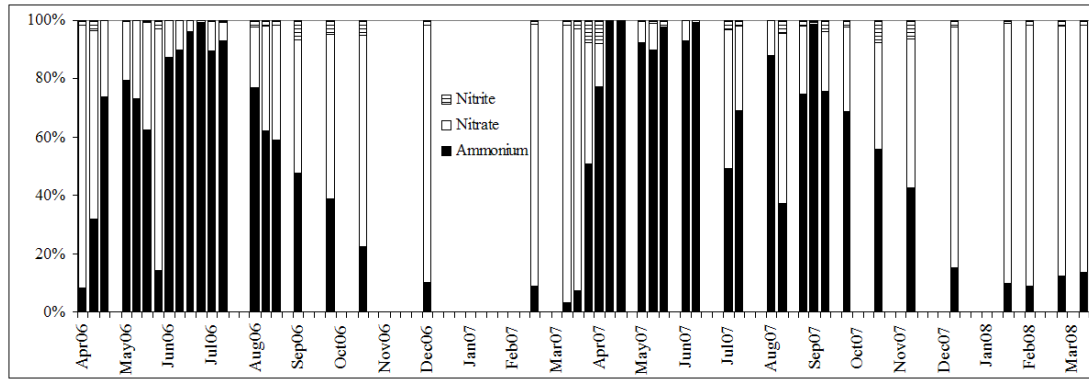


Figure 2.7. The percentage contribution of nitrite (stripes), nitrate (white) and ammonium (black) to DIN for the water column (average of 1 m depth and 4 m depth concentrations), at station CLNBuoy in Carlingford Lough, between April 2006 and March 2008.

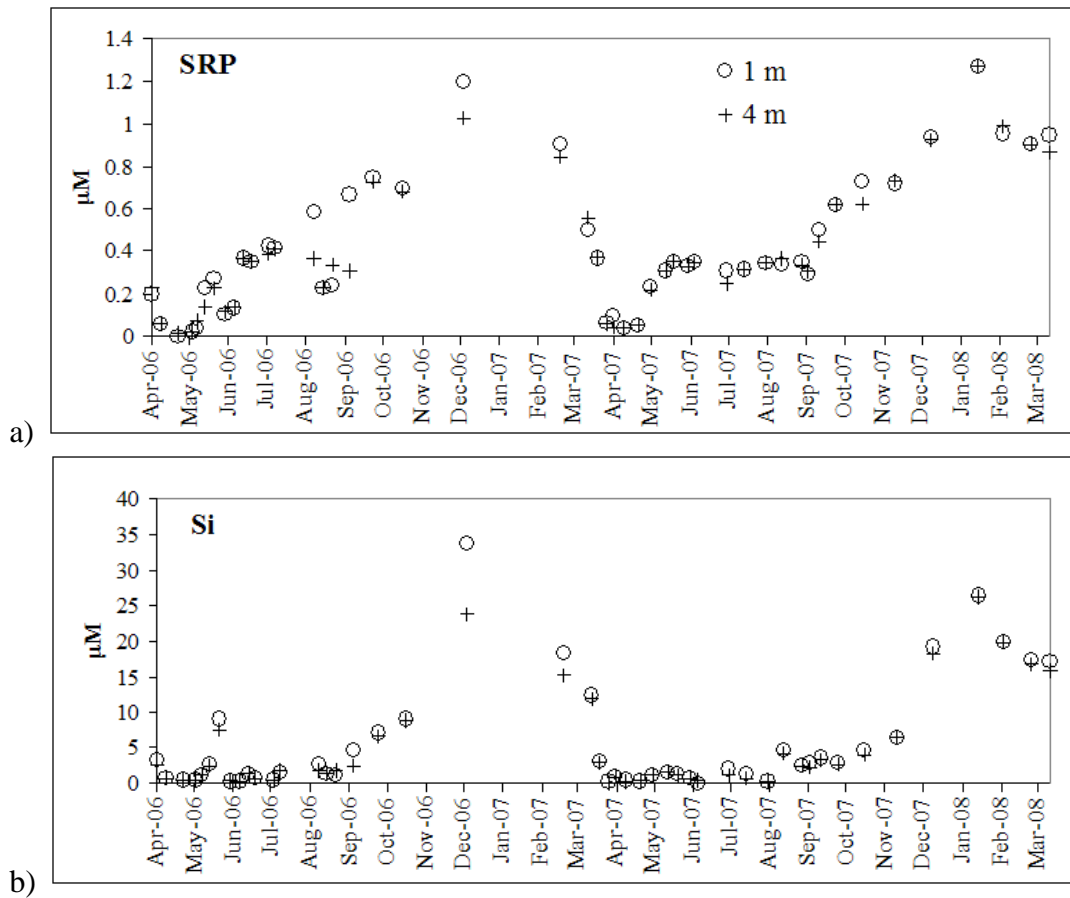


Figure 2.8. The temporal patterns of: a) Soluble Reactive Phosphorus – SRP (μM) and b) silicate – Si (μM), at 1 m (o) and 4 m (+) depth, at station CLNBuoy in Carlingford Lough, between April 2006 and March 2008.

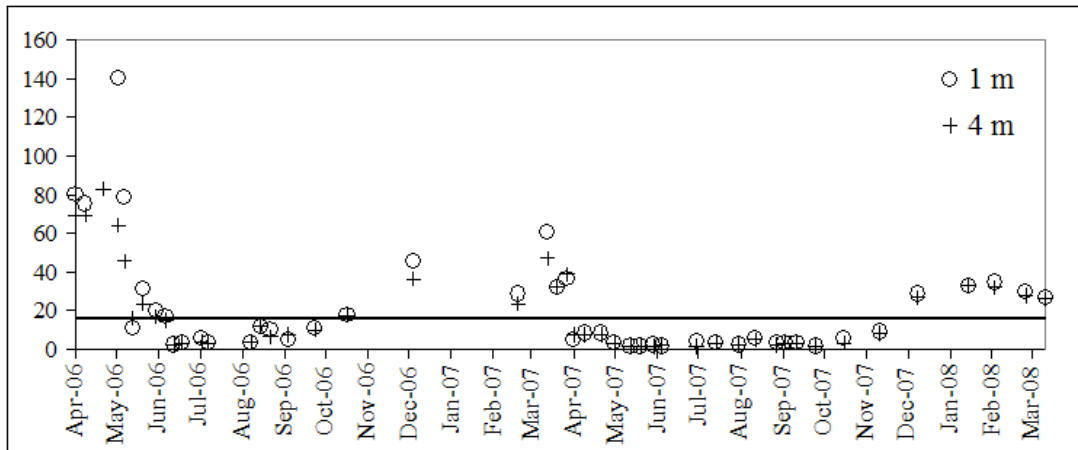


Figure 2.9. The temporal pattern of the DIN/SRP ratio for 1 m (o) and 4 m (+) depth, at station CLN Buoy in Carlingford Lough, between April 2006 and March 2008. The black line represents the Redfield ratio of 16:1.

The linear regressions in Figure 2.10 show the ratio of nutrient accumulation during winter (November to February) and nutrient assimilation by phytoplankton during the spring bloom (March and April) and summer (June to September). Regressions were calculated using nutrient concentrations from 1 m and 4 m depth to increase the number of data (n) for each plot. The regressions for winter and spring were statistically significant (analysis of variance, $p < 0.05$) however the intercept was significantly different from 0 only in plots a, b and d (Figure 2.10).

Regressions of DIN versus SRP gave a N:P ratio of accumulation of 69.1 for winter (Figure 2.10 a) and an uptake ratio of 32.0 during the spring bloom (Figure 2.10 c). The DIN versus silicate ratio was equal to 1.8 during the winter (Figure 2.10 b), and 1.7 for the spring bloom (Figure 2.10 d). Considering the plots for summer (Figure 2.10 e and f), two points are marked in red (26th September 2006, 1 m and 4 m depth); these are nutrient concentrations measured after a week of intense precipitation and an average Clanrye River outflow of $12 \text{ m}^3 \text{ s}^{-1}$. The average River flow during summer was usually $< 2 \text{ m}^3 \text{ s}^{-1}$, so nutrient concentrations from this sampling date were removed from the data set and the regression analyses without these data were not statistically significant ($p > 0.05$).

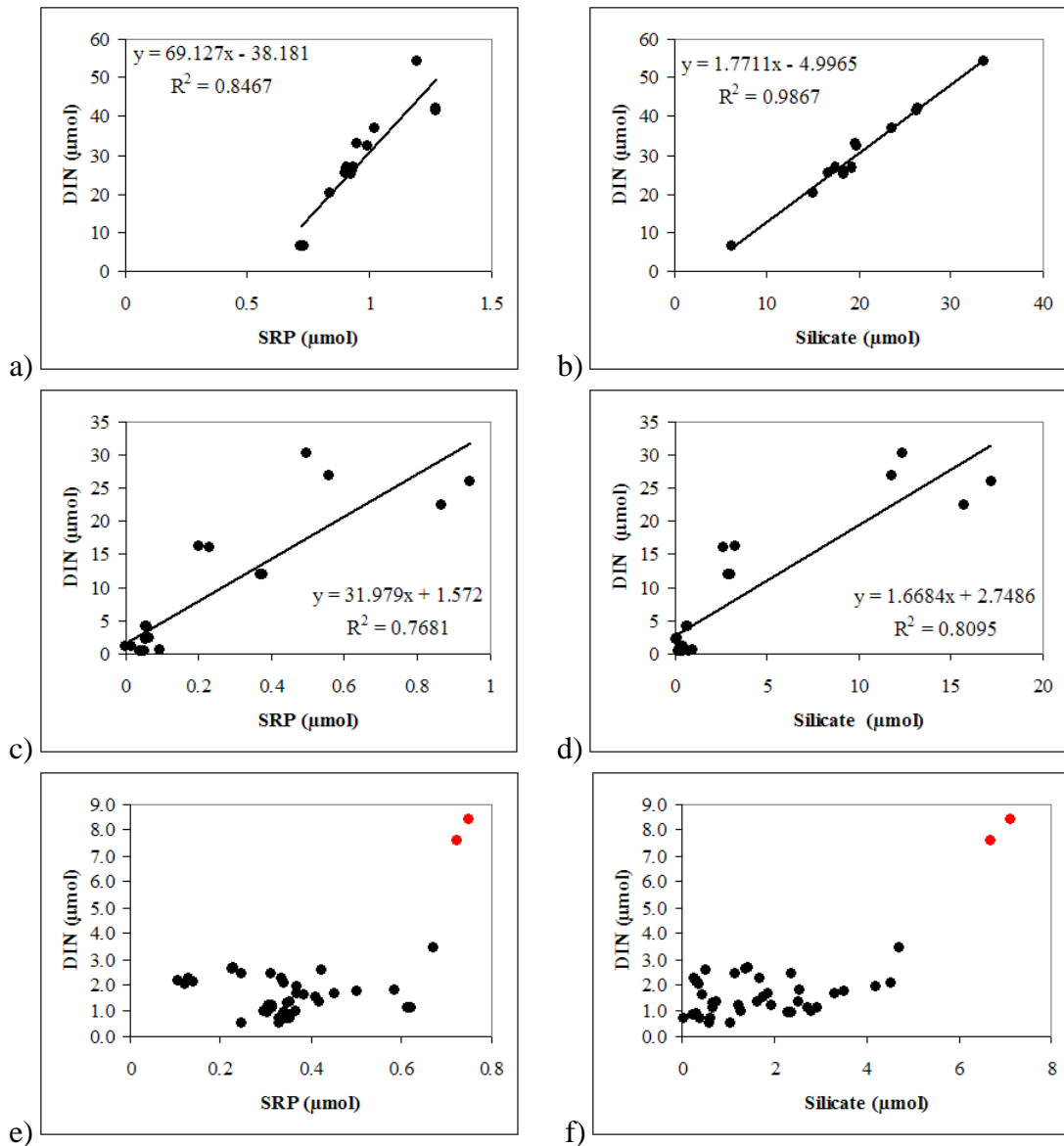


Figure 2.10. Linear regression analyses of DIN versus SRP and DIN versus silicate for winter – November-February (a and b respectively), spring bloom – March and April (c and d respectively), and summer – June-September (e and f respectively) for water column (1 and 4 m depth concentrations), at station CLNBuoy in Carlingford Lough, between April 2006 and March 2008. Number of observations, $n = 14$ for plots a and b, $n = 10$ for plots c and d, and $n = 40$ for plots e and f. All regressions, except e and f, are statistically significant ($p < 0.05$), but only plots a, b and d have intercepts significantly different from 0. A pulse of nutrients at the end of September 2006 is marked by the red circles in plots e and f. Regression analyses of the summer nutrient concentrations without the data from the pulse are not statistically significant ($p > 0.05$).

2.3.3 Chlorophyll and Suspended Particulate Matters

Chlorophyll concentration varied between 0.28 and 21.37 mg m⁻³ (Table 2.5), with an average concentration of 4.47 mg m⁻³. The concentration at 1 m depth was significantly different from the concentration at 4 m depth (paired T-test, T-value = 2.96, n = 47, p < 0.005). In particular, the subsurface concentration was generally higher than the 4 m depth, and the difference between the average concentrations measured at the two depths was 0.57 mg m⁻³. The highest concentration was measured on the 29th March 2007 (Figure 2.11 a), while the lowest was measured during winter on the 17th January 2008. Chlorophyll standing stock ranged between 1.72 (17th January 2008) and 125.10 mg Chl m⁻² (29th March 2007), with an average of 26.91 mg Chl m⁻² (Table 2.5).

The temporal pattern in chlorophyll concentration can be observed in Figure 2.11 a or in Figure 2.12 as chlorophyll standing stock. The years 2006 and 2007 showed slightly different patterns. In 2006, there were two main peaks on the 4th of April (68.4 mg Chl m⁻²), and on the 1st June (59.0 mg Chl m⁻²). After the second peak, chlorophyll standing stock remained approximately constant (around 18.5 mg Chl m⁻²), until a small increase in mid (19th) October (26.5 mg Chl m⁻²). In 2007, the highest chlorophyll standing stock (125.1 mg Chl m⁻²) was measured at the end of March (29th), followed by low values (average 15 mg Chl m⁻²) until the end of May. From June, chlorophyll standing stock increased progressively until the end of August (44.4 mg Chl m⁻²). An autumn peak of 66.7 mg Chl m⁻² was measured on the 18th October. Average winter (November to February 2006 and 2007) chlorophyll standing stock was 4.6 mg Chl m⁻² (chlorophyll concentration <1 mg m⁻³).

Phaeopigments presented a variable temporal distribution (Figure 2.11 b), and ranged between 0 (23rd April 2007) and 3.06 mg m⁻³ (22nd March 2007), with an average of 1.53 mg m⁻³ (Table 2.5). Subsurface phaeopigments concentration was not significantly different from the concentration at 4 m (one-sample T-test, T-value = 0.11, n = 47, p > 0.05).

The ratio between phaeopigments and chlorophyll (Phaeo/Chl) varied between 0 (23rd April 2007), when phaeopigments concentration was not detectable and 2.77 (11th December 2007), when phaeopigments concentration was approximately 3-fold higher than the chlorophyll concentration. The average ratio was 0.58 (Table 2.5), indicating that chlorophyll concentration was usually double the phaeopigments concentration.

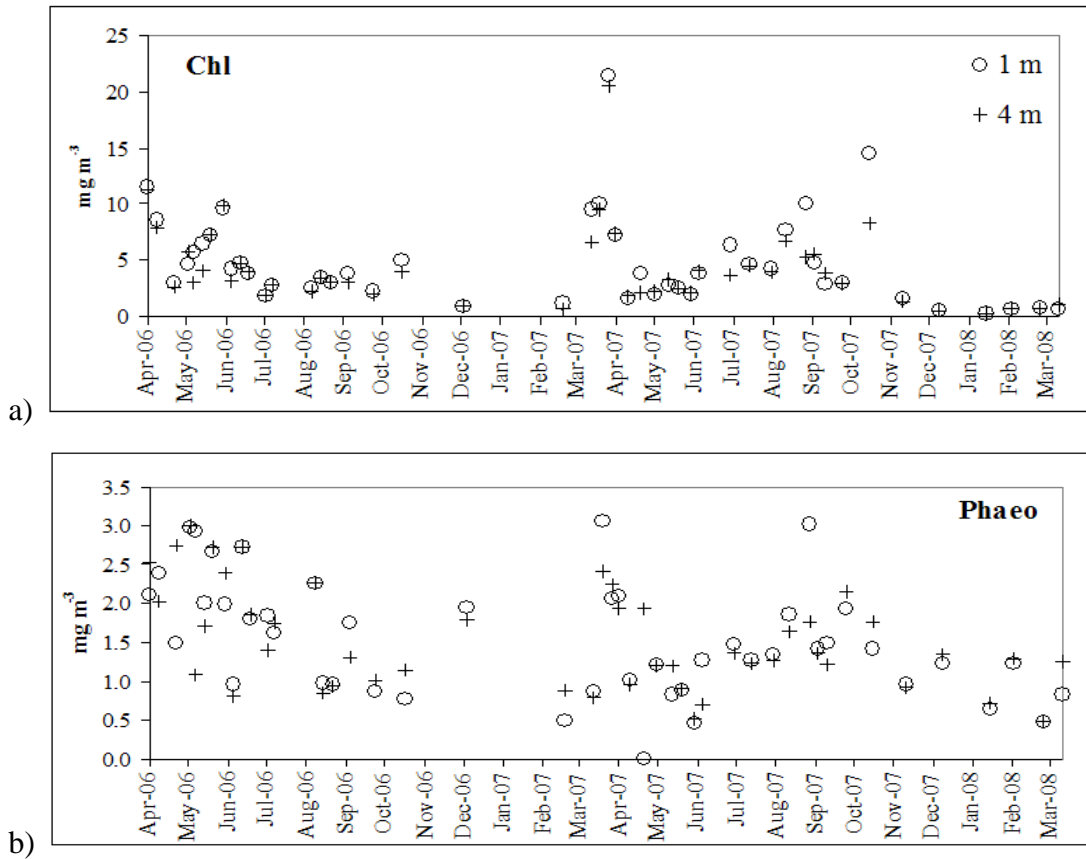


Figure 2.11. The temporal patterns of a) chlorophyll, Chl (mg m^{-3}), and b) phaeopigments, Phaeo (mg m^{-3}), at 1 m (o) and 4 m (+) depth, at station CLNBuoy in Carlingford Lough, between April 2006 and March 2008.

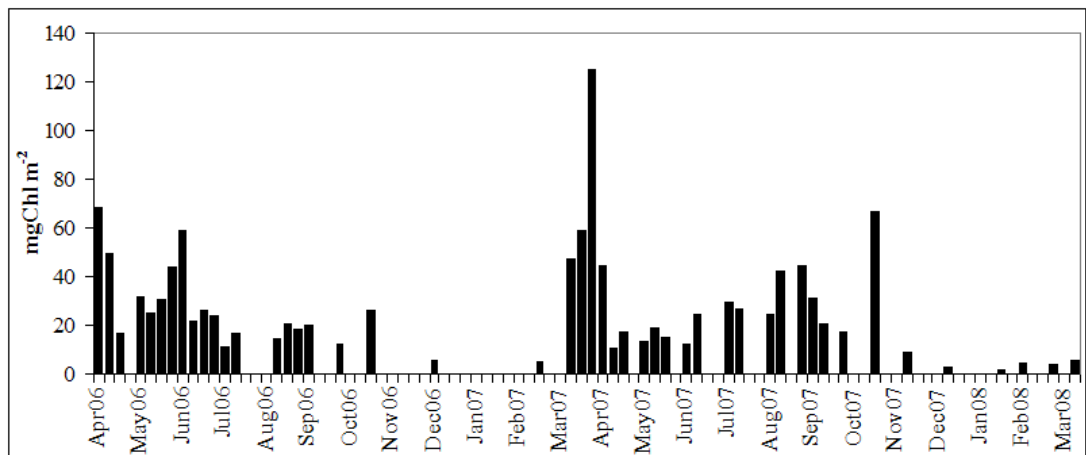


Figure 2.12. The temporal pattern of chlorophyll standing stock (mg Chl m^{-2}), based on an average water column of 5.5 m and linear interpolation between depths of chlorophyll observations, at station CLNBuoy in Carlingford Lough, between April 2006 and March 2008.

Total Suspended Particulate Matter (SPM) ranged between 2.08 and 18.14 mg L⁻¹ (Table 2.5), and reached the lowest concentration on the 8th June 2006 and the 12th April 2007. The highest concentration was reached on the 13th March 2008 (Figure 2.13 a). The subsurface concentration of the total SPM was not statistically different from the concentration at 4 m depth (paired T-test, T-value = -1.85, n = 23, p-value = 0.077), and organic and inorganic SPM concentrations were not statistically different between the two depths (paired T-test, T-value = -1.22 for organic SPM, T-value = -1.67 for inorganic SPM, n =23, p-value > 0.05). Organic matter in the water column (average of 1 m and 4 m depth concentrations) ranged between 1.25 and 8.60 mg L⁻¹ (Table 2.5), and constituted between 21% and 85% of the total SPM and on average 48% (Figure 2.13 b). Organic SPM accounted for the main part of the total SPM on the 12th April 2007 (82%) and on the 22nd May 2007 (85%). Inorganic SPM ranged between 0.13 and 14.77 mg L⁻¹ (Table 2.5), and represented between 15% and 79% of the total suspended matter, with an average of 52% (Figure 2.13 b). The total SPM was mainly constituted by inorganic suspended material from December 2007 to the middle of March 2008 (in particular on the 13th March 2008 with 79%), and on the 22nd March 2007 (74%).

The linear regression of organic SPM against chlorophyll concentration was statistically significant (analysis of variance, n = 44, p = 0.013) but with a low R² (0.14). Regression of organic SPM against phytoplankton biomass (µg C L⁻¹) was also statistically significant (analysis of variance, n= 21, p = 0.011) with an R² of 0.29.

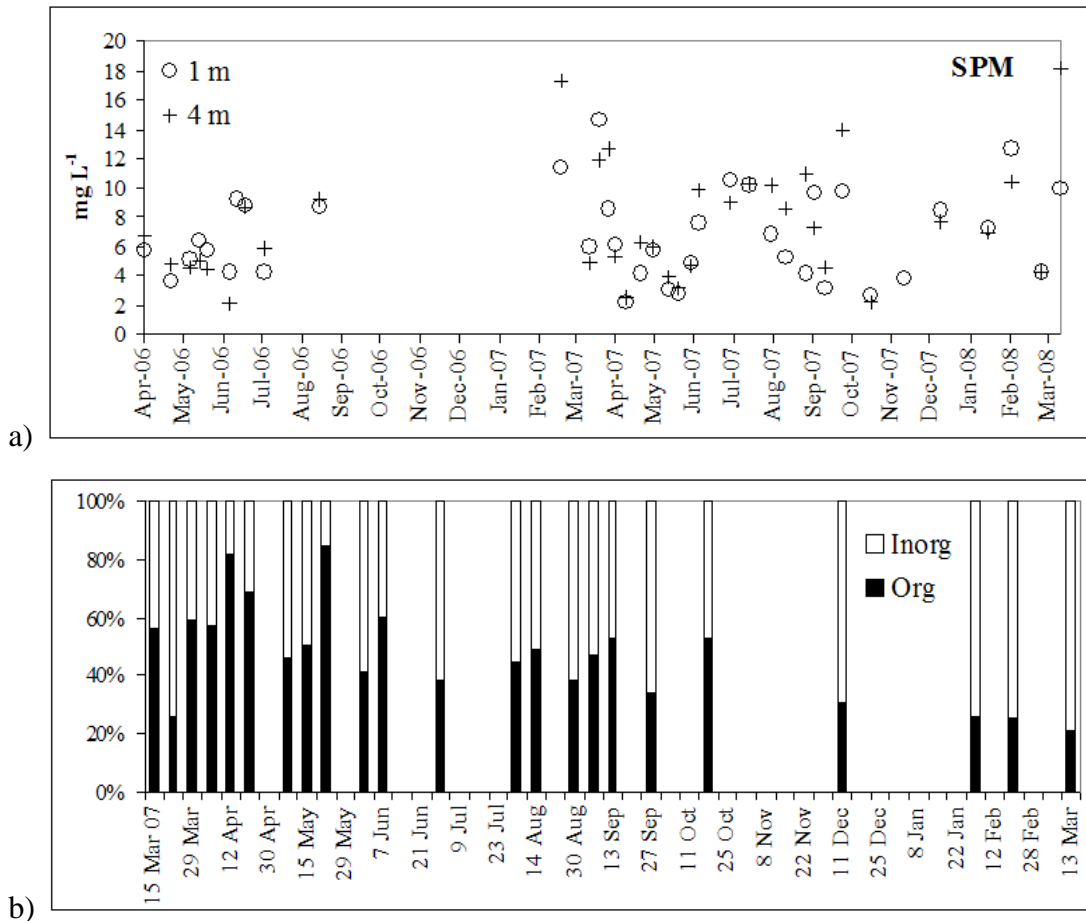


Figure 2.13. The temporal patterns of a) total SPM (mg L^{-1}) at 1 m (o) and 4 m (+) depth, and b) SPM composition (organic ■, and inorganic □), for the water column (average 1 m and 4 m depth concentrations), at station CLNBuoy in Carlingford Lough, between April 2006 and March 2008 for plot a. Information on SPM composition (plot b) were available only for the period between March 2007 and March 2008.

2.3.4 Phytoplankton population

Phytoplankton samples collected in December 2006 and March 2008 could not be counted due to the high SPM content of the sample. Phytoplankton cells sedimented at the bottom of the chamber were covered by a layer of detritus which made species identification difficult.

Based on the analysis of 69 phytoplankton samples, 128 taxa were identified from Carlingford Lough. Of these, 65% were diatoms (54% centric diatoms), 25% dinoflagellates and the remaining 10% were flagellates e.g. coccolithophorids, dictyochophytes, prasinophytes (Table 2.6). In particular, 13 species of *Chaetoceros*

were identified, 6 species each of *Thalassiosira* and *Prorocentrum*, and 5 species each of *Nitzschia* and *Protoperidinium*.

The temporal variations in phytoplankton abundance is shown in Figure 2.14 a. Phytoplankton abundance reached a maximum of over 2.6×10^6 cell L⁻¹ on the 21st June 2006 (Table 2.5), 85% of which were centric diatoms (*Leptocylindrus danicus*, *L. minimum*, *Chaetoceros* sp. and *Thalassiosira* sp.). The lowest abundance, approximately 20×10^3 cell L⁻¹, was observed on the 21st February 2007, while the average abundance during the study period was 809×10^3 cell L⁻¹. Other peaks in abundance $\geq 2 \times 10^6$ cell L⁻¹ were observed on the 24th April 2006, the 14th August 2007, and the 5th September 2007. Low concentrations ($< 90 \times 10^3$ cell L⁻¹) were usually recorded during winter (December to February).

In terms of abundance, diatoms were usually the dominant group in all samples, representing from 9% (23rd May 2006) to 94% (11th April 2006) of the total phytoplankton abundance, and on average 66% (Table 2.7). Only exceptions were the 16th and 23rd May 2006 when dinoflagellates (in particular *Heterocapsa triquetra*) represented 75% of the total abundance, and on the 17th January 2008 when unidentified nanoflagellates ($< 20 \mu\text{m}$) constituted 70% of the microalgal abundance (Figure 2.14 a). On average, dinoflagellates contributed 5% but ranged between 0% and 75% of the total abundance (Table 2.7). Unidentified flagellates constituted from 5% to 70% of the total microalgal abundance and on average 26%, while the other phytoplankton groups (coccolitophorids, dictyochophytes, prasinophytes, cryptophytes, chlorophytes, euglenophytes and cyanophytes) never represented more than 8% each (Table 2.7).

The most abundant taxa were *Thalassiosira* (*nordenskioldii* and *gravidia*), *Chaetoceros* (*compressus*, *socialis*, *curvisetus*, *neglectus*, *debilis* and unidentified species), *Leptocylindrus* (*danicus* and *minimum*), *Heterocapsa triquetra*, *Asterionellopsis glacialis*, *Paralia sulcata* and unidentified nanoflagellates. Each of these taxa dominated the phytoplankton population in at least one sample.

Phytoplankton biomass varied between 3.3 (21st February 2007) and 310.4 $\mu\text{gC L}^{-1}$ (4th April 2006), with an average of 96.8 $\mu\text{gC L}^{-1}$ (Table 2.5). Considering temporal variability, microalgal biomass showed a main peak in spring (4th April 2006 and 29th March 2007) and minor peaks at the end of spring (205 $\mu\text{gC L}^{-1}$, 23rd May 2006) and summer (196 $\mu\text{gC L}^{-1}$, 5th September 2007; Figure 2.14 b). In 2007, an autumn bloom was also observed (109 $\mu\text{gC L}^{-1}$, 18th October 2007). Low

phytoplankton biomass ($< 10 \mu\text{gC L}^{-1}$) was usually observed during winter (November to February).

Diatoms were the main contributors to the microplankton biomass with an average of 77% of the phytoplankton biomass in all samples (Table 2.7). Exceptions to the diatom dominance were observed during the *Heterocapsa triquetra* bloom, in May 2006 (dinoflagellates accounted for 75% of the phytoplankton biomass), and during winter 2007-2008 (unidentified nanoflagellates accounted for 34% of the biomass, Table 2.7). On average, the other microalgal groups never represented more than 7% of phytoplankton biomass in any sample.

The taxa that showed the highest biomass in the samples were the same previously listed as the most abundant. However *Guinardia* (*striata* and *delicatula*), *Cerataulina pelagica*, *Rhizosolenia* (*styliiformis/imbricata* and *setigera*), *Pleurosigma* spp., *Prorocentrum micans*, and *Akashiwo sanguinea*, while never dominant in terms of abundance, were occasionally dominant in terms of biomass. As an example, *Guinardia* spp. and *Cerataulina pelagica* were the taxa with the highest biomass in the samples collected on the 5th May 2006, 17th August 2006, 15th and 22nd May 2007, and 1st and 7th June 2007, while *Rhizosolenia* spp. accounted for the highest biomass on the 1st June 2006, 2nd and 16th July 2007.

Benthic pennate diatoms (Table 2.6, taxa marked with a star) represented on average 3% of the total phytoplankton abundance and 11% of the total phytoplankton biomass. The maximum abundance and biomass of these diatoms (27% and 44% of the total phytoplankton abundance and biomass respectively) were reached on the 21st February 2007.

Table 2.6. A list of taxa identified in the 69 phytoplankton samples from 1 m and 4 m depth at station CLNBuoy in Carlingford Lough, between April 2006 and March 2008. Pennate diatom taxa marked with the star (*) were considered benthic diatoms. *Rhizosolenia styliformis/imbricata* (***) is indicated with 2 species names due to difficulties during identification; this taxon had characteristics of both *R. styliformis* and *R. imbricata*.

Bacillariophytes (Diatoms)	
<i>Amphiprora</i> sp.*	<i>Gyrosigma fasciola</i> *
<i>Amphora laevissima</i> *	<i>Gyrosigma</i> sp.*
<i>Amphora</i> sp.*	<i>Lauderia annulata</i>
<i>Asterionellopsis glacialis</i>	<i>Leptocylindrus danicus</i>
<i>Bacillaria</i> cf. <i>paxillifera</i> *	<i>Leptocylindrus minimus</i>
<i>Bacillaria</i> sp.*	<i>Licmophora</i> sp.*
<i>Bellerochea</i> sp.*	<i>Lithodesmium undulatum</i>
<i>Biddulphia alternans</i>	<i>Melosira nummuloides</i>
<i>Biddulphia</i> sp.	<i>Navicula cryptocephala</i> *
<i>Cerataulina pelagica</i>	<i>Navicula lira</i> *
<i>Chaetoceros affinis</i>	<i>Navicula</i> sp.*
<i>Chaetoceros brevis</i>	<i>Nitzschia frustulum</i> *
<i>Chaetoceros compressus</i>	<i>Nitzschia longissima</i> *
<i>Chaetoceros curvisetus</i>	<i>Nitzschia lorenziana</i> *
<i>Chaetoceros danicus</i>	<i>Nitzschia panduriformis</i> *
<i>Chaetoceros debilis</i>	<i>Nitzschia</i> sp.*
<i>Chaetoceros decipiens</i>	<i>Odontella granulata</i>
<i>Chaetoceros densus</i>	<i>Odontella mobiliensis</i>
<i>Chaetoceros lacinosus</i>	<i>Odontella</i> sp.
<i>Chaetoceros neglectus</i>	<i>Paralia sulcata</i>
<i>Chaetoceros simplex</i>	<i>Plagiogramma</i> sp.*
<i>Chaetoceros socialis</i>	<i>Pleurosigma</i> sp.*
<i>Chaetoceros</i> sp.	<i>Proboscia alata</i>
<i>Cocconeis scutellum</i> *	<i>Pseudo-nitzschia delicatissima</i>
<i>Coscinodiscus granii</i>	<i>Pseudo-nitzschia seriata complex</i>
<i>Coscinodiscus</i> sp.	<i>Pseudo-nitzschia</i> sp.
<i>Coscinoscira polychorda</i>	<i>Rhizosolenia setigera</i>
<i>Cyclotella</i> sp.	<i>Rhizosolenia</i> sp.
<i>Cylindrotheca closterium</i>	<i>Rhizosolenia styliformis/imbricata</i> **
<i>Cylindrotheca fusiformis</i> *	<i>Skeletonema costatum</i>
<i>Dactyliosolen fragilissimus</i>	<i>Stephanopyxis turris</i>
<i>Diploneis bombus</i> *	<i>Striatella unipunctata</i> *
<i>Diploneis</i> sp.*	<i>Surirella</i> sp.*
<i>Ditylum brightwellii</i>	<i>Thalassiosira angulata</i>
<i>Eucampia cornuta</i>	<i>Thalassiosira anguste-lineata</i>
<i>Eucampia zodiacus</i>	<i>Thalassiosira gravida</i>
<i>Fragilariopsis</i> sp.*	<i>Thalassiosira nordenskioldii</i>
<i>Gomphonema</i> sp.*	<i>Thalassiosira rotula</i>
<i>Guinardia delicatula</i>	<i>Thalassiosira</i> sp.
<i>Guinardia flaccida</i>	<i>Triceratium</i> sp.
<i>Guinardia striata</i>	Unidentified centric
	Unidentified pennate*

Table 2.6. Continued.

Dinophytes (dinoflagellates)	Dictyochophytes
<i>Akashiwo sanguinea</i>	<i>Dictyoca fibula</i>
<i>Alexandrium sp.</i>	<i>Dictyocha speculum</i>
<i>Amphidinium sp.</i>	
<i>Ceratium furca</i>	Prymnesiophytes (Coccolitophorids)
<i>Ceratium fusus</i>	<i>Emiliana huxleyi</i>
<i>Ceratium lineatum</i>	Unidentified coccolitophorids
<i>Dinophysis acuminata</i>	
<i>Dinophysis acuta</i>	Prasinophytes
<i>Dinophysis rotundata</i>	<i>Pyramimonas sp.</i>
<i>Dinophysis sp.</i>	Unidentified prasinophytes
<i>Diplopsalis lenticula</i>	
<i>Diplopsalis sp.</i>	Cryptophytes
<i>Goniaulax sp.</i>	Unidentified cryptophytes
<i>Gymnodinium sp.</i>	
<i>Gyrodinium sp.</i>	Flagellates
<i>Heterocapsa triquetra</i>	Flagellate $\geq 10 \mu\text{m}$
<i>Oxytoxum sp.</i>	Flagellate $< 10 \mu\text{m}$
<i>Prorocentrum aporum</i>	
<i>Prorocentrum compressum</i>	Chlorophytes
<i>Prorocentrum lima</i>	<i>Pediastrum sp.</i>
<i>Prorocentrum micans</i>	Unidentified chlorophytes
<i>Prorocentrum minimum</i>	
<i>Prorocentrum sp.</i>	Euglenophytes
<i>Protooperidinium bipes</i>	Unidentified euglenophytes
<i>Protooperidinium breve</i>	
<i>Protooperidinium divergens</i>	
<i>Protooperidinium sp.</i>	Cyanophytes
<i>Protooperidinium steinii</i>	Unidentified cyanophytes
<i>Scripsiella sp.</i>	
<i>Scripsiella trochoidea</i>	
Unidentified naked	
Unidentified tecate	

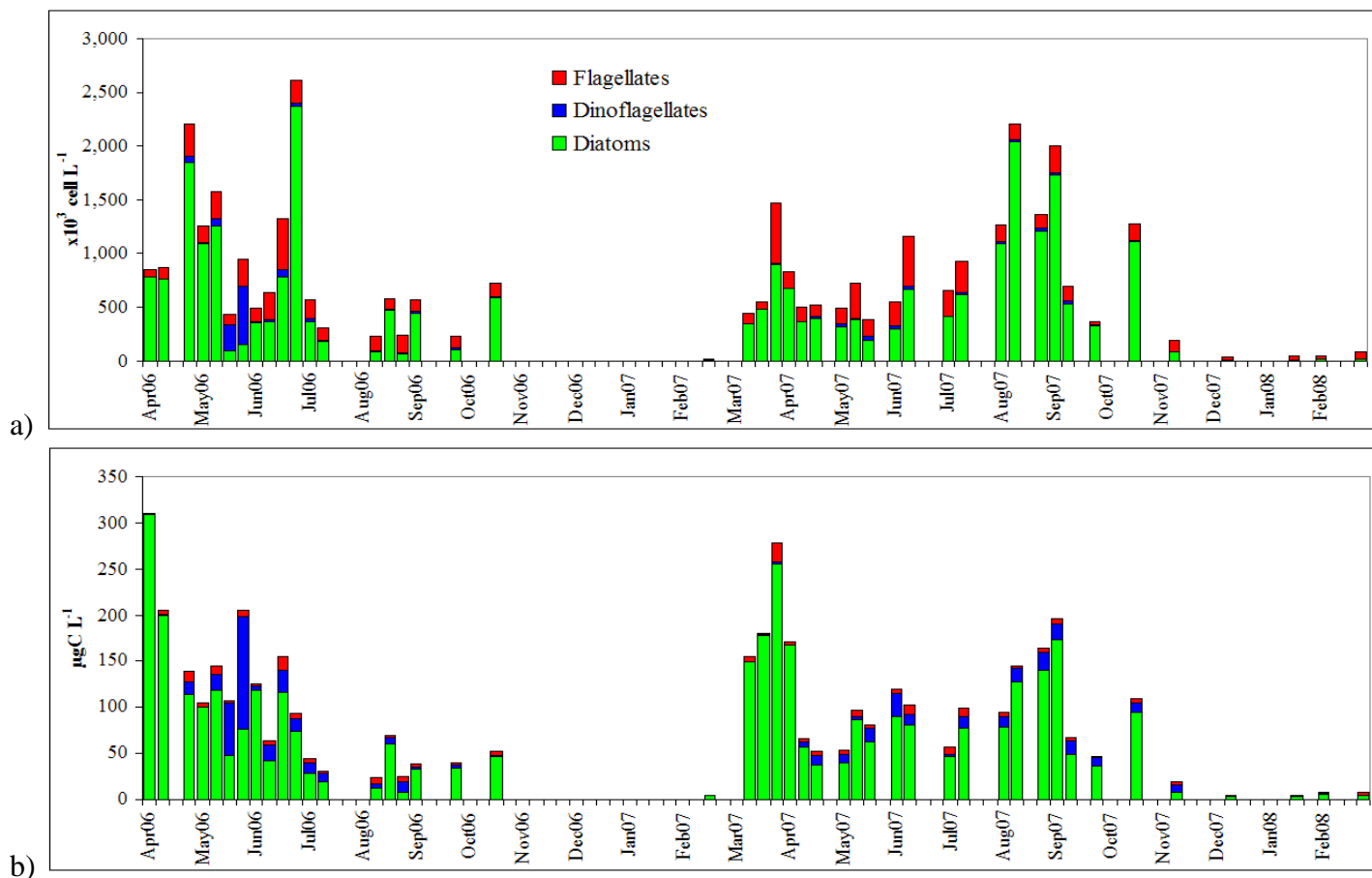


Figure 2.14. The temporal patterns of phytoplankton a) abundance (cell L^{-1}), and b) biomass ($\mu\text{gC L}^{-1}$) of 4 m depth samples, at station CLNBuoy in Carlingford Lough, between April 2006 and March 2008. The colour green represents diatoms, blue dinoflagellates and red all other phytoplankton organisms (flagellates).

Table 2.7. The descriptive statistics (mean, minimum and maximum) for phytoplankton abundance (Abu, cell L⁻¹), percent abundance with respect to total abundance (Abu %), phytoplankton biomass (Bio, µg C L⁻¹) and percent biomass with respect to total biomass (Bio %), of the phytoplankton groups identified in samples from 1 m and 4 m depth, collected at station CLNBuoy in Carlingford Lough, between April 2006 and March 2008. In particular: Dia = diatoms; Dino = dinoflagellates; Coc = coccolithophorids; Dic = dictyochophytes; Pra = prasinophytes; Cry = cryptophytes; Fla = unidentified flagellates; Chlo = chlorophytes; Eug = euglenophytes; Cya = cyanophytes.

Group	Abu (x10 ³ cell L ⁻¹)			Abu %			Bio (µg C L ⁻¹)			Bio %		
	mean	min	max	mean	min	max	mean	min	max	mean	min	max
Dia	565	12	2,367	66	9	94	73	2	309	77	23	100
Dino	36	0	856	5	0	75	13	1	200	15	0	75
Coc	0.9	0	13	0	0	5	0	0	0	0	0	2
Dic	0.06	0	4	0	0	1	0	0	2	0	0	4
Pra	7	0	53	1	0	6	0	0	2	0	0	4
Cry	9	0	105	2	0	5	0	0	3	1	0	2
Fla	130	4	525	26	5	70	3	0	19	7	0	34
Chlo	1	0	62	0	0	8	0	0	1	0	0	1
Eug	0.9	0	10	0	0	4	0	0	2	0	0	9
Cya	0.3	0	11	0	0	2	0	0	0	0	0	0

The temporal patterns in the biomass of the groups that on average contributed the most to the phytoplankton biomass (diatoms, dinoflagellates, cryptophytes and unidentified flagellates, see Table 2.7) are shown in Figure 2.15. Diatoms were identified in every sample therefore the plot a in Figure 2.15 also provides information on the number of observations (black circles) and sampling frequency. The biomass of diatoms started to increase from the end of March (between day 59 and 90), and maintained a high level during spring and summer until the end of August (day 243). From September the biomass declined, except for a small peak in the middle of October (between day 273 and 304). Dinoflagellate biomass increased to a peak in mid May (between day 120 and 151; Figure 2.15 b), and it was relatively constant until mid October. Cryptophytes were generally observed from February to November (from day 59 to 320; Figure 2.15 c) and their biomass was approximately constant during the year. Unidentified flagellates <20

μm were observed all year round, including winter, and there was generally little variations in their biomass (Figure 2.15 d).

The temporal patterns in the biomass of the dominant phytoplankton species and genus (in term of abundance and biomass) are shown in Figures 2.16 and 2.17. *Paralia sulcata* was observed in samples from January to the end of October (from day 0 to 304, Figure 2.16 a), and showed a slightly higher biomass from January to March (from day 0 to 90). *Thalassiosira* spp. (sum of 5 species, see list in Table 2.6) was observed all year round; in particular, the higher biomass was reached at the end of March/start of April during the spring bloom (Figure 2.16 b), when the genus represented up to 99% of the phytoplankton biomass (4th April 2006). *Chaetoceros* spp. biomass (sum of 12 species, see Table 2.6) started to increase in early March (day 59, Figure 2.16 c) and reached a maximum biomass in April-May (around day 120), after the peak in *Thalassiosira*. The genus *Chaetoceros* was generally well represented during the rest of the year up to mid November (day 320, Figure 2.16 c). Other genera, such as *Guinardia*, *Rhizosolenia* and *Leptocylindrus* (Figure 2.16 d and e, Figure 2.17 a), reached high biomass at the start of the summer (day 120-181). These three genera were not identified from December to February. Furthermore, the genus *Leptocylindrus* showed peaks at the end of March (day 90, Figure 2.17 a) and at the end of August/start of September (around day 243). The pennate diatom *Asterionellopsis glacialis* had the highest biomass in September and October (day 243-304, Figure 2.17 b), and accounted for a maximum of 52% of the phytoplankton biomass (7th September 2006). *Pleurosigma* spp. was observed all year round and its biomass showed an increase from May to the end of September (from day 120 to 278, Figure 2.17 c). Considering the dinoflagellates, *Heterocapsa triquetra* reached the highest biomass at the end of May (Figure 2.17 d), and it was mainly observed between May and July (day 120-212). *Prorocentrum micans* was present in the samples from mid April to October (day 105-304, Figure 2.17 e).

Considering potential harmful microalgae, *Pseudo-nitzschia* spp. was present in samples from mid February to November, and showed a higher biomass at the end of August/start September (around day 243, Figure 2.18 a). *Alexandrium* spp. and *Dinophysis* spp. were observed from April to mid September (day 90-258) and from May to early September (day 120-243) respectively (Figure 2.18 b and c). In particular, the genus *Alexandrium* was identified in 10 samples in 2006 and in 2

samples in 2007. Finally, *Akashiwo sanguinea* was identified in samples from September to December (day 243-349, Figure 2.18 d), but only in 2007.

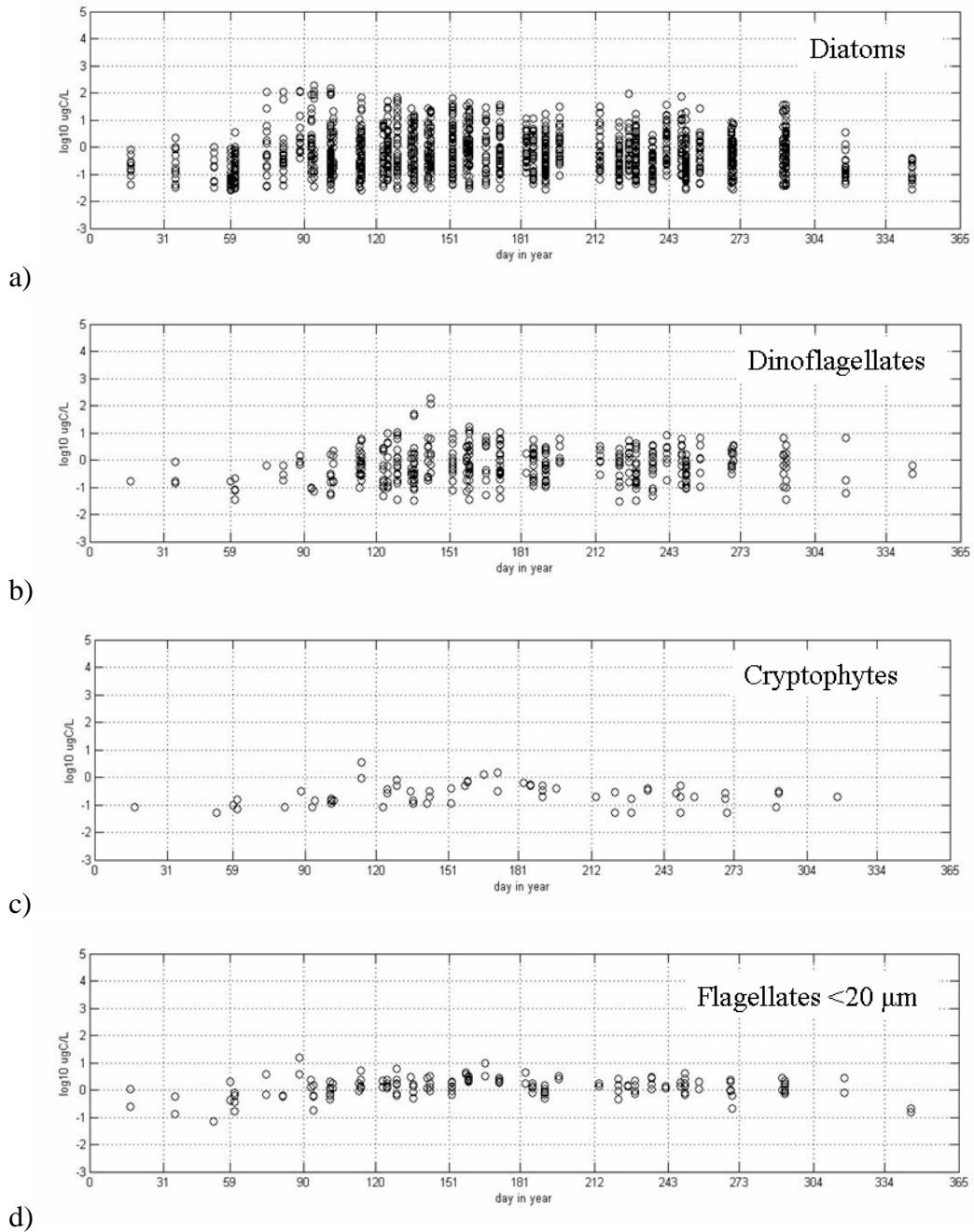


Figure 2.15. The temporal variations in log₁₀ transformed phytoplankton biomass of a) diatoms, b) dinoflagellates, c) cryptophytes, and d) flagellates <20 μm, for a standard year. Data from 1 and 4 m depth samples, collected at station CLNBuoy in Carlingford Lough, between April 2006 and March 2008. Each empty circle is a taxon.

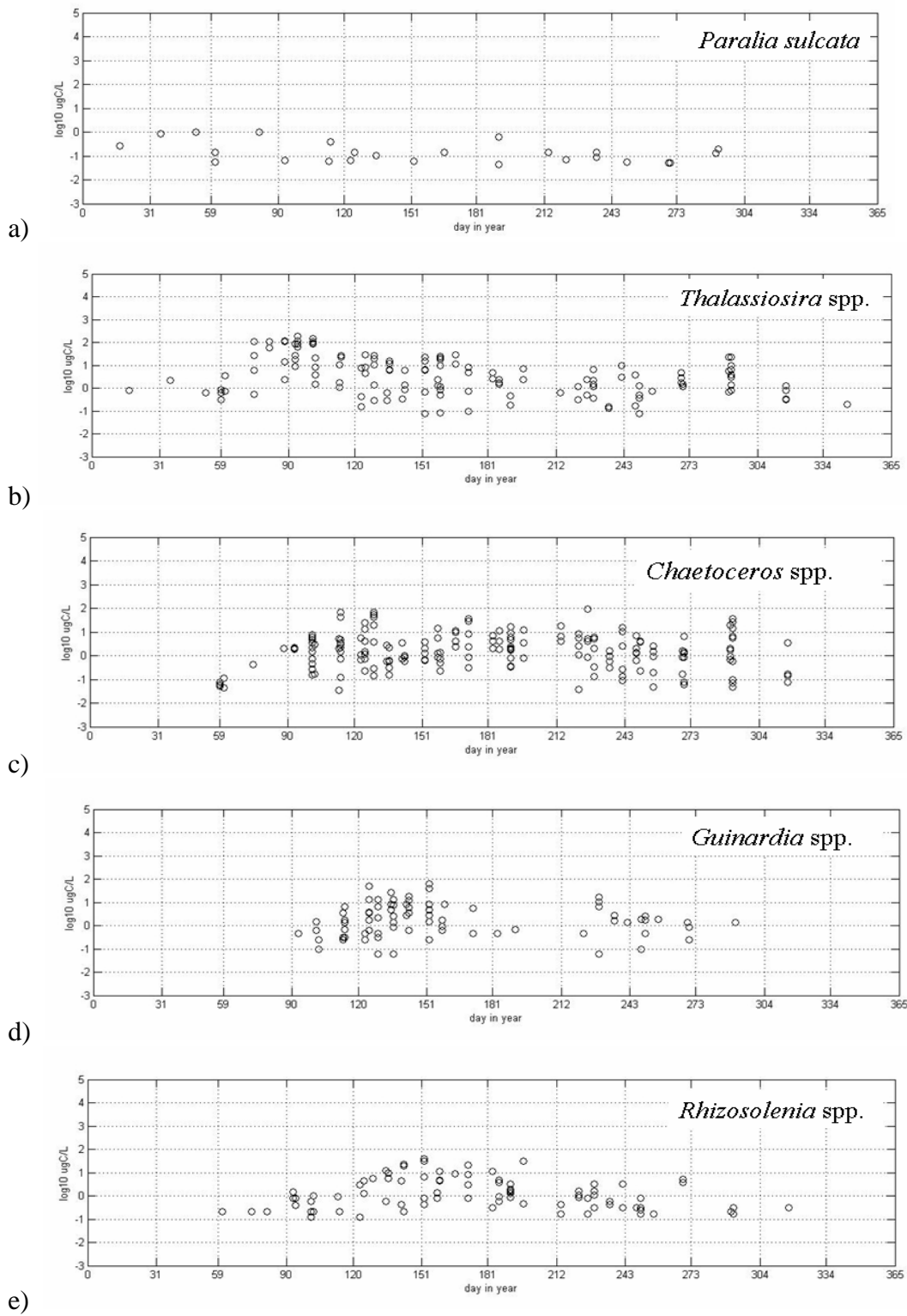


Figure 2.16. The temporal variations in \log_{10} transformed phytoplankton biomass of a) *Paralia sulcata*, b) *Thalassiosira* spp., c) *Chaetoceros* spp., d) *Guinardia* spp., and e) *Rhizosolenia* spp., for a standard year. Data from 1 and 4 m depth samples, collected at station CLNBuoy in Carlingford Lough, between April 2006 and March 2008. Each empty circle is a taxon.

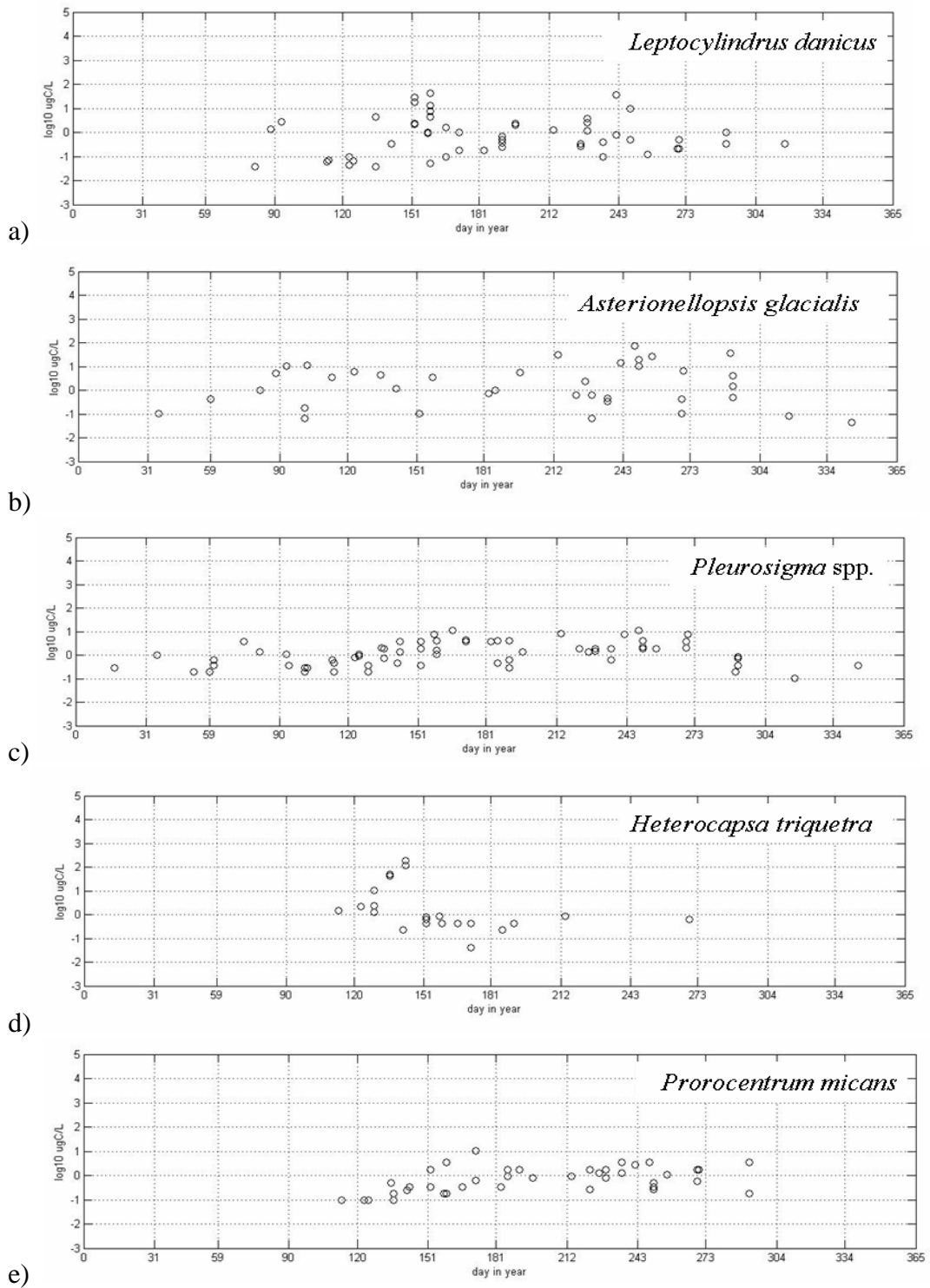


Figure 2.17. The temporal variations in \log_{10} transformed phytoplankton biomass of a) *Leptocylindrus danicus*, b) *Asterionellopsis glacialis*, c) *Pleurosigma* spp. d) *Heterocapsa triquetra* and e) *Prorocentrum micans*, for a standard year. Data from 1 and 4 m depth samples, collected at station CLNBuoy in Carlingford Lough, between April 2006 and March 2008. Each empty circle is a taxon.

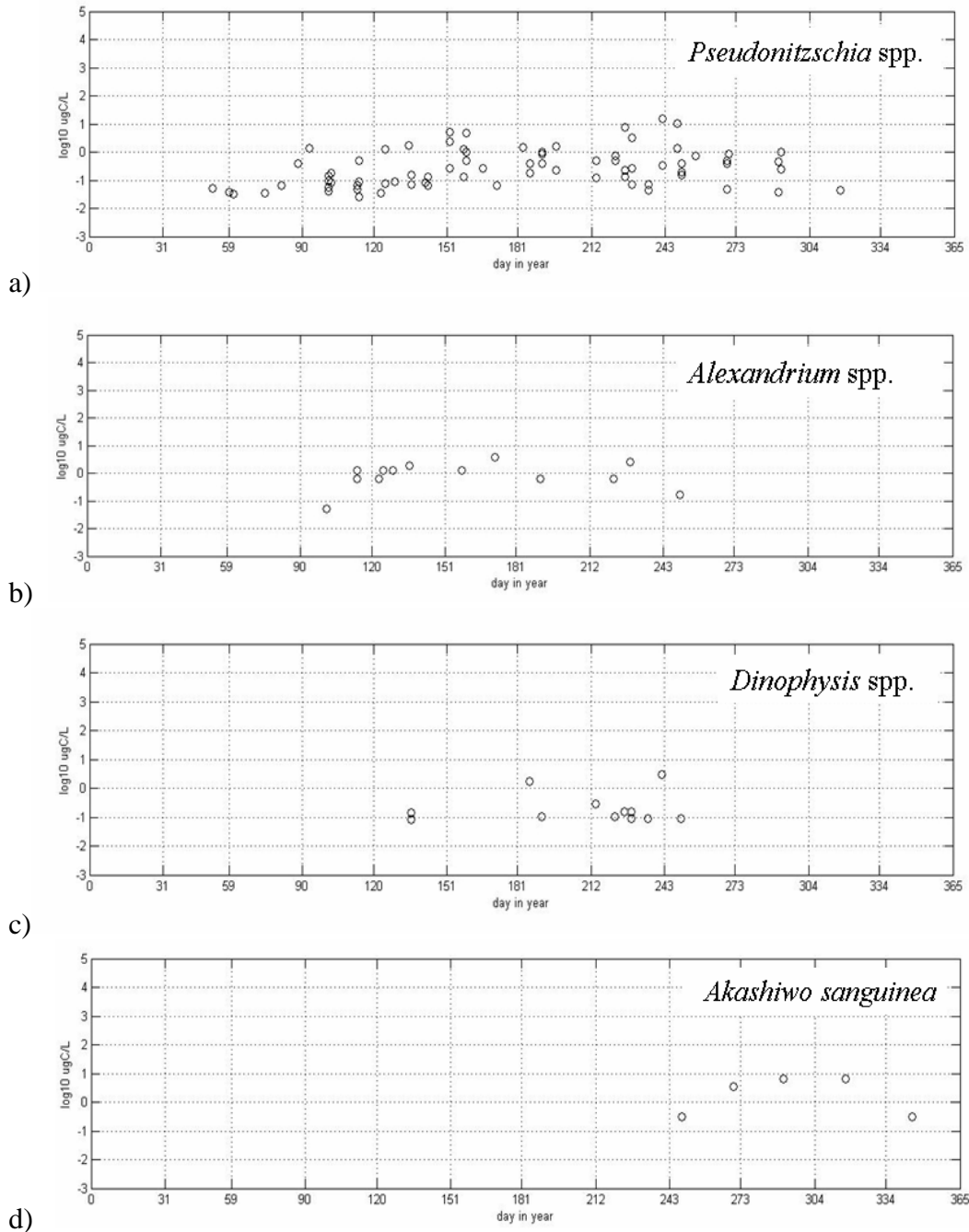


Figure 2.18. The temporal variations in \log_{10} transformed phytoplankton biomass of potentially harmful microalgae a) *Pseudo-nitzschia* spp., b) *Alexandrium* spp., c) *Dinophysis* spp., and d) *Akashiwo sanguinea*, for a standard year. Data from 1 and 4 m depth samples, collected at station CLNBuoy in Carlingford Lough, between April 2006 and March 2008. Each empty circle is a taxon.

The average phytoplankton cell volume (ACV) was calculated as the ratio of phytoplankton biovolume ($\mu\text{m}^3 \text{L}^{-1}$) to phytoplankton abundance (cell L^{-1}) of each sample, and varied between 0.47 and $11.07 \times 10^3 \mu\text{m}^3 \text{cell}^{-1}$, with an average of $2.34 \times 10^3 \mu\text{m}^3 \text{cell}^{-1}$ (Table 2.5). The ACV temporal trend (Figure 2.19 a) showed that microalgae on the 4th April 2006, 15th and 22nd March 2007 had the highest cell volume, followed by organisms observed on the 1st June 2006.

The ratio between chlorophyll concentration ($\mu\text{g L}^{-1}$) and phytoplankton biovolume ($\mu\text{m}^3 \text{L}^{-1}$) provides information on the average phytoplankton chlorophyll content (ACC) per cell volume. ACC varied between 0.96 and $13.44 \times 10^{-9} \mu\text{g} \mu\text{m}^3$, with an average of $3.83 \times 10^{-9} \mu\text{g} \mu\text{m}^3$. From the temporal plot in Figure 2.19 b, it can be seen that the highest chlorophyll concentration per unit volume were reached on the 24th August 2006, the 21st February 2007 and the 11th December 2007.

The chlorophyll/carbon (Chl/C) ratio was calculated from chlorophyll concentration ($\mu\text{g L}^{-1}$) and phytoplankton biomass ($\mu\text{g L}^{-1}$). The ratio ranged between a minimum of 0.02 and a maximum of 0.19, with an overall average of 0.06 (Table 2.5).

The results of the correlation matrix (Pearson coefficient) between salinity, temperature, nutrients (nitrogen compounds, phosphorus and silica), total SPM, and log-transformed River Clanrye outflow, chlorophyll, phaeopigments, phytoplankton abundance, and phytoplankton biomass are given in Table 2.11. Other environmental variables, such as chlorophyll standing stock, ACV, were not considered in the analysis because they were derived from other variables. Temperature, salinity, nutrients, and River flow were significantly correlated ($p < 0.05$). In particular, nutrients showed a negative correlation with salinity and temperature, and a positive correlation with the River flow. Chlorophyll and phytoplankton abundance and biomass (log-transformed) were positively correlated; furthermore, they were negatively correlated with nutrients ($p < 0.05$), and they did not show a significant relationship with salinity, temperature or River flow (with the exception of a positive correlation between phytoplankton abundance and temperature). Phaeopigments showed a negative correlation with phosphate and silica, and a positive correlation with River outflow, chlorophyll, and phytoplankton abundance and biomass. Total SPM was correlated (positively) only with nutrients and River flow.

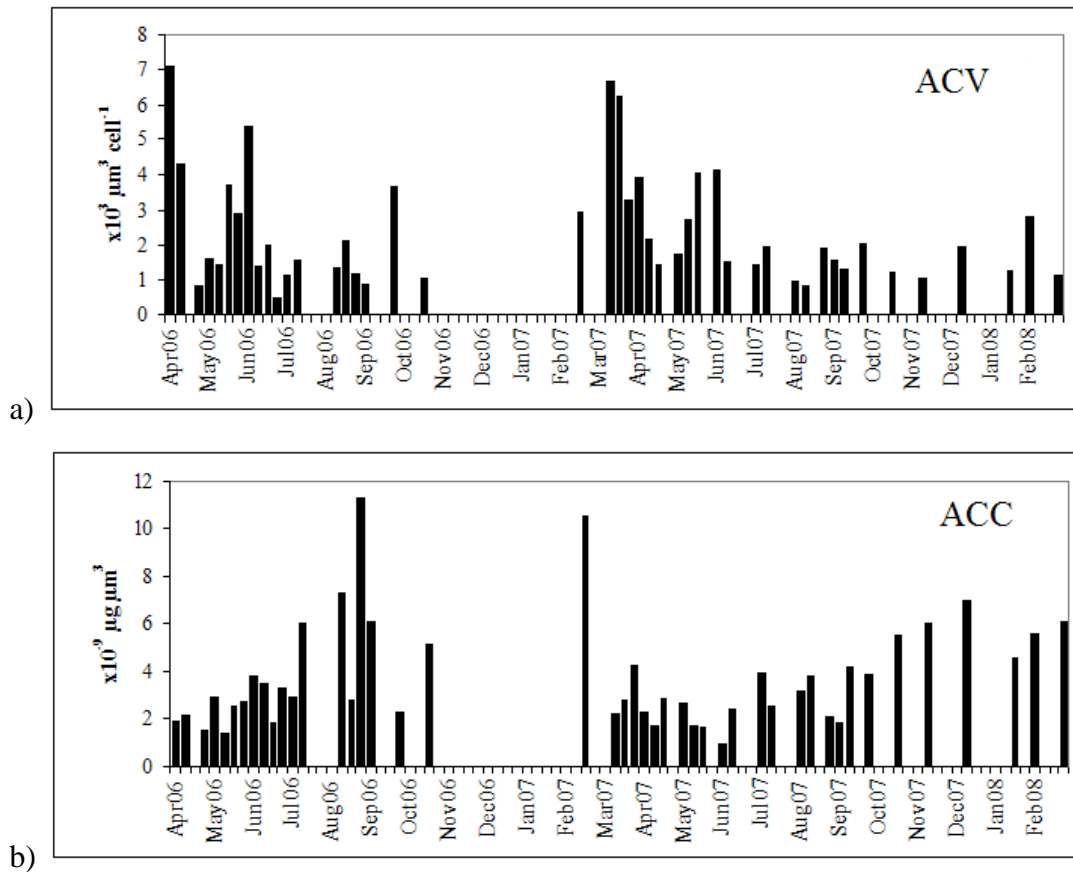


Figure 2.19. The temporal trends of a) average phytoplankton cell volume (ACV, $\times 10^3 \mu\text{m}^3 \text{cell}^{-1}$), and b) average phytoplankton chlorophyll content per cell volume (ACC, $\times 10^{-9} \mu\text{g} \mu\text{m}^3$), from 4 m depth samples, at station CLNBuoy in Carlingford Lough, between April 2006 and March 2008.

Table 2.11. Correlation matrix (Pearson coefficient) of the main physical, chemical and biological variables. Temperature (Temp), salinity (Sal), ammonium (NH₄), phosphate (phosph), nitrate, silica, nitrite, SPM total (SPMtot), log-transformed Clanrye River outflow (logRiv), chlorophyll (logChl), phaeopigments (logPhae), phytoplankton abundance (logAbu), and phytoplankton biomass (logBio). Two stars (**) indicated p-value ≤ 0.001, one star (*) indicated p-value < 0.05. Data from 1 m and 4 m depth, collected at station CLNBuoy in Carlingford Lough, between April 2006 and March 2008.

	Temp	Sal	NH₄	Phosph	Nitrate	Silica	Nitrite	SPMtot	logRiv	logChl	logPhae	logAbu
Sal	0.63**											
NH₄	-0.42**	-0.58**										
Phosph	-0.31*	-0.42**	0.74**									
Nitrate	-0.68**	-0.75**	0.73**	0.78**								
Silica	-0.58**	-0.71**	0.80**	0.88**	0.95**							
Nitrite	-0.59**	-0.65**	0.79**	0.80**	0.85**	0.87**						
SPMtot	-0.19	-0.14	0.14	0.31*	0.27*	0.26*	0.25*					
logRiv	-0.60**	-0.87**	0.56**	0.44**	0.75**	0.72**	0.61**	0.35*				
logChl	0.10	0.07	-0.54**	-0.63**	-0.46**	-0.58**	-0.36**	-0.06	-0.10			
logPhae	-0.07	-0.14	-0.16	-0.30*	-0.18	-0.21*	-0.17	0.15	0.25*	0.50**		
logAbu	0.29*	0.16	-0.48**	-0.66**	-0.62**	-0.68**	-0.47**	-0.23	-0.11	0.65**	0.41**	
logBio	0.02	-0.04	-0.54**	-0.72**	-0.49**	-0.65**	-0.42**	-0.22	0.06	0.85**	0.46**	0.85**

2.4 Discussion

2.4.1 Physical and chemical variables

Carlingford Lough is a semi-enclosed (on three sides) water body, having restricted exchange with the sea, and it can be classified as a Region of Restricted Exchange or RRE (Tett *et al.* 2003; Tett *et al.* 2007). The water circulation in a RRE, such as Carlingford Lough, is mainly regulated by the freshwater run off and the tidal flow of water into and out of the lough. The result is a two-layer circulation or estuarine circulation. Salt water, entering the Lough on the flood tide, forms a dense high-salinity bottom layer moving toward the inner lough, while the freshwater runoff mixes with water already in the Lough to form a low salinity surface layer which leaves the Lough on the ebb tide (Wood, Tett and Edwards 1973). The rate at which the water in the lough exchanges with the near coastal water (flushing rate) depends on different factors such as the topography of the lough, the tidal range, the volume of the freshwater inflow and the turbulent mixing (Jones and Gowen 1990). A flushing rate higher than the rate of phytoplankton growth (e.g. < 2.5 day) could limit the development of phytoplankton biomass in the lough; whereas, loughs with a slower flushing rate (e.g. > 6 days), such as the inner/mid Carlingford Lough, can provide favourable conditions for enhancement of the *in situ* phytoplankton production, if nutrients and light regimes are appropriate (Jones and Gowen 1990).

The reduced-salinity surface layer and the solar heating of the surface layer can create stratification of the water column while turbulence derived from wind and/or current action can mix the water column, homogenising its physical and chemical properties from surface to bottom. Analysis of the $\Delta(T+S)$ at the station CLNBuoy in Carlingford Lough suggests that the water column was stratified on more than half of the sampling occasions and that stratification was mainly induced by a difference in salinity between the subsurface and bottom layers, rather than a difference in temperature. This result is in contradiction with previous observations that the Lough is well mixed (Douglas 1992). The occurrence of higher ΔSal coincided with peaks in Clanrye River outflow (e.g. mid May 2006, December 2006, Figure 2.5) and it suggests that the freshwater outflow was the main driver of the salinity gradient. The few occasions on which the stratification was induced by a thermal gradient were recorded during summer (8th June 2006, 1st June 2007) on sunny days, with no cloud cover (0%), no wind and low River outflow ($< 1.76 \text{ m}^3 \text{ s}^{-1}$

¹). Sampling occasions when the water column was vertically mixed (e.g. 22nd March 2006, 1st June 2006 and 30th August 2006) were characterised by strong wind (state of the sea between force 4 and 6) and incoming or high tide. The vertical salinity gradient, mainly caused by freshwater runoff, is the main driver of the water column stratification in Carlingford Lough and also in Scottish sea lochs such as Loch Etive and Loch Creran (Wood, Tett and Edwards 1973; Tett, Drysdale and Shaw 1981).

As a consequence of the freshwater outflow and the presence of shallow waters, the temperature in Carlingford Lough during winter (minimum of 6.02 °C in 2006-2008) can be lower than the temperature in the coastal area of the western Irish Sea (8 °C in 1992; Gowen *et al.* 1995), and vice versa during summer (maximum temperature in the Lough was 16.55 °C, compared with 15 °C in the Irish Sea).

Temperature and salinity ranges in Carlingford Lough are similar to the ranges in other RREs in Northern Ireland, such as Belfast Lough (2-21 °C and 31.0-33.5 respectively) and Strangford Lough (2-19 °C and 32.5-34.5 respectively; Service *et al.* 1996 and Ferreira *et al.* 2007), and to the Scottish sea loch Striven (6-14 °C and 29-33 respectively; Tett *et al.* 1986). Carlingford Lough showed other similarities with the two sea lochs in NI in the temperature and salinity temporal trends and the presence of weak stratification (Service *et al.* 1996).

The Clanrye River outflow influenced the physical properties of the water column and also the nutrient concentrations. The positive correlation between River flow and nitrogen compounds (ammonium, nitrate and nitrite), phosphate and silicate concentrations indicates that the River was the main source of nutrients for the Lough, as previously observed by Taylor, Charlesworth and Service (1999). However the same authors showed that SWTs were the main source of ammonium in the Lough. Sewage outflow increases with precipitation, as does the River outflow, so this provides one explanation for the positive correlation between NH_4^+ concentration and Clanrye outflow.

The temporal trends in nutrients observed in Carlingford Lough showed the typical pattern of temperate coastal water with maximum concentration during winter and minimum concentration during spring and summer. Nitrogen compounds, phosphate and silicate accumulate during winter due to nutrient remineralisation, when assimilation by phytoplankton is limited by low solar radiation and the short days. In spring, with an increase in illumination, the phytoplankton population starts to build up, utilising dissolved nutrients in the water for growth. Therefore, plotting

nitrogen concentration versus phosphate concentration (DIN:SRP) and nitrogen versus silicate concentration (DIN:Si) for winter months provide a measure of the relative nutrient accumulation ratio in the water column, while plotting the same ratios for the spring bloom period provides an indication of the phytoplankton draw-down ratio (see for example Gowen *et al.* 2000).

The high winter DIN:SRP ratio of 69.1 (Figure 2.10 a) suggests that from November to February (2006-2007 and 2007-2008) Carlingford Lough was enriched in nitrogen relative to phosphorus. During the spring bloom the DIN:SRP ratio fell to 32 (Figure 2.10 c) and the intercept of the regression line (ratio of nutrient assimilation) was not significantly different from zero indicating that nitrogen and phosphorus were depleted at the same time. Measurements of nutrient assimilation ratios in Irish coastal water near Carlingford Lough during the spring bloom in 1997 gave a lower N:P ratio, equal to 11.3 (Gowen *et al.* 2000). The comparison of the DIN:SRP assimilation ratio of 32:1 with the Redfield ratio of 16:1 indicates that the nitrogen assimilation was higher than expected for phytoplankton, suggesting that nitrogen was removed by a process other than phytoplankton assimilation or that the phosphorus was re-supplied (Gowen *et al.* 2000). However some studies (Geider and La Roche 2002; Tett, Hydes and Sanders 2003; Klausmeier *et al.* 2004) have demonstrated that the N:P ratio in marine phytoplankton is variable and that the Redfield ratio of 16:1 can be considered the average stoichiometry of phytoplankton in oceanic waters. Geider and La Roche (2002) derived nutrient ratios in marine microalgae from nutrient-replete and nutrient-limited algal cultures, from the biochemical composition of algae (physiologically achievable N:P ratio) and from marine particulate matter. The authors obtained different nutrient ranges (N:P from cultures 20-50, from biochemical composition 15-30, and from particulate matter 5-34) and they concluded the average elemental composition of phytoplankton is not fixed. Klausmeier *et al.* (2004) used a stoichiometric model of phytoplankton physiology to derive the optimal phytoplankton stoichiometry under different ecological scenarios and they arrived at the same conclusion as Geider and La Roche (2002) that the N:P can be variable. Based on their model, Klausmeier *et al.* (2004) predicted a range of optimal N:P ratio varying between 8.2 and 45.0. In fact phytoplankton elemental composition, in particular N:P ratio, is species-specific and depends on the biology and stoichiometry of ribosomes and proteins in the algal cell (Klausmeier *et al.* 2004). It is also influenced by the ecological conditions (if the

algae are in exponential growth or equilibrium phases) and by environmental conditions such as light regime (Litchman, Klausmeier and Bossart 2004). The N:P ratio measured in Carlingford Lough during spring (32:1) falls within the ranges identified by Geider and La Roche (2002) and Klausmeier *et al.* (2004).

The DIN:SRP ratio in summer 2006 was significantly higher than the ratio measured in summer 2007 (8.18 and 3.15 respectively; two-sample T-test, T-value = 3.50, DF = 19, p-value = 0.002). Although in both years the average summer DIN concentration from June to August was low and $< 2 \mu\text{M}$, summer 2007 was characterised by a significantly lower average DIN concentration than summer 2006 (1.05 and 1.87 μM respectively; $p < 0.001$), while SRP concentrations in the two summers were comparable ($p > 0.05$). The DIN:SRP ratio for summer 2006 is at the lower limit of the Klausmeier *et al.* (2004) optimal stoichiometry range while the ratio for 2007 falls out with all the ranges. In both years, the low N:P ratios may indicate nitrogen limitation for phytoplankton growth in summer.

Taylor, Charlesworth and Service (1999) argued that other processes may be responsible for N removal from the water column during summer; in particular, these processes could be: deposition of organic N in the sediments, denitrification, or uptake by macrophytes and microphytobenthos. Furthermore, denitrification is controlled by the temperature and the organic content of the sediments (Livingstone, Smith and Laughlin 2000), so it could be an important process in the shallow area of the Lough during summer. In this context, Livingstone, Smith and Laughlin (2000) estimated an annual denitrification rate for Belfast Lough and Strangford Lough of 28 tonnes of N km^{-2} . The intertidal area in Carlingford Lough is approximately 15 km^2 and assuming the same denitrification rate measured in Belfast and Strangford Loughs, the denitrification process may remove up to 420 tonnes of nitrogen per year, equal to 1/3 of the annual N loading in Carlingford Lough.

The DIN:Si ratios measured in Carlingford Lough (1.8 and 1.7 for winter and spring respectively; Figure 2.10 b and d) were lower than the value presented in Gowen *et al.* (2000) for Irish coastal water (2.2), but they were comparable to the range identified by Brzezinski (1985) for 27 diatoms species (0.69-1.27), and also they fall in the range suggested by Tett, Hydes and Sanders (2003) for North-West European seas during winter (0.8-2.7). Furthermore, the intercept of the DIN:Si regression for the spring bloom was significantly different from zero indicating that silicate was depleted quicker than nitrogen. This suggests that silicate was likely to

have been the nutrient limiting phytoplankton production towards the end of the spring bloom, and this could be justified considering that the phytoplankton population in Carlingford Lough was dominated by diatoms over this period (on average 83% of the phytoplankton abundance during March and April 2006 and 2007).

A comparison of the physical and chemical variables measured during this study with earlier data (Douglas 1992; Taylor, Charlesworth and Service 1999; Ferreira *et al.* 2007) show that the temperature and salinity ranges were similar while nutrient concentrations (DIN and SRP) were approximately half of the concentrations reported by Ferreira *et al.* (2007) for the period 1994-2000. This difference in N and P concentrations can be related to the location of sampling stations used by Ferreira *et al.* (2007). In particular, they derived the nutrient concentrations from stations in the inner, mid and outer Lough. However it is also possible that there could have been a reduction in nutrient loading in the Lough in the last 15 years due to the upgrade of the sewage system (personal communication M. Service, AFBI, Belfast).

Comparing Carlingford Lough to other Northern Irish sea loughs, Strangford Lough has a similar annual load of nitrogen (1,981 tonnes y^{-1}) and there is evidence of phytoplankton N limitation during summer (Service *et al.* 1996). Belfast Lough has a higher nutrient load from sewage (N load is 5-fold higher than in Carlingford Lough; Service *et al.* 1996) and only the outer Lough has nutrient concentrations in the same range as Carlingford Lough.

2.4.2 Biological variables

Considering the biological variables (e.g. chlorophyll), the spring bloom in Carlingford Lough occurred between the end of March and the start of April. According to previous studies of Carlingford Lough, the timing of the spring bloom has been shown to be variable. Douglas (1992) recorded the main chlorophyll peak in May, and Ball, Raine and Douglas (1997) in mid April. Based on these observations, Ball, Raine and Douglas (1997) argued that the spring bloom in the Lough occurred later than other locations around the Irish Coast (e.g. start of April in Galway Bay and neighbouring inlets; Raine and Patching 1980) and suggested this

was a consequence of the dilution effect of the large tidal prism. However, the above authors based their study on monthly sampling and this frequency may not have been sufficient to characterise short term variability. To support this hypothesis, Taylor, Charlesworth and Service (1999) used a sampling frequency similar to the present study and they observed the spring bloom at the end of March.

The spring bloom at the end of March - start of April also occurs in Belfast Lough and in general in the Irish Sea coastal region between Carlingford Lough and Dublin, while in the central area of the Irish Sea the spring bloom typically occurs in April/May (Gowen *et al.* 1995; Gowen and Bloomfield 1996). In the Scottish sea lochs Creran, Striven and Etive the phytoplankton spring bloom has been shown to occur slightly earlier than in Carlingford Lough, in the middle of March (Wood, Tett and Edwards 1973; Tett and Wallis 1978; Tett *et al.* 1986). The difference in the timing of the spring bloom between these areas could be related to different hydrodynamic conditions of the water column or to underwater light limitation. The variables influencing the timing of the spring bloom in Carlingford Lough will be fully discussed in the chapter describing the underwater light field (Chapter 3).

The other peaks in chlorophyll concentration measured in the Lough during the summer (in June and August) were recorded after peaks in River Clanrye outflow which introduced new dissolved nutrients in the Lough. Ball, Raine and Douglas (1997) observed a peak in chlorophyll at the end of August 1992 after low riverine inputs. The authors suggested that the peak could have been driven by regeneration of nutrients from sediments. However, Gowen *et al.* (2000) estimated a nitrate and ammonium efflux rate for Irish coastal water during summer of $29 \mu\text{mol N m}^{-2} \text{ h}^{-1}$; considering a water column of 5.5 m depth (such as at the station CLNBuoy), the N efflux from sediments would have been equal to $0.127 \mu\text{M N d}^{-1}$, which was probably not sufficient to support a peak in chlorophyll. It is possible then that the peak in August 1992 was associated to a phytoplankton bloom occurring outside the Lough, in the Irish Sea coastal waters.

The maximum and the average chlorophyll concentrations in 2006-2008 were higher than the concentration measured by Ball, Raine and Douglas (1997), Taylor, Charlesworth and Service (1999), and Ferreira *et al.* (2007). Explanations for this difference could be the different sampling frequency adopted in these studies and the different sampling station locations. Comparing Carlingford Lough to other RREs in NI, Belfast Lough showed a wider range of chlorophyll concentration ($0\text{-}45 \text{ mg m}^{-3}$;

Service *et al.* 1996) probably due to the higher nutrient loads. In contrast, Strangford Lough supported a smaller chlorophyll range (0.5-15 mg m⁻³; Service *et al.* 1996) than Carlingford Lough although characterised by a similar nutrient range. This suggests that other variables, such as light, may limit phytoplankton growth in Strangford Lough as also suggested by the late spring bloom (early May according to Service *et al.* 1996).

The phytoplankton population in Carlingford Lough was dominated by diatoms all year round and this could be explained considering the high nutrient concentration in the mid Lough and the hydrodynamic condition (intermittent mixed and stratified) of the water column. Diatoms are not motile organisms and turbulence helps to retain cells in the euphotic zone; alternatively, stratified conditions may favour the sinking of the non motile diatoms and also favour the presence of dinoflagellates which can swim actively to remain in the euphotic zone (Margalef 1978; Jones and Gowen 1990). In this context, the only occasion of dinoflagellate dominance (mid/late May 2006) at the sampling station in Carlingford Lough coincided with the strongest stratification ($\Delta\text{Sal}_{1-4} = 1.59$).

Phytoplankton abundance (Figure 2.14 a) showed a different seasonal pattern than phytoplankton biomass (Figure 2.14 b) due to the variable size and biovolume of the microalgae cells. In fact, the peaks in abundance were characterised by organisms with a relatively small volume ($< 1 \times 10^3 \mu\text{m}^3 \text{ cell}^{-1}$; Figure 2.19 a) but highly abundant ($> 10^6 \text{ cell L}^{-1}$), such as *Chaetoceros* spp. and *Asterionellopsis glacialis*. In contrast, the peaks in phytoplankton biomass were produced by microalgae with a large cell volume (on average $7 \times 10^3 \mu\text{m}^3 \text{ cell}^{-1}$; Figure 2.19 a) but with abundance $< 500 \times 10^3 \text{ cell L}^{-1}$, such as *Thalassiosira* spp. Furthermore *Chaetoceros* spp. reached the highest abundances (24th April 2006, 21st June 2006 and 14th August 2007) in condition of relative low nutrient concentration (e.g. DIN $< 2 \mu\text{M}$), while *Thalassiosira* spp. blooms occurred with high nutrient concentration (e.g. DIN $> 15 \mu\text{M}$). The ability of *Chaetoceros* spp. to bloom in condition of relative low nutrients could be related to its high cell surface area to volume ratio (1.04 for *C. socialis*) compared to *Thalassiosira* spp. ratio (0.35 for *T. nordenskioldii*). With high surface area/volume ratio, nutrients and metabolites can be moved quicker within the cell, improving the growth rate of the organism (Margalef 1978; Reynolds 1996).

Some of the main phytoplankton taxa, in terms of abundance and biomass, identified in 2006-2008 (e.g. *Thalassiosira nordenskioldii*, *T. rotula*, *Rhizosolenia*

spp., *Leptocylindrus danicus*, *Chaetoceros* spp.) were also observed during the previous studies of the Lough (Table 2.3). However there are some differences between the historical data and the present data that could be related to different sampling techniques. Douglas (1992) used a net with mesh of 60 μm diameter to collect phytoplankton samples, consequently the samples were probably not representative of the smaller fraction of the phytoplankton population (e.g. microflagellates and naked dinoflagellates). Different sampling location and sampling frequency could also explain other differences between the historical data and the 2006-2008 data. The summer population was dominated by *Leptocylindrus danicus*, *Guinardia delicatula* and *Rhizosolenia* spp., which were also common in the western Irish Sea coastal waters in 1995 and 1997 (McKinney, Gibson and Stewart 1997; Gowen *et al.* 2000).

Thalassiosira spp. characterised the spring bloom in Carlingford Lough and also in Scottish RREs; however, in Scottish sea lochs (such as Loch Creran) the phytoplankton spring bloom was also dominated by *Skeletonema costatum* (Marshall and Orr 1930; Wood, Tett and Edwards 1973; Tett, Drysdale and Shaw 1981; Boney 1986; Tett *et al.* 1986). In particular, in 1973 and 1979, in the Inner Firth of Clyde and in Loch Creran respectively, *S. costatum* dominated the algal community with abundance up to 10×10^6 cell L^{-1} (Tett, Drysdale and Shaw 1981; Boney 1986). In term of abundance and biomass, *Skeletonema* spp. never represented an important part of the phytoplankton population in Carlingford Lough (Douglas 1992; Ball, Raine and Douglas 1997; Taylor, Charlesworth and Service 1999); in fact it never exceeded 50×10^3 cell L^{-1} in 2006-2008, and also in the past (1993) its abundance was 27×10^3 cell L^{-1} (Ball, Raine and Douglas 1997). However it is important to note that from 1981 to 2003 a substantial decrease in *Skeletonema* abundance has been observed in Loch Creran (P. Tett personal communication) as well as other coastal regions. For example, Borkman and Smayda (2009) reported a reduction of $\approx 45\%$ in *Skeletonema* spp. abundance from 1959 to 1997 in Narragansett Bay, USA. The reduction has been related to variation in the North Atlantic Oscillation (NAO) index while it is not clear what caused the reduction in Loch Creran. Unfortunately there are no data available on phytoplankton populations in Carlingford Lough in the 1980s or earlier, therefore it is not possible to know if *Skeletonema* has ever been abundant in the Lough or if the environmental conditions in Carlingford Lough are not suitable for this taxon.

The similarities between the phytoplankton composition of Carlingford Lough and the Scottish sea lochs (e.g. Loch Creran and Loch Striven) are not limited to *Thalassiosira* spp., in fact *Chaetoceros* spp., *Leptocylindrus danicus*, *Eucampia zodiacus*, *Rhizosolenia* spp., *Heterocapsa* spp., *Guinardia delicatula* were also common in these RREs (Boney 1986; Tett *et al.* 1986; Tett, Drysdale and Shaw 1981).

Finally the observation of the phytoplankton average chlorophyll content (ACC; Figure 2.19 b) temporal trend suggests that microalgae during spring and early summer had a lower chlorophyll content per cell compared to the microalgae present at the end of August 2006 and during winter (December to February). The three main peaks in ACC were characterised by the dominance, in terms of biomass, of *Chaetoceros compressus* (August), *Paralia sulcata* and unidentified naked dinoflagellates (during winter). Considering the two winter peaks, it is possible that phytoplankton abundance and biomass in these samples were underestimated, because the samples had a high sediment content which made the enumeration of the cells very difficult. ACC was calculated by dividing chlorophyll concentration by phytoplankton biovolume; consequently underestimation of biovolume would lead to an overestimation of the average chlorophyll content. However, it is also the case that in conditions of low irradiance phytoplankton cells tend to have higher chlorophyll content compared to conditions of high irradiance as shown by data from experiments with *Skeletonema costatum* and *Gonyaulax tamarensis* (Langdon 1987).

2.5 Conclusions

From the analysis of the chemical, physical and biological variables of Carlingford Lough it is possible to understand that:

- the outflow of the Clanrye River at the head of Carlingford Lough has a strong influence on the vertical structure of the water column and the chemical, physical and biological variables of the inner/mid region of the Lough (e.g. nutrient concentrations, phytoplankton abundance and biomass); the water column was stratified in more than half of the sampling occasions despite earlier claims that it is well mixed;
- silicate and nitrogen are the nutrients potentially limiting phytoplankton growth during spring and summer respectively;
- diatoms are favoured to dominate the phytoplankton population during the year, due to the high nutrient concentration in the Lough and mixed/stratified water column conditions;
- temperature, salinity, and nutrient ranges in Carlingford Lough are similar to other RREs in Northern Ireland (Belfast Lough and Strangford Lough) and in Scotland (e.g. Loch Creran), as well as the phytoplankton composition except for a marked reduction in *Skeletonema* spp.

CHAPTER 3

Underwater light field

3.1 Introduction

This chapter is a complement to Chapter 2 and provides information on the underwater light field and water column transparency measurements at station CLNBuoy in Carlingford Lough. In particular, Chapter 3 aims: to provide a description of the seasonal variability of the diffuse light attenuation coefficient for downward irradiance (K_d); to identify and quantify the effect of the different optical compounds of the water medium on the variability of K_d ; and to discuss the influence of the underwater light field on the timing of the phytoplankton spring bloom.

3.1.1 The electromagnetic spectrum

In addition to inorganic carbon, H_2O and nutrients, phytoplankton require energy in the form of solar radiation to photosynthesise. Light availability can limit phytoplankton growth in turbid estuaries (e.g. Cloern 1987; Devlin *et al.* 2008) and it influences the timing of the starting of the spring bloom (e.g. Gieskes and Kraay 1975; Peeters *et al.* 1991; Peeters *et al.* 1993).

The electromagnetic radiation from the Sun, expressed as quanta or photons, can be described by a wavelength (λ) and a frequency (ν) in accordance to Equation 3.1 (Kirk 1994).

$$\lambda = \frac{c}{\nu} \quad (3.1)$$

Where c is the speed of the light ($300 \times 10^6 \text{ m s}^{-1}$). While the energy (ε) associated to a photon is given by the product of the photon's frequency by Planck's constant ($h = 6.63 \times 10^{-34} \text{ J s}$); the energy is inversely related to the wavelength (Equation 3.2; Kirk 1994).

$$\varepsilon = h \cdot \nu = \frac{h \cdot c}{\lambda} = \frac{1988}{\lambda} \cdot 10^{-19} \quad (3.2)$$

The part of spectrum relevant for photosynthesis is called PAR (Photosynthetically Available Radiation; Tett 1990; Kirk 1994) and includes the wavelengths between approximately 400 and 700 nm. PAR represents 38% of the extraterrestrial solar irradiance (Kirk 1994).

A photon, emitted by the Sun and arrived at the upper atmosphere, has to travel through the atmosphere, the air-water interface and part of the water column

before being available to a phytoplankton cell. During this journey, components of the atmosphere (e.g. clouds) or of the aquatic medium (e.g. water itself, suspended matter) can deviate the photon from its original path or absorb it, competing with phytoplankton for its utilization. The upper part of the atmosphere reflects back to space $\approx 34\%$ of the incoming solar radiation, while another 19% is absorbed by clouds and other components of the atmosphere (see review by Kirk 1994). Consequently only 47% of the extraterrestrial solar radiation reaches the Earth surface.

The atmosphere absorbs and scatters the bands of the electromagnetic spectrum in a different way. As an example, the intensity of PAR is diminished by scattering and absorption by ozone, oxygen and water vapour while the intensity of the infrared band (> 700 nm) is mostly reduced by absorption by water vapour. The infrared band is absorbed by the atmosphere more than the PAR band, consequently PAR accounts for a higher proportion of the solar radiation at the Earth surface than outside the atmosphere. In particular, PAR is 45% of the solar radiation at the Earth surface (Kirk 1994). When the light arrives at the surface of the water, 4-6% of the solar radiation is reflected back to the atmosphere (Tett 1990). The proportion of light reflected changes with the angle that the light beam approaches the surface of the water. The amount of light reflected can vary from 2% for a vertical incident beam to 100% for a beam that is almost parallel to the water surface (Kirk 1994). The state of the sea can also affect the proportion of light reflected at the sea surface. For example, newly formed whitecap waves can reflect up to 55% of the incident solar radiation (see review by Kirk 1994).

Once the light photons pass through the air-water interface, they change their direction from the vertical due to refraction. The latter is a phenomenon derived from the changes of the speed of the light passing from the air to the water. The refraction of the light from air to water varies with the temperature, salinity of the water and with the wavelength of the incident radiation (Kirk 1994).

3.1.2 Inherent optical properties

Once a photon has passed through the air-water interface only 2 phenomena can happen: the photon is absorbed or scattered. The latter occurs when a photon

diverges from its original path due to interaction with some components of the water medium (e.g. particles). The scattering does not remove the photon from the water, but makes the photon follow a zigzag path which impedes the penetration of the photon down the water column and increases its chances to be absorbed by some component of the water medium (Kirk 1994).

The absorption and scattering properties of a water body are expressed in terms of the absorption coefficient (a) and the scattering coefficient (b). Considering an infinitesimally thin layer of medium and a parallel beam of monochromatic light hitting the layer at right angles, a is defined as the fraction of the light absorbed by the layer divided by the thickness of the layer, while b is the fraction of the light beam that is scattered, divided by the thickness of the layer. The coefficients a and b vary with the type of substances constituting the water medium and not with the geometry of the light field (e.g. the sun angle), therefore they are called inherent optical properties (see review by Kirk 1994). From the sum of the absorption and scattering coefficients another inherent optical property can be derived, the beam attenuation coefficient c . The latter is the fraction of the incident beam that is absorbed and scattered by an infinitesimal layer of the water medium, divided by the thickness of the layer.

The main components of the water medium that absorb and/or scatter the light photons are considered to be: plankton component (including phytoplankton, microzooplankton and non-living detritus), inorganic suspended particulate matter, yellow substances (also referred to as Coloured Dissolved Organic Material, CDOM), and water itself (IOCCG 2000). Water absorbs mainly in the red region of the electromagnetic spectrum (> 550 nm) and a layer of 1 m of pure water absorbs approximately 35% of the incident light at 680 nm (Kirk 1994). The yellow substances (mainly humic substances derived from plant decomposition) and inorganic suspended solids have a stronger absorption towards low wavelength such as blue and UV (around 400 nm). The chlorophylls and other pigments in the phytoplankton have two main peaks of absorption, in the blue and in the red band (approximately 440 and 670 nm respectively). As a result, in oligotrophic oceanic waters, blue and green light both penetrate deeply in the water column, while in productive coastal waters green light penetrates deeper than blue light (Kirk 1994).

The individual contribution of the components of the water medium to the absorption and scattering of light (assuming the contribution of water as constant)

varies between water bodies. As an example, CDOM was responsible for 70% and 66% of the light absorption in three shallow estuaries in New England and in a macrotidal estuary in south-western Australia, respectively (Branco and Kremer 2005; Kostoglidis, Pattiaratchi and Hamilton 2005). In other regions, such as the North Sea-Baltic Sea estuarine transition and a Mediterranean coastal lagoon in the Balearic Islands, the light reduction was mainly associated with absorption by chlorophyll pigments with an average of 32% and 47% respectively (Lund-Hansen 2004; Obrador and Petrus 2008). In UK marine waters, suspended solids are responsible for more than 90% of the light reduction in the water medium (Devlin *et al.* 2009).

The inherent optical properties are additive which means that a and b can be expressed as the sum of the contributions due to the different constituents of the water medium. Furthermore they are linear properties, indicating that the absorbing/scattering effect of a component is proportional to its concentration (Kirk 1994; Bowers and Mitchelson-Jacob 1996; Gallegos 2001). This is summarised in Equations 3.3 and 3.4 for absorption and in Equations 3.5 and 3.6 for scattering.

$$a = a_w + a_y + a_i + a_p \quad (3.3)$$

$$a = a_w + a_y^* [Y] + a_i^* [I] + a_p^* [P] \quad (3.4)$$

$$b = b_w + b_i + b_p \quad (3.5)$$

$$b = b_w + b_i^* [I] + b_p^* [P] \quad (3.6)$$

Where a_w , a_y , a_i , a_p are the absorption by water, yellow substances (CDOM), inorganic particulate matter and phytoplankton component (same symbols for the scattering coefficients). The coefficients with the star are the specific absorption or scattering coefficients (absorption or scattering per unit concentration), while the symbols in brackets are the concentrations of the components. CDOM is not included in Equations 3.5 and 3.6 because it is not expected to contribute to scattering (Bowers and Mitchelson-Jacob 1996).

3.1.3 Vertical attenuation coefficient (apparent optical properties)

The radiant flux per unit area of a surface (E), resulting from the absorption and scattering of photons in the water, can be measured in $W m^{-2}$, quanta (or

photons) $s^{-1} m^{-2}$ or mol quanta (or mol photons or Einstein) $s^{-1} m^{-2}$ (Kirk 1994). In the water column the radiant flux can move downward (downward irradiance E_d), and upwards (upward irradiance E_u), as a result of the scattering of photons in the water medium. E_u is usually much smaller than E_d , however there are some exceptions. In shallow water bodies where enough light reaches the seabed, E_u increases near the bottom due to reflection of the light from it. E_u can also be important in highly turbid water bodies due to greater scattering of photons by suspended particles (Kirk 1994).

The downward irradiance ($E_d(z)$) available for phytoplankton at a certain depth z can be derived from the Lambert-Beer equation, using the downward irradiance just below the surface ($E_d(0)$) and the vertical attenuation coefficient for downward irradiance (K_d) between the surface and the depth z (Equation 3.7; Kirk 1994).

$$E_d(z) = E_d(0) \cdot e^{-K_d \cdot z} \quad (3.7)$$

The Equation 3.7 describes the attenuation with depth of a monochromatic light with constant angular distribution, propagating in a homogeneous medium, and it shows that light decreases in an exponential manner with depth (Kirk 1994; Kirk 2003).

The term $K_d \cdot z$ in Equation 3.7 is called ‘optical depth’ and can be used to compare the photosynthetic potential of different water bodies (Tett 1990; Kirk 1994). A given optical depth can correspond to different physical depth in waters with different transparency. As an example, in turbid water (high K_d) a given optical depth will correspond to a shallower physical depth compare to the same optical depth in clear water (low K_d). The ratio between E_d and $E_d(0)$ is called the average cosine for downwelling light or $\overline{\mu_d}$, and it specifies the angular structure of the downwards light field as a result of the sun angle, the proportion of diffuse sky irradiance and the sea state (Kirk 1994; Gallegos 2001). The reciprocal of the average cosine for downwelling light is called distribution function (D_d) for downwelling light (Preisendorfer 1961 as cited by Kirk 1994).

The vertical attenuation coefficient can be calculated from Equation 3.7, and for a given depth interval z_1 - z_2 , $K_{d(z_1-z_2)}$ can be derived as shown in Equation 3.8 (Kirk 2003).

$$K_{d(z_1-z_2)} = \frac{1}{(z_2 - z_1)} \ln \left[\frac{E(z_1)}{E(z_2)} \right] \quad (3.8)$$

Where $E_d(z_1)$ is the downward irradiance at depth z_1 and $E_d(z_2)$ is the downward irradiance at the depth z_2 . A more accurate way to calculate K_d is to derive the coefficient of the linear regression of ln-transformed E_d versus depth over the depth interval z_1 - z_2 . Usually for most oceanographic studies, the depth interval chosen coincides with the layer of water from the surface to the depth at which E_d is 1% of $E_d(0)$, which represents the area of the water column in which the major part of the light is attenuated (Kirk 2003).

In reality, as already discussed, downward PAR is composed of different wavelengths which are absorbed and/or scattered in different ways by the water medium. For most marine waters, the attenuation of PAR is stronger in the first few meters of water (higher K_d) than deeper in the water column where the wavebands (mainly blue-green) have similar attenuation coefficient (Kirk 1994). For marine water, this can result in a biphasic curve when plotting ln-transformed E_d versus depth (Figure 3.1). In the upper part of the curve, the slope (K_d) increases with depth, while in the second part, where the curve becomes approximately linear, the value of the slope stabilises. In turbid water the biphasic character of the curve is not evident because the change in slope of the curve occurs near the surface of the water due to the stronger absorption of the light (Kirk 1994). Even in water bodies where the biphasic character of the total PAR attenuation curve is evident, the change of slope (K_d) with depth is not very big. Thus the attenuation of total PAR in a water body can be described by a single value of K_d or two (one for the upper part of the curve and one for the linear part; Kirk 1994 and Kirk 2003).

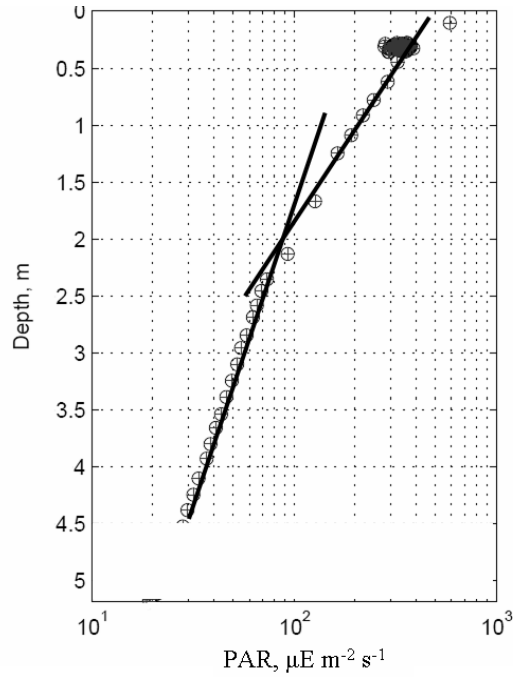


Figure 3.1. Example of a biphasic curve of logarithm of downward irradiance PAR ($\mu\text{E m}^{-2} \text{s}^{-1}$) versus depth (m), for the sampling station CLNBuoy in Carlingford Lough.

Tett (1990) suggested a modification of the Equation 3.7 to correct for the rapid attenuation of polychromatic light near the water surface (Equation 3.9).

$$E_d(z) = m_2 \cdot E_d(0) \cdot e^{-K_{d(\min)} \cdot z} \quad (3.9)$$

Where $K_{d(\min)}$ is the minimum value of the attenuation coefficient (e.g. between K_d of different wavebands of monochromatic light), m_2 is a correction factor for the quicker attenuation of polychromatic light near the surface and its value depends on the method used to derive $K_{d(\min)}$. For turbid coastal, fjordic and oceanic waters, m_2 ranges between 0.34 and 0.39 (see Tett 1990).

The vertical attenuation coefficient is a function of the geometrical properties of the light field, but at the same time K_d is also largely influenced by the absorption and scattering properties of the water medium. Thus K_d is classified as an apparent optical property or semi-inherent optical property (Kirk 1994; Gordon 1989). Inherent and apparent optical properties can be related using the Gershun equation (Equation 3.10; Kirk 1994; Bowers and Mitchelson-Jacob 1996; Kirk 2003).

$$K_E = \frac{a}{\mu} \quad \text{where} \quad \bar{\mu} = \frac{\vec{E}}{E_0} \quad (3.10)$$

K_E is the diffuse attenuation coefficient for net downward irradiance which is given by the downward irradiance minus the upward irradiance. If the latter is a constant fraction of the downward irradiance, K_E can be approximated to K_d (Bowers and Mitchelson-Jacob 1996). $\bar{\mu}$ is the average cosine of the light field (the cosine of the angle the photons make with the vertical) and is derived as the ratio between the net downward irradiance (\bar{E}) and the scalar irradiance (E_0). As an example, for the Irish Sea, $\bar{\mu}$ was estimated to be equal to 0.7 (Bowers and Mitchelson-Jacob 1996).

Kirk (1994) identified an empirical relationship between K_d and the absorption and scattering coefficients (Equation 3.11). This relationship can be applied to a wide range of water bodies and solar incidence angles.

$$K_d = \frac{1}{\mu_0} \left[\mu_a + G(\mu_0) \mu_s \right] \quad \text{where } G(\mu_0) = \frac{g_1 \mu_0 - g_2}{\mu_0} \quad (3.11)$$

In the equation, μ_0 is the cosine of the solar zenith angle, accounting for refraction at the air-water interface (assuming a flat surface, it can be derived from the location and the time of the day). $G(\mu_0)$ is a function of the relative effect of scattering on the total rate of attenuation and g_1 and g_2 are constants of a scattering phase function (see Kirk 1994).

Phytoplankton cells can absorb photons regardless of their direction. Therefore both E_d and E_u are important for microalgal photosynthetic activity. In terms of the irradiance available to phytoplankton it is more correct to refer to the scalar irradiance (E_0), which is the total radiant flux per m^{-2} from all directions at a given point in the water medium. E_0 includes E_d and E_u . Although $E_0 > E_d$, the light attenuation coefficient for the scalar irradiance (K_0) is approximately equal to the attenuation coefficient for downward irradiance K_d for water bodies with a scattering/absorption ratio ranging from 0.3 to 30 (Kirk 1994). The difference between K_d and K_0 increases with the turbidity of the water medium. In fact, in very turbid water bodies, underwater light is more diffuse due to high scattering and E_0 is higher than E_d ($E_0/E_d = 2.0$ to 2.5 ; Kirk 1994).

Phytoplankton photosynthesis takes place in a layer of the water called the 'euphotic zone' which goes from the surface down to the depth (z_{eu}) at which $E_d > 1\%$ of E_d at the surface (Kirk 1994). Assuming that K_d is approximately constant with depth, z_{eu} can be calculated as shown in Equation 3.12.

$$z_{eu} = \frac{4.6}{K_d} \quad (3.12)$$

However Tett (1990) defined the euphotic zone as “*all layers in which photoautotrophic production exceeds heterotrophic consumption on the time-scale under investigation*”, therefore linking the definition of euphotic zone to the concept of the critical depth. In fact, the latter was defined by Sverdrup (1953) as the depth at which the depth-integrated photosynthesis is equal to the depth integrated respiration. Tett (1990) argued that the compensation depth (and therefore the lower limit of the euphotic zone) could occur lower than the depth of 1% $E_d(0)$, in particular at 0.1% of $E_d(0)$ (see Tett 1990). The contrast between critical and compensation depths is a consequence of the way the two depths are calculated; the compensation depth is derived taking into account the balance between production and respiration at discrete depth, whereas the critical depth is derived taking into account the balance between production and respiration integrated along a layer of water column.

3.1.4 Measurements of the underwater light field

Irradiance is the most frequently measured property of the underwater light field, and it provides information on how much light is available for photosynthesis by phytoplankton. Generally an irradiance meter consists of a collector (e.g. a flat disk of translucent diffusive plastic), which collects the radiant flux, a photoelectric detector (generally positioned beneath the collector), and occasionally a photomultiplier (if a narrow waveband is measured). The irradiance meter can be connected to a data logger, such as a CTD, which stores the data collected (Kirk 1994). Irradiance meters are designed to respond equally to all the wavebands (wide-band detector), others are sensitive to a specific range of wavebands such as PAR. A second type of irradiance meter is called a quanta meter, and it responds equally to all the quanta within the PAR range, regardless of their wavelengths. An irradiance meter can have a flat collector (known as cosine or 2π collector) or a spherical collector (4π). The response of a cosine collector to the incident light depends on how much of the collector surface is projected towards the radiant flux. The area of the collector intercepting the light is proportional to the cosine of θ ; where the latter is the angle between the vertical of the collector and the direction of the radiant flux (see Figure 3.2). If the flat collector is oriented toward the surface, it measures the

downwards irradiance, and when oriented downwards it measures upward irradiance (Figure 3.3 a and b). Spherical collectors measure the irradiance coming from all directions and consequently measure scalar irradiance (Figure 3.3 c; Kirk 1994).

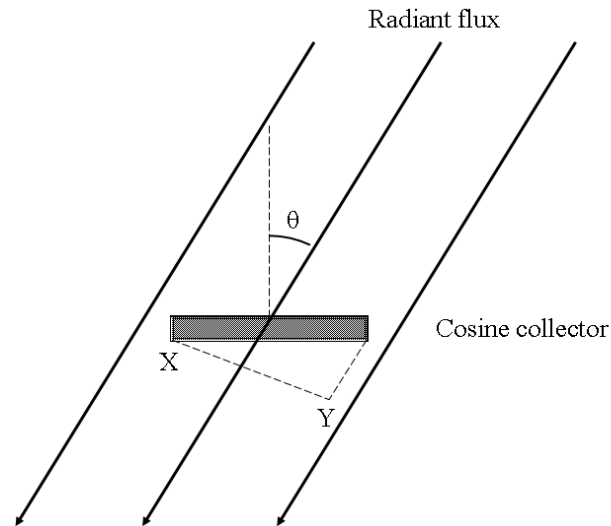


Figure 3.2. Dependence of a cosine collector on the direction of the radiant flux. The area of the collector that intercept the radiant flux is related to XY , which is proportional to $\cos\theta$ (from Kirk 1994).

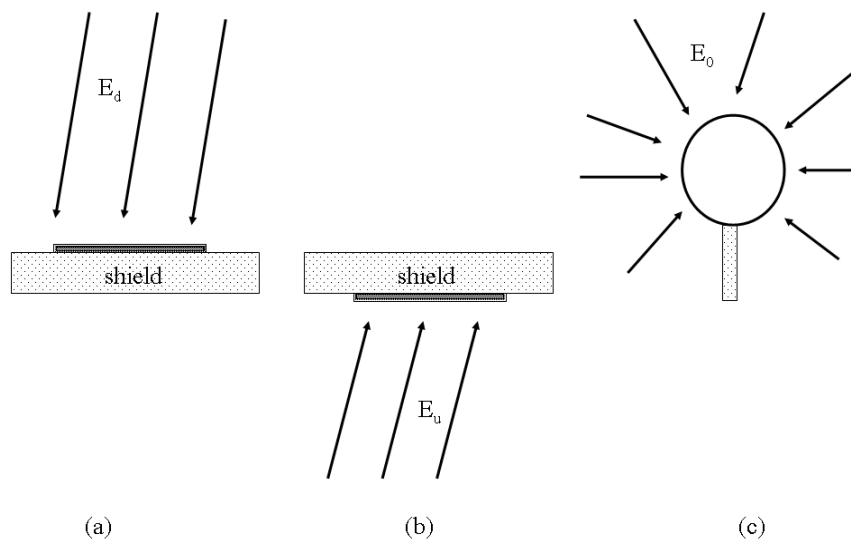


Figure 3.3. Radiant flux measured by cosine and spherical collectors. A cosine collector facing upward (a) measures downward irradiance E_d ; while the same collector facing downward (b) measures upwelling irradiance E_u . A spherical collector receives light from all directions (c), therefore it measures scalar irradiance E_0 .

The main sources of error when measuring the underwater light field are: 1) wave action; 2) fluctuation in irradiance due to clouds; and 3) perturbation of the light field due to the presence of the boat (Kirk 1994). Considering the first source of error, the convex part of a surface wave focuses the incident light at some depth within the water column. Fluctuations in irradiance due to clouds are slower than fluctuation in irradiance due to waves, and they affect the whole illuminated water column. These fluctuations can be identified by monitoring the solar radiant flux on deck and comparing these data with the underwater measurements. The third type of error can be overcome by manoeuvring the vessel so that measurements of irradiance are made on the “sunny side” of the ship.

3.1.5 How to derive K_d

From measurements of underwater light and Secchi depth

The attenuation coefficient for downward irradiance is commonly derived from measurements of the underwater light field (from light meters) using Equation 3.8, or calculating the coefficient of the linear regression of ln-transformed E_d versus depth.

A simple visual method of estimating K_d is the Secchi disk. This is a white disk, with a diameter of 20/30 cm, that is lowered down the water column until it just disappears from view. The depth at which the disk disappears is the ‘Secchi depth’ (z_{SD}) or ‘Secchi disk transparency’. K_d can be calculated from z_{SD} using Equation 3.13, with a value of f equal to 1.7 (Poole and Atkins 1929) or, for turbid waters, with f equal to 1.44 (Holmes 1970). Devlin *et al.* (2008) analysed the relationship between K_d and Secchi depth in 382 locations in transitional, coastal and offshore waters around the United Kingdom (Equations 3.14 for transitional waters and Equations 3.15 for coastal/offshore waters). The relationships between K_d and Secchi depth gave R^2 values of 0.79 for transitional waters, and 0.86 for coastal/offshore waters.

$$K_d = \frac{f}{z_{SD}} \quad (3.13)$$

$$\text{Transitional waters: } \ln K_d = 0.253 - 1.029 \ln(z_{SD}) \quad (3.14)$$

$$\text{Coastal/offshore waters: } \ln K_d = -0.010 - 0.861 \ln(z_{SD}) \quad (3.15)$$

Preisendorfer (1986) showed that relationships between Secchi depth and K_d are a function of where the measurements are made, the time of the year and local meteorological conditions. Consequently, the author suggested caution in the application of K_d -Secchi depth relationships in locations other than those from which the relationships were derived.

From theoretical and empirical models

The vertical attenuation coefficient, the absorption coefficient and the scattering coefficient can be derived using Equations 3.3 – 3.6, 3.10 and 3.11. The study of Bowers and Mitchelson-Jacob (1996) provides a clear example of how Equations 3.4 and 3.10 can be combined for predicting the attenuation coefficient for the Irish Sea (Equations 3.16 – 3.18).

$$a_{550} = 0.03 + 0.027 [I] + 0.019 [P] + 0.05 [Y] \quad (3.16)$$

$$K_{550} = \frac{1}{\mu} \cdot a_{550} \quad (3.17)$$

$$K_{PAR} = 0.01 + 1.11 \cdot K_{550} \quad (3.18)$$

Where the symbols in square brackets are the concentration of inorganic particles, phytoplankton pigments and yellow substances respectively; $a(550)$ is the absorption coefficient at 550 nm; K is the attenuation coefficient for the 550 nm waveband or for PAR; and μ is the mean underwater cosine.

It is not always possible to measure absorption and attenuation at different wavebands, therefore the application of Equations 3.3 – 3.6, 3.10 and 3.11, and the creation of relationships for deriving $K_d(\text{PAR})$ can be difficult. A simple solution is to linearly partition $K_d(\text{PAR})$ as the contribution of the attenuation of the different OACs (Equations 3.19 and 3.20) as done for absorption and scattering coefficients in Equations 3.3 – 3.6.

$$K_d(\text{PAR}) = K_w + K_y + K_i + K_p \quad (3.19)$$

$$K_d(\text{PAR}) = K_w + k_y [Y] + k_i [I] + k_p [P] \quad (3.20)$$

Where w, y, i and p refer to water, yellow substances (CDOM), inorganic particulate matter and phytoplankton component respectively. k_y , k_i and k_p are the specific attenuation coefficients, while the letters between squared brackets are concentrations.

However, when using the linear relationships showed in Equations 3.19 and 3.20, K_d is treated incorrectly as an inherent optical property. In fact, K_d is an apparent optical property and as such it does not depend linearly on the concentration of the water medium components. It is also true that under certain conditions (e.g. correcting the downward irradiance for the geometric structure of the underwater light field), K_d can be considered a property of the medium (Gordon 1989). This last assumption was demonstrated by Gordon (1989) for Case 1 waters, and for Case 2 waters with low concentration of non absorbent particles. In this context, Case 1 waters indicates water in which phytoplankton and water are the dominant OACs (e.g. oceanic waters), while Case 2 waters refers to waters in which CDOM and suspended solids are important OACs (e.g. coastal waters). Considering the small error that is usually associated with Equation 3.20 and its simplicity, K_d is commonly predicted by linear regression of the concentration of OACs. Some examples of these linear models are provided in Table 3.1, while a more detailed list can be found in Branco and Kremer (2005). It is not always possible to derive K_d from a linear model of OACs concentrations. For a shallow water estuary, Gallegos (2001) compared a linear regression model of K_d (using chlorophyll, CDOM and suspended solids as predictors) to a more realistic model of light attenuation and observed that the linear model underestimated $K_d(\text{PAR})$ at high attenuation.

The light attenuation coefficient can be derived from ocean colour remote sensing. Lee *et al.* (2005) grouped the different types of algorithms that calculate $K_d(\lambda)$ into 3 main types. The first type is based on an empirical relationship between $K_d(490)$ and the ratio of the blue/green light leaving the water and measured by satellite; the second category uses an empirical relationship to derive chlorophyll concentration (based on the ratio of the blue/green radiation detected by satellite), which is then used for deriving $K_d(\lambda)$. Finally the third type derives the absorption and backscattering coefficients (from satellite measurements), and uses them as input to a semi-analytical model that estimates the light attenuation coefficient (Lee *et al.* 2005). The first two types of models are generally applicable for clear oceanic waters, while the third type can be applied to coastal and turbid waters. Examples of algorithms to calculate K_d from remote sensing for clear and turbid waters can be found in Lee *et al.* (2005 a and b), and Wang, Son and Harding (2009).

Table 3.1. Examples of linear models for deriving K_d from concentrations of the constituent of the water medium. Tripton is defined as the non-algal particulate matter; g_{440} is the absorption coefficient at 440 nm and represents CDOM; TSS is total suspended solids; D is a statistic used to quantify the error in the prediction of K_d from SPM.

Equation	R^2	p-value	Location	Reference
$K_d=0.0163[\text{Chl}]+0.7627$	0.93	< 0.001	Mediterranean coastal lagoon	Obrador and Pretus (2008)
$K_d(\text{PAR})=0.06402[\text{tripton}]+0.521$	0.96	0.0025	Indian River Lagoon	Christian and Sheng (2003)
$K_d=0.346g_{440}+0.063[\text{TSS}]+0.31$	0.74	< 0.0001	Estuary SW Australia	Kostoglidis, Pattiaratchi and Hamilton (2005)
$K_d=0.039+0.067[\text{SPM}]$	0.98	D=24.1%	Coastal and offshore waters UK	Devlin <i>et al.</i> (2008)

3.2 Methods

3.2.1 *In situ* measurements of the underwater light field

Information on the sampling station, the sampling frequency and the variables measured during each sampling trip can be found in section 2.2.1 of Chapter 2. Measurements of the underwater light field were carried out from April 2006 until June 2006 with a Li-Cor cosine quantum sensor positioned on a Seabird 19 CTD belonging to Cefas (hereafter referred to as the Cefas light meter; Figure 3.4 a). From June 2007 to March 2008, measurements were made with two Li-Cor spherical quantum sensors connected to a Seabird 19 CTD (hereafter referred to as the AFBI light meter; Figure 3.4 b and c). The AFBI light meter (Figure 3.4 b and c) was designed by Professor P. Tett and assembled at AFBI by Mr. W. Clarke. This light meter consisted of two spherical collectors fixed on an aluminium frame so that the sensors were a fixed distance apart. The distance between the two collectors could be changed from 2 m for clear offshore or coastal waters, to 1 m for turbid waters. Measurements made with this instrument provided estimates of:

- a. the light attenuation at the air-water interface (positioning the bottom sensor underwater and the top one above the surface; Figure 3.4 c);
- b. K_0 (assumed approximately equal to K_d , Kirk 1994) by regression of each sensor $\ln E_d$ on depth;
- c. the instantaneous K_0 or K_d (from simultaneous light measurements by the two sensors, and knowing the distance between them).

Estimates of K_d derived from the two sensors were influenced by clouds and waves effects but they were not affected by the inclination of the light meter when underwater. Estimates of instantaneous K_d were not affected by the clouds and waves effects but they required the instrument to be vertical during the measurement for guaranteeing a constant distance between the sensors.

Secchi disk depth was also recorded on each sampling occasion. Solar radiation measurements (in $W m^{-2}$) were recorded at an AFBI weather station located in Hillsborough (approximately 25 miles from Carlingford Lough).

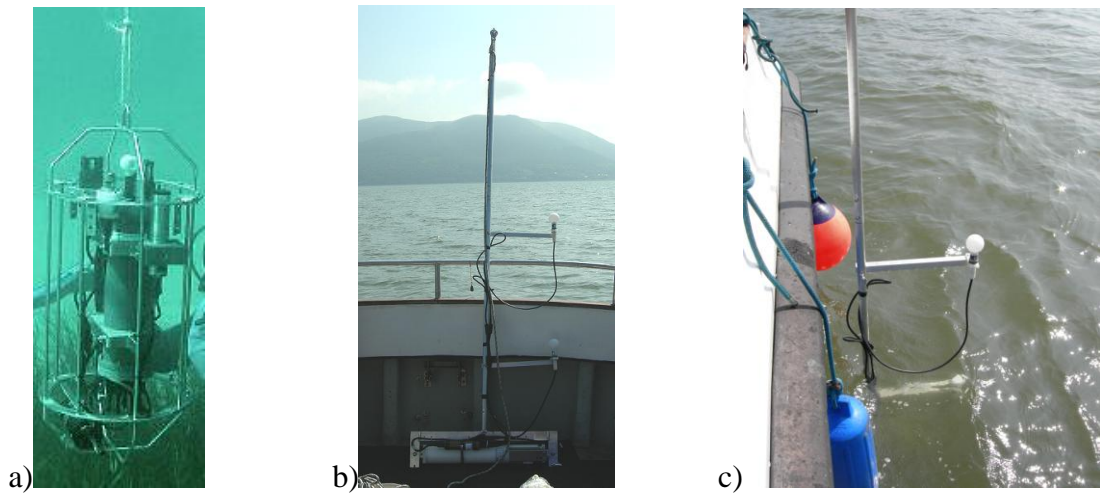


Figure 3.4. Details of the light meters used during this study. a) Cefas light meter, used from April to June 2006 (the photo shows a spherical light collector however during this study a cosine collector was used); b) AFBI light meter used from June 2007 to March 2008, and c) measurements of the light above and below the surface for estimating the light attenuation at the interface, with the AFBI light meter.

3.2.2 Estimates of K_d

Two Matlab scripts (*UWLight0.M* and *UWLight1.M*) were written to analyse the irradiance profiles collected by the AFBI light meter, while a modification of '*UWLight1.M*' (called '*UWLight1b_1s1d.M*') was used to analyse the underwater irradiance profiles measured by the Cefas light meter. The scripts divided the water column into optical depths and calculated K_0 (which can be approximated to K_d according to Kirk 1994) for each 0.5 increment in optical depth. An average value of K_d from the different optical depths was used as the final K_d for the water column.

'*UWLight0.M*' (Listing 3.1 in the Appendix 2) was run only in combination with '*UWLight1.M*'. The script '*UWLight0.M*' calculated the depth of the light sensors (based on the depth derived by the CTD) and the ratio between the irradiance measurements of the two sensors. The latter was called p1p2 in the script commands, and was equal to 1.23 indicating that the top sensor had a higher reading than the bottom sensor. The depth reading and p1p2 were then introduced in '*UWLight1.M*' to calibrate the depth of the CTD and the irradiance readings from the two sensors. The first part of the analysis of a given profile with '*UWLight1.M*' (Listing 3.2 in the

Appendix 2) was the calculation of instantaneous K_d for the down cast and the up cast. The instantaneous K_d at a given time “t” of the cast was equal to:

$$K_d(t) = \frac{-\ln((PAR_{bot}(t) \cdot p1p2) / PAR_{top}(t))}{sepd} \quad (3.21)$$

Where $PAR_{bot}(t)$ was the PAR reading of the lower sensor at the time “t”; $PAR_{top}(t)$ was the PAR reading of the top sensor at the time “t”; $p1p2$ was the ratio of the PAR readings between the two sensors; and $sepd$ was the distance between the two spherical sensors (set to 1 m for Carlingford Lough). The down cast and up cast provided a series of instantaneous K_d values, and the mean of these estimates (K_{dI}) was calculated and use in the next step of the analysis.

In the second part of the script, mean K_d was used to calculate the maximum number of optical depths for the profile, $odmax$. The latter was calculated as the product between mean K_d and the maximum depth ($zmax$) recorded by the CTD.

$$od\ max = meanKd \cdot z\ max \quad (3.22)$$

If $odmax > 1$ optical depth, the script calculated K_d from the optical depth of 0.5 ($odstart$) and incremented the optical depth of 0.5 ($odstep$) until reaching $odmax$. If $odmax \leq 1$, smaller increments were used. The physical depth interval over which K_d was calculated was defined as the depth interval between $ztop$ and $zbot$, where:

$$ztop = \frac{odstart}{meanKd} \quad (3.23)$$

$$zbot = ztop + \frac{odstep}{meanKd} \quad (3.24)$$

For each depth interval, K_d ($regKd$ in the script) was calculated as the slope of the regression line of the ln-transformed PAR in that given interval. At the end of the analysis of a given profile, the script outputs $regKddown$, which is the matrix containing $regKd$ for the down cast for the top and bottom sensors, and $regKdup$, is another matrix showing $regKd$ for the up cast for the top and bottom sensors. The mean of these four series of $regKd$ was calculated to give a final K_{dR} for the whole water column.

For a given irradiance profile the script produced two estimates of K_d of the water column:

1. K_{dI} from instant measurements (mean of instant K_d from down-cast and up-cast);
2. K_{dR} from regressions (mean of $regKd$ from down-cast and up-cast, top sensor and bottom sensor).

The underwater PAR profiles measured in 2006 (derived by the Cefas light meter) were analysed with ‘*UWLight1b_Is1d.M*’ (a modification of ‘*UWLight1.M*’ made during the course of this study). These profiles were recorded by one sensor and calculation of instantaneous K_d (K_{dI}) was not possible. The first stage of the analysis with ‘*UWLight1b_Is1d.M*’ was the calculation of K_d for the water column as the slope of the interpolation line of the ln-transformed PAR for the whole down cast. This value of K_d was then used instead of mean K_d in the following steps of the analysis. The resulting value of the light attenuation coefficient (average of the values of K_d calculated from regression of ln-PAR based on optical depths) was called K_{dCefas} .

Incomplete profiles (e.g. measurements of underwater light for only the first meter of the water column) or profiles made when shading influenced the profile (Figure 3.5) were not considered in the analysis. A total of 2 profiles were excluded from the analysis due to the above. Example of output plots of the script ‘*UWLight1.M*’ are showed in Figure 3.6.

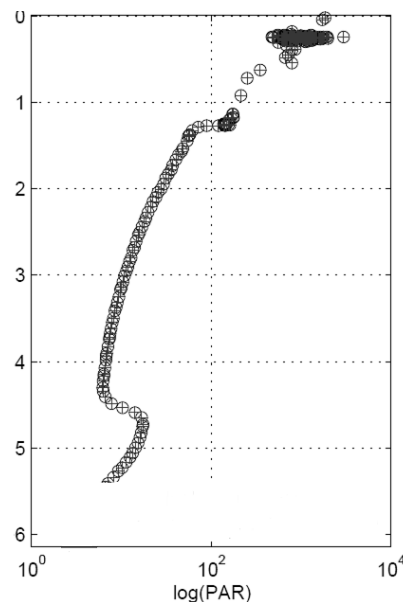


Figure 3.5. An example of an underwater light profile not considered in the analysis, because of shading by the boat (seen as the decrease in E_d below 1 m, and increase in E_d at 4.5 m). PAR, on the x-axes was expressed in $\mu E m^{-2} s^{-1}$, while depth (on the y-axes) was expressed in meters.

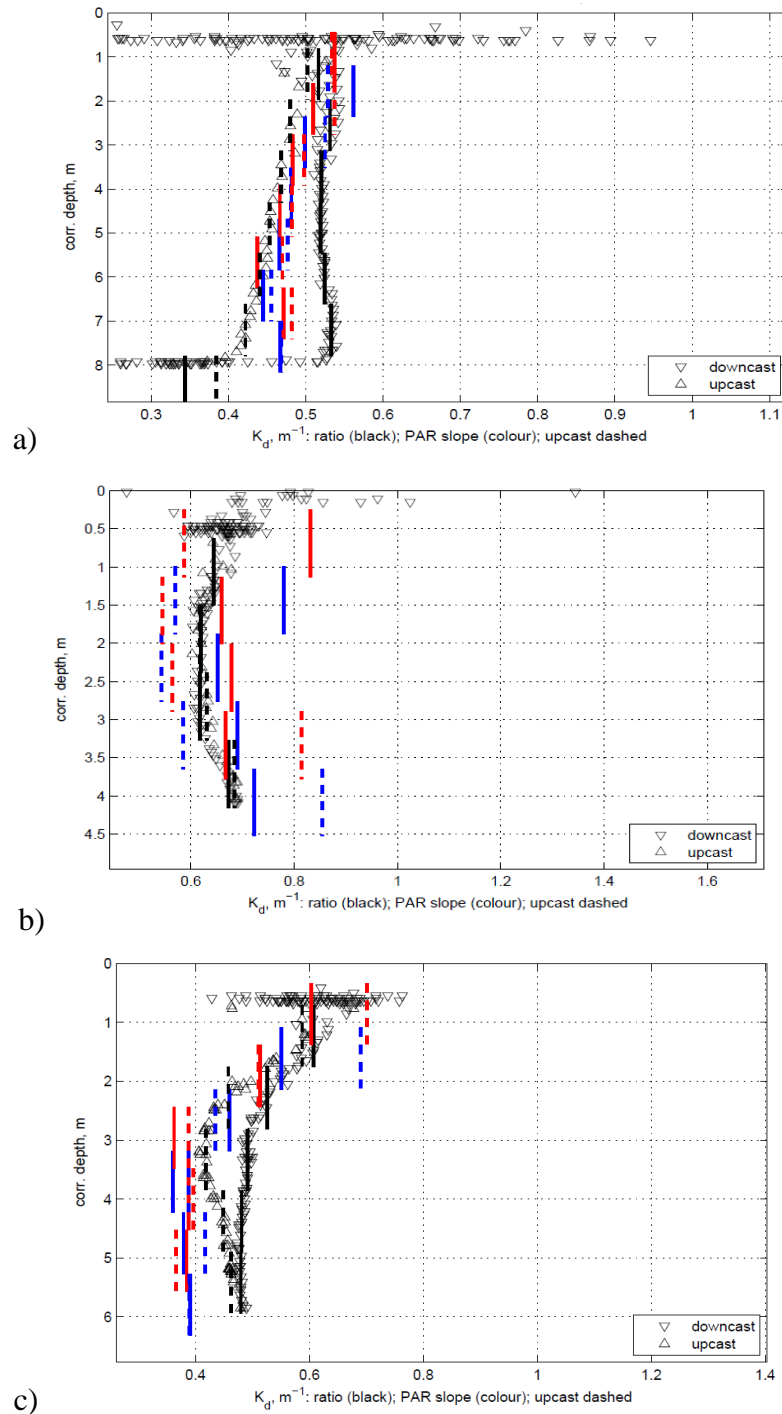


Figure 3.6. Examples of output plot from ‘*UWLight1.M*’; a) 16th July 2007, b) 2nd August 2007 and c) 13th September 2007. The triangles represent the instantaneous K_d for the down cast (∇) and the up cast (Δ). Solid lines represent regKd for the down cast and dashed lines regKd for the up cast. Red is the colour for the top sensor, blue for the bottom sensor and black for the instantaneous K_d . For example, a solid red line symbolises the regKd calculated in that depth interval from the down cast of the top sensor.

3.2.3 Calculation of surface incident PAR and daily surface mixed layer irradiance

Global solar radiation measurements were recorded on an hourly basis at the AFBI weather station in Hillsborough. The script '*dailySLM*' was used to calculate the total daily surface incident PAR during the sampling period. The script (Listing 3.3 in the Appendix 2) calculated the sum of the hourly solar radiation measurements for each day, expressed in W m^{-2} . The daily solar radiation was then converted into PAR multiplying by 0.45 (Kirk 1994).

Daily surface mixed layer irradiance (E_{SML}) was calculated using Equation 3.25 (Riley 1967).

$$E_{\text{SML}} = \frac{E_0}{K_d \cdot h} \cdot (1 - e^{-K_d \cdot h}) \quad (3.25)$$

Where E_0 is the surface irradiance and h is the depth of the surface mixed layer (see section 2.2.7 in Chapter 2). E_0 was calculated as the sum of the hourly PAR measured by the Hillsborough weather station for a given day and multiply by 0.94 (6% reduction in irradiance due to surface reflection; Tett 1990). h was set to 5.5 m (the average depth of the water column), therefore the equation derived the daily water column irradiance.

3.2.4 Data analysis

Descriptive statistics of the data, together with the graphs showing seasonal variation of K_d , Secchi depth, z_{eu} and daily surface incident irradiance were prepared using Microsoft Office Excel 2003. The difference between K_{dI} and K_{dR} was tested statistically using a 2-sample T-test. The software package Minitab 15.1.1.0 was used to run the analysis. Normality distribution of K_{dI} and K_{dR} was tested according to Barnes (1952) as described in Chapter 2 (section 2.2.7).

Single and multiple regression analyses between estimates of K_{dR} , and other environmental variables (chlorophyll, SPM concentrations, and Secchi depth) were carried out using Minitab 15.1.1.0. To evaluate the prediction of the relationship between K_d and Secchi depth, the observed values of the diffuse attenuation coefficient (derived from the light meters) were regressed against predicted values estimated from the relationship. Regression of observed versus predicted values was

chosen instead of predicted versus observed as suggested by Piñeiro *et al.* (2008), who observed that using the predicted versus observed lead to incorrect estimates of the slope and intercept of the regression equation, although the R^2 value does not change.

During the study it was not possible to measure the concentration of CDOM, although it is one of the variables influencing K_d . Foden *et al.* (2008) observed a negative correlation between CDOM concentration and salinity in UK marine waters (Equation 3.26; $n = 585$, $p < 0.05$, $R^2 = 0.81$). Therefore, Equation 3.26 was used to estimate CDOM concentrations in Carlingford Lough.

$$CDOM = -0.174 \cdot Salinity + 6.288 \quad (3.26)$$

3.3 Results

3.3.1 Seasonal trends of surface irradiance, Secchi depth, OACs and K_d

The seasonal pattern of total daily surface PAR is shown in Figure 3.7. The highest daily incident PAR (sum of hourly surface PAR for a given day) of 3660 W m^{-2} was measured the 11th June 2006, while the lowest of 27.5 W m^{-2} on the 26th December 2006.

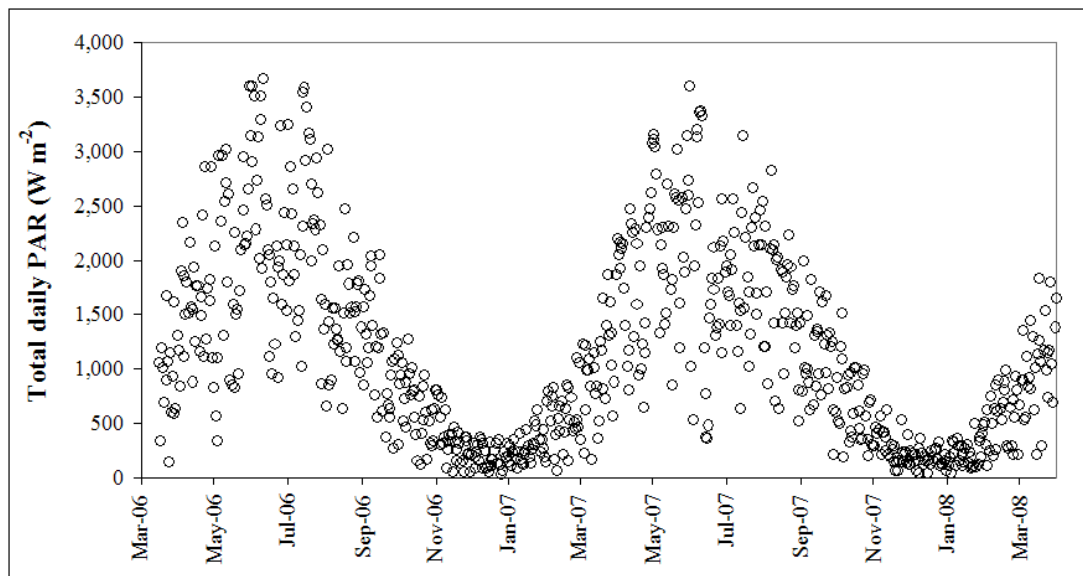


Figure 3.7. Seasonal pattern of total daily surface incident PAR (sum of hourly surface incident PAR for a given day) in W m^{-2} . Hourly solar irradiance data were measured by the AFBI weather station in Hillsborough, between March 2006 and December 2008. Data provided by Mr. Harry Nicholson (AFBI).

A total of 37 underwater irradiance profiles were measured in Carlingford Lough from April 2006 to March 2008. Of these, 19 were recorded at the sampling station CLNBuoy and 18 were measured in other locations along the Lough. Furthermore, of the 37 profiles, 8 were recorded with the Cefas light meter and 29 with the AFBI light meter. Descriptive statistics for Secchi depth, SPM concentration (as shown in Chapter 2), CDOM concentration (derived from salinity using Equation 3.26) K_{dI} , K_{dR} and K_{dCefas} are given in Table 3.2.

Table 3.2. Descriptive statistics (number, mean, standard deviation, median, minimum, and maximum) of: Secchi depth z_{SD} (m), SPM total – organic and inorganic from 1 m and 4 m depth (SPM_{tot}), CDOM of the water column (derived from salinity using Equation 3.26), K_{dI} (m^{-1}), K_{dR} (m^{-1}) and K_{dCefas} (m^{-1}); at station CLNBuoy in Carlingford Lough, between April 2006 and March 2008.

	Unit	n	Mean	SD	Median	Min	Max
z_{SD}	m	47	2.6	0.9	2.5	1.0	5.0
SPM_{tot}	$mg\ L^{-1}$	72	7.08	3.54	6.17	2.08	18.14
CDOM	m^{-1}	47	0.64	0.18	0.60	0.41	1.11
K_{dI}	m^{-1}	9	0.57	0.11	0.57	0.42	0.71
K_{dR}	m^{-1}	9	0.61	0.11	0.63	0.45	0.76
K_{dCefas}	m^{-1}	8	0.47	0.14	0.51	0.24	0.63

The seasonal variation in Secchi disk depth is shown in Figure 3.8. Secchi depth varied between 1 m (5th December 2006, 22nd March 2007, 5th February 2008 and 13th March 2008) and 5 m (12th April 2007 and 1st June 2007). The mean Secchi depth was 2.6 m. Variability of SPM (organic and inorganic) has been discussed in Chapter 2 (see section 2.3.3); the seasonal trend can be observed in Figure 3.9. Total Suspended Particulate Matter (SPM) reached the lowest concentration (2.08 $mg\ L^{-1}$) on the 8th June 2006 and the 12th April 2007 while the highest concentration (18.14 $mg\ L^{-1}$) was measured on the 13th March 2008. The seasonal trend of the derived concentration of CDOM is shown in Figure 3.10. The average CDOM concentration was 0.64 and varying between 0.41 and 1.11 (Table 3.2). CDOM was calculated from a negative relationship with salinity (Equation 3.26) therefore it shows maximum values (1.11, 6th December 2006) during periods of high river outflow ($> 4\ m^3\ s^{-1}$). The average K_{dI} for station CLNBuoy was $0.57\ m^{-1}$, and varied between 0.42 (7th June 2007) and $0.71\ m^{-1}$ (27th September 2007). The range of variability of K_{dR} ($0.45 - 0.76\ m^{-1}$) was similar to the range of K_{dI} , while the average was slightly higher ($0.61\ m^{-1}$). K_{dCefas} had average of $0.47\ m^{-1}$ and ranged between 0.24 and $0.63\ m^{-1}$. The values of K_{dR} , K_{dI} and K_{dCefas} are shown in Figure 3.11. Profiles of the light attenuation coefficient derived from the AFBI and Cefas light meters are shown in Figure 3.12.

Due to strong current during some sampling events, it was not possible to record vertical profiles and it is likely that in these cases K_{dI} could have been

underestimated (distance between the sensors < 1 m). To test this hypothesis, the similarity between K_{dI} and K_{dR} was compared using a two-sample T-Test. All measurements of K_{dI} and K_{dR} available for Carlingford Lough were used to test the hypothesis. The output of the test (T-value = 0.15, n = 34, p = 0.885) shows that there is no statistical difference between the two data sets. K_{dR} was used in the next stage of the analysis because each estimate of K_{dR} was derived as average of 4 light measurements (down cast and up cast for each light sensor).

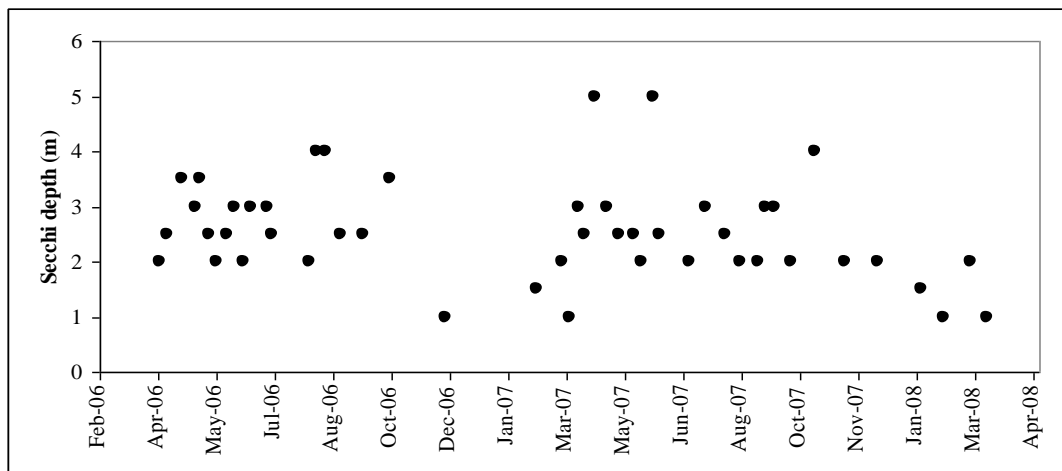


Figure 3.8. Seasonal variability of Secchi depth (m) at station CLNBUoy in Carlingford Lough, between April 2006 and March 2008.

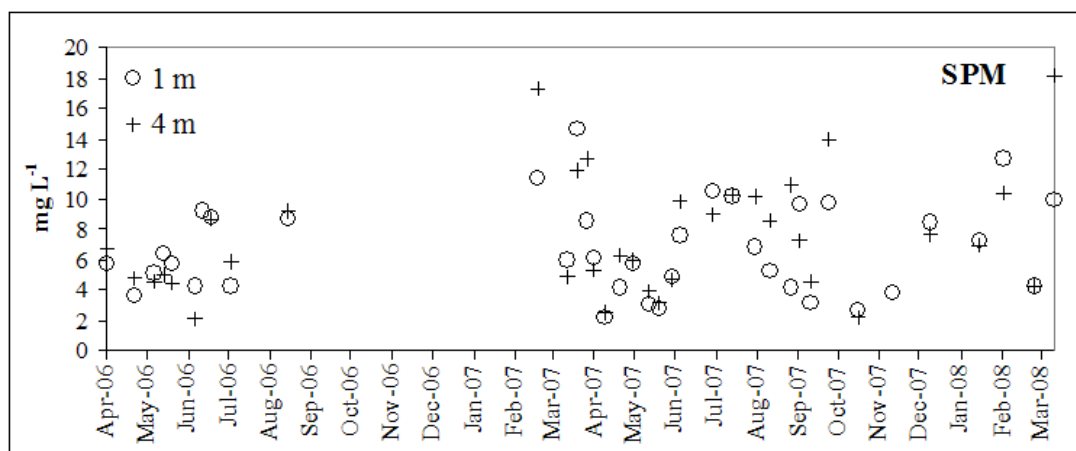


Figure 3.9. Seasonal patterns of total SPM (mg L^{-1}) at 1 m (o) and 4 m (+) depth, at station CLNBUoy in Carlingford Lough, between April 2006 and March 2008.

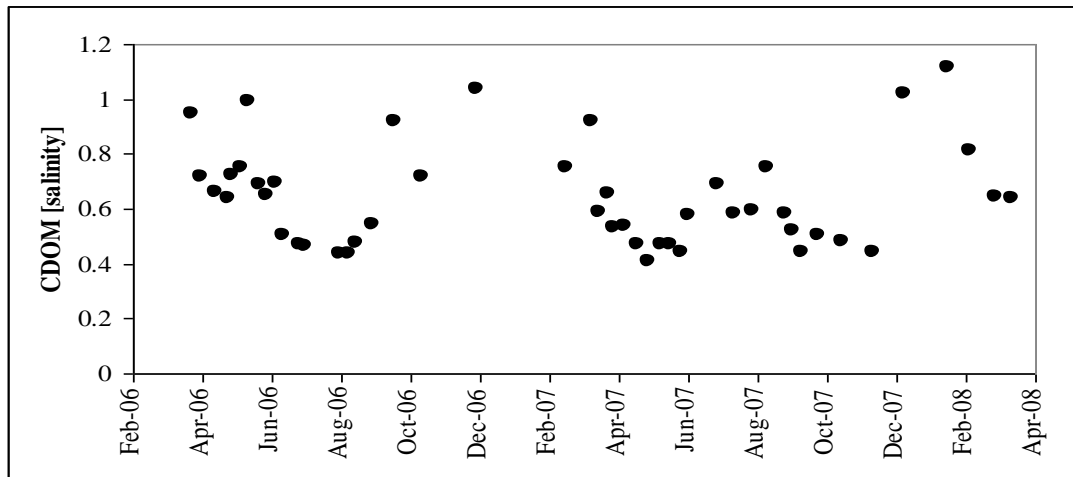


Figure 3.10. Seasonal pattern of CDOM, calculated from salinity using Equation 3.26, at station CLNBUoy in Carlingford Lough, between April 2006 and March 2008.

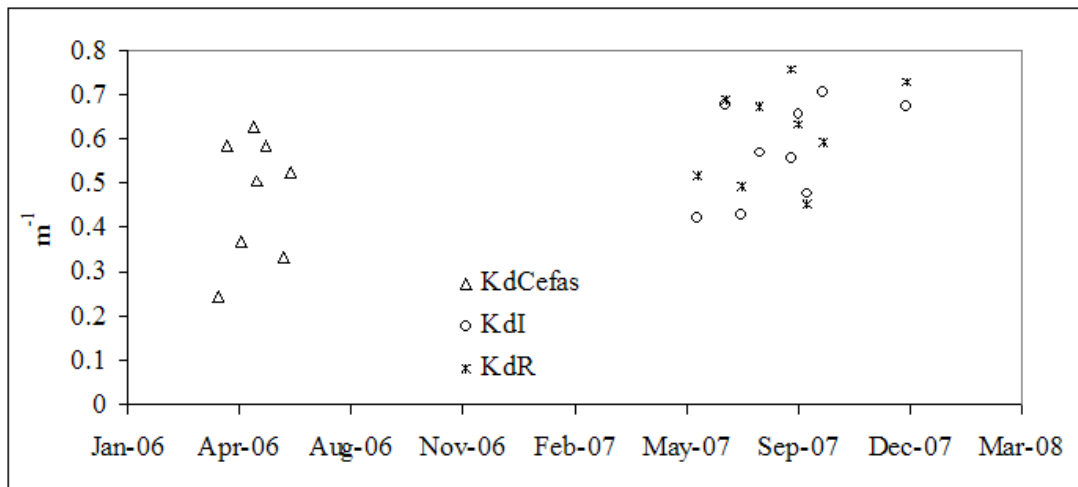


Figure 3.11. Values of K_{dR} , K_{dI} and K_{dCefas} (m^{-1}) at station CLNBUoy in Carlingford Lough, between April 2006 and March 2008.

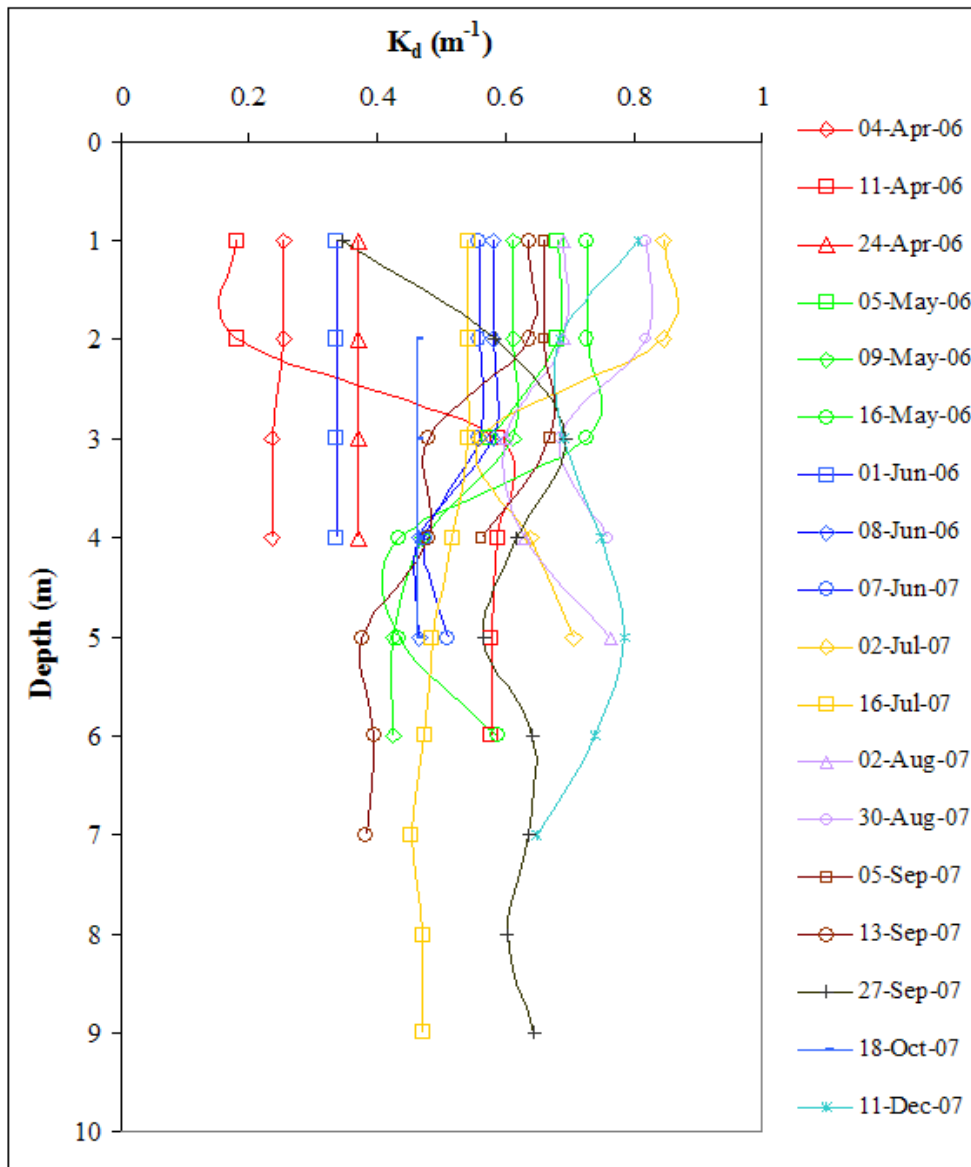


Figure 3.12. K_d profiles (m^{-1}) derived from measurements with Cefas and AFBI light meters, for station CLNBuoy in Carlingford Lough, between March 2006 and March 2008. The variability in depth between profiles is due to sampling being carried out at different states of the tide.

3.3.2 Empirical relationships for deriving K_d

Values of K_{dR} and K_{dCefas} were regressed against SPM concentration and against Secchi depth to find the best relationship to calculate K_d for sampling trips in which the light meters were not available. All estimates of the light attenuation coefficient available for Carlingford Lough (from CLNBuoy and other stations along

the Lough) were used in the regressions. The regression of K_{dR} and K_{dCefas} versus SPM concentrations (mg L^{-1}) was significant (analysis of variance, $n = 29$, $p < 0.001$) with $R^2 = 0.60$ (Equation 3.27). Considering only K_{dR} values ($n = 23$), the R^2 of the regression improved to 0.71 (Figure 3.13 and Equation 3.28).

$$\text{Using } K_{dR} \text{ and } K_{dCefas}: K_d = 0.0498SPM + 0.195 \quad (3.27)$$

$$\text{Using } K_{dR}: K_d = 0.0522SPM + 0.1898 \quad (3.28)$$

The regression of K_{dR} and K_{dCefas} versus $1/(\text{Secchi depth})$ was statistical significant (analysis of variance, $n = 34$, $p < 0.001$) and gave $R^2 = 0.73$ (Equation 3.29). For the K_{dR} data set only, the R^2 of the regression was 0.92 ($n = 27$, Figure 3.14 and Equation 3.30).

$$\text{Using } K_{dR} \text{ and } K_{dCefas}: K_d = 1.1245 \cdot \frac{1}{z_{SD}} + 0.1022 \quad (3.29)$$

$$\text{Using } K_{dR}: K_d = 1.1822 \cdot \frac{1}{z_{SD}} + 0.0887 \quad (3.30)$$

Equation 3.30 gave the best fit to the data ($R^2 = 0.92$), and was therefore used to calculate the K_d values for those surveys (a total of 29) carried out when it was not possible to made irradiance profiles. The observed K_{dR} for the period June 2007-March 2008 (AFBI light meter) were regressed against the predicted K_d (from Equation 3.30) for the same period. The regression was statistically significant (analysis of variance, $n = 27$, $p < 0.001$) and had an R^2 of 0.93 (Equation 3.31 and Figure 3.14); the slope was significantly different from 1 ($p < 0.001$), while the intercept was not significantly different from 0 ($p = 0.792$).

$$K_{d\text{observed}} = 0.975 \cdot K_{d\text{predicted}} + 0.0087 \quad (3.31)$$

Where K_d observed is K_{dR} , and K_d predicted refers to K_d derived from Secchi depth measurements and using Equation 3.30.

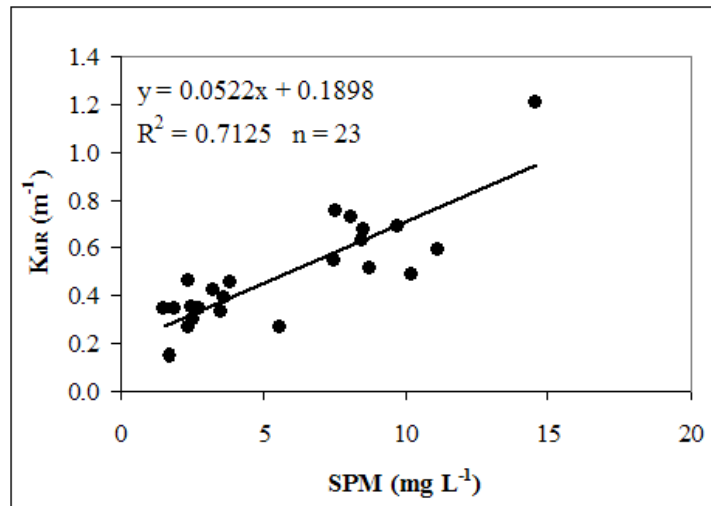


Figure 3.13. Regression of K_{DR} (m⁻¹) against SPM concentration (mg L⁻¹), for Carlingford Lough, between June 2007 and March 2008 (AFBI light meter).The solid line is the interpolation line of the points.

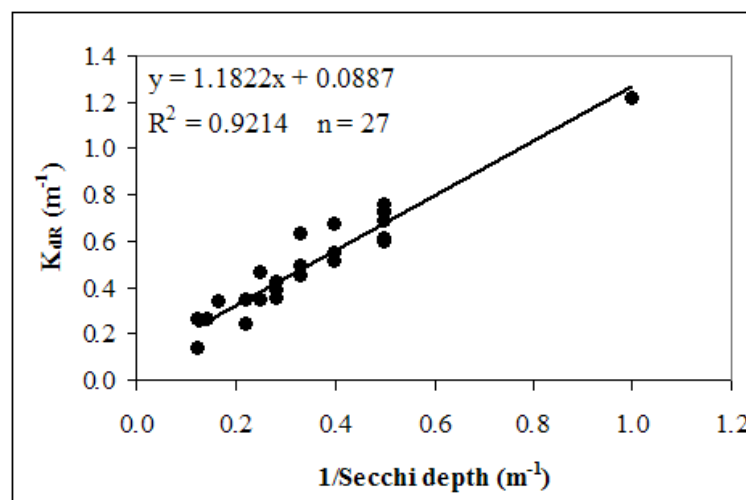


Figure 3.14. Regression of K_{DR} (m⁻¹) against 1/Secchi depth (m⁻¹), for Carlingford Lough, between June 2007 and March 2008 (AFBI light meter).The solid line is the interpolation line of the points.

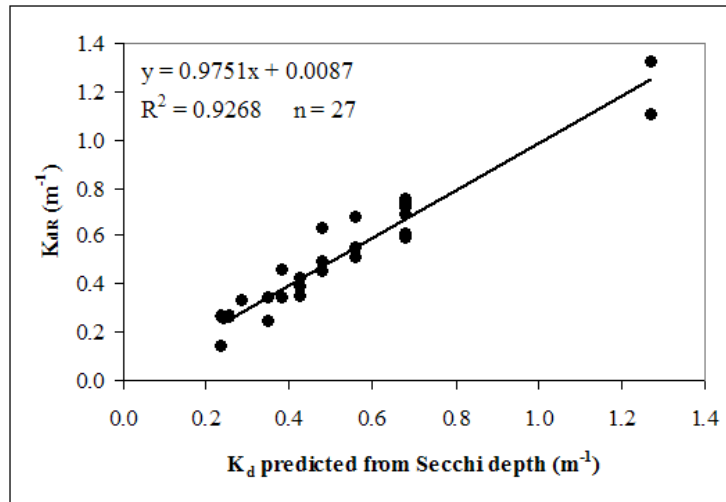


Figure 3.15. Regression of K_{dR} (m^{-1} ; AFBI light meter) versus K_d predicted by Secchi depth using Equation 3.30, for Carlingford Lough, between June 2007 and March 2008. The solid line is the interpolation line of the points.

3.3.3 Seasonal variability of modelled K_d and relationship with OACs

The seasonal trend in K_d derived from Equation 3.30 together with the K_d derived from light profiles (K_{dCefas} and K_{dR}) is shown in Figure 3.16. Of the 47 estimates of K_d , 8 were derived from light profiles using the Cefas light meter (K_{dCefas}), 10 from light profiles using the AFBI light meter (K_{dR}), and the remaining 29 from Secchi depth measurements and Equation 3.30. The figure shows that the highest estimate of K_d ($1.27 m^{-1}$) were observed on the 5th December 2006, 22nd March 2007, 5th February 2008 and 13th March 2008. The lowest K_d ($0.24 m^{-1}$) was on the 4th April 2006. The average K_d was $0.62 m^{-1}$ (Table 3.3).

Using Equation 3.12, K_d estimates were used to calculate the depth at which the irradiance was 1% of the surface irradiance (z_{eu}). Descriptive statistics of z_{eu} are given in Table 3.3. The depth of the 1% irradiance level ranged between 3.6 and 18.9 m, with average of 8.4 m. Therefore, except for the winter period, on average the euphotic zone encompassed the whole of the water column. The seasonal trend in z_{eu} was the inverse of the seasonal trend of K_d (Figure 3.17).

To understand the contribution of the different Optically Active Components (OACs) to the variability in K_d , estimates of K_d (see Figure 3.16) were regressed

against the main OACs (SPM, log-chlorophyll and log-CDOM concentrations). The regression was statistically significant (analysis of variance, $n = 37$, $p < 0.001$,) and R^2 was approximately 0.48 (Equation 3.32). SPM accounted for 36% of K_d variability and chlorophyll concentration for approximately 9%. CDOM concentration was not significantly related to K_d ($p > 0.05$). If CDOM was not included in the analysis, the regression was statistically significant (analysis of variance, $n = 37$, $p < 0.001$) with an R^2 of 0.45 (Equation 3.33); the amount of variability of K_d explained by ln-transformed chlorophyll and SPM are the same as for Equation 3.32.

$$K_d = 0.499 - 0.167 \cdot \ln Chl + 0.0402 \cdot SPM_{tot} + 0.338 \cdot \ln CDOM \quad (3.32)$$

$$K_d = 0.415 - 0.178 \cdot \ln Chl + 0.0426 \cdot SPM_{tot} \quad (3.33)$$

Where Chl is the chlorophyll concentration.

Table 3.3. Unit of measure and descriptive statistics (number, mean, standard deviation, median, minimum, and maximum) of: K_d (m^{-1}) from light profiles (K_{dCefas} and K_{dR}) and Secchi depth measurements (from Equation 3.30), and depth of 1% surface light (z_{eu}), at station CLNBuoy in Carlingford Lough, between April 2006 and March 2008.

	Unit	n	Mean	SD	Median	Min	Max
K_d	m^{-1}	47	0.62	0.24	0.56	0.24	1.27
z_{eu}	m	47	8.4	3.0	8.2	3.6	18.9

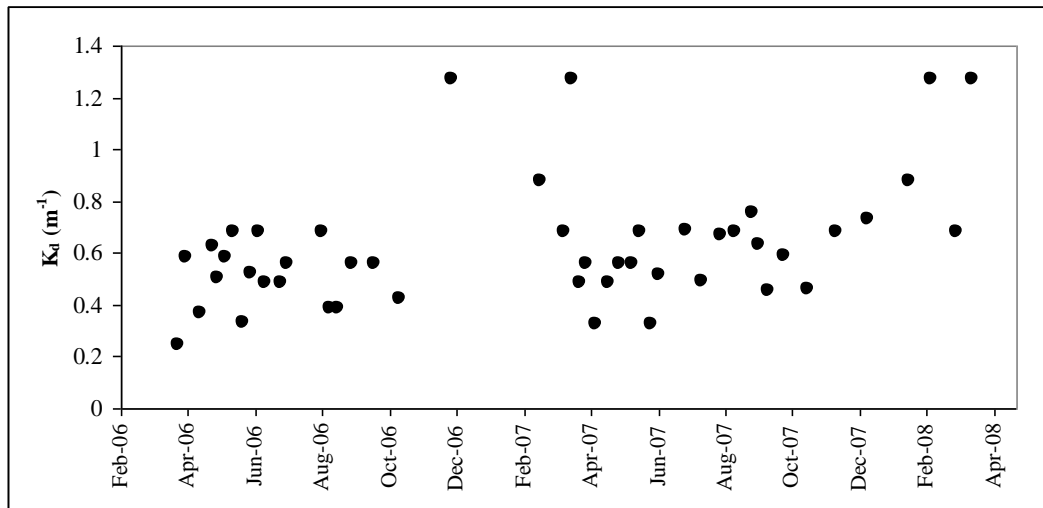


Figure 3.16. Seasonale pattern of K_d (m^{-1}), derived from measurements with Cefas and AFBI light meters (K_{dCefas} and K_{dR}) and from Secchi depth measurements using Equation 3.30, for station CLNBUoy in Carlingford Lough, between March 2006 and March 2008.

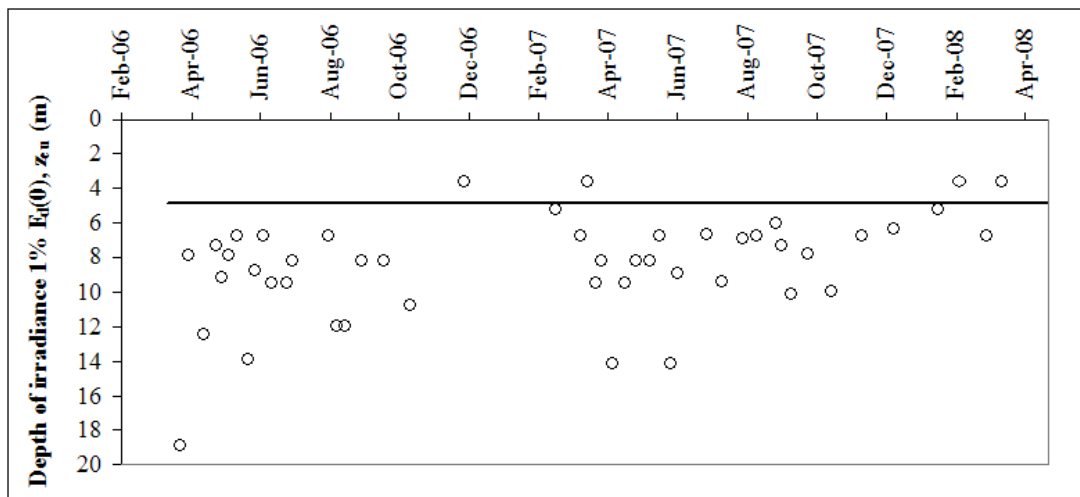


Figure 3.17. Seasonal trend of the depth at which irradiance was 1% of $E_d(0)$, z_{eu} (m), as derived from Equation 3.12, for station CLNBUoy in Carlingford Lough, between March 2006 and March 2008. The solid line represents the average depth (5.5 m) at the station.

3.4 Discussion

3.4.1 K_{dI} and K_{dR}

The availability of PAR is one of the main factors controlling primary production, and it is usually used in models for predicting primary production (e.g. Varela *et al.* 1995; Moll 1998; Skogen and Moll 2000). The reduction of light with depth is regulated by the attenuation coefficient K_d , which can be derived from *in situ* measurements of light, from Secchi disk depth, or from theoretical or empirical models (see section 3.1.5). In this study, attenuation coefficients were derived from PAR measurements by light meters following two approaches which gave two estimates of K_d for each light profile (K_{dI} and K_{dR}).

Considering the entire data set, the two types of K_d were not statistically different, however their estimates were influenced by different environmental conditions (such as wave and cloud effects or the angle of inclination of the light meter). As an example, Figures 3.6 a and b show the variability in profiles of K_d instantaneous and K_d from regressions derived from down cast and up cast of two profiles. In Figure 3.6 a, estimates of K_d derived from regressions from the 2 sensors for the up and down casts (in blue and red) are almost overlapping while the estimates of instantaneous K_d for the down cast (in black) are different. A requirement for the measurements of instantaneous K_d is that the distance between the sensors should be constant, which implies that the light meter should be lowered vertically down the water column. In Figure 3.6 a, the different estimates of the instantaneous K_d are probably due to a change in the angle of inclination of the light meter during the down cast, which altered the distance between the sensors.

Figure 3.6 b shows the opposite. In this example, the up cast and down cast estimates of K_d from regressions differ while the estimates of K_d instantaneous were similar. In this case, the explanation could be related to the effect of clouds or waves which affect estimates of K_d derived from regressions but not those derived from instantaneous measurements. The calculation of the instantaneous K_d was used for checking the estimates of K_d from regressions.

3.4.2 A model for predicting K_d

Estimates of K_d for Carlingford Lough have been obtained from light meter (K_{dR} and K_{dCefas}) and from a relationship with Secchi depth, which was shown to be a good predictor of K_d ($R^2 = 0.92$), and a better predictor than SPM ($R^2 = 0.71$). This result is in contrast with results from Devlin *et al.* (2008) for UK transitional and coastal water, where SPM explained 98% of the variability in K_d for coastal/offshore waters and Secchi depth only 86%. This discrepancy could be explained considering that the equation adopted in this study (3.30) has been derived from a single location (Carlingford Lough) and based on data for one year (2007), while the relationships in Devlin *et al.* (2008) were calculated using data from different sites in UK coastal waters and during a period of two years time (2004 and 2005).

Regression of K_d versus OACs for Carlingford Lough showed that SPM explained approximately 30% of the variability in K_d , followed by chlorophyll concentration which explained 9%. The importance of SPM as the main source of variation of K_d is in agreement with the results of Devlin *et al.* (2009) for UK waters, although in the study in Carlingford Lough the variance explained by SPM is three-fold smaller than in the Devlin *et al.* paper. This difference could be related to the smaller data set used for the Carlingford Lough study. It is also important to note that part of the variability in K_d could be related to other variables which have not been taken into account in the regression. These include variation in the spectral distribution of the submarine light, the variability in the scattering property of SPM in relation to the particle size, or the different light absorption ability of different types of phytoplankton organisms (Devlin *et al.* 2009).

Although the variation in K_d explained by chlorophyll was small (9%), chlorophyll concentration was significantly and negatively related to the diffuse attenuation coefficient. In this context, phytoplankton blooms with chlorophyll concentrations $> 10 \text{ mg m}^{-3}$ (4th April 2006, 1st June 2006 and 29th March 2007) occurred when K_d was low $< 0.5 \text{ m}^{-1}$. In Figure 3.12 it is possible to see that the K_d profiles for the 4th April 2006 and for the 1st June 2006 were characterised by some of the lowest K_d estimates derived from light meters for the sampling station. The association of phytoplankton blooms in Carlingford Lough with low K_d is in agreement with observations for the Solent where chlorophyll concentration $> 10 \text{ mg}$

m^{-3} during the spring bloom occurred only when K_d was $\approx \leq 0.5 \text{ m}^{-1}$ (Iriarte and Purdie 2004).

3.4.3 Seasonal variability of K_d

The highest K_d values were observed in Carlingford Lough between December and March (2006-07 and 2007-08, Figure 3.16) when SPM concentrations were $> 10 \text{ mg L}^{-1}$ (Figure 3.9). Estimates of $K_d > 1 \text{ m}^{-1}$ were generally associated with windy weather (e.g. Beaufort scale 5-6 on the 22nd March 2006 and 5th February 2008) and with period of high freshwater run off from the Clanrye River (e.g. $> 12 \text{ m}^3 \text{ s}^{-1}$ on the 5th December 2006). This suggests that the high SPM concentrations, and consequently the stronger attenuation of underwater light, were caused by bottom sediment resuspension (due to the stirring action of strong wind), or that suspended materials were introduced in the Lough with freshwater outflow.

The range of variability of K_d in Carlingford Lough ($0.24 - 1.27 \text{ m}^{-1}$, Table 3.3) is comparable to ranges of K_d calculated for the Scottish Sea Loch Etive ($0.20 - 0.92 \text{ m}^{-1}$, Wood, Tett and Edwards 1975), the Solent in the South of England ($0.3 - 1.9 \text{ m}^{-1}$, Iriarte and Purdie 2004), and in general corresponds to the water type “coastal sheltered marine lagoons” ($0.1 - 1.3 \text{ m}^{-1}$) in the classification by Devlin *et al.* (2008). However, the average diffuse attenuation coefficient in Carlingford Lough (0.62 m^{-1} ; Table 3.3) is higher than K_d estimated for the Scottish sea loch Creran ($0.17 - 0.38 \text{ m}^{-1}$, Tett and Wallis 1978), the Western Irish Sea ($0.14 - 0.35 \text{ m}^{-1}$, Gowen and Bloomfield 1996), Irish coastal waters ($0.19 - 0.57 \text{ m}^{-1}$, Gowen *et al.* 2000), and the North Sea – Baltic sea transition region (average 0.23 m^{-1} , Lund-Hansen 2004).

Only measurements of Secchi depths were available for comparison with other Northern Ireland sea loughs, such as Belfast Lough and Strangford Lough (Parker, Rosell and MacOscar 1988; Service *et al.* 1996). The range of Secchi depths for Carlingford Lough (1 - 5 m) is similar to the range for the outer Belfast Lough ($< 1 - 6 \text{ m}$; Parker, Rosell and MacOscar 1988; Service *et al.* 1996), but smaller than the range measured in Strangford Lough (1.5 – 10 m, Service *et al.* 1996).

Considering the variability of the attenuation coefficient with depth, different type of K_d profiles could be observed (Figures 3.6 and 3.12). In Figure 3.6 a, K_d was

approximately constant with depth (suggesting that the OACs in the water column were homogeneously distributed), while in graphs b and c of the same figure, K_d varied with depth. In graph b (Figure 3.6) K_d was higher near the bottom while in graph c it was higher at the surface and decreased towards the bottom, suggesting that the distribution of the OACs in the water column was not homogeneous. The same variability in vertical profiles can also be seen in Figure 3.12 which shows the profiles of the average K_d from regressions on each occasion that measurements were made. In this figure, the profiles measured on the 4th of April and 1st of June 2006, K_d was approximately constant with depth, while other profiles (e.g. 9th and 16th of May 2006) K_d was higher closer to the surface. Vertical stratification calculated for the 4th April and the 1st June 2006 was weaker ($\Delta(T+S) = 1.2$; see section 2.3.1) than stratification estimated for May 2006 (average $\Delta(T+S) = 3.8$). Considering that the salinity gradient was the main driver of stratification, the higher K_d at the surface in May could have been related to a higher concentration of OACs in the less saline surface layer.

3.4.4 Timing of the start of the phytoplankton spring bloom

Focusing on the phytoplankton spring bloom and the environmental variables influencing its timing, observations from 2006 and 2007 suggest that low light attenuation coefficient ($< 0.5 \text{ m}^{-1}$) is one of the factors that allows the phytoplankton population to increase. During winter, nutrients were abundant (section 2.4.1), due to remineralisation processes, and phytoplankton was limited by the low solar radiation and the short days. In fact, between December and mid March (2006 – 2008) there were events when $z_{eu} < 5.5 \text{ m}$ with $K_d > 1 \text{ m}^{-1}$ (5th December 2006, 22nd March 2007, 5th February 2008 and 13th March 2008). In March/April the light level began to increase and z_{eu} started to exceed the depth of the water column, allowing the phytoplankton population to receive enough light to increase the rate of photosynthesis and utilisation of nutrients. During the rest of the year, the water column at the sampling station in the Lough had irradiance $> 1\%$ of $E_d(0)$ (Figure 3.17).

It has also been suggested that the phytoplankton spring bloom occurred when a certain threshold of daily irradiance in the Surface Mixed Layer (SML) has

been reached (Riley 1967; Gowen *et al.* 1995). Gowen *et al.* (1995) observed that in the N-W Irish Sea the spring increase in phytoplankton production was associated with a daily irradiance in the surface mixed layer between 183 and 245 $\text{W m}^{-2} \text{d}^{-1}$. In 2006, the sampling activity in Carlingford Lough started on the 4th April when the spring bloom was already in progress (chlorophyll concentration of 11.42 mg m^{-3}) and the daily irradiance of the water column was 1214 W m^{-2} . The variability in the daily column irradiance for station CLNBuoy in Carlingford Lough from mid February 2007 to the end of March 2007 is shown in Figure 3.18. It is possible to observe that on the 21st of February chlorophyll concentration was 0.9 mg m^{-3} (suggesting that the spring bloom had not started yet) and the daily irradiance of the water column was 101 W m^{-2} . At the time of the next sampling event, on the 15th March, the average chlorophyll concentration for the water column was 8.1 mg m^{-3} and the daily irradiance of the water column was 206 W m^{-2} . Measurements of surface chlorophyll from the automated mooring in Carlingford Lough from the end of February 2007 to the end of April 2007 (Figure 3.19) suggest that phytoplankton growth started to increase slowly from the end of February but peaked on the 14/15th March; therefore the value of daily irradiance measured on the 15th March is in agreement with the range identified by Gowen *et al.* (1995) for the Irish Sea. Furthermore, the average daily water column irradiance for the week prior to the start of the spring bloom was 209 W m^{-2} .

Similar observations have been made for the spring bloom in the Solent. Iriarte and Purdie (2004) concluded that chlorophyll concentrations $> 10 \text{ mg m}^{-3}$ occurred when daily irradiance of the SML was approximately 200 $\text{W m}^{-2} \text{d}^{-1}$. In Carlingford Lough concentration of chlorophyll $> 10 \text{ mg m}^{-3}$ occurred on the 29th March 2007 (20.9 mg m^{-3}) when daily irradiance of the water column was 184 W m^{-2} . Although this value for the 29th of March is slightly lower than the one derived for the Solent, it is important to note that the average irradiance in the week prior to the peak in chlorophyll concentration in Carlingford Lough was 319 W m^{-2} .

The peak in chlorophyll of the 29th March 2007 is in agreement with the observations by Taylor, Charlesworth and Service (1999), who measured the highest chlorophyll concentration (10 mg m^{-3}) at the end of March in 1997. In contrast, Ball, Raine and Douglas (1997) measured a peak (6 to 9 $\text{mg chlorophyll m}^{-3}$) in April 1992, and Douglas (1992) recorded a peak (19.44 mg m^{-3}) in early May 1990 and 1991. This difference might reflect differences in sampling frequency. Ball, Raine

and Douglas (1997) and Douglas (1992) sampled monthly and it is possible that they missed the spring bloom. Taylor, Charlesworth and Service (1999) adopted a weekly sampling frequency similar to the one used in this study.

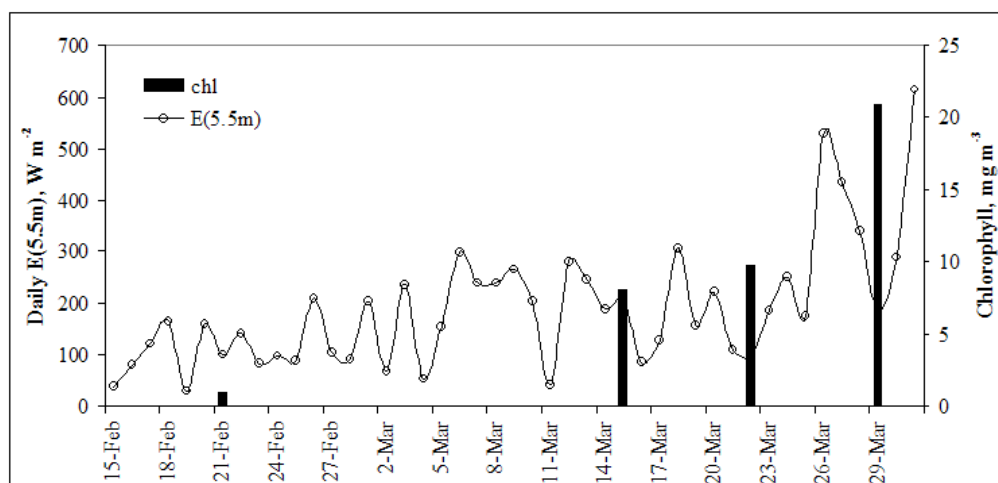


Figure 3.18. Variability in daily average irradiance of the water column (E(5.5m)) expressed in $W m^{-2}$, and chlorophyll concentration ($mg m^{-3}$) for the period 15 February 2007 to 31 March 2007, at the station CLNBuoy.

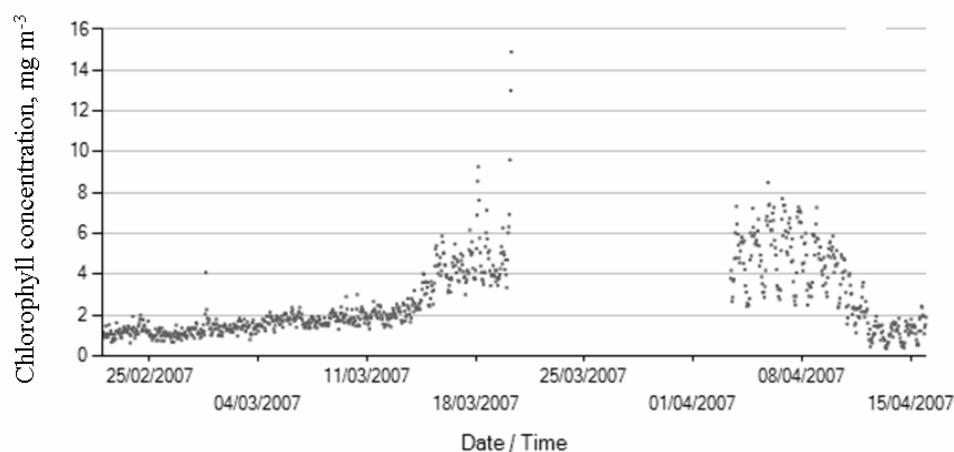


Figure 3.19. Chlorophyll concentration ($mg m^{-3}$) from the automated buoy in Carlingford Lough (CLNBuoy) for the period 22nd February 2007 to 16th April 2007. The plot was generated by the AFBI website (<http://www.afbini.gov.uk/index/services/services-specialist-advice/coastal-science/coastal-monitoring/monitored-sites/carlingford-lough-north.htm>) and the data were not quality assured.

3.5 Conclusions

From the analysis of the underwater light field in Carlingford Lough and its attenuation with depth, it was possible to observe that:

- the calculation of K_{dI} was useful as a check on the estimates of K_{dR} ;
- the estimates of the light attenuation coefficient in Carlingford Lough showed a seasonal variability (with maximum during the winter months) and also vertical variability;
- the estimates of K_d derived for Carlingford Lough were comparable with estimates of the attenuation coefficient for the Scottish Sea Loch Etive and the Solent in the South of England;
- suspended solids were the Optically Active Constituent that explained the higher proportion of variability in K_d (30%), followed by chlorophyll concentration (9%). Secchi depth proved to be the best predictor of K_d ($R^2 = 92\%$). However it was not fully understood what controlled the light extinction in the Lough and it was not possible to define the typical shape of the K_d profile;
- the sub-surface light climate was considered to be the main factor controlling the beginning of the phytoplankton production season. In 2007, the phytoplankton spring bloom started during the 14 and 15th March when the daily irradiance of the water column was 206 W m^{-2} . The timing of the peak in chlorophyll concentration (approximately 21 mg m^{-3}) at the end of March 2007 is in agreement with previous observations by Taylor, Charlesworth and Service (1999);
- chlorophyll concentrations $> 10 \text{ mg m}^{-3}$ have been observed when $K_d < 0.5 \text{ m}^{-1}$.

CHAPTER 4

The ^{14}C technique

4.1 Introduction

This chapter aims to provide a review of the main techniques used for measuring primary production (highlighting advantages and disadvantage) with particular focus on the ^{14}C technique. Chapter 4 also aims to give a description of the standard operating procedure developed during the primary production experiments with samples from Carlingford Lough, and the problems encountered in the setting up of the method.

4.1.1 Primary production measurements

Primary production is the rate of fixation of inorganic carbon (CO_2) into organic carbon ($(\text{CH}_2\text{O})_n$) during photosynthesis. The latter involves a number of different processes (e.g. carbon assimilation, oxygen production) which can be measured and used as a proxy for estimating primary production (Beardall, Ihnken and Quigg 2009).

The techniques for measuring primary productions can be grouped into 4 types that focus on different parts of the photosynthetic process. The first group of techniques involves the use of a tracer, a radioisotope (^{14}C) or a stable isotope (^{13}C or ^{18}O), that is added to water samples and taken up by phytoplankton organisms during an incubation. The ^{14}C tracer is added to the sample as bicarbonate (H^{14}CO_2). After incubation, the ^{14}C incorporated into the phytoplankton cells is assayed using standard radioisotope techniques (Steemann Nielsen 1952). The procedure based on ^{13}C is similar to the ^{14}C procedure with the exception that a mass spectrometer is used for estimating the ^{13}C incorporated into the cell (Slawyk, Collos and Auclair 1977; Mousseau *et al.* 1995). The $^{18}\text{O}_2$ is added as H_2^{18}O and after incubation the dissolved gasses in the sample are extracted by vacuum degassing. The recovered O_2 (containing the $^{18}\text{O}_2$) is combusted to CO_2 and analyzed in a mass spectrometer (Bender *et al.* 1987). The ^{14}C method measures gross or net production depending on the length of the incubation. If the incubation is short (1-3 hours), the technique estimates gross photosynthesis (the ^{14}C has not returned to the water following respiration). With longer incubations (12-24 hours) the method gives results that are less than gross primary production (because some of the ^{14}C has returned to the water

following respiration) and can be approximated to net production (Marra 2009). The ^{18}O technique provides an estimate of gross primary production.

The second type of technique is also called the “light and dark bottle oxygen method” and involves changes in dissolved oxygen or total inorganic carbon concentrations over a known time (typically 12-24 h) in a water sample. The duration of incubation should be long enough to include a light period when both photosynthesis and respiration occur, and a dark period when only respiration occurs. Change in oxygen concentration over this period in the light bottles gives a measure of net microplankton community production which includes respiration of heterotrophic organisms, such as bacteria and protozoa (Williams, Raine and Bryan 1979). Gross primary production can be estimated by adding the respiratory loss of oxygen in the dark bottle to the net production measured in the light bottle. It is assumed that respiration in the dark is equal to respiration in the light.

The third type of techniques for measuring production involves measurements of the ratios and anomaly of isotopes ($^{17}\text{O}:^{16}\text{O}$, $^{18}\text{O}:^{16}\text{O}$ and $\text{O}_2:\text{Ar}$) in water and in the atmosphere. The triple isotope O_2 method, or ^{17}O anomaly ($\Delta^{17}\text{O}$), is based on the estimation of the ratios of $^{17}\text{O}:^{16}\text{O}$, and $^{18}\text{O}:^{16}\text{O}$. This method is based on the principle that atmospheric O_2 is depleted in ^{17}O , due to photochemical reactions in the stratosphere. This non-biological isotope signature of ^{17}O is removed by the photosynthetic process and can be used to derive oxygen production by photosynthesis (Luz and Barkan 2009). In relation to the other method ($\text{O}_2:\text{Ar}$), O_2 concentration in the ocean is affected by both physical and biological processes, while argon (Ar) which has similar physical properties to oxygen has no biological sink or source. Thus, estimating Ar physical supersaturation and removing it from oxygen concentration it is possible to obtain the “biological O_2 supersaturation” (Luz and Barkan 2009). Detailed description of the triple isotope O_2 method and the $\text{O}_2:\text{Ar}$ method can be found in the review by Luz and Barkan (2009). The $\Delta^{17}\text{O}$ method determines gross O_2 production because it is affected by photosynthesis (and also oceanic dynamics and gas exchange at the air-water interface) but not by respiration. On the other hand, the $\text{O}_2:\text{Ar}$ method provides estimates of net O_2 production (Luz and Barkan 2009).

The fourth group of techniques (Pulse Amplitude Modulated – PAM – Fluorometry and Fast Repetition Rate fluorometry- FRRf) focus on changes of the cellular fluorescence in microalgae. These techniques consider the activities of

photosystem II (PSII) during light reactions and in particular the change in chlorophyll *a* fluorescence yield of the PSII. During photosynthesis, NADP reduction and ADP phosphorylation (which are detected as changes in fluorescence) are carried out by electron transport. The electrons needed for these processes have been withdrawn from water molecules, together with protons, leading to O₂ evolution. Thus the electron transport rates (ETRs) can be related to the gross O₂-evolution (see reviews by Beardall, Ihnken and Quigg 2009 and Suggett *et al.* 2009).

The technique that has been used most widely is the ¹⁴C technique, developed by Steemann Nielsen (1952). Furthermore, the techniques described above are generally assessed against ¹⁴C uptake experiments. It is also important to highlight that although the ¹⁴C technique is considered to be the “*pre-eminent means of measuring primary production*” (Marra 2009), it is not a ‘gold standard’ for primary production measurements. In fact it is still not completely clear whether ¹⁴C assimilation in long term incubations measures net primary production (Marra 2009).

Comparisons between results from ¹⁴C with ¹³C incubations generally show good agreement although differences have been observed that are related to biological and/or environmental conditions such as phytoplankton biomass and/or irradiance (Mousseau *et al.* 1995). The ¹³C technique eliminates the health risk associated with the radioactive nature of ¹⁴C but it requires a larger sample volume due to the lower sensitivity.

Grande *et al.* (1989) compared estimates of primary production obtained with the ¹⁸O₂, O₂ light and dark bottles and ¹⁴C techniques and found good agreement between *in situ* incubations. ¹⁸O₂ rates of gross production were similar to those estimated with the light and dark bottle oxygen method, but ¹⁴C estimates only represented 60-100% of the production measured with the ¹⁸O₂. In contrast, rates estimated with simulated *in situ* ¹⁸O₂ incubations were twice the values derived from light/dark bottles and 2-3 times the ¹⁴C estimates. One explanation for the higher production measured by the ¹⁸O₂ method compared to estimates derived from the ¹⁴C method could be associated with the re-fixation of the respired CO₂ by the cell (Ryther 1956). If re-fixation occurs in the cell, the ambient CO₂ will be taken up proportionally less than the ambient H₂O (because there is a source of C within the cell). Thus in this situation the application of the ¹⁸O method would give an estimate of production higher than the ¹⁴C method (Marra 2009).

Generally there is close agreement between ^{14}C method and light and dark bottle oxygen method; however there are some discrepancies especially in conditions of low nutrient concentrations, high levels of irradiance, or low production/respiration ratios (Peterson 1980).

General limitations for the first and second types of techniques (tracer techniques and light and dark bottle oxygen method) are related to the “bottle effect” (Marra 2009) and the measurements of respiration. These techniques require incubation of the samples; consequently there are concerns about the effects of enclosing a water sample in a container (e.g. loss of turbulence, damage to organisms, grazing by micro- and mesozooplankton). With respect to the light and dark bottle oxygen method, the long incubation time can result in no, or even negative, net microplankton community production due to respiration by the heterotrophic community.

The third and fourth types of techniques for measuring production (e.g. $\text{O}_2:\text{Ar}$, FRRf) do not require an *in vitro* incubation but they estimate primary production from *in situ* measurements. Comparisons of ^{14}C uptake rates with oxygen production during experiments off Bermuda in 2000 showed that gross oxygen production derived by the $\Delta^{17}\text{O}$ technique was higher than production estimated using the ^{14}C technique. At the same time, production derived from ^{14}C assimilation was higher than net oxygen production derived from $\text{O}_2:\text{Ar}$ ratio (Luz and Barkan 2009). The authors associated the higher gross oxygen production (compared to production estimated with ^{14}C) to very rapid rates of O_2 cycling in PSII, or to mechanisms, such as photorespiration, which involve O_2 consumption with little CO_2 release. They also advise caution when comparing rates of carbon and oxygen production because their ratio varies over a wide range.

Electron transport rate (ETR) has been used in aquatic productivity studies since the 1990s. FRRf provides extremely rapid *in situ* measurements (μ to milli seconds, and no requirement of incubation). However the conversion from electron transport to changes in CO_2 or O_2 is still not well characterised (Suggett *et al.* 2009). As an example, Suggett *et al.* (2009) simultaneously measured ETR_{PSII} (by FRRf), gross and net O_2 evolution (^{18}O technique and using a mass inlet membrane spectrometry, MIMS) and C fixation (^{14}C technique) for 6 microalgal species under different growth conditions. The relationship between ETR_{PSII} and gross O_2

evolution was good ($R^2 = 0.81$) while ETR_{PSII} exceeded ^{14}C uptake by a factor between 5.4 and 11.6.

Finally, primary production over large geographical scales can be derived from remotely-sensed visible spectral radiometry (ocean colour; e.g. Platt *et al.* 2008). This provides a synoptic view of a variable (e.g. chlorophyll concentration) which would not be possible with traditional sampling methods from research vessels. However, in the context of primary production the implementation of remote sensing requires the development of local algorithms that relate pigment biomass to primary production, and ^{14}C uptake is generally used to validate these algorithms (Marra 2009; Tilstone *et al.* 2009).

Considering that the ^{14}C method is used for comparison with other techniques and it is well recognised for its high sensitivity, it was chosen as the technique for estimating primary production in this study of Carlingford Lough.

4.1.2 The ^{14}C technique

The principle and technique of the ^{14}C incubation was described first by Steemann Nielsen (1952) and outlined, with some small changes, by Strickland and Parsons (1967).

This method gives an estimation of the uptake of dissolved inorganic carbon (DIC) from the water by phytoplankton, during photosynthesis. A known amount of $H^{14}CO_3^-$ is added to a water sample with known volume and content of CO_2 (the latter calculated from salinity following the method indicated by Strickland and Parsons 1968). Samples are incubated for a known period of time under ambient conditions of temperature and light. During the incubation, phytoplankton take up ^{14}C . After the incubation phytoplankton organisms, with their assimilated organic radioactive carbon, are separated from the water and the remaining inorganic carbon by filtration. The radioactivity of each filter is counted using a scintillation counter (Peterson 1980).

Steemann Nielsen (1952) required three conditions to be met so that the method could provide a measure of gross production:

1. $^{14}CO_2$ should be incorporated only through photosynthesis;
2. $^{14}CO_2$ assimilation rate should be equal to $^{12}CO_2$ assimilation rate;

3. $^{14}\text{CO}_2$ should not be lost through respiration.

In fact none of these conditions are exactly met and some corrections are necessary. Carbon dioxide is also assimilated in the dark (dark fixation). This value can be measured in a dark bottle and subtracted from values of carbon fixation for each light bottle (Cadée 1983). Dark fixation is usually 1-3% of fixation at saturating irradiances (Cadée 1983; Steemann Nielsen 1952) and it is partly biological (probably largely due to bacteria and phytoplankton reactions light-initiated) and partly non-biological. For the second condition, ^{14}C has a different atomic mass compared to ^{12}C and it is assimilated slower. Steemann Nielsen (1952) estimated that ^{14}C is assimilated 6% slower than ^{12}C . Finally, ^{14}C is lost during experiments through respiration (dark respiration and photorespiration) and excretion processes as extracellular products. The latter refer to the release from the cell of products synthesized during photosynthesis or related to it (e.g. glycolate). Steemann Nielsen (1952) estimated that 4% of the organic matter produced during photosynthesis was lost through respiration, in a 4-hour experiment. Normally cells release no more than 5% of fixed carbon (Vegter 1983).

Steemann Nielsen (1952) also discussed a number of conditions under which the ^{14}C method may not give good results, such as low irradiance or high heterotrophic bacterial activity. Finally, another source of error can be sample filtration: some phytoplankton organisms pass through the filter and/or dissolved organic matter released during incubation may be absorbed by the filter (Maske and Garcia-Marquez 1994).

Although this technique is not free from errors, the ^{14}C method has been used worldwide since the 1970s. According to Marra (2002) the reasons for this include:

1. the isotope is safe to handle and simple to obtain (compared with other isotopes). ^{14}C is an ideal isotope because it is added in small concentrations; the form is specific to one metabolic pathway; given that phytoplankton organisms are unicellular, it is acceptable to assume that the isotope is quickly mixed through cellular organelles;
2. the method is relatively easy to undertake;
3. it is not possible to get a negative result: there will always be uptake even if is not connected with photosynthetic fixation;
4. it is the most sensitive method available.

In relation to the last point, Strickland and Parsons (1967) stated that the sensitivity of the technique depended to a greater part on the amount of ^{14}C added and on the precision of the radiochemical part of the procedure. They identified the lower limit as 0.01 mg C m^{-3} .

As stated above, the ^{14}C technique requires the incubation of water samples and according to Brown (1982) there are three types of incubation which are mainly used:

- 1) *in situ* (IS): incubation of water samples in the sea at the depths from which the samples are collected;
- 2) simulated *in situ* (SIS): this type of incubation uses natural light. Typically it takes place on the deck of a research ship in a water bath at constant temperature. The sun light is appropriately reduced using neutral-density filters placed over the bath to reproduce irradiance at different depths;
- 3) artificial light incubator: this type of incubation is carried out in the laboratory in an incubator with a constant light source. Using a combination of neutral density filters, it is possible to obtain a light gradient, so that samples are incubated at different irradiance levels. An example of a light gradient incubator is the photosynthetron (Lewis and Smith 1983).

Each of these incubation methods introduces some errors and limitations (Brown 1982). *In situ* measurements are considered the simplest and most reliable type of incubation, but during the incubation onboard a research ship, the vessel has to remain or return to a given location, thus limiting the area that can be sampled and monopolizing ship time (Lohrenz *et al.* 1992). Furthermore, samples incubated by the IS method are exposed at fixed light depths compared to natural conditions where phytoplankton can be subjected to vertical movement through the water column. SIS and artificial light incubator measurements in part overcome the problem of ship time and increase the temporal and spatial resolutions of primary production measurements (Lohrenz *et al.* 1992). Nevertheless, for SIS measurements, it is important to incubate the sample at the *in situ* temperature otherwise estimates of production derived with SIS incubations can differ by more than 50% from estimates derived with IS incubation (Lohrenz *et al.* 1992). Considering the limitations of the artificial light incubations, the light source should be an approximation of natural submarine light and the equipment (e.g. photosynthetron) necessary for this type of incubation can be quite expensive (Lohrenz *et al.* 1992);

The literature regarding the reliability of the results obtained with the three types of incubation is extensive and sometimes contradictory. Some studies (e.g. Brown 1982; Colijn, Cadée and Hegeman 1983; Head 1976; Lohrenz 1992; Lohrenz *et al.* 1992) have found good agreement between the *in situ*, the simulated *in situ* and the artificial light incubator methods, with small differences between the results (e.g. less than 15% or within a factor of 2). However, some of these studies (Brown 1982; Lohrenz *et al.* 1992) also show that there can be large (e.g. 50%) difference between the three types of incubation.

4.2 Standard operating procedure for primary production incubations

4.2.1 Sampling

Water samples for ^{14}C incubations were collected from 4 m depth at the sampling station in Carlingford Lough (CLNBuoy) and kept in a 5 L plastic bottle, wrapped in black plastic bags to avoid exposure to light. Water samples were transferred from the sampler into the 5 L bottle using a plastic tube ending in a 250 μm net to remove mesozooplankton (e.g. copepods). Incubations were usually started within 3 hours of the sample being collected from the Lough.

4.2.2 Light gradient incubators (photosynthetrons)

Water samples from the Lough were incubated in the laboratory using a light gradient incubator called a photosynthetron (Lewis and Smith 1983). An artificial light incubator method was chosen rather than an *in situ* incubation method to reduce the time spent sampling and the use of the boat. Two types of photosynthetron were used in this work. The first type (type 1; Figure 4.1 a and c), used during 2006, was a unit with dimensions of 46 x 27 x 27 cm and a weight of 10.75 kg. It held 24 vials of 25 mm diameter and 20 mL volume, and illumination was provided by two 250 W quartz-halogen lamps. The second type (type 2; Figure 4.1 b and d) was used during 2007 and 2008 and it had a structure similar to the type 1, with the exception that the illumination was provided by 24 halogen bulbs (Aluline Pro, 20W). Experiments from 1 to 19 were run with the type 1 photosynthetron while the others (from 20 to 43) with the type 2 photosynthetron.

These incubators have the benefit of requiring a small volume of seawater (Babin, Morel and Gagnon 1994; Lewis and Smith 1983). Consequently water samples were incubated in scintillation vials reducing sample manipulation and the amount of glassware used. Furthermore, samples do not require filtration at the end of the incubation, and acidification is used to remove the unused ^{14}C , thereby further reducing sample manipulation. The photosynthetrons were connected to a temperature controlled water bath that maintained a constant temperature during the incubation. A glass window chamber connected to the tap water, and positioned between the bulbs and the sample holder, was also required for the type 2

photosynthetron to reduce the heat produced by the bulbs. Incubations were run at the same temperature as the water from which the water sample was collected.

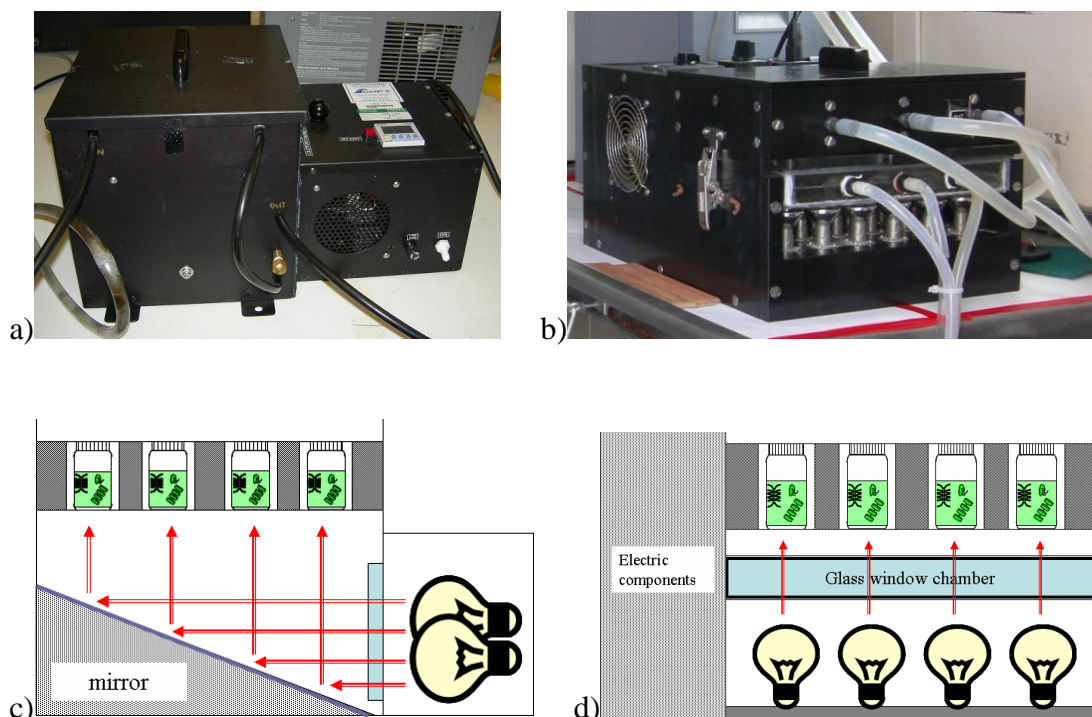


Figure 4.1. Type 1 photosynthetron (a) and type 2 photosynthetron (b), and schemes of their internal functioning system (c for type 1 and d for type 2).

Irradiance levels in each position of the sample holder of the photosynthetrons were modified using neutral density filters. In the type 1 photosynthetron the filters were cut into circles with diameters slightly larger than the base of the vials, and held in place by an ‘O’ ring, while in the type 2 photosynthetron the filters were cut into squares and placed in a small tray positioned underneath each sample holder. A combination of different filters was used to obtain the desired range of light levels.

The irradiance levels in each position of the sample holder were checked using a Biospherical QSL 100 sensor, before and after the incubation. During the measurement, the light gathering sensor head was immersed in a vial containing 5 mL of water. Incubations were run with a range of irradiance between 1 and 1400 $\mu\text{E m}^{-2} \text{s}^{-1}$. Up to experiment 21 the maximum irradiance in the photosynthetron was less

than $700 \mu\text{E m}^{-2} \text{s}^{-1}$, while from experiment 22 to 43 the irradiance was up to 1200-1400 $\mu\text{E m}^{-2} \text{s}^{-1}$.

Some functional limitations of the photosynthetrons were observed. These were primarily related to the filter placement, overheating of the samples and light variation during incubation. In the type 1 photosynthetron the filters were difficult to place in position at the bottom of the sample holder, and often the surface of the filters was concave instead of flat. In the type 2, the presence of a small tray underneath the sample holder made this operation easier. Overheating of the sample was a major problem in the type 2 photosynthetron due to the positioning of a light bulb a few centimetres below each vial. The use of the glass chamber, connected to running supply of cold water reduced the heating but restricted the photosynthetron to a position close to a water supply. In the type 1 photosynthetron overheating was not a problem because the light bulbs were located in a different section of the photosynthetron, which was separated by a glass window (see Figure 4.1 c).

In relation to the light variation during incubations, the type 2 photosynthetron exhibited a bigger variation in irradiance during the incubation (Figure 4.2 b). Variations in light intensity during the incubation occurred during all the experiments however the differences in irradiance before/after the incubation were bigger using the second type of photosynthetron (Figure 4.2). With the type 1 photosynthetron the variation was always less than $20 \mu\text{E m}^{-2} \text{s}^{-1}$, except for experiment 17, position C5, which showed a variation of $40 \mu\text{E m}^{-2} \text{s}^{-1}$. Variations in irradiance in the type 2 reached 200-300 $\mu\text{E m}^{-2} \text{s}^{-1}$ (Figure 4.2 b), representing a reduction of up to 61% in irradiance during the incubation. Usually the greatest variation occurred in positions set at the higher irradiance of the light gradient. The smaller light variation in the type 1 photosynthetron suggests that the use of two bulbs with the reflection system was more reliable than the use of 24 single bulbs.

Based on the previous consideration, the use of a type 1 photosynthetron is recommended for further incubations. Furthermore, it is also recommended that the irradiances in the sample positions are measured before and after each incubation and to use a mean of these two values in further analysis.

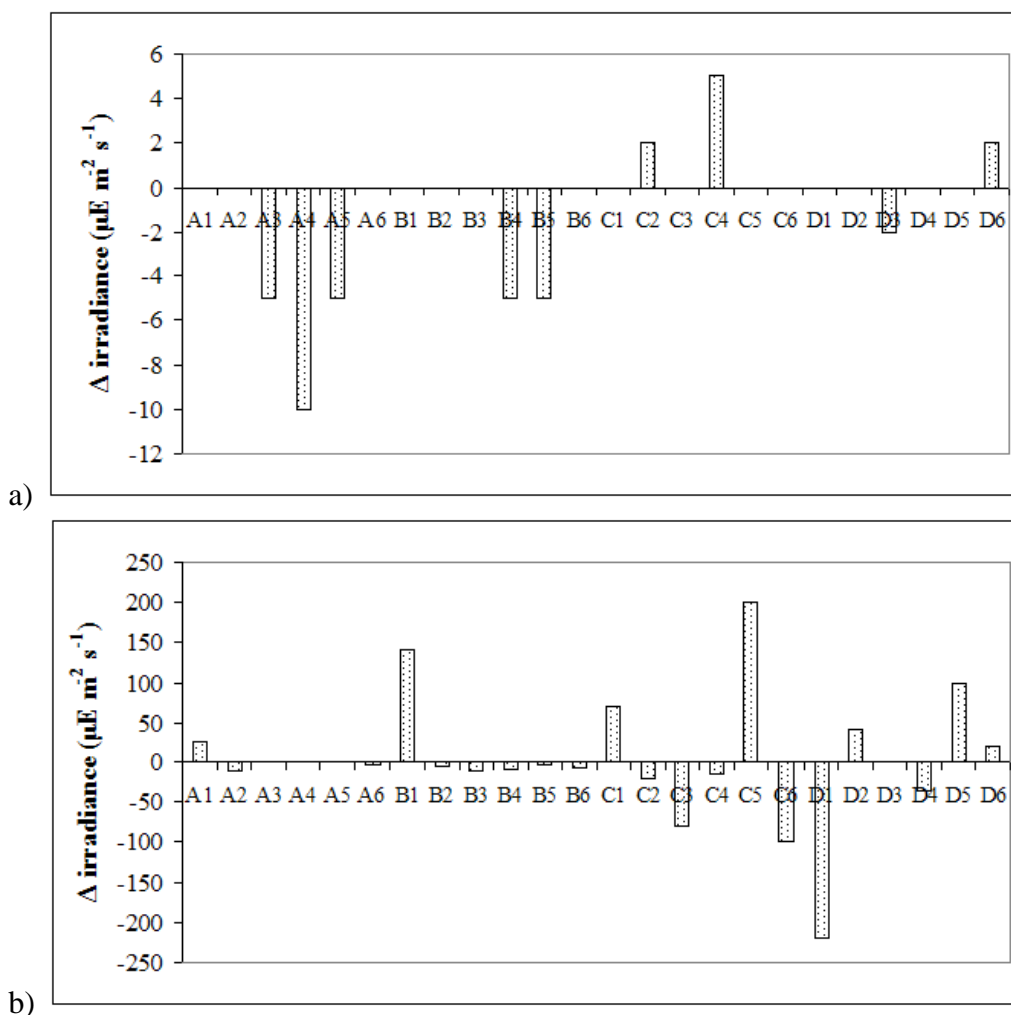


Figure 4.2. Example of variation in light intensity before/after incubation (Δ irradiance in $\mu\text{E m}^{-2} \text{s}^{-1}$), using the type 1 photosynthetictron (a) and the type 2 (b). The letter-number code on the x-axes refers to the positions of the vials in the photosynthetictrons.

4.2.3 ^{14}C incubations

Preparation of the stock solution

A ^{14}C stock solution was prepared in March 2006 and used in all experiments providing a standard source of isotope for each incubation. When not in use the solution was stored in a fridge. ^{14}C has a half life estimated as 5730 ± 40 y, which means that a solution can be stored for all of the sampling period without any significant loss in activity. The stock solution was prepared by adding 1 mCi (37 MBq) of ^{14}C to 20 mL of low nutrient sea water (salinity 35, batch LNS15, nutrient

less than 1 μM , Ocean Scientific International Limited, OSIL). For each experiment 100 μL of stock solution, with a theoretical activity of 185 KBq, were used.

In reality, the activity inoculated in the seawater samples ranged between 85 KBq (experiment 43) and 188 KBq (experiment 4). The activity of the stock solution decreased linearly during the study period, as shown by the plot of the average total activity (TA) of each experiment (Figure 4.3). The trend was particularly clear from 2007 (Figure 4.3 b), when an average reduction of 2% of the stock solution activity was observed between one experiment and the following one.

In general during incubations, phytoplankton used approximately 0.1-0.4% of the ^{14}C added, suggesting that the radioisotope inoculated into the sample was well in excess of that required by the phytoplankton. The estimates of a phytoplankton consumption $\leq 0.4\%$ was confirmed during an independent study of the primary production of the Irish Sea, carried out in May and July 2010 (data not shown).

Bacteria consumption could be one of the explanations for the reduction in activity of the stock solution, while ^{14}C natural decay could be excluded considering the ^{14}C half life of 5730 ± 40 y.

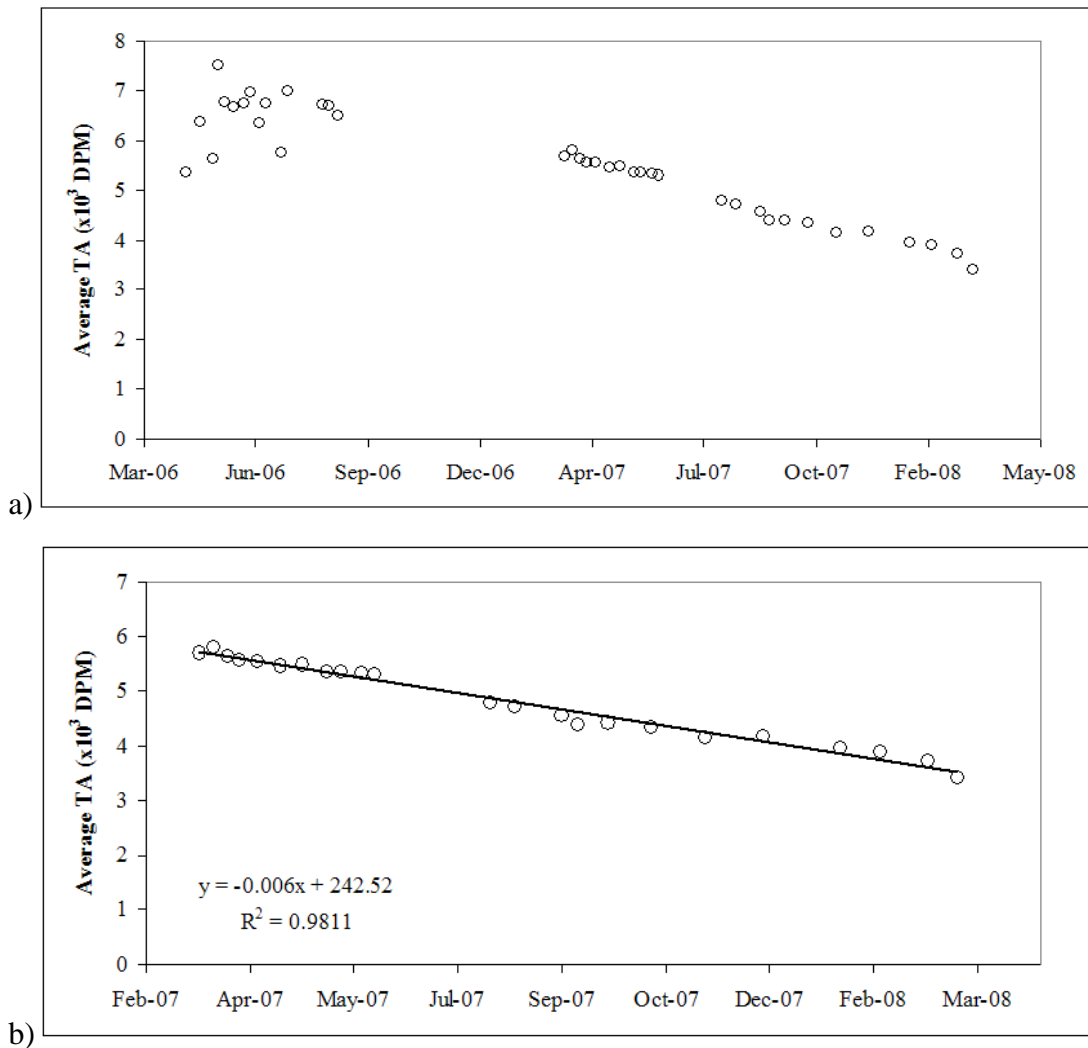


Figure 4.3. Average total activity (TA) calculated for each experiment (a); and highlight of the period March 2007 – March 2008 showing the equation and R^2 of the linear regression (b). The total activity is expressed in $\times 10^3$ DPM.

Incubation procedure

The photosynthetron and the water bath were switched on 30-45 minutes before the start of the experiment. Before each incubation, 32 scintillation vials were labelled:

- 24 'sample vials' with the positions of the sample holder (columns A to D and rows 1 to 6, see Figure 4.4);
- 3 with ' t_0 ' (time-zero);
- 3 with 'TA' (total activity);
- 2 with 'dark' (dark incubation).

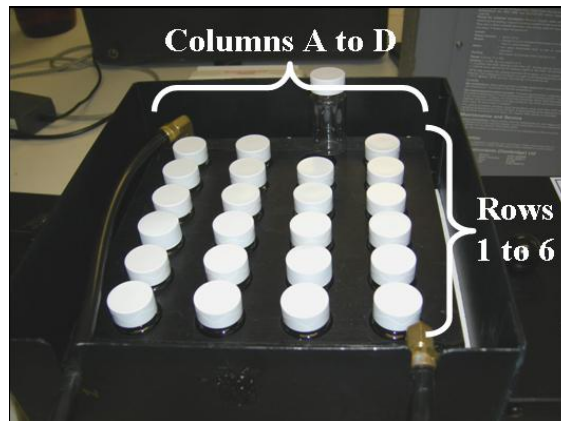


Figure 4.4. View of the vials arrangement in the type 1 and type 2 photosynthetrons.

Once all of the vials had been prepared, the 5 L bottle with the water sample was gently mixed and 150 mL of seawater sample was transferred to a polycarbonate bottle, using a graduated cylinder. Lighting was kept to a minimum in the experimental area to avoid exposing the sample to light before an experiment began. A known volume, 100 μL , of ^{14}C stock solution was added by pipette to the polycarbonate bottle which was gently mixed 10 times to disperse the isotope.

Three 250 μL aliquots of ethanolamine were added to the vials labelled 'TA' prior to the addition of 100 μL of the inoculated seawater sample to each vial. The total activity provided a means of estimating the activity added to the seawater sample and is therefore an internal standard. Three 5 mL aliquots of inoculated seawater sample were added to each of the vials labelled ' t_0 ' prior to the addition of 250 μL of formaldehyde (40%) to each vial to fix the microphytoplankton in the water sample. The three t_0 vials were shaken and stored until analysis. 5 mL aliquots of inoculated seawater sample were pipetted into the 24 'sample vials', which were immediately placed into the correct position in the sample holder of the photosynthetron to start the incubation. Finally, aliquots of 5 mL of inoculated seawater sample were pipetted into the two remaining vials (labelled 'dark') and immediately wrapped in aluminium foil and incubated in the dark at the same temperature and for the same duration as the 24 'sample vials'. During winter, when the chlorophyll concentration was below 1 mg m^{-3} , 10 mL aliquots were used. For these experiments, a double amount of ^{14}C stock solution was added to each vial. The

remaining unused inoculated sea water sample was disposed of down the designated sink in the radioisotope laboratory.

Strickland and Parsons (1967) suggested an incubation time of between 2 and 6 hours, but Lewis and Smith (1983) argued that in just 3-4 hours photoacclimation could take place in the phytoplankton population. Babin, Morel and Gagnon (1994) suggested an incubation time of between 20 and 120 minutes. Incubation time was set for two hours, as suggested in Gargas, Nielsen and Lønholdt (1976), Harding, Meeson and Fisher (1986), Macedo *et al.* (2001) and Tillmann, Hesse and Coljin (2000). For the experiments run during winter 2007-08 the incubation time was set to 3 hours because of the low phytoplankton abundance (chlorophyll concentration < 1 mg m⁻³).

At the end of each incubation, the 24 vials were removed from the photosynthesetron and 250 µL of formaldehyde (40%) added to each vial, including the dark incubation vials, to stop the photosynthetic process. To remove the inorganic ¹⁴C not used by the phytoplankton, 400 µL of 6M (or 6N) HCl were added to the 29 vials (24 'sample vials', 2 'dark' and 3 't₀'). The vials were placed in a tray on a shaking table, inside a desiccator, and the entire apparatus placed in a fume cupboard. Sodium hydroxide pellets were placed in two small plastic basins, on the bottom of the desiccator, in order to trap ¹⁴CO₂ released during acidification. Finally, after acidification for approximately 16 hours, 10 mL of scintillation cocktail (Optiphase Supermix or Ultima Gold) were added to each of the 29 vials and the three 'TA' vials. All the vials were shaken and allowed to stand for 12 hours until the content became clear. The activity of each sample in Disintegrations Per Minutes (DPM) was counted with a Tri-Carb 3100TR Liquid Scintillation Analyser (Perkin Elmer). Scintillation counter internal standards were run before every analysis.

The sodium hydroxide pellets used during the acidification process were dissolved in distilled water in a glass bottle and the resulting solution was disposed of down the designated sink in the radioisotope laboratory. Samples from the sodium hydroxide solution were analysed to check activity and it was found that the pellets trapped 80% of the ¹⁴C released from vials during acidification. The remaining 20% was probably lost in the air (as ¹⁴CO₂) and in the plastic basins containing pellets.

The process from the preparation of the stock solution to analysis in the scintillation counter is summarised in Figure 4.5.

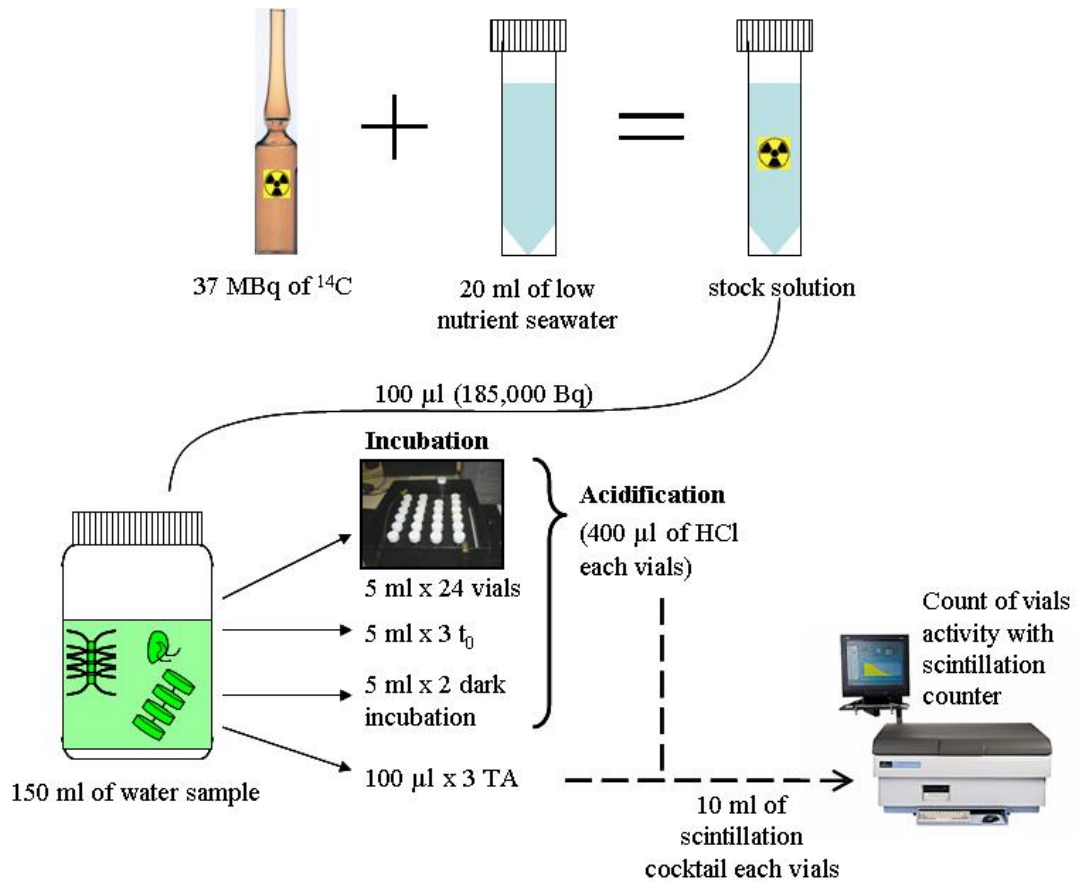


Figure 4.5. Diagram showing the different phases of the ^{14}C technique adopted in this study, from the preparation of the stock solution to the sample analysis with a scintillation counter.

4.2.4 Acidification problem

Steemann Nielsen (1952) and Lewis and Smith (1983) observed that inorganic ^{14}C was completely removed by acidification with HCl 6N in 20-30 minutes and for the first 6 experiments the vials were left to acidify for one hour. However, in these 6 experiments the DPM/irradiance plots (Figure 4.6) did not give the expected curves but flat lines.

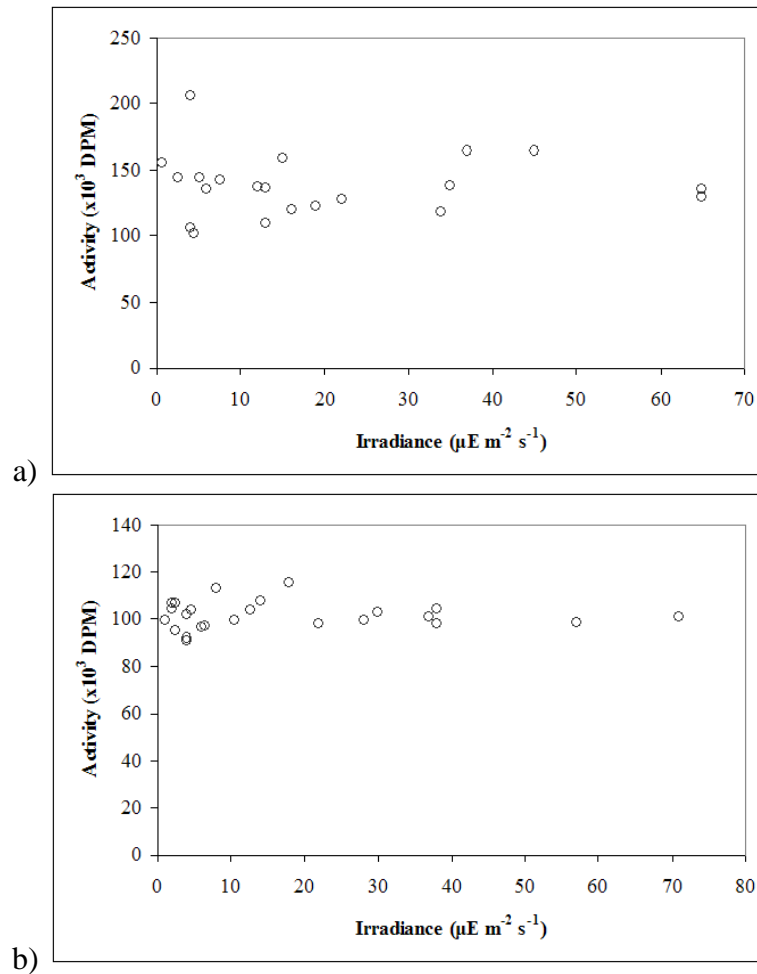


Figure 4.6. Examples of carbon assimilation (DPM) and irradiance ($\mu\text{E m}^{-2} \text{s}^{-1}$) plots obtained after one hour acidification. a) Experiment 2 (24th April 2006) and b) experiment 4 (9th May 2006).

On account of a mechanical fault with the scintillation counter during the first two months of sampling, counting of samples from these experiments was delayed, and this prevented early identification of the problem. When the problem was identified, samples were filtered after incubation on membrane filters (0.45 μm), using a manual pump. With filtration, phytoplankton cells were mechanically separated from the inorganic ^{14}C . Each sample vial and the filtration apparatus was rinsed with 10 mL of distilled water each time a sample was filtered. Filters were placed in clean scintillation vials and 10 mL of scintillation cocktail were added. Samples were subsequently read as normal using the scintillation counter.

The filtration process requires more handling of the samples compared to the acidification process, and there was a higher chance of contamination of the samples. Therefore the acidification problem was investigated by conducting three short experiments (A, B and C) in which the amount of HCl added to the samples and the duration of the acidification phase were varied as follow.

A) After incubation of inoculated water samples, normal and double amounts of HCl (400 and 800 μL) were added to pairs of vials incubated at the same irradiance, then acidified for one hour. The resulting set of data was analysed with one-way Anova and no significant difference ($DF = 11$, $F = 0.934$, $p > 0.05$) was found between the two treatments.

B) In experiment B, 5 mL aliquots of inoculated distilled water were added to 20 vials. Five vials (control) were fixed with 10 mL of scintillation cocktail while the others were acidified: 5 with 200 μL , 5 with 400 μL and 5 with 800 μL of HCl. Acidification lasted one hour then 10 mL of scintillation cocktail were added to each of the 15 vials. The results are presented in Figure 4.7. The 3 sets of samples were significantly different from the control and there was also a significant difference between them (one-way Anova, $DF = 9$, $p < 0.05$). None of the acidification treatments completely removed all of the activity. In fact, increasing the amount of acid reduced the quantity of ^{14}C removed. With 200 μL of acid, 71% of ^{14}C was removed, with 400 μL 63% and 59% with 800 μL of HCl.

C) During experiment C, the effect of a longer period of acidification was investigated. Three incubations were run, in three consecutive weeks, with water samples collected on different trips in Carlingford Lough. After each incubation, the samples were acidified for ≈ 16 hours using 400 μL of acid. The resulting activity versus irradiance values of these incubations gave curves when graphed (Figure 4.8).

Experiments A, B and C demonstrated that the initial acidification problem was related to the duration of the acidification phase and not to the amount of HCl added to the sample. For the remaining experiments, samples were acidified at the end of the incubation and left shaking with acid over night.

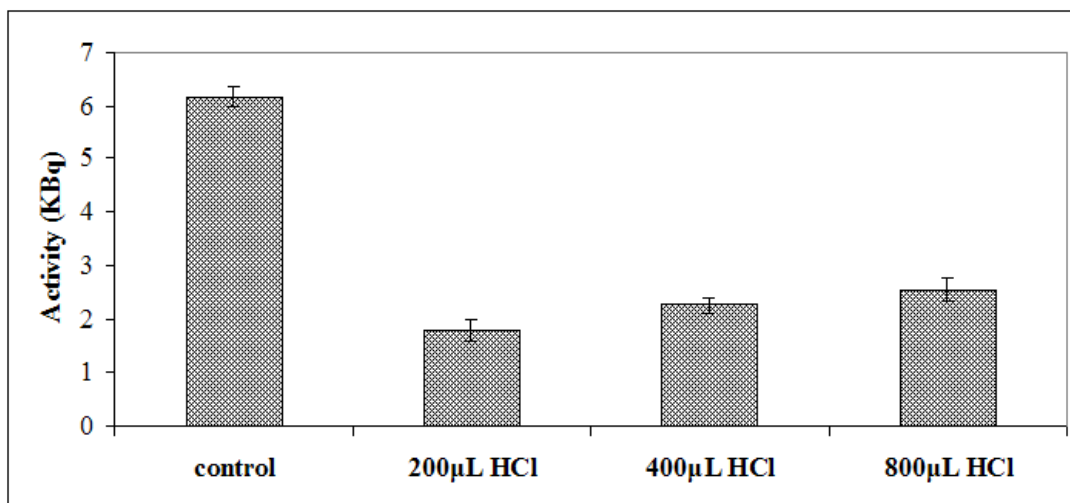


Figure 4.7. Results of the experiment B, showing the mean activities (KBq) of the solutions acidified with 200, 400 and 800 μL of HCl. Control = solution (distilled water + ^{14}C) + scintillation cocktail. Error bar is the standard deviation of the mean for the 5 replicates.

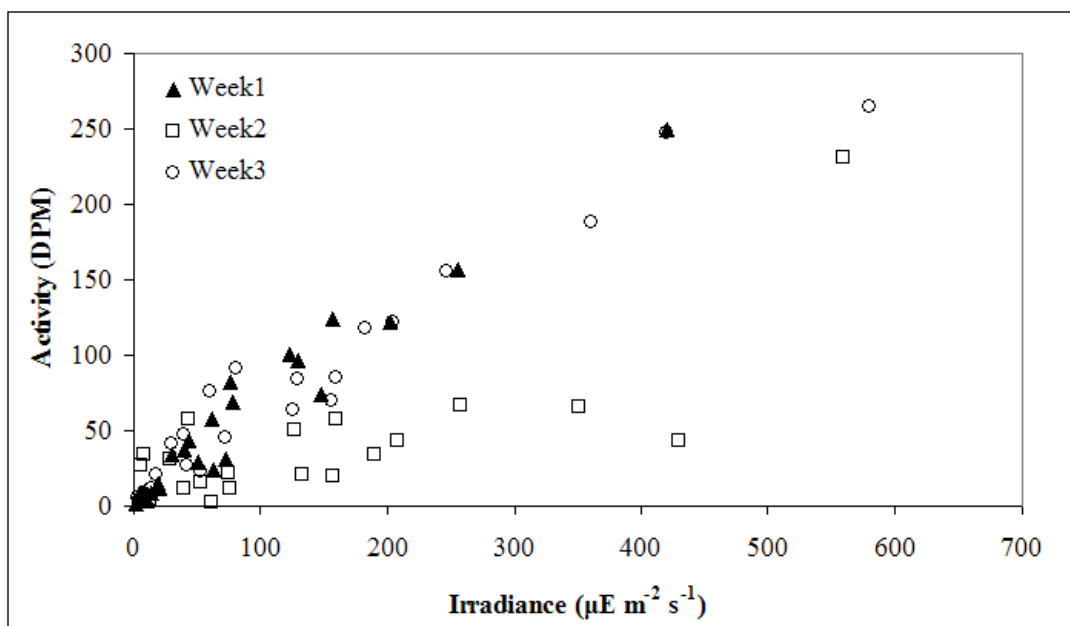


Figure 4.8. Activity (DPM) / irradiance ($\mu\text{E m}^{-2} \text{s}^{-1}$) curves for experiment C, weeks 1, 2 and 3, after ≈ 16 hours of acidification.

Experiment C was also used to investigate the effect of filtration and acidification on the removal of the excess inorganic ^{14}C . The water sample from the Lough collected in Week 1 was used for running two incubations, one after the other; the contents of the incubated vials from the first incubation were filtered while the vials from the second incubation were acidified. The same procedure was repeated with the water samples from the Lough collected in Week 2 and Week 3, with the only exception that the order of the treatment was reversed each week (Table 4.1). Considering that only one photosynthetron was available, the second incubation was usually carried out approximately 3 hours after the start of the first incubation. The results of the incubations carried out in Weeks 1 and Week 2 are shown in Figure 4.9. Results from the incubations in Week 3 could not be used due to contamination of the filtered samples.

The values obtained from acidified samples from Week 1 were higher than values from the filtered samples incubated at the same irradiances (Figure 4.9 a). In Week 2, samples treated with filtration showed the highest activity (Figure 4.9 b). It appears that the order with which the incubations were carried out (first or second) was more important than the treatment chosen for removing the excess ^{14}C ; in fact the second incubation gave the highest activity in both Week 1 and 2. Physiological modifications may have occurred in phytoplankton cells during the 3 hours gap between the first and second incubation which could explain the different responses the cells gave when exposed to light. Acidification was preferred to filtration to minimise handling of samples and cross contamination.

Table 4.1. Simple description of experiment C, identifying which samples were treated with filtration and which with acidification.

	Filtration	Acidification
Week 1	1	2
Week 2	2	1
Week 3	1	2

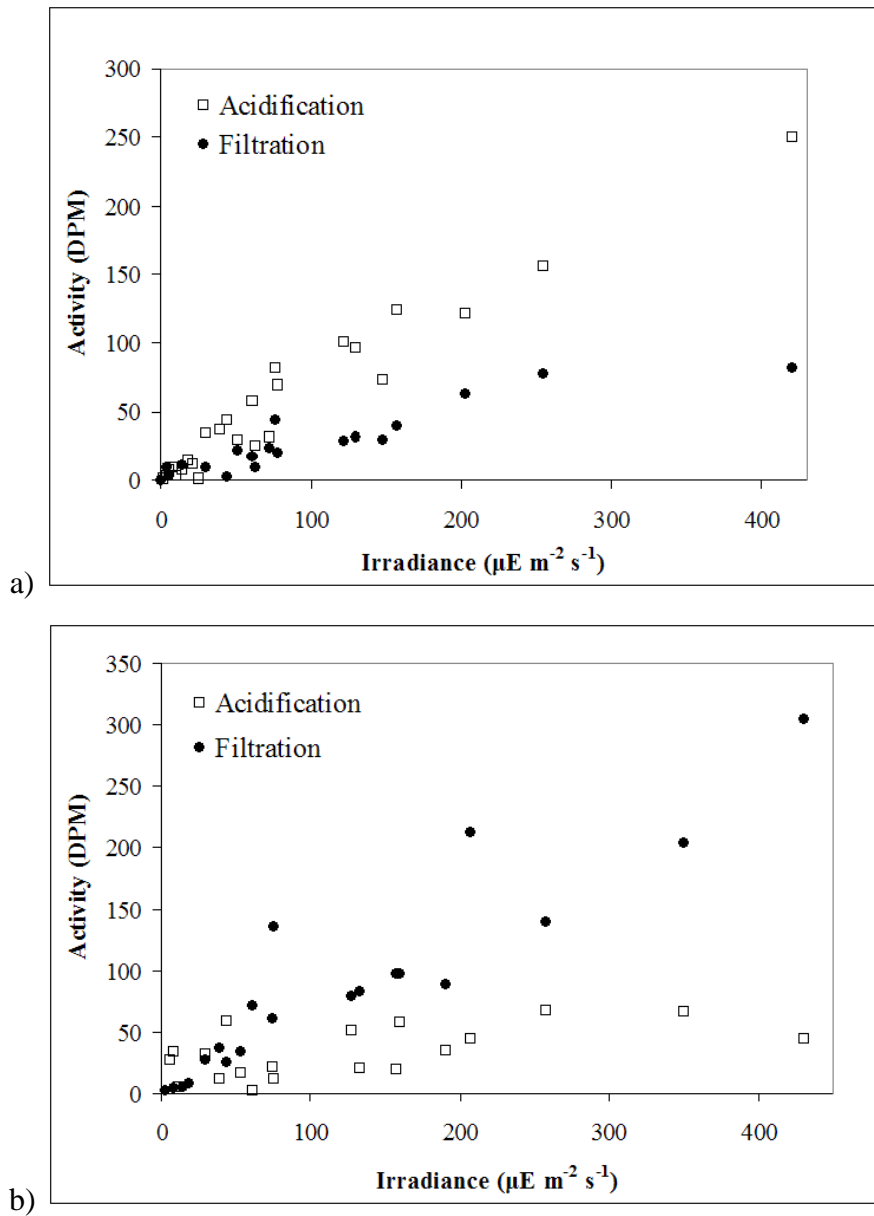


Figure 4.9. Comparison of acidification versus filtration treatments for Experiment C, Week 1 (a) and Week 2 (b). Activity (DPM) versus irradiance ($\mu\text{E m}^{-2} \text{s}^{-1}$) curve derived from acidified samples is shown as empty squares, while the curve derived from filtered sample is marked by the filled circles.

4.3 Conclusions

After considering the different techniques available for deriving primary production:

- the ^{14}C technique was chosen for estimating primary production of Carlingford Lough, due to its high sensitivity;
- a standard operating procedure was developed for deriving estimates of production of the Lough, that involved the use of a photosynthetron and short term incubations;
- the acidification phase should be ≈ 16 hours.

CHAPTER 5

Photosynthetic parameters

5.1 Introduction

Chapter 5 aims to test whether the photosynthetic parameters in Carlingford Lough show significant correlation with temperature, nutrient concentrations, light availability and phytoplankton community. This chapter also aims to identify the light saturation model that consistently produces a good fit to the P/E curves derived from primary production experiments with water samples from Carlingford Lough.

5.1.1 Photosynthetic parameters

The rate of photosynthesis depends on the amount of light to which phytoplankton are exposed (Tett 1990), and on the efficiency with which the light is utilised by phytoplankton for driving photosynthetic reactions (Falkowski and Raven 1997). Plotting the rate of photosynthesis against irradiance produces a curve which is commonly called photosynthesis/irradiance curve or P/E curve. In a photosynthesis/irradiance curve three different parts can be generally identified (Figure 5.1):

1. an initial part where increasing light intensity induces an increment in the rate of photosynthesis (light-limited region);
2. an intermediate part where the rate of photosynthesis is not influenced by changes in irradiance (light-saturated region);
3. a terminal part where an increase in light causes a decrease in photosynthesis (photoinhibited region, Falkowski and Raven 1997; Gargas, Nielsen and Lønholdt 1976).

The first part of the curve represents the light-dependent processes of photosynthesis (e.g. harvesting of photon energy by photosystems I and II, PSI and PSII, see Chapter 1 for more details). In particular, at the origin of the curve where the irradiance is low, photosynthesis is limited by the light harvesting capacity of the photosystem II (Falkowski and Raven 1997; Behrenfeld, Esaias and Turpie 2002), and fixation of CO₂ is approximately a linear function of irradiance.

The second part of the curve corresponds to the photosynthetic dark processes (Calvin cycle, see Chapter 1). At this level of irradiance (saturation light), photosynthesis is limited by the rate at which carbon is fixed (Behrenfeld, Esaias and

Turpie 2002), because the rate of photon absorption is higher than the rate of the electron transport from water to carbon dioxide (Falkowski and Raven 1997).

Part 3 of the curve, with a negative slope, represents a process called photoinhibition which is a reduction in the photosynthetic capacity caused by exposure to high irradiance. This reduction depends on both the duration of the exposure and the intensity of the light (Falkowski and Raven 1997). Photoinhibition occurs in the electron transfer chain located in photosystem II (Han *et al.* 2000), and leads to a reduction in PSII photochemical efficiency (see review by Falkowski and Raven 1997). Reduction in photosynthetic capacity can occur in phytoplankton living at the surface during hours of elevated irradiance or in phytoplankton that are suddenly transported into surface waters from greater depth (Han *et al.* 2000). The reduction in photosynthetic rate in the last part of the P/E curve can also be caused by photo-oxidation of chlorophyll *a* molecules (Gargas, Nielsen and Lønholdt 1976; Han *et al.* 2000) that, unlike photoinhibition, causes a permanent damage to chlorophyll molecules.

From photosynthesis/irradiance curves, it is possible to derive three important parameters; α , P_{\max} (Figure 5.2), and β (if photoinhibition occurs). The efficiency of biomass-related photosynthesis under low irradiance (α) can be represented by the initial slope of the P/E curve (Equation 5.1), and is usually denoted with unit $\text{mgC } \mu\text{E m}^{-2} \text{ s}^{-1}$. If the slope is normalised to chlorophyll biomass the superscript “B” is added, α^{B} (Falkowski and Raven 1997). The units of the normalised photosynthesis efficiency are $\text{mgC (mgChl)}^{-1} \mu\text{E m}^{-2} \text{ s}^{-1}$.

$$\alpha = \frac{dP}{dE} \quad (E \rightarrow 0) \quad (5.1)$$

P_{\max} is the rate of light-saturated photosynthesis (Tett 1990), the plateau of the P/E curve. As for α , the superscript “B” is added when the light-saturated photosynthesis is normalised to chlorophyll. The units of P_{\max}^{B} include also time (e.g. $\text{mgC (mgChl)}^{-1} \text{ h}^{-1}$). Finally, β is the rate of decline in photosynthetic rate when photoinhibition occurs; it is analogous to α but with the opposite sign (Falkowski and Raven 1997).

The ratio $P_{\max}^{\text{B}} : \alpha^{\text{B}}$ is called E_k (Figure 5.2) and “*corresponds to the point at which the linear part of the light-saturation curve intersects the plateau*” (Côté and Platt 1983).

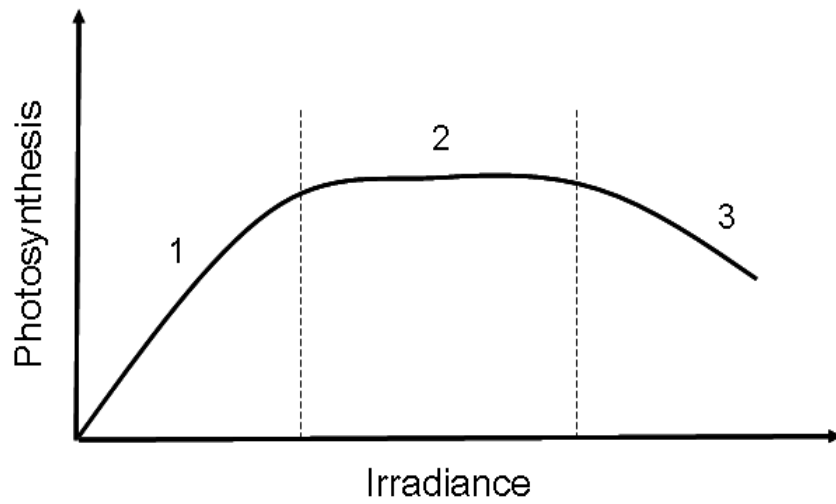


Figure 5.1. An example of a photosynthesis/irradiance curve or P/E curve.

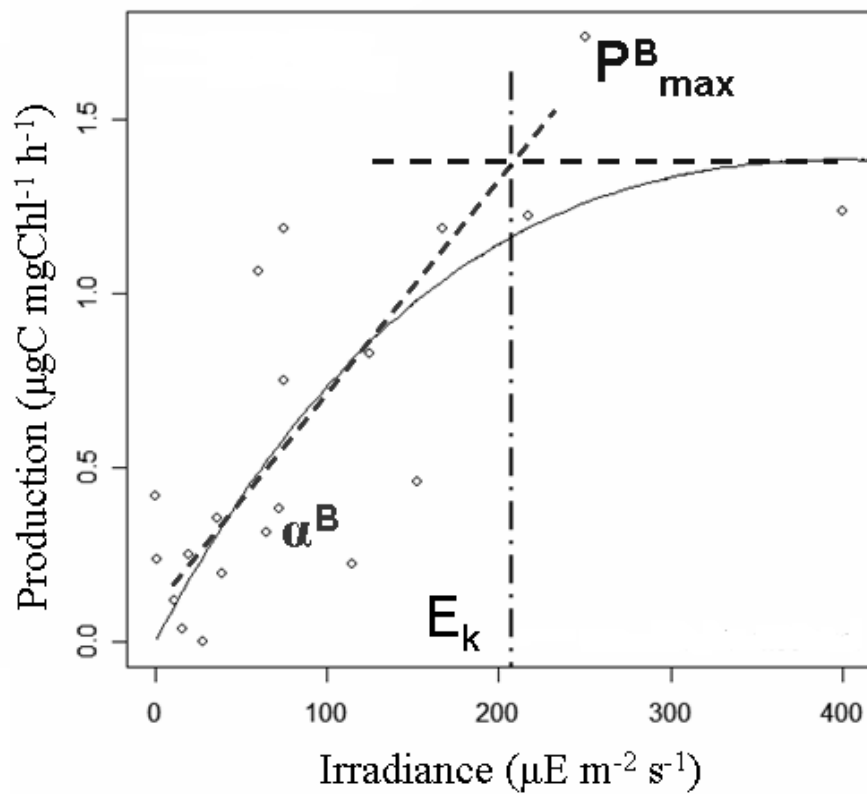


Figure 5.2. A P/E curve showing the photosynthetic parameters (α^B and P_{max}^B) and E_k . Photosynthetic rate is expressed in $\mu\text{gC mgChl}^{-1} \text{h}^{-1}$ and irradiance (PAR) in $\mu\text{E m}^{-2} \text{s}^{-1}$.

5.1.2 Variability of the photosynthetic parameters

Values of the photosynthetic parameters depend on the physiological characteristics of the microalgae cells, consequently changes in environmental conditions can be identified by variations in the photosynthetic parameters (Côté and Platt 1983; Macedo *et al.* 2002). Côté and Platt (1983) reviewed the main factors influencing the photosynthetic parameters and these are listed below:

- P_{\max}^B is a function of enzymatic processes and depends on temperature (Platt and Jassby 1976) and other factors such as nutrient regime, light history, time of the day, biochemical composition and species composition of the phytoplankton, phaeopigments/chlorophyll *a* ratio and phytoplankton cell volume;
- variation in α^B can be potentially related to phytoplankton cell size, pigment composition, adaptation to sun and shade conditions, light quality and nutrient availability;
- E_k is related to physiological modification in response to changes in the environmental conditions such as temperature, phytoplankton species composition and light history.

On the basis of the light saturation index E_k , variability in photosynthetic parameters can be divided into two categories: the first one is associated with independent changes in α^B and P_{\max}^B values; the second category is related to co-occurring changes in α^B and P_{\max}^B (Behrenfeld *et al.* 2004). The E_k -dependent variability (the first category) induces changes in E_k values and is generally related to photoacclimation (physiological cell modification in response to variation in the light). The E_k -independent variability does not change the value of E_k and it is more difficult to explain considering that α^B and P_{\max}^B are influenced by different factors (see above) so they should not co-vary. Behrenfeld *et al.* (2004) suggested that nutrient availability and taxonomic composition may play an important role in the covariance of α^B and P_{\max}^B .

The photosynthetic parameters can vary over a range of time scales including daily and seasonal scales (Côté and Platt 1983). In particular, the daily scale acquires more importance in middle latitudes where the local meteorological environmental forcing (e.g. the passage of frontal disturbance) presents a time scale of a few days (Heath 1973). The diurnal variability of α^B and P_{\max}^B had been shown by different

studies (e.g. MacCall and Platt 1977; Côté and Platt 1983; Jouenne *et al.* 2005; Yoshikawa and Furuya 2006), but while P_{\max}^B showed a distinct diurnal pattern with maximum at noon, the daily cycle of α^B was less obvious. Harding *et al.* (1981) observed that different taxa can show different amplitude and timing of the daily oscillation. Furthermore some taxa, such as *Ditylum brightwellii* and *Biddulphia mobiliensis*, did not show daily variation. In estuaries, lagoon and coastal ecosystems, the tidal cycle can also cause short term variability in photosynthetic parameters (Lizon *et al.* 1995; Jouenne *et al.* 2005). The vertical mixing generated by tidal shear may move phytoplankton up and down the water column exposing it to different light conditions, inducing photoinhibition.

5.1.3 Estimates of α^B and P_{\max}^B and models of the photosynthesis/irradiance relationship

As discussed in section 5.1.1, the photosynthetic parameters can be derived from photosynthesis/irradiance curves. A number of models have been used to fit P/E curves and some of the most well-known models are given in Table 5.1. The models (Table 5.1) do not account for photoinhibition and are summarised as a general form in Equation 5.2, where the instantaneous rate of photosynthesis (normalised by chlorophyll), P^B , is a function of the irradiance (E) and the photosynthetic parameters (normalised by chlorophyll). The equation below is valid for irradiances below the irradiance at which photoinhibition occurs.

$$P^B = f(E, \alpha^B, P_{\max}^B) \quad (5.2)$$

Where f is function.

Of the models listed in Table 5.1, it is possible to identify a linear model (Blackman 1905) and hyperbolic models (Burk and Lineweaver; Smith 1936/Talling 1957). The remaining equations (e.g. Webb, Newton and Star 1974; Jassby and Platt 1976) have exponential functions (McBride 1992). The models in Tables 5.1 (except for Steele 1962) are light saturation models which means they do not account for photoinhibition.

Jassby and Platt (1979) assessed the performance of each of the models in Table 5.1 using model ability to fit empirical data from natural marine phytoplankton populations. The authors adopted a two-stage fitting procedure to fit the data to a

given model. They first estimated α^B from linear regression, and then P_{\max}^B by a non-linear least-squared fit, keeping α^B fixed to the value determined at stage one. The success of each model to fit the data was determined using two indices: 1. the mean scatter around the fitted line (mean squared deviation); 2. the number of times a given model gave the best fit based on an unweighted least-squared criterion (Jassby and Platt 1979). Jassby and Platt showed that the Burk and Lineweaver (1935) and Steele (1962) equations gave the poorest fit (the second one because it takes into account photoinhibition). The authors concluded that “*the light-saturation curve (up to the onset of photoinhibition) for natural population of coastal phytoplankton is best described by a hyperbolic tangent function*” (Jassby and Platt 1979).

Lederman and Tett (1981) also fitted the data set used by Jassby and Platt (1976), together with a simulated data set, to the same 8 equations but derived the photosynthetic parameters by both simultaneous and independent estimations. A minimum sum of squared differences (or SSE) between the observed values and the predicted values were used as criteria for goodness of fit. Lederman and Tett (1981) found that most of the models (e.g. Talling 1957; Jassby and Platt 1976; modification of Steele 1962; Webb, Newton and Star 1974) were not distinguishable on this basis of the goodness of fit. Furthermore, Lederman and Tett (1981) concluded that the Jassby and Platt equation could not be considered the most successful model, instead on the basis of their criteria they concluded that the Smith/Talling equation gave the best fit.

In a more recent study, Grangeré *et al.* (2009) tested the fit of the Webb *et al.* (1974), Platt *et al.* (1975), Monod (1950) (=Burk and Lineweaver 1952), Smith (1936) and Steele (1962) equations on 18 months of photosynthetic data from the Baie des Veys (France). After performing linear regression of the predicted versus observed production values for each model, the authors concluded that the Webb *et al.* (1974), Platt *et al.* (1975) and Smith (1936) models gave the best fit to their data set.

Based on the above, it appears that there is no single best model for describing photosynthesis/irradiance relationships, and the choice of which model to use may depend on the criterion adopted for assessing the goodness of fit. In this study it was decided to use all 8 models (Table 5.1) with the P/E curves from Carlingford Lough, and to use a set of criteria for identifying the best model, which was then used in the final stage to model primary production in the Lough.

Table 5.1. Sources and equations of the 8 models used by Jassby and Platt (1976) and Lederman and Tett (1981). P^B is the instantaneous rate of photosynthesis normalised by chlorophyll, α^B is the efficiency of photosynthesis at low irradiance normalised by chlorophyll, P^B_{\max} is the maximum rate of light-saturated photosynthesis normalised by chlorophyll, and E is the irradiance.

Sources	Equations
Blackman (1905)	$P^B = \alpha^B \cdot E \quad \left(0 \leq E \leq \frac{P^B_{\max}}{\alpha^B} \right)$ $P^B = P^B_{\max} \quad \left(E > \frac{P^B_{\max}}{\alpha^B} \right)$
Burk and Lineweaver (1935)	$P^B = P^B_{\max} \cdot \frac{\alpha^B \cdot E}{P^B_{\max} + \alpha^B \cdot E}$
Smith (1936); Talling (1957)	$P^B = P^B_{\max} \cdot \frac{\alpha^B \cdot E}{\sqrt{P^B_{\max}{}^2 + (\alpha^B \cdot E)^2}}$
Steele (1962)	$P^B = \alpha^B \cdot E \cdot e^{-\left(\frac{\alpha^B \cdot E}{P^B_{\max} \cdot e}\right)}$
Jassby and Platt (1976) modification of Steele (1962)	$P^B = \alpha^B \cdot E \cdot e^{-\left(\frac{\alpha^B \cdot E}{P^B_{\max} \cdot e}\right)} \quad \left(0 \leq E \leq \frac{P^B_{\max} \cdot e}{\alpha^B} \right)$ $P^B = P^B_{\max} \quad \left(E > \frac{P^B_{\max} \cdot e}{\alpha^B} \right)$
Webb, Newton and Star (1974)	$P^B = P^B_{\max} \cdot \left(1 - e^{-\frac{\alpha^B \cdot E}{P^B_{\max}}} \right)$
Jassby and Platt (1976), modification of Platt <i>et al.</i> (1975)	$P^B = \alpha^B \cdot E - \frac{(\alpha^B \cdot E)^2}{4 \cdot P^B_{\max}} \quad \left(0 \leq E \leq \frac{2 \cdot P^B_{\max}}{\alpha^B} \right)$ $P^B = P^B_{\max} \quad \left(E > \frac{2 \cdot P^B_{\max}}{\alpha^B} \right)$
Jassby and Platt (1976)	$P^B = P^B_{\max} \cdot \tanh\left(\frac{\alpha^B \cdot E}{P^B_{\max}}\right)$

5.2 Methods

5.2.1 Estimates of photosynthetic parameters using ‘*PIcurvefit4.R*’

Each ^{14}C incubation carried out with a photosynthetron (Chapter 4) produced 24 paired values of irradiance ($\mu\text{E m}^{-2} \text{s}^{-1}$) and ^{14}C activity expressed in DPM (Disintegrations Per Minute). Activity of ^{14}C as DPM was converted to carbon assimilation, normalised to chlorophyll concentration and used to plot a P/E curve and estimate the photosynthetic parameters. The script, ‘*PIcurvefit4.R*’ (Listing 5.1), and the software R version 2.2.0 (2005) were used for performing the steps described above.

The scripts fitted each P/E curve from Carlingford Lough using 9 photosynthesis/irradiance models (the 8 models used by Jassby and Platt 1976 and an unpublished model by P. Tett, see Table 5.2) and the photosynthetic parameters were derived simultaneously. The activity in DPM was converted to carbon assimilation per unit mass of chlorophyll ($\text{mgC mgChl}^{-1} \text{h}^{-1}$) using Equation 5.3 from Strickland and Parsons (1967).

$$C = \frac{[(DPM_{\text{sample}} - DPM_{\text{dark}}) \cdot W \cdot 1.05]}{(t_{\text{incubation}} \cdot DPM_{\text{added}} \cdot \text{Chl})} \quad (5.3)$$

Where: DPM_{sample} is the activity of the vial (in DPM) after the incubation and acidification; DPM_{dark} is the average activity of the vials incubated in the dark after acidification; W is the weight of carbonate carbon content in sea water in mgC m^{-3} (Equation 5.4); 1.05 is a correction for differential uptake of ^{14}C compared with ^{12}C ; $t_{\text{incubation}}$ refers to the length of the incubation, expressed in hours. DPM_{added} is the activity of each vial before the start of the incubation and it was calculated from the mean total activity (TA vials in Chapter 4); Chl is the chlorophyll concentration of the sample in units of mg m^{-3} .

W was calculated using Equation 5.4 from Parsons *et al.* (1984).

$$W = 12000 \cdot (0.96 \cdot ((S \cdot 0.067) - 0.05)) \quad (5.4)$$

Where S is the salinity of the water sample.

The average DPM and standard deviation of samples incubated in the dark for 2 hours were 57 ± 8 ($n = 31$). Occasionally one of the 2 samples incubated in the dark during an experiment had an anomalously high activity (e.g. for experiment 13, 675 DPM). These anomalous values was compared to the average of the t_0 samples and if the value was over 3 standard deviations from the mean it was not included in

the analysis. In fact, the average values of t_0 and dark samples derived from all incubations were not statistically different (two-sample T-test, T-value = -1.02, n = 31, p-value = 0.310) therefore the average t_0 value was used as a check on the values of the dark samples.

After transformation of DPM counts to C assimilation, the script was used to plot the photosynthesis/irradiance data set and to fit the 9 equations (Table 5.2). For each data set, the best, the second best and the worst fit are shown in an output plot (see Figure 5.3 a as example). Furthermore, for each P/E curve the script also produces a box-plot of the residuals of the fit of each model (see example in Figure 5.3 b), calculated as the distance between the observed value and the expected value predicted by the model.

In experiments 7, 16, 17, 18 and 21 the light in the photosynthesetron was not high enough to reach the maximum photosynthetic rate (P_{max}^B), consequently all 9 models failed to fit the data sets. For these experiments a simple linear model was used to fit the data sets and only α^B was estimated.

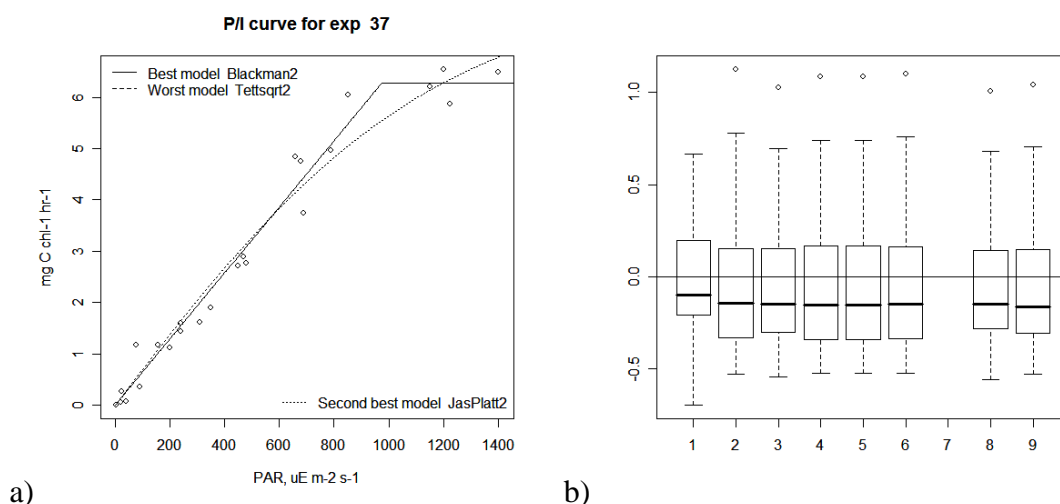


Figure 5.3. An example of the standard output of the script '*PIcurvefit4.R*': a) best, second best and worst models fitting the data set; b) boxplot of the residuals for the 9 models where 1 = Blackman, 2 = BurkLine, 3 = STalling, 4 = Steele, 5 = modSteel2, 6 = Webbexp, 7 = Tettsqrt, 8 = JasPlatt, 9 = modPlatt (see Table 5.2 for explanation of model name). The worst fitting model and the boxplot of the model number 7 (Tettsqrt) are missing because the model could not fit the data set.

Table 5.2. Sources, abbreviations used in ‘*PIcurvefit4.R*’, and equations of the 9 models used to fit P/E curves from Carlingford Lough. P^B is the instantaneous rate of photosynthesis normalised by chlorophyll, α^B is the efficiency of photosynthesis at low irradiance normalised by chlorophyll, P^B_{\max} is the maximum rate of light-saturated photosynthesis normalised by chlorophyll, and E is the irradiance.

Sources	Model name	Equations
Blackman (1905)	Blackman	$P^B = \alpha^B \cdot E \quad \left(0 \leq E \leq \frac{P^B_{\max}}{\alpha^B} \right)$ $P^B = P^B_{\max} \quad \left(E > \frac{P^B_{\max}}{\alpha^B} \right)$
Burk and Lineweaver (1935)	BurkLine	$P^B = P^B_{\max} \cdot \frac{\alpha^B \cdot E}{P^B_{\max} + \alpha^B \cdot E}$
Smith (1936); Talling (1957)	STalling	$P^B = P^B_{\max} \cdot \frac{\alpha^B \cdot E}{\sqrt{P^B_{\max}{}^2 + (\alpha^B \cdot E)^2}}$
Steele (1962)	Steele	$P^B = \alpha^B \cdot E \cdot e^{-\left(\frac{\alpha^B \cdot E}{P^B_{\max} \cdot e}\right)}$
Jassby and Platt (1976) modification of Steele (1962)	modSteel	$P^B = \alpha^B \cdot E \cdot e^{-\left(\frac{\alpha^B \cdot E}{P^B_{\max} \cdot e}\right)}$ for $\left(0 \leq E \leq \frac{P^B_{\max} \cdot e}{\alpha^B} \right)$ $P^B = P^B_{\max} \quad \left(E > \frac{P^B_{\max} \cdot e}{\alpha^B} \right)$
Webb, Newton and Star (1974)	Webbexp	$P^B = P^B_{\max} \cdot \left(1 - e^{-\frac{\alpha^B \cdot E}{P^B_{\max}}} \right)$
Jassby and Platt (1976), modification of Platt <i>et al.</i> (1975)	modPlatt	$P^B = \alpha^B \cdot E - \frac{(\alpha^B \cdot E)^2}{4 \cdot P^B_{\max}}$ for $\left(0 \leq E \leq \frac{2 \cdot P^B_{\max}}{\alpha^B} \right)$ $P^B = P^B_{\max} \quad \left(E > \frac{2 \cdot P^B_{\max}}{\alpha^B} \right)$
Jassby and Platt (1976)	JasPlatt	$P^B = P^B_{\max} \cdot \tanh\left(\frac{\alpha^B \cdot E}{P^B_{\max}}\right)$
Tett (not published)	Tettsqrt	$P^B = P^B_{\max} \cdot \sqrt{\frac{\alpha^B \cdot E}{P^B_{\max} + \alpha^B \cdot E}}$

The results of fitting the 9 models were ranked from the best to the worst, based on a goodness of fit coefficient R^2 , calculated as shown in Equation 5.5.

$$R^2 = 1 - \frac{RSS}{TSS} = 1 - \frac{\sum (Y - \hat{Y})^2}{\sum (Y - \bar{Y})^2} \quad (5.5)$$

Where RSS is the residual sum of squares; TSS is the total sum of squares; Y refers to an observed value of carbon assimilation, \hat{Y} is the correspondent value of production predicted by the model; \bar{Y} is the average production.

The total sum of squares provides information on the total amount of variability between the Y values, while the residual sum of squares provides information on the amount of variability of Y remaining after fitting the model (Zar 1998). The model with the lowest residual sum of squares (and the highest R^2) should provide the best fit to the data set.

Two other coefficients, based on R^2 , were used to quantify the ability of each model to fit the data. The number of data sets for which a given model gave the best fit (N_i), and a coefficient based on the rank position derived from the R^2 calculation. Focusing on this last coefficient, the model which gave the best fit (highest R^2) received a score of 8, the second best model a score of 7 and so on such that the model which gave the worst fit received a score of 1. Where the model was not able to fit the data, a score of zero was assigned. The overall performance of a given model was determined by summing the scores; thus the model with the highest score was considered to be the one with the best overall performance.

5.2.2 Initial values of α^B and P_{\max}^B

'*Pcurvefit4.R*' is an algorithm that repeatedly recalculates α^B and P_{\max}^B until the best fit (which gives the R^2 closer to 1) is obtained. The script requires initial guessed values for α^B and P_{\max}^B to start the iteration process. It is really important to use the correct initial values; in fact if the latter are too far from the 'expected' values the algorithm could give erroneous final estimates of α^B and P_{\max}^B . On the other hand, we don't know which the 'expected' values are.

To determine the sensitivity of the initial values on the final estimates of the photosynthetic parameters, a simple test was performed. Using the data set from experiment 10, the initial value of P_{\max}^B was set as 7 mgC mgChl⁻¹ h⁻¹, and the initial

value of α^B as 0.001 (mgC mgChl⁻¹ ($\mu\text{E m}^{-2} \text{s}^{-1}$) h⁻¹). With these initial conditions no models were able to fit the data set. Changing the initial value of α^B to 0.01, and leaving P_{max}^B unaltered, 4 models were now able to fit the data set. Finally setting $\alpha^B = 0.1$ (leaving P_{max}^B unaltered), all the equations except Tettsqrt were able to fit the data set. The results from this test are summarised in Table 5.3. The same results were obtained varying the initial value of P_{max}^B , maintaining the value of α^B unaltered.

For a better understanding of the importance of the initial values, the above numerical test was repeated but with the data set from experiments 25 and 34, using 13 initial values of α^B (varying from 0.001 to 0.5 mgC mgChl⁻¹ ($\mu\text{E m}^{-2} \text{s}^{-1}$) h⁻¹) and 13 initial values for P_{max}^B (varying from 2 to 24 mgC mgChl⁻¹ h⁻¹). One photosynthetic parameter was varied at a time, while the other was left unaltered. For each of the 9 models, the initial values of α^B or P_{max}^B were plotted against the corresponding values derived from the model. An example of this type of plot can be seen in Figure 5.4 which shows the final estimates of α^B associated to the 13 initial estimates for JasPlatt model (leaving P_{max}^B unaltered). The initial values of the photosynthetic parameters influenced the number of models able to fit the data sets but not the final estimates of α^B and P_{max}^B derived from the model, i.e. if the model was able to fit the data set it would give consistently the same final estimates of the photosynthetic parameters (Figure 5.4).

Based on the above, the initial value for P_{max}^B was chosen in the following way: a) the P/E curve was plotted in Microsoft Excel; b) the two or three points at the highest irradiance (which form a plateau) were used to calculate the initial value of P_{max}^B . If a plateau was not present the highest carbon assimilation was considered as initial P_{max}^B . For α^B , an initial value of 0.01 mgC (mg Chl)⁻¹ $\mu\text{E m}^{-2} \text{s}^{-1} \text{h}^{-1}$ was used for all the experiments.

Table 5.3. Summary of the test, using experiment 10 data, on the initial value of α^B ($\text{mgC mgChl}^{-1} (\mu\text{E m}^{-2} \text{s}^{-1}) \text{h}^{-1}$), showing the number of models able to fit the data set with varying initial values of α^B and leaving P_{max}^B unaltered at $7 \text{ mgC mgChl}^{-1} \text{h}^{-1}$.

Initial value of α^B ($\text{mgC mgChl}^{-1} (\mu\text{E m}^{-2} \text{s}^{-1}) \text{h}^{-1}$)	Number of models from Table 5.2 able to fit the data set
0.001	0
0.01	4
0.1	8

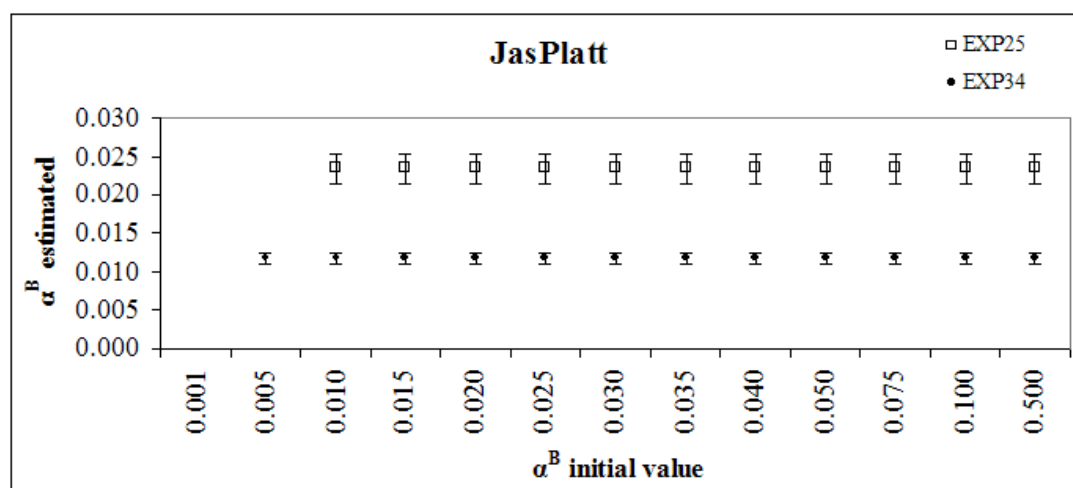


Figure 5.4. A plot showing the estimated α^B ($\text{mgC mgChl}^{-1} (\mu\text{E m}^{-2} \text{s}^{-1}) \text{h}^{-1}$) by the Jassby and Platt (1976) equation with various initial values of α^B ($\text{mgC mgChl}^{-1} (\mu\text{E m}^{-2} \text{s}^{-1}) \text{h}^{-1}$). Data set from experiments 25 and 34.

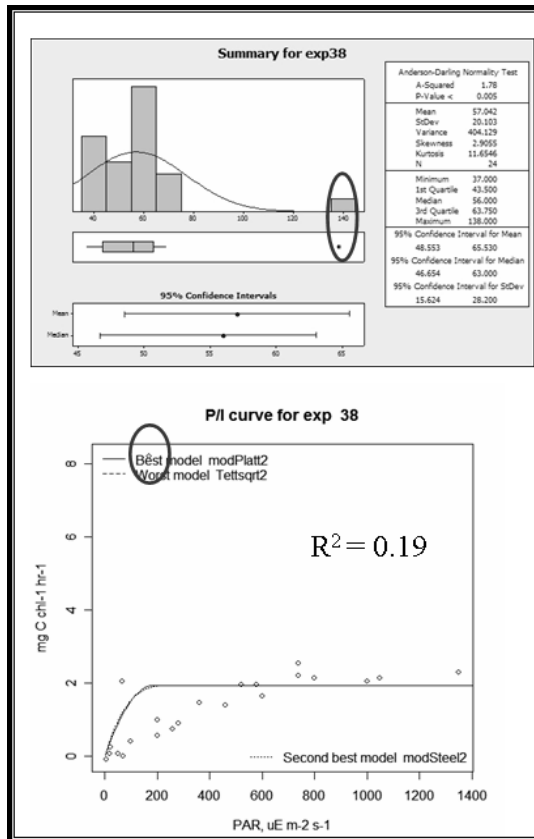
5.2.3 Identification of outliers

During an incubation experiment in a photosynthetron, different errors (e.g. variation in pipetted sample volume between vials or contamination of the vials) may occur and cause anomalously high activities in one or some of the 24 incubated vials. The presence of outliers in the data set decreases the ability of the script '*Pcurvefit4.R*' to fit the data thus producing incorrect final estimates of α^B and P_{max}^B . For this reason, descriptive statistics (e.g. mean, median and standard

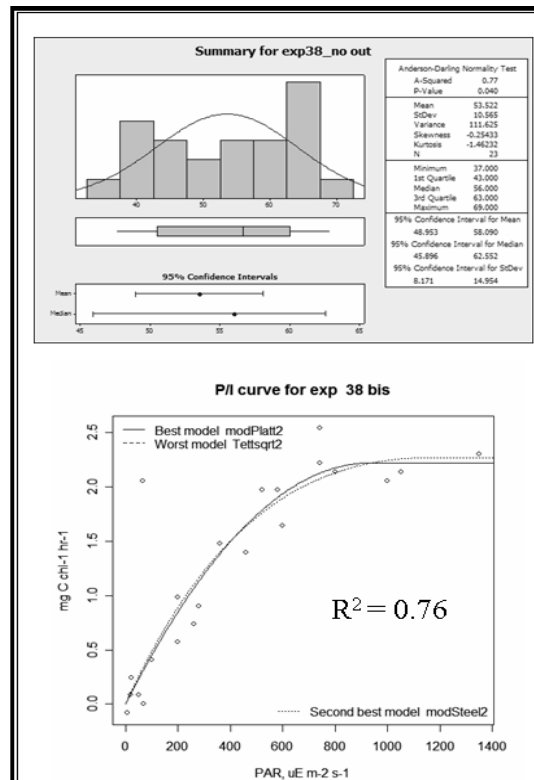
deviations) of the activities of the 24 incubated samples of each experiment were derived, using Minitab 15. Values of activity deviating more than 3 standard deviations from the mean were classified as outliers. Any data set containing outlier/s was then analysed in R (version 2.2.0, 2005) with '*PIcurvefit4.R*', with and without the outlier, and the R^2 derived for the 2 analyses were compared. If the exclusion of the outlier increased the value of R^2 , the outlier was removed from the dataset. Descriptive statistics were then recalculated for the new data set (without the outlier) and the new data set retested to ensure that no other outliers were present. An example of the process for identifying outliers is shown in Figure 5.5.

Outliers were identified in the data sets from experiments 16, 17, 18, 20, 38, 39 and 40, and could be grouped in 2 types (Figure 5.6). Type 1 outliers (experiments 16, 17, 18 and 20) were from a vial incubated at the higher irradiance (Figure 5.6 a). In these experiments the light in the incubator was not high enough to reach P_{\max}^B and the light gradient was not reproduced homogeneously in the incubator (e.g. missing values between 400 and 600 $\mu\text{E m}^{-2} \text{s}^{-1}$). Based on this consideration, the values classified as outliers, in the experiments 16 to 18 and 20, were not considered real outliers but part of the linear part of the P/E curve and were retained in the data set.

The type 2 outlier (Figure 5.6 b), observed in the data set from experiments 38, 39 and 40, was a vial incubated at low/medium irradiances (e.g. $< 200 \mu\text{E m}^{-2} \text{s}^{-1}$). In these experiments there was a good light gradient, up to 1400 $\mu\text{E m}^{-2} \text{s}^{-1}$, and the maximum photosynthetic rate was reached. In all 3 experiments, the anomalous values were well above the asymptote of the curve. The removal of type 2 outlier considerably improved the goodness of the fit. For experiment 38, R^2 increased from 0.19 to 0.76 (Figure 5.5), from 0.07 to 0.53 for experiment 39; from 0.08 to 0.23 for experiment 40. Therefore, outliers in each data set from these experiments were not included in the analysis.



a)



b)

Figure 5.5. Descriptive statistics and P/E curve for the data set from experiment 38, a) with outlier (indicated by the circle) and b) without the outlier. The R^2 of the best fit (modPlatt) are also shown. The worst fitting model is not represented because the model could not fit the data set.

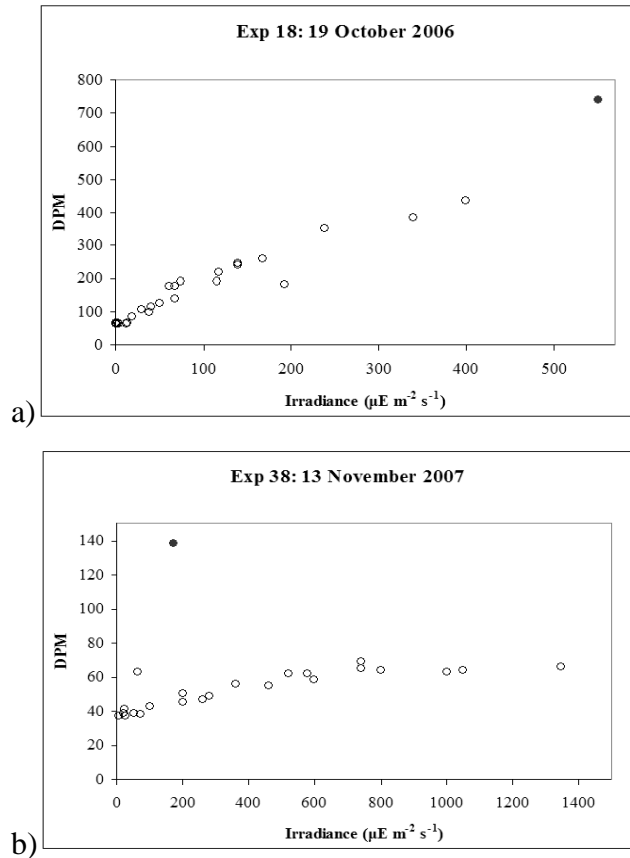


Figure 5.6. The two types of outlier identified in the data sets. a) An example of a type 1 outlier from experiment 18 and b) an example of the second type identified in data set from experiment 38. The outlier is marked as a full black circle.

5.2.4 Data analysis

Descriptive statistics of the data were calculated using Microsoft Office Excel 2003, together with the plots showing the temporal variability of photosynthetic parameters and E_k .

Multiple regression analyses of estimates of photosynthetic parameters against other environmental variables were carried out using Minitab 15.1.1.0, after log-transformation of some variables (see section 2.2.7 on criteria for transformation). The best fitting regression model was identified by the Minitab function “Best Subset Regression”. The latter examines all the possible subsets of the predictors, and shows, for the two best models of each number of predictors, the R^2 and standard deviation of the residuals (S) of the regression. The lower the value of S, the better the model predicts the response.

5.3 Results

From the 11th of April 2006 until the 13th of March 2008, 43 ¹⁴C incubations were carried out. Of these 33 were successful and produced P/E curves from which photosynthetic parameters were derived. The failure of 10 experiments (1 to 6, 14-15, 31 and 41) was related to problems with the treatment of the vials after the incubation (see Chapter 4 in relation to the length of the acidification phase); damage of the vials; inability of the models to fit the data set and derive the photosynthetic parameters.

5.3.1 Comparison of the models

Table 5.4 shows the list of experiments performed together with the date, the method of treatment of the samples (filtration or acidification over night, see Chapter 4), the model that gave the best fit to the P/E curves, estimates of the photosynthetic parameters with standard errors for the best model, estimates of E_k and the value of R^2 (for the best model). Examples of P/E curves are given in Figure 5.7. The mean, standard deviation, median, minimum and maximum estimates of α^B , P_{max}^B and E_k derived from the models are shown in Tables 5.5, 5.6 and 5.7 respectively. The square-root model of Tett (unpublished) did not fit any of the data sets and is not shown in the tables.

Focusing on α^B (Table 5.5), the averages derived from the models were slightly different, with Blackman (see Table 5.2 for abbreviations) giving the lowest average of $0.0089 \text{ mgC mgChl}^{-1} (\mu\text{E m}^{-2} \text{ s}^{-1}) \text{ h}^{-1}$ and BurkLine the highest average of $0.0115 \text{ mgC mgChl}^{-1} (\mu\text{E m}^{-2} \text{ s}^{-1}) \text{ h}^{-1}$. Comparing the model estimates of α^B , the minimum estimate ranged between $0.0031 \text{ mgC mgChl}^{-1} (\mu\text{E m}^{-2} \text{ s}^{-1}) \text{ h}^{-1}$ (Blackman) and $0.0042 \text{ mgC mgChl}^{-1} (\mu\text{E m}^{-2} \text{ s}^{-1}) \text{ h}^{-1}$ (Steele, modSteel), while the maximum estimate varied between $0.0170 \text{ mgC mgChl}^{-1} (\mu\text{E m}^{-2} \text{ s}^{-1}) \text{ h}^{-1}$ (linear model) and $0.0279 \text{ mgC mgChl}^{-1} (\mu\text{E m}^{-2} \text{ s}^{-1}) \text{ h}^{-1}$ (BurkLine). The temporal variability in α^B derived from the models is shown in Figure 5.8. It is possible to observe that the models gave similar estimates except for a few occasions (e.g. December 2006, January 2008). In particular, estimates of α^B derived from the experiment in January 2008 showed considerable variability between models and generally high standard errors of the estimates. As suggested by the descriptive statistics in Table 5.5,

BurkLine gave the highest estimates of α^B for all the data sets analysed, while Blackman gave the lowest estimates (Figure 5.8).

The estimates of P_{\max}^B calculated from the models were variable as suggested by the mean values given in Table 5.6. Comparing the estimates of P_{\max}^B derived by the models, the average rate of light-saturated photosynthesis varied from 5.93 mgC (mg Chl)⁻¹ h⁻¹ (Blackman) to 26.12 mgC (mg Chl)⁻¹ h⁻¹ (BurkLine). The minimum values of P_{\max}^B from the models were generally similar and in the range 1.01 mgC (mg Chl)⁻¹ h⁻¹ (modPlatt) to 2.00 mgC (mg Chl)⁻¹ h⁻¹ (BurkLine). There was a much wider range of the maximum values including values up to 185.24 mgC (mg Chl)⁻¹ h⁻¹ (BurkLine). Blackman gave the lowest maximum estimate of P_{\max}^B of 15.33 mgC (mg Chl)⁻¹ h⁻¹. The temporal variability in P_{\max}^B is depicted in Figure 5.9. From the plot it appears that, as in the case of α^B , of all the models, BurkLine gave the highest estimates for all the data sets analysed. It is also possible to see that the estimates were particularly variable (with very high standard errors) for the experiment in mid August 2007. To better observe the trend in P_{\max}^B , Figure 5.9 has been redrawn without BurkLine and leaving out part of the standard error bars for the mid August experiment (Figure 5.10). It is then possible to see that the models gave different estimates for all the experiments from spring, summer and autumn 2007, while they produced very similar estimates of P_{\max}^B for the experiments from November 2007 to March 2008. Excluding BurkLine, Webbexp gave the highest estimates (Figure 5.10), followed by Steele and modSteel.

The descriptive statistics for E_k are shown in Table 5.7. As for P_{\max}^B , the models gave different average estimates of E_k , varying between 654.8 $\mu\text{E m}^{-2} \text{s}^{-1}$ (Blackman) and 2602.2 $\mu\text{E m}^{-2} \text{s}^{-1}$ (BurkLine). The minimum estimates of E_k ranged between 129.6 $\mu\text{E m}^{-2} \text{s}^{-1}$ (Steele) and 226.4 $\mu\text{E m}^{-2} \text{s}^{-1}$ (Blackman). For the maximum estimates the variability was higher with estimates ranging between 1051.4 $\mu\text{E m}^{-2} \text{s}^{-1}$ (Blackman) and 18733.1 $\mu\text{E m}^{-2} \text{s}^{-1}$ (BurkLine). The BurkLine model gave the highest estimates of E_k (Figure 5.11) for all data sets, followed by Webbexp, Steele and modSteel.

Table 5.4. A list of experiments performed, showing date, method of treatment of the samples (Filtr = filtration; Acid2 = acidification over night), best model to fit the data set (see Table 5.2 for explanation of the abbreviations), α^B (mgC mgChl⁻¹ ($\mu\text{E m}^{-2} \text{s}^{-1}$) h⁻¹), standard error of α^B , P_{max}^B (mgC mgChl⁻¹ h⁻¹), standard error of P_{max}^B , E_k ($\mu\text{E m}^{-2} \text{s}^{-1}$) and R^2 . The photosynthetic parameters, E_k and R^2 are from the model that best fitted the data.

n exp	Date	Method	Model	α^B	se- α^B	P_{max}^B	se- P_{max}^B	E_k	R^2
7	01-Jun-06	Filtr	LinearModel	0.0039	0.0002	---	---	---	0.95
8	08-Jun-06	Filtr	JassPlatt	0.0077	0.0006	2.53	0.73	328.4	0.94
9	15-Jun-06	Filtr	Blackman	0.0041	0.0003	1.25	0.15	306.7	0.89
10	21-Jun-06	Filtr	modPlatt	0.0055	0.0010	1.01	0.22	182.2	0.67
11	05-Jul-06	Filtr	modPlatt	0.0145	0.0024	2.19	0.37	150.8	0.68
12	10-Jul-06	Filtr	Stalling	0.0058	0.0005	4.37	2.26	748.3	0.90
13	10-Aug-06	Filtr	Blackman	0.0047	0.0003	1.43	0.16	300.7	0.88
16	07-Sep-06	Acid2	LinearModel	0.0118	0.0009	---	---	---	0.89
17	26-Sep-06	Acid2	LinearModel	0.0170	0.0010	---	---	---	0.93
18	19-Oct-06	Acid2	LinearModel	0.0103	0.0005	---	---	---	0.95
19	05-Dec-06	Acid2	BurkLine	0.0216	0.0061	9.42	4.16	436.7	0.59
20	15-Mar-07	Acid2	Stalling	0.0115	0.0005	16.24	4.57	1408.5	0.98
21	22-Mar-07	Acid2	LinearModel	0.0136	0.0011	---	---	---	0.88
22	29-Mar-07	Acid2	Blackman	0.0083	0.0004	3.82	0.13	461.9	0.96
23	03-Apr-07	Acid2	Blackman	0.0123	0.0007	7.00	0.43	569.8	0.93
24	12-Apr-07	Acid2	Blackman	0.0135	0.0005	9.26	0.36	688.6	0.97
25	23-Apr-07	Acid2	Blackman	0.0213	0.0013	15.33	0.74	718.2	0.94
26	03-May-07	Acid2	Blackman	0.0079	0.0003	5.60	0.17	707.1	0.97
27	15-May-07	Acid2	Blackman	0.0091	0.0003	8.50	0.35	936.6	0.97
28	22-May-07	Acid2	BurkLine	0.0122	0.0026	15.50	5.03	1268.7	0.85
29	01-Jun-07	Acid2	BurkLine	0.0059	0.0006	41.12	32.12	7006.9	0.97
30	07-Jun-07	Acid2	JassPlatt	0.0069	0.0005	9.06	1.28	1316.3	0.97

Table 5.4. Continued.

n exp	Date	Method	Model	α^B	se- α^B	P_{\max}^B	se- P_{\max}^B	E_k	R^2
32	02-Aug-07	Acid2	Blackman	0.0100	0.0004	8.79	0.41	877.8	0.96
33	14-Aug-07	Acid2	Blackman	0.0098	0.0003	10.30	0.27	1051.4	0.98
34	05-Sep-07	Acid2	Blackman	0.0105	0.0003	9.84	0.27	933.6	0.98
35	13-Sep-07	Acid2	Blackman	0.0110	0.0004	10.44	0.55	950.6	0.94
36	27-Sep-07	Acid2	Stalling	0.0098	0.0008	20.15	5.75	2065.0	0.94
37	18-Oct-07	Acid2	Blackman	0.0064	0.0002	6.27	0.17	974.5	0.98
38	13-Nov-07	Acid2	modPlatt	0.0048	0.0007	2.22	0.22	466.5	0.76
39	11-Dec-07	Acid2	Blackman	0.0031	0.0007	1.77	0.26	563.8	0.53
40	17-Jan-08	Acid2	Steele	0.0126	0.0063	2.72	0.66	215.5	0.23
42	28-Feb-08	Acid2	Stalling	0.0040	0.0013	2.54	0.68	638.7	0.52
43	13-Mar-08	Acid2	Stalling	0.0198	0.0029	6.32	0.41	319.1	0.88

Table 5.5. Descriptive statistics (number of estimates, mean, standard deviation, median, minimum and maximum value) for α^B (mgC mgChl^{-1} ($\mu\text{E m}^{-2} \text{s}^{-1}$) h^{-1}) estimated by the 8 models and the linear model. Tettsqrt model is not shown because it could not be fitted to any of the data sets. The abbreviations of the names of the models are explained in Table 5.2.

α^B	Blackman	BurkLine	JassPlatt	Steele	modSteele	STalling	Webbexp	modPlatt	Linear mod
n	23	28	28	28	28	27	28	28	5
Mean	0.0089	0.0115	0.0097	0.0107	0.0107	0.0098	0.0110	0.0103	0.0113
Standard Dev	0.0045	0.0062	0.0048	0.0053	0.0053	0.0050	0.0056	0.0051	0.0049
Median	0.0083	0.0102	0.0094	0.0101	0.0101	0.0095	0.0101	0.0098	0.0118
Minimum	0.0031	0.0041	0.0039	0.0042	0.0042	0.0040	0.0041	0.0039	0.0039
Maximum	0.0213	0.0279	0.0238	0.0261	0.0261	0.0238	0.0262	0.0257	0.0170

Table 5.6. Descriptive statistics (number of estimates, mean, standard deviation, median, minimum and maximum value) for P_{\max}^B ($\text{mgC mgChl}^{-1} \text{ h}^{-1}$) estimated by the 8 models. Tettsqrt model is not shown because it could not be fitted to any of the data sets. The abbreviations of the names of the models are explained in Table 5.2.

P_{\max}^B	Blackman	BurkLine	JassPlatt	Steele	modSteele	STalling	Webbexp	modPlatt
n	23	28	28	28	28	27	28	28
Mean	5.93	26.12	8.11	11.17	11.16	9.74	14.34	8.75
Standard Dev	3.68	35.33	5.98	12.92	12.92	7.22	17.61	8.84
Median	5.60	16.45	8.16	8.62	8.62	9.59	10.32	7.42
Minimum	1.25	2.00	1.10	1.07	1.07	1.24	1.27	1.01
Maximum	15.33	185.24	24.34	67.59	67.59	29.70	92.14	45.67

Table 5.7. Descriptive statistics (number of estimates, mean, standard deviation, median, minimum and maximum value) for E_k ($\mu\text{E m}^{-2} \text{ s}^{-1}$) estimated by the 8 models; Tettsqrt model is not shown because it could not be fitted to any of the data sets. The abbreviations of the names of the models are explained in Table 5.2.

E_k	Blackman	BurkLine	JassPlatt	Steele	modSteele	STalling	Webbexp	modPlatt
n	23	28	28	28	28	27	28	28
Mean	654.8	2602.2	846.3	1113.7	1114.8	1011.4	1428.7	881.8
Standard Dev	263.6	3606.2	563.3	1305.0	1304.2	687.7	1787.9	875.7
Median	665.4	1730.4	704.5	782.2	782.2	905.3	990.4	671.6
Minimum	226.4	181.1	168.8	129.6	134.3	178.7	141.1	150.8
Maximum	1051.4	18733.1	2463.9	6824.9	6824.9	3007.8	9308.1	4603.1

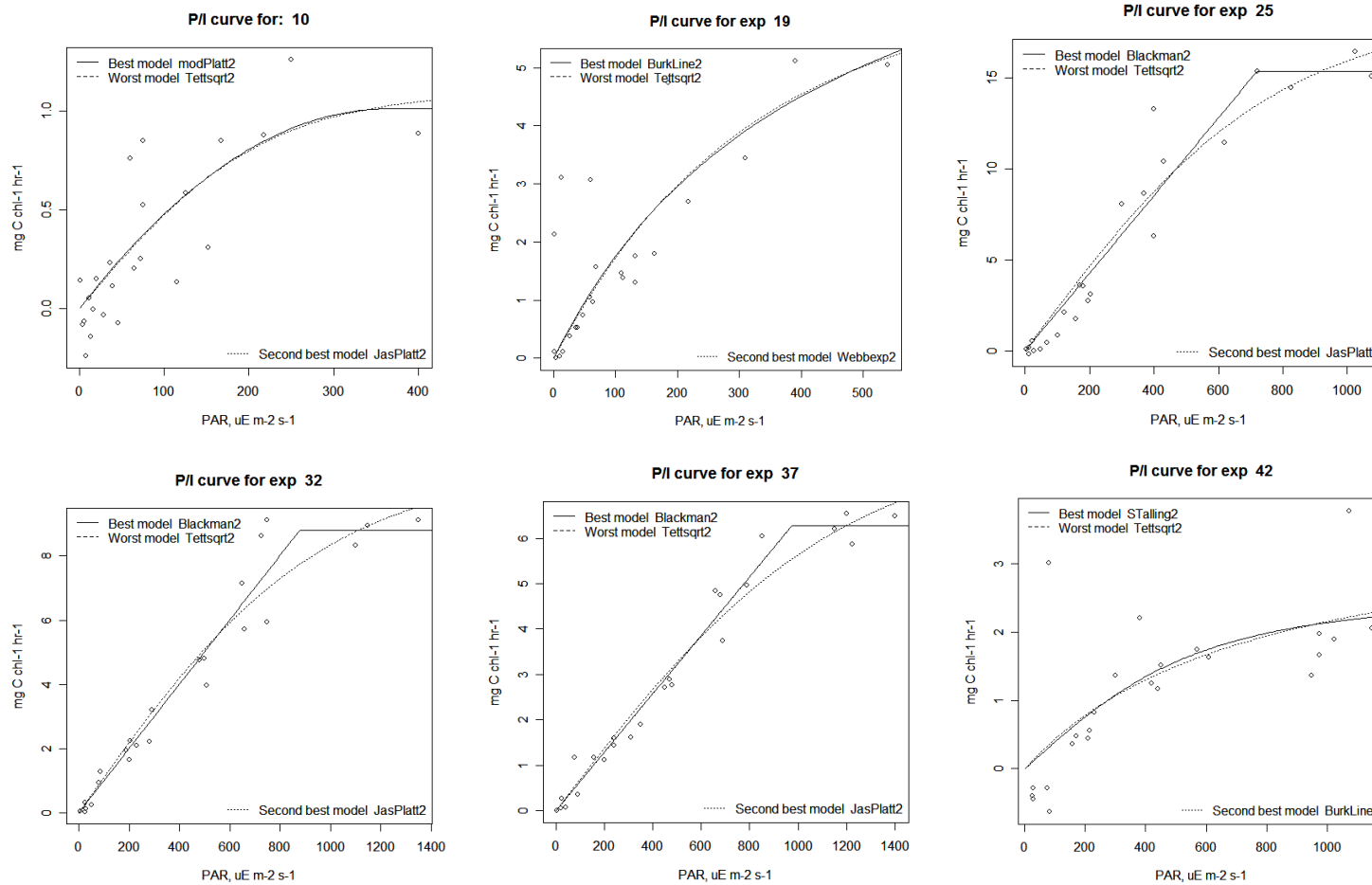


Figure 5.7. Examples of P/E curves showing the best and second best models fitting the data. The worst fitting model (Tettsqrt) is missing because the model could not fit the data set.

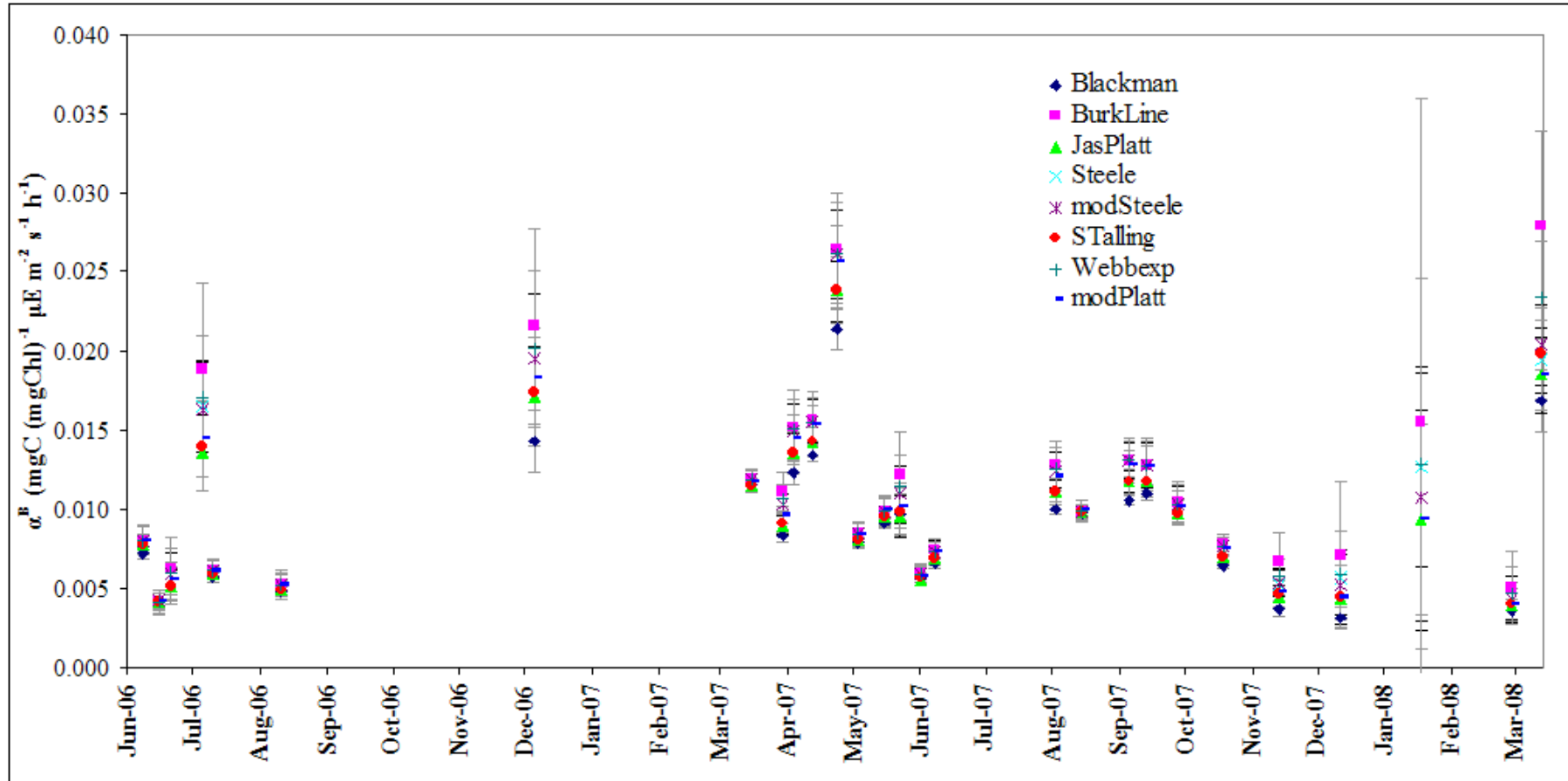


Figure 5.8. Variability in α^B ($\text{mgC mgChl}^{-1} (\mu\text{E m}^{-2} \text{s}^{-1}) \text{h}^{-1}$) from June 2006 to March 2008 estimated from P/E models (see Table 5.2 for explanation of the abbreviations). Error bars are the standard error. Estimates from Tettsqrt model are not shown because the model could not be fitted to any of the data sets.

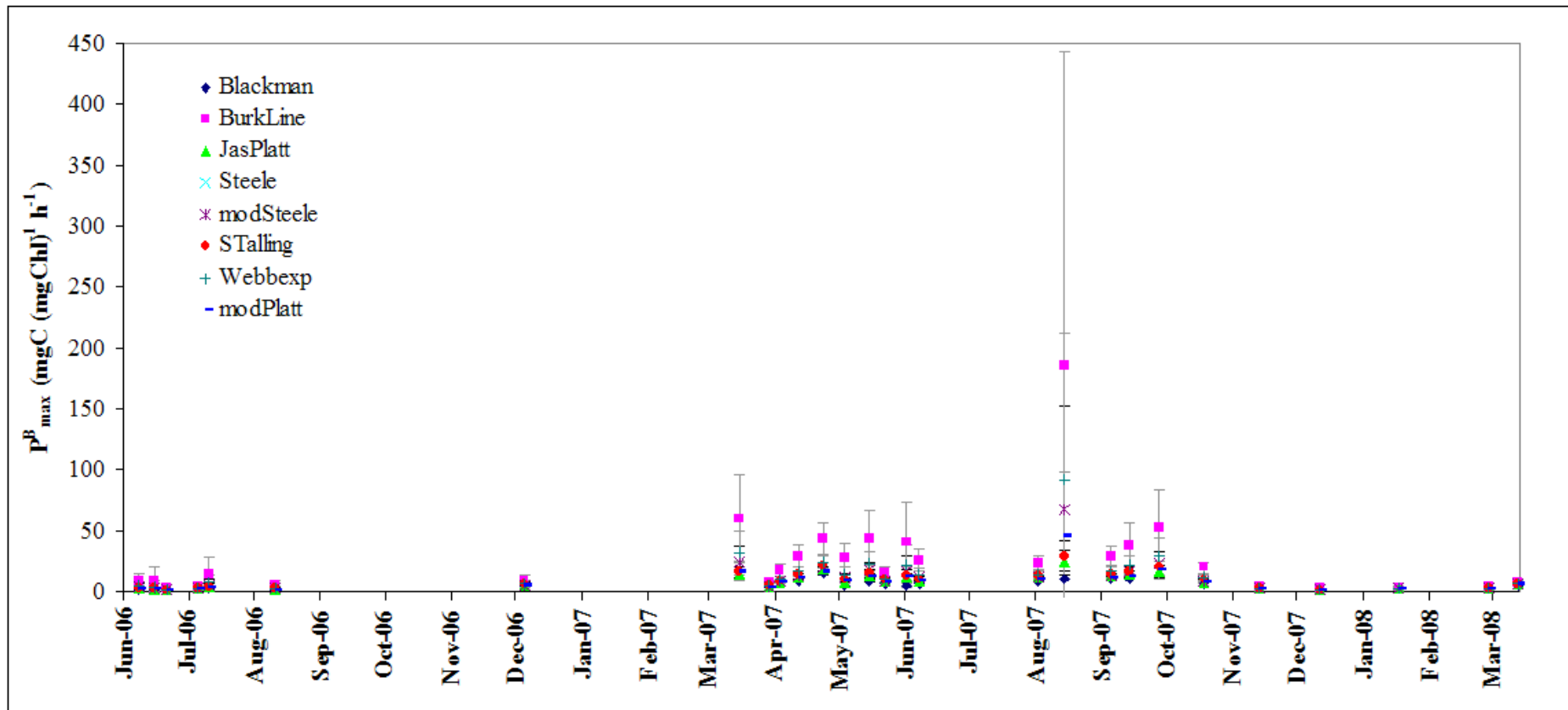


Figure 5.9. Variability in P^B_{\max} ($\text{mgC mgChl}^{-1} \text{h}^{-1}$) from June 2006 to March 2008 estimated from 8 models (see Table 5.2 for explanation of the abbreviations). Error bars are the standard error. Estimates from Tettsqrt model are not shown because the model could not be fitted to any of the data sets.

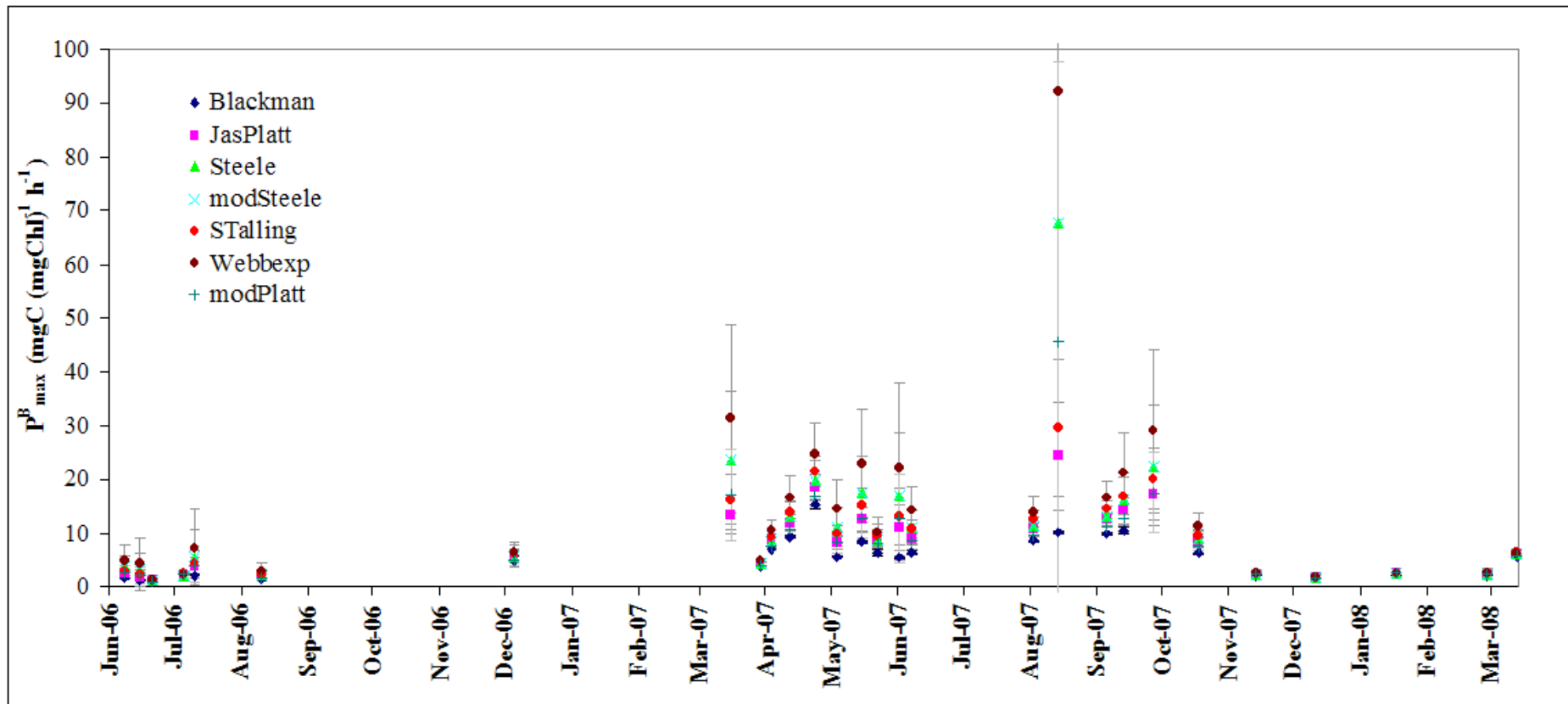


Figure 5.10. Variability of P_{\max}^B ($\text{mgC mgChl}^{-1} \text{h}^{-1}$) from June 2006 to March 2008 estimated from 7 models (see Table 5.2 for explanation of the abbreviations) with exclusion of the Burk and Lineweaver (1935) model. Error bars are the standard error. The upper parts of the standard error bars for Webbexp, Steele and modSteele models are not shown (see Figure 5.9 for the graph with full error bars). Estimates from Tettsqrt model are not shown because the model could not be fitted to any of the data sets.

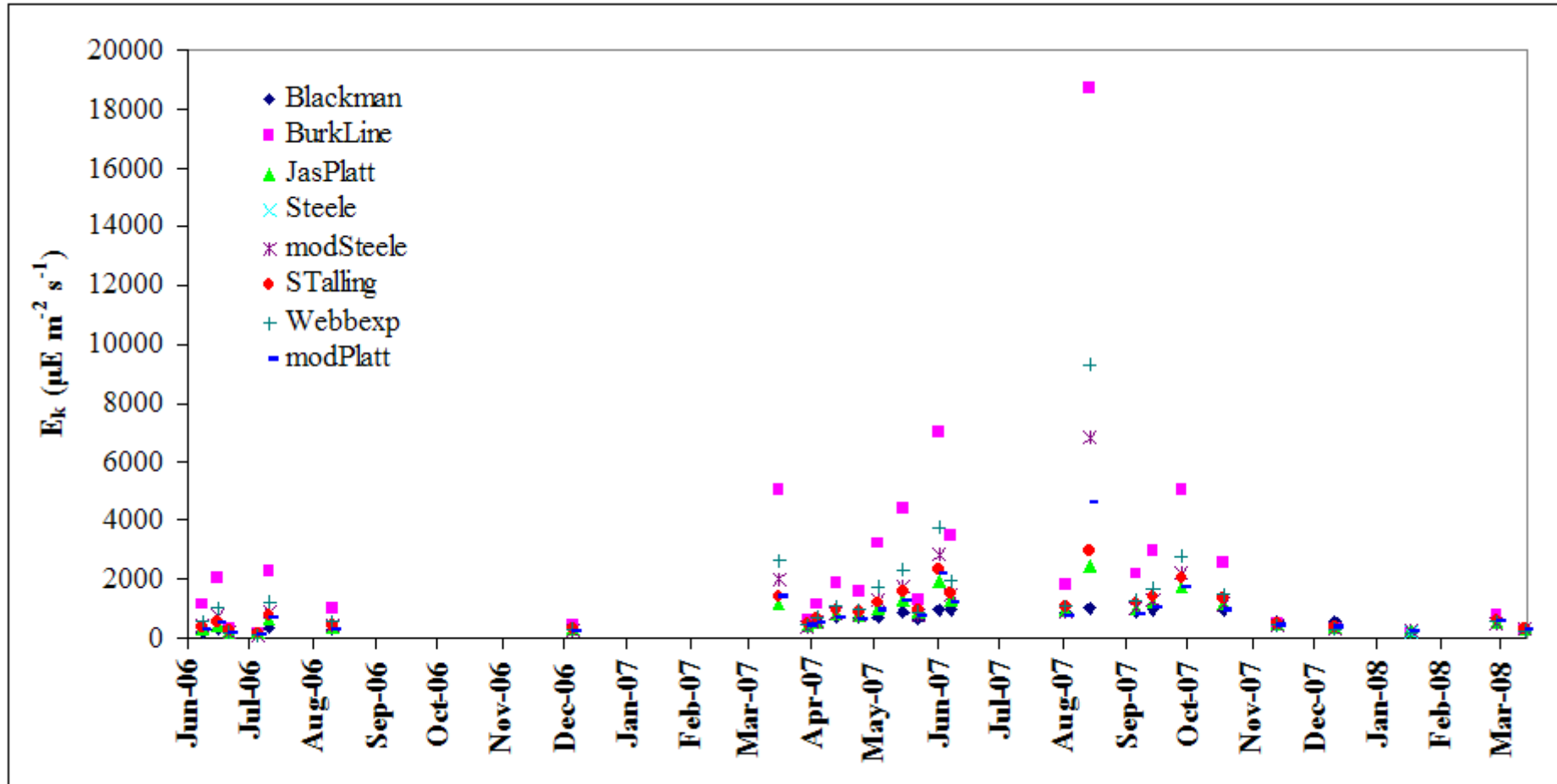


Figure 5.11. Variability of E_k ($\mu E m^{-2} s^{-1}$) estimated from 8 models (see Table 5.2 for explanation of the abbreviations), from June 2006 to March 2008. Estimates from Tettsqrt model are not shown because the model could not be fitted to any of the data sets.

The estimates of the three indices used to identify the best overall model for fitting Carlingford Lough data sets are shown in Table 5.8. For the 33 data sets, each index gave a different 'best' model. JasPlatt and modPlatt had the highest average indices of goodness R^2 (0.713), although the difference in R^2 from other models such as Steele, modSteel, Webbexp, BurkLine, and Stalling, was small. Based on the number of times a model fitted the data sets as the best one (N_i), Blackman scored the highest (best model in 14 out of 33 cases), followed by STalling and the linear model with 5 times each. According to the third index (which was ranking the models based on the R^2), JasPlatt scored the highest suggesting that this model was consistently providing good fit of the data sets, although it was only the best model fitting in 2 out of 33 cases. The second best model based on this third index was STalling.

Excluding the linear model (which was only used to fit the P/E data sets when none of the 9 models could fit the data) and Tett unpublished model (which did not fit any of the data), Blackman had the lowest average R^2 (0.608), although it was the best model based on N_i . Webbexp and modSteele were never the best model fitting the data set, followed by Steele which was the best model in only 1 situation. Considering the rank index, BurkLine had a score that was 2.5 fold smaller than JasPlatt, followed by Webbexp with a score approximately half of the JasPlatt model. Based on these results, it was decided to use JasPlatt estimates of the photosynthetic parameters for the next stage of the analysis. This model was preferred to the others because of its good R^2 and overall consistency in fitting all the data sets (highest score of the rank index).

Table 5.8. The average R^2 , N_i (number of times a model gave the best fit) and Rank index (based on the R^2 of the fit of the model) for the 10 models. The rank number between square brackets is the overall performance of the model with 1 being the best. See Table 5.2 for explanation of the model names.

Model	Average R^2	N_i	Rank
Blackman	0.608 ± 0.426	14	131 [5]
BurkLine	0.707 ± 0.352	3	67 [8]
JassPlatt	0.713 ± 0.352	2	169 [1]
Steele	0.712 ± 0.350	1	133 [4]
modSteele	0.711 ± 0.351	0	108 [6]
Stalling	0.706 ± 0.363	5	156 [2]
Tettsqrt	0.000 ± 0.000	0	0 [10]
Webbexp	0.709 ± 0.351	0	91 [7]
modPlatt	0.713 ± 0.351	3	146 [3]
Linear mod	0.139 ± 0.334	5	40 [9]

5.3.2 Variability in estimates of α^B and P_{\max}^B (JasPlatt model)

Trends in estimates of photosynthetic parameters and E_k derived from the JasPlatt model are shown in Figures 5.12, 5.13, and 5.14. α^B showed peaks in December 2006, April 2007 and March 2008 (Figure 5.12); the highest estimates were derived for March 2008 and April 2007, while the lowest for mid June 2006. The trend in P_{\max}^B was less clear with main peaks in April and August 2007 (Figure 5.13). The trend in E_k followed closely that of the P_{\max}^B trend (Figure 5.14).

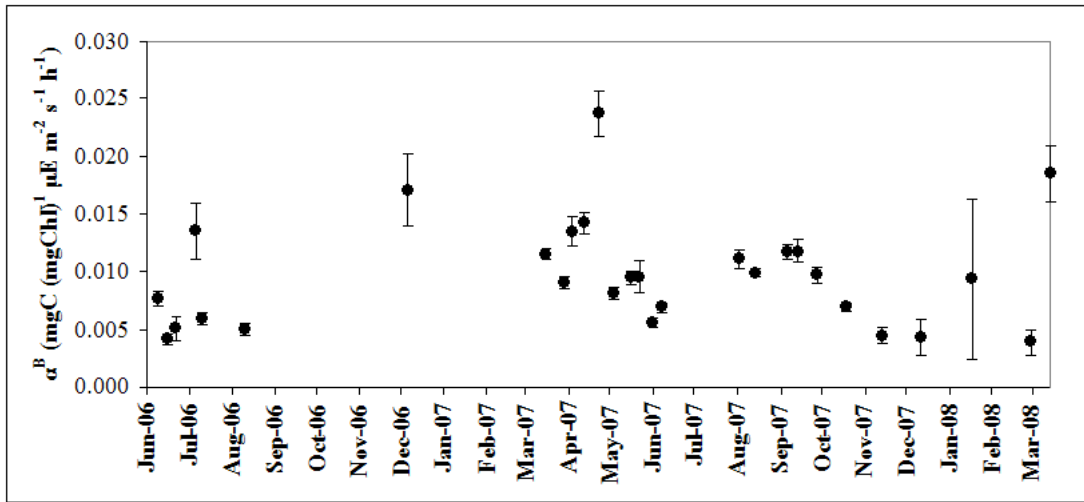


Figure 5.12. Variability in α^B (mgC mgChl⁻¹ (μ E m⁻² s⁻¹) h⁻¹) from June 2006 to March 2008 estimated using Jassby and Platt (1976) model. Error bars are the standard error.

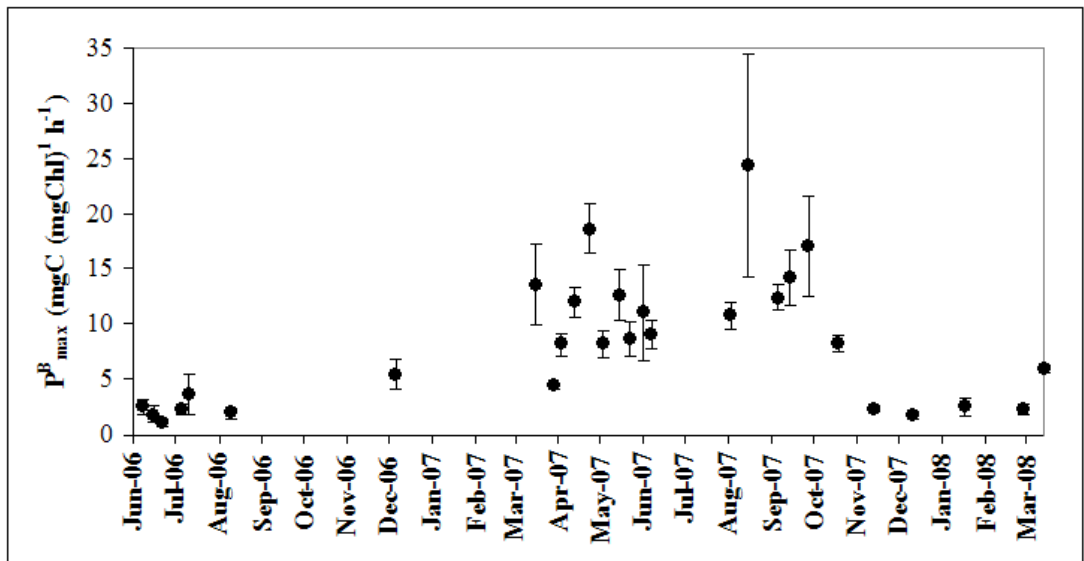


Figure 5.13. Variability in P^B_{max} (mgC mgChl⁻¹ h⁻¹) from June 2006 to March 2008 estimated using Jassby and Platt (1976) model. Error bars are the standard error.

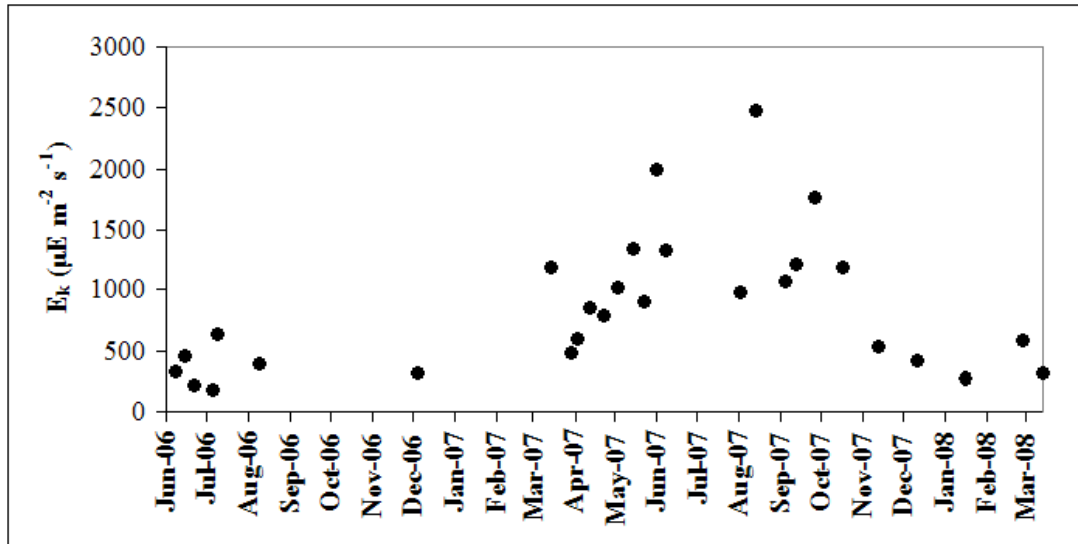


Figure 5.14. Variability in E_k ($\mu\text{E m}^{-2} \text{s}^{-1}$) from June 2006 to March 2008 estimated from Jassby and Platt (1976) model.

Multiple regressions of α^B and P_{\max}^B estimates (derived from JasPlatt) and other environmental variables were performed to identify which environmental variables were influencing the variability in the photosynthetic parameters. Log-transformed α^B and P_{\max}^B were regressed against time of sampling, CTD temperature and salinity, nutrient (ammonium, nitrite, nitrate, phosphate, silicate) concentrations, temperature of incubation, K_d , and log-transformed phaeopigments/chlorophyll ratio, average phytoplankton cell volume ($\log\text{ACV}$), average chlorophyll concentration per phytoplankton cell ($\log\text{ACC}$), surface irradiance at the time of sampling ($\log I_{\text{samp}}$), average surface irradiance in the 24 hours before sampling ($\log I_{24}$), and Clanrye River flow. The normality distribution of the variables was tested before performing the regressions (see section 2.2.7).

Log-transformed P_{\max}^B , log-transformed phaeopigment/chlorophyll ratio and phosphate explained 46.9 % (R^2) of the variability in α^B . The regression (Equation 5.6) was statistically significant (analysis of variance, $DF = 27$, $F = 7.05$, $n = 28$, $p = 0.001$), as well as the regression coefficients of $\log P_{\max}^B$ and \log phaeopigments/chlorophyll ratio ($p < 0.05$). The regression coefficient of phosphate was not statistically significant ($p > 0.05$). $\log P_{\max}^B$ explained 36.8% of the variance, \log phaeopigments/chlorophyll ratio 7.1% and phosphate the remaining 3%.

$$\log \alpha^B = -2.23 + 0.405 \cdot \log P_{\max}^B + 0.25 \cdot \log \frac{Phaeo}{Chl} - 0.151 \cdot \log Phosphate \quad (5.6)$$

The variability in $\log P_{\max}^B$ was mainly explained by $\log \alpha^B$, and NH_4 ($R^2 = 58.3\%$, $DF = 27$, $F = 17.45$, $n = 28$, $p < 0.001$; see Equation 5.7). NH_4 explained 36.8% of the variance in $\log P_{\max}^B$, and $\log \alpha^B$ 21.5% (the regression coefficients were statistically significant with $p < 0.05$).

$$\log P_{\max}^B = 2.91 + 0.926 \cdot \log \alpha^B - 0.158 \cdot NH_4 \quad (5.7)$$

The Pearson correlation coefficient of the photosynthetic parameters and the environmental variables listed below (Table 5.9), showed that $\log \alpha^B$ was negatively correlated to the average chlorophyll content per cell (coefficient = -0.438, $p < 0.05$) and positively to $\log P_{\max}^B$ (coefficient = 0.607, $p \leq 0.001$). Log-transformed P_{\max}^B was positively correlated to $\log \alpha^B$ (as noted above) and was also correlated negatively to ammonium concentration (coefficient = -0.570, $p < 0.05$), log-transformed average chlorophyll content (coefficient = -0.510, $p < 0.05$); and log-transformed phaeopigments/chlorophyll ratio (coefficient = -0.439, $p < 0.05$).

Table 5.9. Pearson correlation coefficient for each comparison of a photosynthetic parameter and the main environmental variables, and its statistical significance (* = $p < 0.05$; ** = $p \leq 0.001$; no star = $p > 0.05$). Ts is the sampling time; T and S are temperature and salinity from CTD; NH₄, Phosp, Nitra, Si, Nitri are ammonium, phosphate, nitrate, silicate, and nitrite respectively; T_inc is temperature of incubation; K_d; logRiv is the log-transformed river flow; logACV and logACC refer to average cell volume and average chlorophyll per cell respectively (log-transformed); logE₂₄ and logE_s indicate the irradiance in the 24 hours before the sampling event and the irradiance during the sampling event (log-transformed); logph/chl is the ratio of phaeopigments to chlorophyll (log-transformed).

	Ts	T	S	NH₄	Phosp	Nitra	Si	Nitri	T_inc
logP_m^B	0.211	0.162	0.203	-0.570*	-0.318	-0.227	-0.256	-0.304	0.155
log^Bα	-	-0.020	-0.118	-0.128	-0.067	0.103	0.052	0.050	-0.100

	K_d	logRiv	log ACV	log ACC	logE₂₄	logE_s	logph/chl	log P_m^B	log α^B
logP_m^B	-	-0.110	0.316	-0.510*	0.206	0.079	-0.439*		0.607 **
log^Bα	0.280	0.157	0.131	-0.438*	-0.173	-0.098	-0.006	0.607 **	

5.4 Discussion

5.4.1 Comparison of P/E models

For a given data set, the models used (Table 5.2) provided similar estimates of α^B but variable estimates of P_{\max}^B and E_k (overall if observing the maximum estimates). The BurkLine model gave the highest estimates. This last observation is partially supported by the study by Grangeré *et al.* (2009) who compared the fit of 5 photosynthesis/irradiance models (Webbexp, Platt *et al.* 1975, BurkLine, STaylor and Steele) on data from the Baie de Veys (France) and observed that the equations of BurkLine and Steele gave the highest estimates compared to the other 3 models. Furthermore, in the study by Grangeré *et al.* (2009), BurkLine and Steele models also gave extreme values of α^B . In another study for testing the fit of photosynthesis/irradiance models (Frenette, Demers and Legendre 1993), the fit of JassPlatt and Webbexp models were shown to give similar estimates of P_{\max}^B (4% difference between the models), while the estimates of α^B showed a difference of 24% between the two models.

From the above considerations it appears that the different models can give different estimates of the photosynthetic parameters. Therefore the choice of model should be based on the ability of the model to minimize the residual sum of squares of the fit (see Lederman and Tett 1981); in other words, the ability to reduce the distance between the observations and the associated values predicted by the model. This can also be expressed with the determination coefficient R^2 (section 5.2.1). Based on the R^2 value it is possible to identify models that are producing a bad fit. However, the R^2 does not discriminate photosynthesis/irradiance models that produce a good fit, as shown by Lederman and Tett (1981) and in this study (Table 5.8). Other criterion, such as N_i (the number of data sets for which a given model gave the best fit), may help in the selection of which model to use, although Lederman and Tett (1981) warned that N_i is a “*statistic of undefined properties*”, thus differences in N_i are not easy to interpret. One of the risks in using N_i as a selection criterion, is of selecting a model that can fit the data sets quite well in most of the case but also quite badly in others (Lederman and Tett 1981) In fact, this seems to be the case with the Blackman model (Table 5.8). This model gave the best fit (highest R^2) for 14 out of 33 data sets, but had one of the lowest average R^2 suggesting that on average its fit was not as good as the other models. Furthermore, Blackman could not

fit 5 of the 33 data sets, while the other models were able to produce estimates of the photosynthetic parameters for those 5 data sets.

It seems then more important to use a model that consistently produces a good fit, although not necessarily the best or worst. The third type of index used in this study (Rank in Table 5.8) tried to take into account the ‘consistency’ term of the fit. Based on this last index, JassPlatt appeared to be the most consistent model in fitting the data sets (a consideration supported by the highest average R^2). The second best model based on the Rank index was STalling, while the modPlatt, which had the same average R^2 as JassPlatt, came only third with 23 points of difference. At the other end of the scale (excluding the linear model which was used only when P_{\max}^B was not reached, and Tettsqrt), it was possible to find BurkLine and Webbexp.

Based on values of R^2 and on the Rank index it was decided to adopt the hyperbolic function of Jassby and Platt (1976). Although it is not possible to identify an absolute best model, it is interesting to note that in all the cited studies (Jassby and Platt 1976; Lederman and Tett 1981; Grangeré *et al.* 2009) Burk and Lineweaver’s model (1935) gave one of the poorest fit. This could be explained considering that the rectangular hyperbola (Burk and Lineweaver’s model) is frequently used to describe enzyme kinetics, in particular nutrient uptake by microalgae (Jassby and Platt 1976).

The variability in the estimates of the photosynthetic parameters amongst models was not constant suggesting that some data sets may have been more difficult to fit due to scattered data points. For the experiment carried out in mid August 2007 the variability in estimated P_{\max}^B between models was large and the estimates of P_{\max}^B and E_k from all models (except Blackman and JassPlatt) were not considered reliable. In fact, based on the photosynthetic turnover time and on the number of photosynthetic units, the maximum assimilation number (P_{\max}) should be approximately $25 \mu\text{gC h}^{-1}$ (Falkowski 1981). For the data set of mid August 2007, only JassPlatt and Blackman estimated a maximum photosynthetic rate $< 25 \text{ mgC mgChl}^{-1} \text{ h}^{-1}$. For this event (mid August 2007) the STalling model gave P_{\max}^B as $30 \text{ mgC mgChl}^{-1} \text{ h}^{-1}$, while the other model estimates were well above the number suggested by Falkowski (1981).

5.4.2 Variability of the photosynthetic parameters (JassPlat model) and investigations on the estimates of E_k

A comparison of the estimates of the photosynthetic parameters from Carlingford Lough with values reported in literature is shown in Table 5.10. The range in α^B from Carlingford Lough is comparable with the ranges measured in the German Wadden Sea (Tillmann, Hesse and Colijn 2000), in the Baie des Veys (Jouenne *et al.* 2005, 2007), in the Elbe and Gironde estuary (Goosen *et al.* 1999), in the Falkowski estuary (Azevedo, Duarte and Bordalo 2006), in the NW Mediterranean (Morán and Estrada 2005), and off the Baja California (Aguirre-Hernández *et al.* 2004). However, the Carlingford Lough values were lower than those measured in the NW Irish Sea (Gowen and Bloomfield 1996; Gowen *et al.* 1995), in the Dogger Bank in the North Sea (Riegman and Colijn 1991; Weston *et al.* 2005), in the Eastern English Channel (Lizon *et al.* 1995), in San Margaret Bay (Platt and Jassby 1976), and in Bedford Basin (Côté and Platt 1983).

Due to the large variability in the rate of light saturated photosynthesis, all P_{\max}^B values derived by the other authors listed in Table 5.10 fell into the range of estimates of P_{\max}^B measured in Carlingford Lough. However, Carlingford Lough values never reached the minimum values given in some of the papers in Table 5.10 (e.g. Gowen and Bloomfield 1996; Tillmann, Hesse and Colijn 2000; Jouenne *et al.* 2005 and 2007). The average Carlingford Lough value of $8.11 \text{ mgC mgChl}^{-1} \text{ h}^{-1}$ was similar to the average P_{\max}^B reported by Struski and Bacher (2006) for the Marennes-Oléron on the French Atlantic coast ($9.07 \text{ mgC mgChl}^{-1} \text{ h}^{-1}$), but was almost double the average values reported by Platt and Jassby (1976) and Côté and Platt (1983).

Table 5.10. Comparative table of ranges of α^B ($\text{mgC mgChl}^{-1} \text{ h}^{-1} (\mu\text{E m}^{-2} \text{ s}^{-1})^{-1}$), P^B_{max} ($\text{mgC mgChl}^{-1} \text{ h}^{-1}$) and E_k ($\mu\text{E m}^{-2} \text{ s}^{-1}$) derived from this study and literature. The authors of the study, the location, date and model used to fit the P/E curve are also shown.

Authors	Location	Date	Model	α^B ($\text{mgC mgChl}^{-1} (\mu\text{E m}^{-2} \text{ s}^{-1})^{-1}$)	P^B_{max} ($\text{mgC mgChl}^{-1} \text{ h}^{-1}$)	E_k ($\mu\text{E m}^{-2} \text{ s}^{-1}$)
Gowen and Bloomfield (1996)	Western Irish Sea	Mar 1992 – Oct 1993	Talling (1957)	0.02 – 0.52	0.27 – 6.87	---
Gowen <i>et al.</i> (1995)	NW Irish Sea	Summer 1992	Talling (1957)	0.12 – 0.26 (median)	1.39 – 3.71 (median)	---
Shaw and Purdie (2001)	UK coastal water, North Sea	1993 - 1995	Webb, Newton and Star (1974)	0.02 – 2.44 (per day)	8 – 332 (per day)	176 ± 6
Weston <i>et al.</i> (2005)	Dogger Bank (North Sea)	Aug 2001	Jassby and Platt (1976)	0.013-0.0358	1.85-3.86	65.8-215.6
Riegman and Colijn (1991)	Dogger Bank (North Sea)	Jul-Aug 1988	Platt <i>et al.</i> (1980)	0.0464	13.6-13.8	297
Tillmann, Hesse & Colijn (2000)	German Wadden Sea	Mar 1995 – Dec 1996	Platt <i>et al.</i> (1980)	0.007-0.039	0.8-9.9	67 - 538
Jouenne <i>et al.</i> (2005)	Baie des Veys Eastern English Channel (France)	Jun 2003 and Apr 2004	Platt <i>et al.</i> (1980)	Jun 03: 0.015 (estuary), 0.037 (bay) Apr 04: 0.003 (estuary), 0.015 (bay)	Jun 03: 1.8 (estuary), 2.3 (bay) Apr 04: 0.2 (estuary), 0.7 (bay)	Jun 03: 163.7 (est.), 63.5 (bay) Apr 04: 107 (est.), 58 (bay)
Jouenne <i>et al.</i> (2007)	Baie des Veys Eastern English Channel (France)	May 2002 – Oct 2003	Platt <i>et al.</i> (1980)	0.002 – 0.119	0.39 – 8.48	---

Table 5.10. Continued.

Struski and Bacher (2006)	Marennes-Oléron, French Atlantic coast	2001 – 2002	Jassby and Platt (1976)	0.011 – 0.066 (mean 0.025)	5.12 – 13.53 (mean 9.07)	181.7 – 772.7 (mean 390.4)
Lizon <i>et al.</i> (1995)	Eastern English Channel	29-30 Apr – 1 May 1993	Platt <i>et al.</i> (1980)	0.145 – 0.262	9.7 – 16.6	70.6 – 101.6
Goosen <i>et al.</i> (1999)	Elbe estuary (Germany), Westerschelde (The Netherlands), Gironde (France)	April 1994	Eilers and Peeters (1988)	Elbe: 0.006 – 0.015 Westerschelde: 0.015 – 0.020 Gironde: 0.012 – 0.020	Elbe: 2.0 – 4.0 Westerschelde: 4.2 – 18.0 Gironde: 0.6 – 8.6	- - -
Macedo <i>et al.</i> (2001)	Santo André Lagoon Southwest Portugal	Jan 1998 – Jan 1999	Eilers and Peeters (1988)	- - -	2.0 – 22.5	5.2 – 335
Azevedo, Duarte and Bordalo (2006)	Falkowski estuary (Portugal)	Dec 2002 – Dec 2003	Steele (1962)	0.0046 – 0.0194	0.87 – 5.06	373.8 – 723.0
Morán and Estrada (2005)	NW Mediterranean	Mar 1999 – Jan/Feb 2000	Platt <i>et al.</i> (1980), Webb, Newton and Star (1974)	0.006 – 0.032	0.8 – 3.9	52 – 442
Mangoni <i>et al.</i> (2008)	Adriatic Sea (Italy)	Feb – Mar 1997	Platt <i>et al.</i> (1980)	0.1168 (Feb), 0.0245 (Mar)	20.27 (Feb), 2.38 (Mar)	81-174
Harding, Meeson and Fisher (1986)	Chesapeake Bay, Delaware Bay USA	Mar 1982 – Apr 1983	Platt <i>et al.</i> (1980)	0.011 – 0.14	1.2 – 15	70.7 – 486
Platt and Jassby (1976)	San Margaret Bay	Jul 1973 – Mar 1975	Jassby and Platt (1976)	0.03 – 0.50 (mean 0.20)	1.05 – 19.87 (mean 4.52)	35 – 358 (mean 112)

Table 5.10. Continued. * Original data: 0.08 – 0.26 (mean 0.14) mgC mgChl⁻¹ h⁻¹ (W m⁻²)⁻¹; ** 12.53 – 62.51 (mean 37.61) W m⁻².

Côté and Platt (1983)	Bedford Basin (Nova Scotia)	May – Jul 1975	Jassby and Platt (1976)	0.017 – 0.057 (mean 0.030)*	2.04 -8.37 (mean 4.93)	57.6 – 287.5 (mean 173.0)**
Aguirre-Hernández <i>et al.</i> (2004)	Off Baja California	Jul – Sep/Oct 1998	Jassby and Platt (1976)	0.004 – 0.028	0.51 – 11.26	102 – 917
Yoshikawa and Furuya (2006)	Sagami Bay (Japan)	Early/late summer 2002 -2003	Platt <i>et al.</i> (1980)	- - -	0.7 – 9.2	99 – 536
This study	Carlingford Lough Northern Ireland	Jun 2006 – Mar 2008	Jassby and Platt (1976)	0.0039 – 0.0238 (mean 0.0097)	1.10 – 24.34 (mean 8.11)	168.8 – 2463.9 (mean 846.3)

The temporal variability in α^B (Figure 5.12), with peaks in December and in March/April, is comparable with the temporal variability described in the studies by Platt and Jassby (1976), Morán and Estrada (2005), and with the study by Harding, Meeson and Fisher (1986). However, plotting the estimates of α^B against day number (Figure 5.15), the trend appeared slightly different with a peak between March and May, a decrease during summer and another small peak at the start of the autumn. If P_{\max}^B is plotted against day number independent of the year (Figure 5.16), its temporal variability is clearer than in Figures 5.9 and 5.10. In particular, the photosynthetic rate at saturating irradiance showed a minimum during winter, a maximum in spring (April/May), followed by a decrease in summer (June/July) and another maximum in late summer (August/September). A late summer peak in P_{\max}^B is in agreement with observations from the Baie des Veys in France (Jouenne *et al.* 2007), the Falkowski estuary in Portugal (Azevedo Duarte and Bordalo 2006), the NW Mediterranean (Morán and Estrada 2005), and San Margaret Bay (Platt and Jassby 1976).

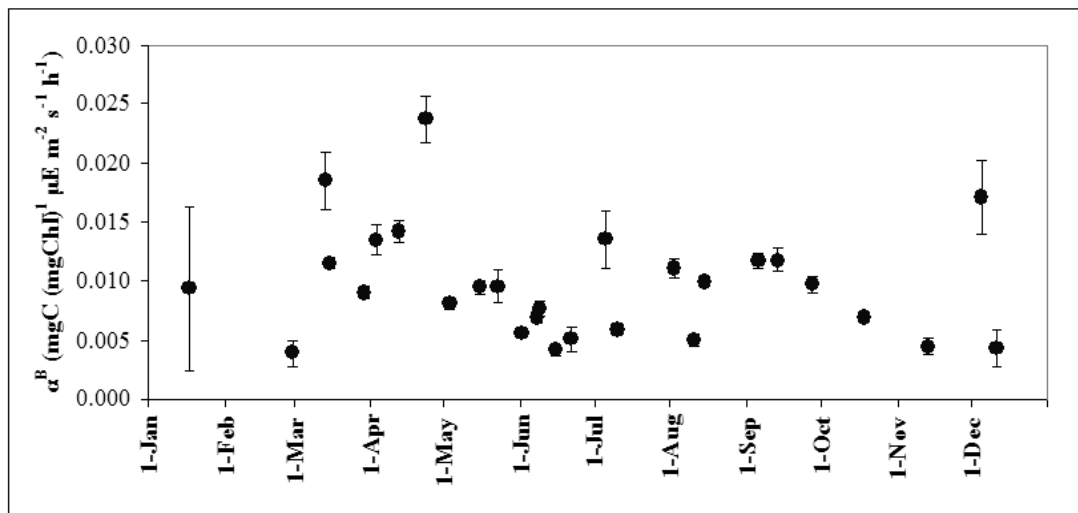


Figure 5.15. Variability of α^B (mgC mgChl⁻¹ (μE m⁻² s⁻¹) h⁻¹) estimated from Jassby and Platt (1976) model, plotted by day number (data from June 2006 to March 2008). Error bar is the standard error.

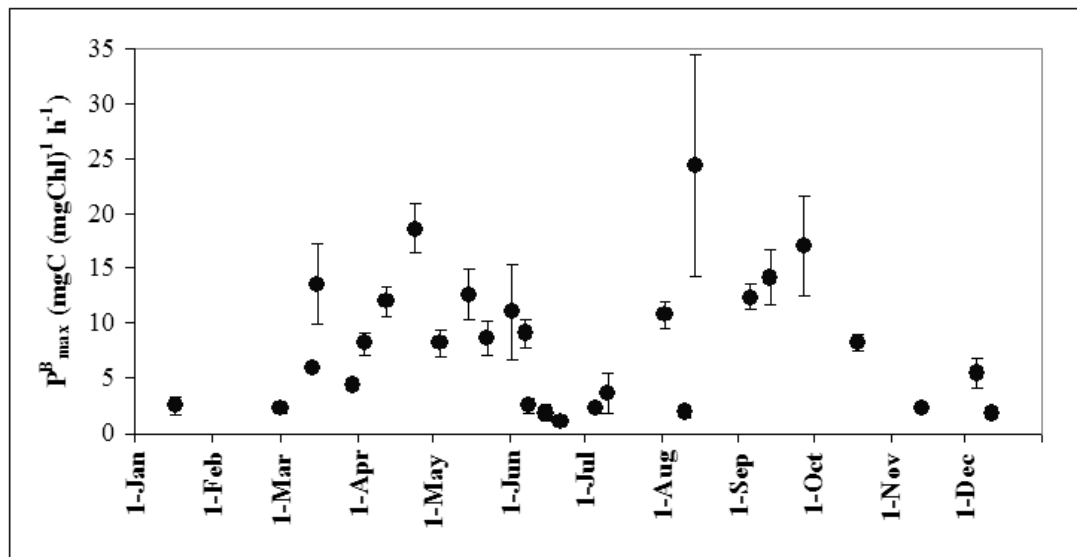


Figure 5.16. Variability of P^B_{max} ($\text{mgC mgChl}^{-1} \text{h}^{-1}$) estimated from Jassby and Platt (1976) model, plotted by day number (data from June 2006 to March 2008). Error bar is the standard error.

The saturation irradiance E_k , was extremely variable and presented unexpectedly high values. The highest values of E_k published in the literature for natural phytoplankton populations are $723.0 \mu\text{E m}^{-2} \text{s}^{-1}$, for the Douro estuary in Portugal (Azevedo, Duarte and Bordalo 2006), $864 \mu\text{E m}^{-2} \text{s}^{-1}$, for the Sagami Bay in Japan (Yoshikawa and Furuya 2006), and $917 \mu\text{E m}^{-2} \text{s}^{-1}$, for the Baja California (Aguirre-Hernández *et al.* 2004). However, the maximum value obtained from the study in Carlingford Lough was over 3 fold higher than the estimates of Azevedo, Duarte and Bordalo (2006) and Yoshikawa and Furuya (2006).

This observation suggests that there may have been an error in some part of the experimental procedure. To examine this possibility, a series of investigations were carried out on the equipment and the method used.

The irradiance measurements (in the 24 positions in the photosynthetron) carried out during the experiments were re-checked to confirm that the unit of measurement were expressed in $\mu\text{E m}^{-2} \text{s}^{-1}$. The biospherical sensor (QSL 100) used for the irradiance measurements was calibrated against a new QSL 100 (< 1 year old) using a range of natural irradiance values. The resulting plot of the calibration is shown in Figure 5.17 and suggests the instrument used during the experimental activity was functioning well.

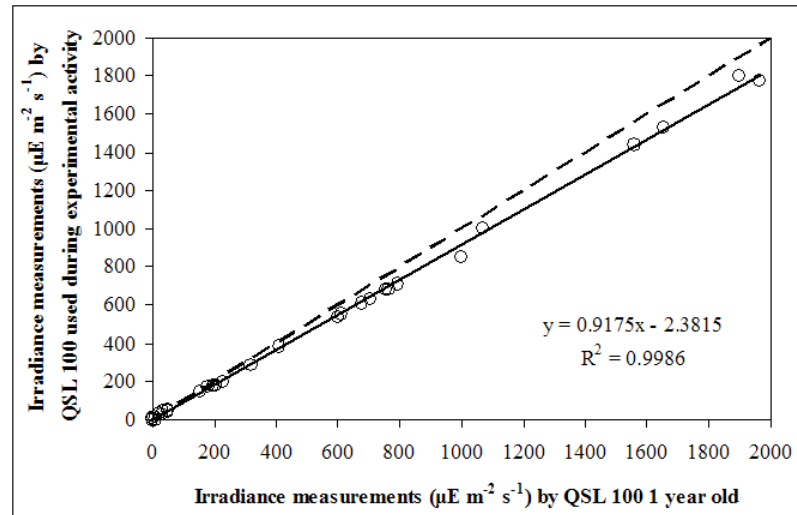


Figure 5.17. Calibration of the Biospherical Sensor (QSL 100) used during the experiments against a new (1 year old) Biospherical Sensor (QSL 100). The 1:1 line is represented by the dashed line.

The measurements of ^{14}C activity derived from the scintillation counter were then considered. The instrument (Tri-Carb 3100TR Liquid Scintillation Analyzer) was calibrated before every batch of analysis using a ^{14}C internal standard. Furthermore, samples from ^{14}C incubations in the Irish Sea (collected during an independent experiment), and analysed with the same scintillation counter, gave estimates of E_k comparable with literature.

The interpolation procedure of the P/E curves was then investigated. An inter-calibration was carried out in January/February 2010 with laboratories in Netherlands (NIOZ) and Finland (SYKE). The participant laboratories analysed the same P/E curve and derived the photosynthetic parameters. The R script used for analysing P/E curves from Carlingford Lough data was adopted for the inter-calibration and it gave estimates of α^B and P_{\max}^B 15-20% higher than the other 2 participants. The discrepancy in the estimates between the participants was associated with the different software (R, Matlab and Excel) used for computing the interpolation of the P/E curve. Although P_{\max}^B and α^B may be overestimated, the overestimation affected the parameters in the same way therefore their ratio (E_k) was not affected.

The ability of the models to fit some P/E curves was then assessed. Observing the P/E plots, it appeared that in some experiments the P/E curves did not reach the light-saturated plateau, therefore the models had to predict where light saturation should have occurred with the possibility of overestimating the value of P_{\max}^B . To test this hypothesis, all the P/E curves were visually checked and only the curves that had a clear light saturation plateau (at least 3-4 points in approximately straight line) were considered. Figure 5.18 shows example of P/E curves with 3-4 points for the plateau and P/E curve where the light saturated production was not clear. After visual screening, the P/E curves were reduced to 13 with a clear plateau (experiments 22-26, 32, 34-35, 37-40 and 42-43), and new descriptive statistics of P_{\max}^B and E_k were calculated for these experiments. P_{\max}^B derived from the screening ranged between 1.76 and 18.62 mgC mgChl⁻¹ h⁻¹ with an average of 7.99 mgC mgChl⁻¹ h⁻¹, while E_k ranged between 275.3 and 1210.5 $\mu\text{E m}^{-2} \text{s}^{-1}$ with an average of 734.2 $\mu\text{E m}^{-2} \text{s}^{-1}$. Although the screening of the P/E curves removed the highest estimates of P_{\max}^B and E_k from the data set, it did not reduce the ranges and averages of these parameters suggesting that the difficulty in fitting the P/E curves with a poorly defined plateau may have been one of the reasons for high E_k values. Screened values of α^B showed the same range of variability shown in Table 5.5 but with a slightly higher mean (0.0107 instead of 0.0097 mgC mgChl⁻¹ ($\mu\text{E m}^{-2} \text{s}^{-1}$) h⁻¹).

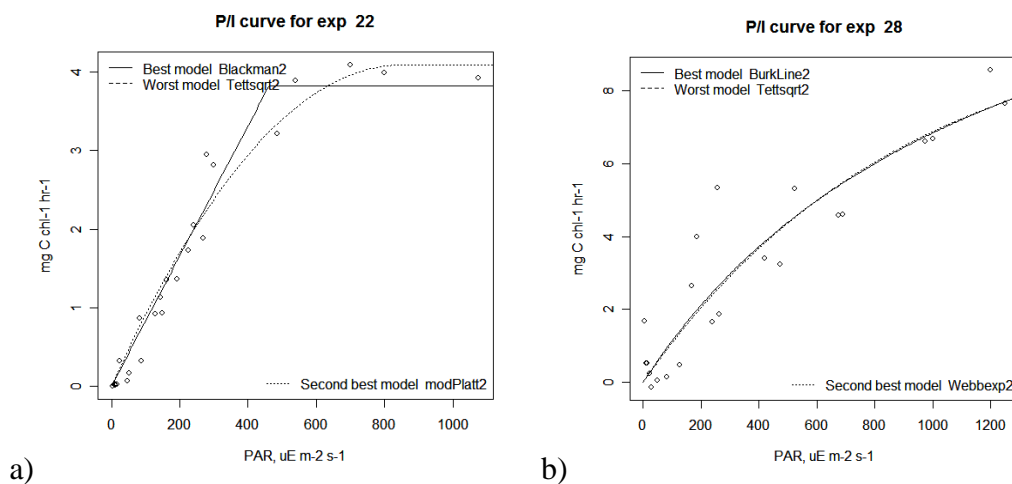


Figure 5.18. Example of P/E curve with 3-4 points identifying light saturation (a) and P/E curve where the plateau was not clear (b).

Another possible explanation for the high values of E_k could be related to the presence of microphytobenthos in the water sample (as suggested by Struski and Bacher 2006). However, as highlighted in Chapter 2, benthic pennate diatoms represented on average only 0.4% of the total phytoplankton abundance, therefore their contribution to photosynthetic efficiency and carbon assimilation was likely to have been minimal.

The anomalously high values of E_k could also be a consequence of the period of dark (usually 2-3 hours) that the phytoplankton experienced during transportation from the sampling site in Carlingford Lough to the laboratory in Belfast. Unfortunately, it was not possible to test if this was the case. However in a study of the Santo André Lagoon, Macedo *et al.* (2001) kept water samples for primary production experiments in the dark for approximately 4 hours before starting the incubation, and their estimates of E_k were comparable with literature values (see Table 5.10).

Finally, in May and July 2010, an independent study was carried out estimating primary production at some sampling stations in the Irish Sea. During this study the standard operating procedure described in Chapters 4 and 5 was applied, and an E_k of approximately $700 \mu\text{E m}^{-2} \text{s}^{-1}$ was derived for a vertically mixed coastal station in May 2010 (data not shown).

Although the estimates of E_k were unusually high in this study, no error was identified in the procedure and no malfunction of the equipment was identified that would have given such high values. On the basis of these investigations, α^B and P_{max}^B values were assumed correct and the values from all 33 experiments were used in the modelling of primary production. Values of E_k were not part of the modelling study.

5.4.3 Environmental control on the photosynthetic parameters

As summarised in the introduction of this Chapter, the photosynthetic parameters are influenced by environmental variables. P_{max}^B is a function of enzymatic processes in photosynthesis and it is influenced by factors such as temperature, nutrient concentration, light history. α^B is a function of photochemical processes and depends on factors such as pigment composition, light quality, and nutrients regime (see review by Côté and Platt 1983).

The relationship between P_{\max}^B and temperature has been described in various studies (e.g. Platt and Jassby 1976; Tillmann, Hesse and Coljin 2000; Macedo *et al.* 2001; Azevedo, Duarte and Bordalo 2006), showing that P_{\max}^B reaches maximum values during summer and minimum during winter. In this study of the photosynthetic parameters of Carlingford Lough there was no statistically significant relationship between P_{\max}^B and temperature (Table 5.9), and contrary to that observed by the authors above, low values of P_{\max}^B were observed during summer 2006 (June to August 2006; Figure 5.10). However, if the values of P_{\max}^B for summer 2006 are removed from the data set, the remaining values showed a positive significant correlation with the incubation temperature (Pearson coefficient = 0.658, p-value < 0.001). Furthermore the incubation temperature explained 43.4% of the variability in log-transformed P_{\max}^B , and the linear regression between temperature and log- P_{\max}^B , excluding summer 2006, was statistically significant (analysis of variance, $F = 15.31$, $DF = 21$, $n = 20$, p-value < 0.001).

The regression of temperature against log- P_{\max}^B is shown in Figure 5.19, where it is possible to observe that the estimates for summer 2006 differed from the rest of the data set. In fact the average estimate of P_{\max}^B for summer 2006 was statistically different from the average estimate for summer 2007 (two-sample T-test, T-value = -3.26, $DF = 3$, p-value = 0.047), and the average P_{\max}^B in the period June-August 2006 was approximately 6 fold smaller than the average P_{\max}^B for the same period in 2007. Considering the other environmental variables and their average values for summer 2006 and 2007, it was observed that there was no statistically significant difference in nitrate, phosphate, and silica concentrations, temperature and solar irradiance between summer 2006 and 2007 (tested with two-sample T-test, p values were all > 0.05). Ammonium concentration was the only environmental variable that showed significant difference between summer 2006 and 2007 (two-sample T-test, T-value = 10.49, $DF = 27$, p-value < 0.001), with an average concentration during summer 2006 more than double the average concentration in summer 2007 (1.55 and 0.70 μM respectively). In fact, considering the entire data set of estimates of P_{\max}^B , ammonium concentration was negatively correlated with P_{\max}^B (Table 5.9) and was one of main predictors of P_{\max}^B , explaining approximately 37% of its variability (Equation 5.7).

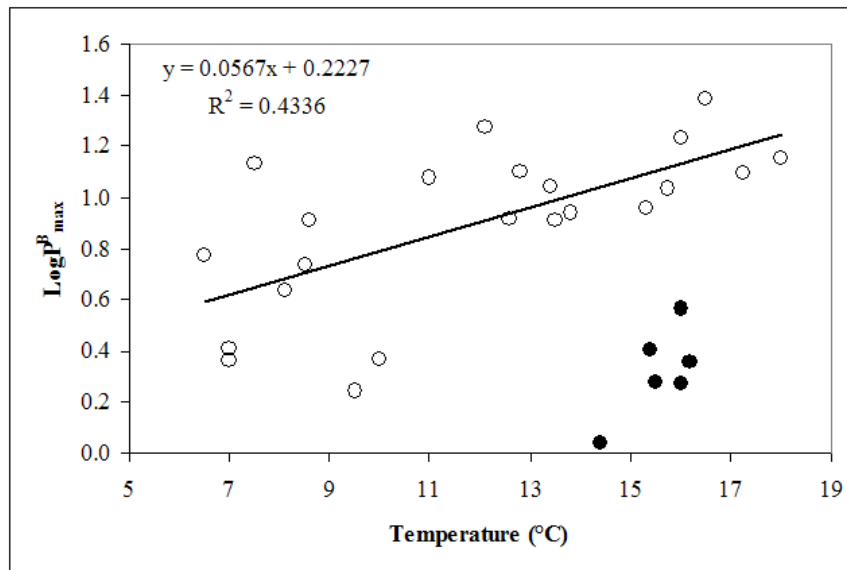


Figure 5.19. Regression of log-transformed P_{\max}^B against temperature ($^{\circ}\text{C}$) for data from December 2006 to March 2008 (empty circles) while summer estimates from June to August 2006 (full black circles) are not included.

The influence of ammonium on the variability of P_{\max}^B was also observed by MacCaull and Platt (1977). Explanations of the negative relationship between ammonium and photosynthetic rate were provided in detail in section 6.4.3 of Chapter 6. In summary, the negative relationship could be an effect of ammonium being assimilated by phytoplankton (Gowen, Tett and Jones 1992), or, contrarily, ammonium could inhibit nitrate-uptake with consequent reduction in production (Dugdale *et al.* 2007).

Considering the strong positive relationship between the photosynthetic parameters, α^B and P_{\max}^B variability fell in the category of E_k -independent variability as defined by Behrenfeld *et al.* (2004). The covariance between the photosynthetic parameters is generally unexpected because it is assumed that different factors limit α^B and P_{\max}^B (Behrenfeld *et al.* 2004). In fact α^B depends on the light reactions of photosynthesis (light-harvesting capacity of the photosynthetic units), while P_{\max}^B is influenced by the dark reactions of photosynthesis (e.g. activity/concentration of the enzyme RUBISCO). Behrenfeld *et al.* (2004) presented different examples of the occurrence of E_k -independent variability *in situ* and in the laboratory. Although the

causes of the E_k -independent variability were not completely clear, the importance of nutrient availability has been highlighted (Behrenfeld *et al.* 2004). The products of photosynthesis (NADPH and ATP) are used in the production of glucose and also in secondary pathways (e.g. nitrogen assimilation). The allocation of NADPH and ATP between these pathways determines the efficiency with which light is utilised for carbon fixation. The allocation of the products is not fixed but varies with the metabolic demands of the cell, that in turn vary with external environmental conditions such as low nutrient concentration (Behrenfeld *et al.* 2004). The significant relationship between photosynthetic parameters and nutrients in Carlingford Lough support this.

Focusing on α^B , the average estimate for summer 2006 was not statistically different from the average estimate in summer 2007 (two-sample T-test, T-value = -0.78, DF = 7, p-value = 0.463). The spring peak in α^B coincided with the minimum in phosphate concentration (Figure 2.8 a). Phosphate explained 3% of the variability in $\log\alpha^B$ however this was not statistically significant (Table 5.9). The relationship between phosphate and $\log\alpha^B$ could be explained by the fact that under conditions of low nutrients, species of phytoplankton reduce the size of the photosynthetic units (PSU) in the cells. Therefore, the cells have to increase the efficiency of light utilisation (α^B) to compensate for the reduction in PSU (Côté and Platt, 1983).

Côté and Platt (1983) observed positive correlation between phaeopigments/chlorophyll and α^B and P_{max}^B during their study of Bedford Basin (Nova Scotia). They explained the positive relationship in term of grazing, suggesting that the photosynthetic parameters would be limited by the rate at which the nutrients were “*being made available through grazing activity*”. At the same time they explained the correlation between α^B and phaeopigments/chlorophyll as the result “*of their mutual correlation with P_{max}^B* ”. In this context, the results from Carlingford Lough seem at odds in that the correlation matrix showed that $\log P_{max}^B$ was negatively correlated to $\log(\text{phaeopigments/chlorophyll})$. It is not clear what was causing the negative correlation between $\log(\text{phaeopigments/chlorophyll})$ and $\log P_{max}^B$ at station CLNBuoy in Carlingford Lough.

The photosynthetic parameters were also negatively correlated with the average chlorophyll content of the phytoplankton. This could be explained by self shading inside the phytoplankton cell. If pigments are tightly packed in the cell their efficiency in absorbing light may be less (Platt and Jassby 1976).

Jouenne *et al.* (2005) found that species composition, and cell size influence the photosynthetic response of phytoplankton in ecosystems characterized by tidal mixing. In this study of Carlingford Lough, the photosynthetic parameters did not show any significant correlation with the average cell volume (ACV; Table 5.9).

5.5 Conclusions

After deriving and analysing the photosynthetic parameters of station CLNBuoy in Carlingford Lough, it was possible to understand that:

- in the study of Carlingford Lough, the hyperbolic tangent of Jassby and Platt (1976) consistently produced a good fit to the data sets;
- α^B estimates were comparable with estimates from estuaries and bays in temperate regions, showing seasonal variability with higher estimates observed in spring (March to May). P_{\max}^B showed seasonal variability as well as α^B , however it also showed variability between years as suggested by the comparison of the summer values for 2006 and 2007. Considering 2007, P_{\max}^B reached the lowest value in winter and the highest at the end of the summer;
- the estimates of E_k were high, but no errors were identified in the procedure and no malfunction of the equipment was observed that would explain these estimates;
- ammonium concentration was negatively correlated to P_{\max}^B ; the incubation temperature was positively correlated to P_{\max}^B , but only if the summer 2006 estimates were not included in the analysis. Phaeopigments/chlorophyll ratio and phosphate concentration were predictors of the variability in α^B . The photosynthetic parameters were also negatively correlated with the average chlorophyll content of the phytoplankton. α^B and P_{\max}^B were positively correlated, therefore falling in the E_k -independent variability category.

CHAPTER 6

Modelling production and respiration

6.1 Introduction

The aim of Chapter 6 is to provide estimates of annual gross phytoplankton production and net microplankton community production at station CLNBuoy in Carlingford Lough. In particular, this chapter aims to present and discuss the two models adopted to derive estimates of daily and annual column productions. The relationship between gross daily column production and chlorophyll standing stock (explaining 70% of the variability in production) is also tested in this chapter.

The previous chapters of this thesis focused on characterising the physical, chemical and biological properties of Carlingford Lough. Chapter 2 and 3 provided information on the sampling, as well as on ranges and trends in temperature, salinity, K_d , surface irradiance, nutrients, chlorophyll and SPM concentrations, and phytoplankton composition. The technique for measuring primary production (^{14}C method) was described in Chapter 4, while Chapter 5 focused on the photosynthetic parameters derived from the photosynthesis/irradiance curves. The data gathered from these chapters were used in two models that are presented in this Chapter for deriving estimates of daily and annual production.

The first model (*day_colum_prod4.M*) was used to derive gross daily column production, based on the photosynthetic parameters, E_0 , K_d , and chlorophyll concentration. Estimates of gross daily column production (GDGP) were regressed against other environmental variables to identify which variables could be used as proxies for estimating GDGP. The second model (*HPLF2d.M*), implementing a truncated Fourier series, identified the annual trend in gross daily column production and derived estimates of gross annual production and the confidence intervals of variability. A schematic diagram of the linkages between the fieldwork and the modelling is shown in Figure 6.1.

Before describing the two models and the results of their applications, a general classification of primary production models existing in literature is given.

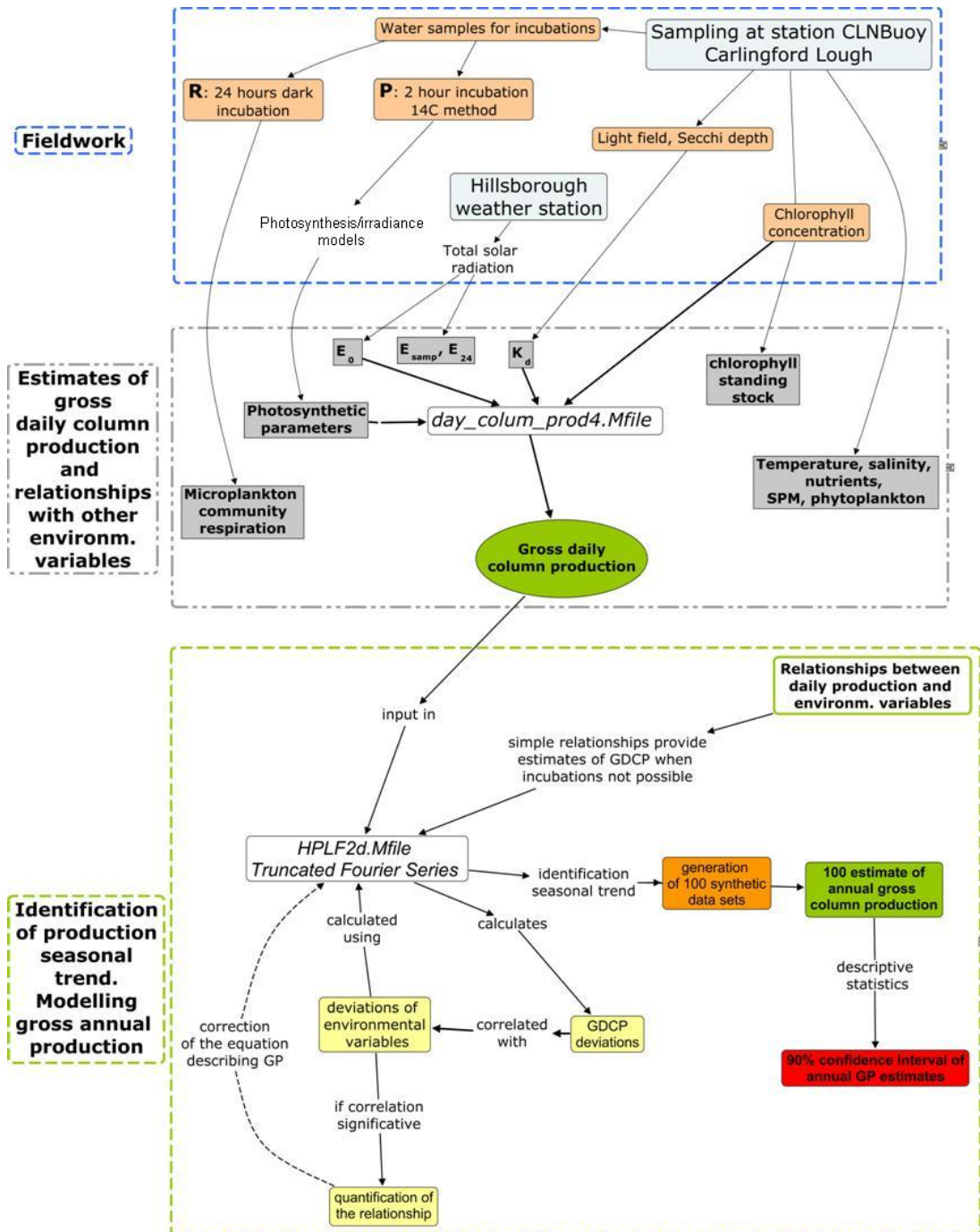


Figure 6.1. A schematic diagram of the linkages between fieldwork, the model for estimating gross daily column production (*day_colum_prod4.M*) and the model for estimating gross annual production (*HPLF2d.M*).

6.1.1. Classification of primary production models

In the initial chapter of this thesis the importance of studying primary production as well as the limitations of the applicability to routine samplings of the most common methodologies for measuring production was highlighted. One way to overcome these limitations is to use models for estimating production. A model can be defined as “*a simple representation of a complex phenomenon*” (Soetaert and Herman 2001). There are different types of models (e.g. conceptual model, mathematical model), but all can be considered an abstraction of the reality which contains only the essential characteristic needed for solving or describing a problem.

Generally, primary production models are used for computing estimates of the daily carbon fixation by phytoplankton, per unit of water bodies. Production models can range from simple relationships between chlorophyll concentration of the water column and column production (e.g. Joint and Pomroy 1993; Gowen and Bloomfield 1996), to more complex models that take in account other factors such as photoacclimation of phytoplankton, nutrient limitation and grazing by zooplankton (e.g. Tett 1981; Tett, Edwards and Jones 1986; Behrenfeld *et al.* 2002). However, more commonly, column production is calculated using irradiance-dependent models, based on the photosynthetic parameters (e.g. α^B and P_{max}^B), integrated over time and down the water column (e.g. Herman and Platt 1986; Gowen *et al.* 1995; Lizon *et al.* 1995; Tillmann *et al.* 2000; Jouenne *et al.* 2005; Weston *et al.* 2005).

All the models that derive column production tend to follow the same steps (Sathyendranath, Platt and Forget 2007). These are:

- a) determination of the light available at the sea surface;
- b) derive phytoplankton biomass at the surface and down the water column (biomass profile);
- c) assign the parameters of the model (e.g. the photosynthetic parameters);
- d) derive the underwater light field (light transmission);
- e) estimate production at each depth and integrate over time and depth.

Considering the examples of primary production models available in literature, some authors created classifications of models, to help scientists select which model to use. As examples, the classification by Behrenfeld and Falkowski (1997) and the classifications by Sathyendranath, Platt and Forget (2007) are described below.

6.1.2 The Behrenfeld and Falkowski classification

Behrenfeld and Falkowski (1997) argued that a classification of the models as empirical, semi-analytical and analytical was not enough for production models, because there were no models that were completely analytical (only based on first principles). In fact, production models depend on empirical parameterization at some level. Therefore the authors suggested a different classification based on the level of integration, and identified 5 types of models.

The first type was called 'WRM' or wavelength-resolved models; the WRMs calculated production at discrete depths, within the illuminated region of the water column, as function of PAR wavelength-specific absorption. They used photosynthesis irradiance variables (e.g. α^B and P^B_{max}) or variables characterizing the photosystem (e.g. absorption), and production was calculated by integration of the discrete production rates over depth, wavelength and time.

The second type was derived from WRMs removing the wavelength dependency; these were called WIMs (wavelength-integrated models). Therefore the production was calculated by integration of discrete production rates over depth and time. WRMs and WIMs calculated net production as gross production minus respiration.

If the time dependence in solar irradiance was removed from the WIMs, it was possible to obtain the third category of models. TIMs, or time-integrated models, maintained the vertical resolution but the discrete estimates of net production were measured directly, rather than derived from gross production and respiration estimates. In particular, TIMs used estimates of net production derived from long term incubations (e.g. 6-24 hours) which were carried under variable irradiance field therefore intrinsically integrating a range of photosynthetic rates.

The fourth category of models was called DIM (depth-integrated models) and included models which were not vertically resolved. These models usually linked the column production to an environmental variable such as chlorophyll concentration of the water column or daily integrated irradiance.

The 4 types of models described above derived daily production while the fifth type derived annual production (APM, annual production models). The APMs related annual production to surface chlorophyll concentration and they did not

consider changes in phytoplankton physiology in space and time (Behrenfeld and Falkowski 1997).

6.1.3. The Sathyendranath, Platt and Forget classifications

As shown in Figure 6.2 the production models can be grouped based on 3 types of classifications (Sathyendranath, Platt and Forget 2007). The classifications are based on the way the photosynthetic process is described, or the light field is described, or according to the state variables used.

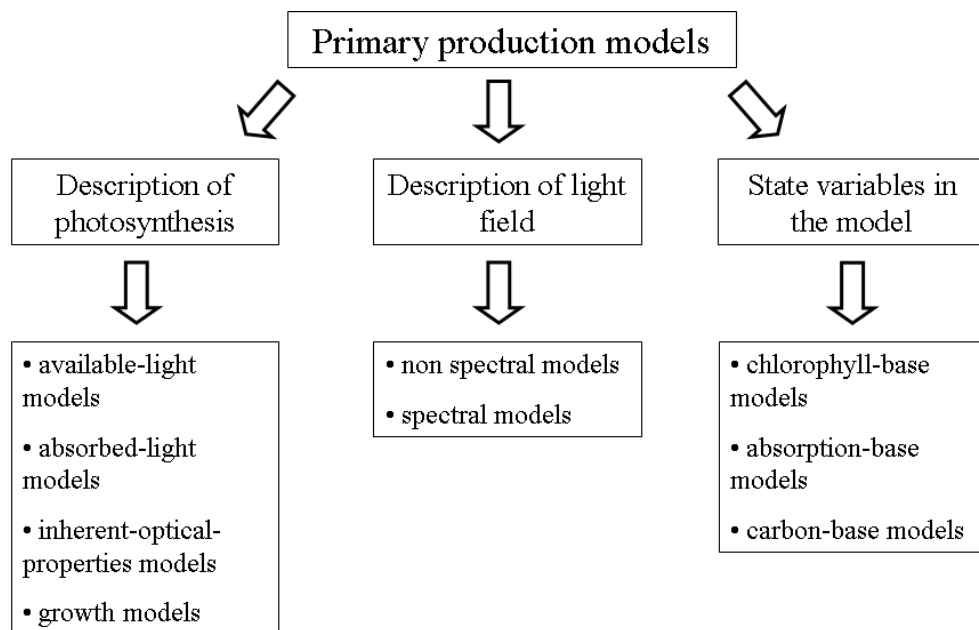


Figure 6.2. Classifications of primary production models according to Sathyendranath, Platt and Forget (2007) and Sathyendranath and Platt (2007). The diagram highlights 3 types of classification based on: the description of photosynthesis; the description of the light field; the state variables used in the model.

Using the first type of classification (description of photosynthesis, Figure 6.2) 4 categories of model could be identified. The ‘available-light model’, or photosynthesis-irradiance model, adopts equations similar to the ones discussed in

Chapter 5 of the present work, where the production is a function of the available light. An example of this equation is given below (Equation 6.1; Platt *et al.* 1980).

$$P = B \cdot P_m^B \cdot \left(1 - \exp \left(- \frac{\langle \alpha^B \rangle}{P_m^B} \cdot E \right) \right) \quad (6.1)$$

Where P is the production; the diamond brackets $\langle \rangle$ indicates a variable derived for the PAR domain, e.g. $\langle \alpha^B \rangle$ is the initial slope measured for flat incident spectral light covering the PAR domain; P_m^B is the assimilation number of the P/E curve; B is biomass derived from the concentration of chlorophyll; and E is the total available PAR. Considering that $P_m^B / \langle \alpha^B \rangle = E_k$ and substituting E/E_k with E_* (dimensionless irradiance), Equation 6.1 can be re-written in the following form (Equation 6.2).

$$P = B \cdot P_m^B \cdot \left(1 - \exp \left(- E_* \right) \right) \quad (6.2)$$

The second type of model (based on the description of photosynthesis) is the ‘absorbed-light model’ and it can be derived by substituting Equation 6.3 (Platt and Jassby 1976) into Equation 6.2.

$$\langle \alpha^B \rangle = \phi_m \cdot \langle a_B^* \rangle \quad (6.3)$$

$$P = B \cdot \langle a_B^* \rangle \cdot \phi_m \cdot E_k \cdot \left(1 - \exp \left(- E_* \right) \right) \quad (6.4)$$

Where ϕ_m is the maximum quantum yield, and $\langle a_B^* \rangle$ is the biomass-specific absorption coefficient for phytoplankton, averaged for the PAR domain.

Equation 6.4, representative of the ‘absorbed- light model’, can be converted into another form typical of the third category of model, ‘inherent-optical-property model’, or ‘biomass-independent’ models. Substituting the biomass-normalised mean total absorption coefficient ($\langle a_B \rangle$) with the biomass-specific absorption coefficient of phytoplankton (Equation 6.5), it is possible to obtain an equation in which the biomass does not appear explicitly (Equation 6.6).

$$\langle a_B \rangle = B \cdot \langle a_B^* \rangle \quad (6.5)$$

$$P = \langle a_B \rangle \cdot \phi_m \cdot E_k \cdot \left(1 - \exp \left(- E_* \right) \right) \quad (6.6)$$

The fourth type of model, based on the description of the photosynthetic process, is the ‘growth model’. This model considers the primary production a

measure of the rate of change of carbon per unit time ($P = dC / dt$), and its general form is exemplified in Equation 6.7.

$$g = \frac{1}{\chi \cdot B} \cdot (P - R) \quad (6.7)$$

Where g is the specific growth rate; χ is the carbon-to-chlorophyll ratio; R is phytoplankton respiration; P is the gross production and can be derived by a light-photosynthesis model. Equation 6.7 can describe the growth rate only if the gross production P is net of the respiration R (see section 6.2.5 for more information on respiration and net production).

The 4 types of model describing photosynthesis can be converted from one to another and should give the same results if run with the same input parameters (Sathyendranath and Platt 2007; Sathyendranath, Platt and Forget 2007). Furthermore, to run all 4 types of model only requires 4 parameters: $\langle \alpha^B \rangle$, P_m^B , $\langle a_B^* \rangle$ and χ ; all the other parameters can be derived from these 4.

Another type of classification (Figure 6.2) considers the way in which the light is described, rather than photosynthesis. With this classification, models are divided into ‘non-spectral’ and ‘spectral’ types. The 4 types of models listed above are all considered ‘non-spectral’ because they use the total irradiance E (covering the whole domain of PAR), as well as a spectral average of the initial slope and of the absorption coefficient. Therefore there is no distinction of the spectral quality of the underwater light field, and no information on the spectral response of the photosynthetic process to this variability. The ‘non-spectral’ models can be converted into ‘spectral’ by simply replacing the product $\langle \alpha^B \rangle \cdot E$ with its spectral equivalent $\int \alpha^B(\lambda) E(\lambda) d\lambda$.

The final type of classification in Figure 6.2 is based on the type of input variables chosen for the model, in particular the state variables. Chlorophyll (chlorophyll-based model) is the most common state variable and this is for different reasons, such as its clear connection to photosynthesis (it is at the heart of photosynthesis), and the simplicity of its measurements. The use of the phytoplankton absorption coefficient as a state variable (absorption-based models) is a variation of the chlorophyll-based models, considering the close relationship between chlorophyll and absorption. Finally the use of carbon as an input variable (carbon-

base models) may have limitations due to the difficulty in distinguishing between phytoplankton carbon from non-phytoplankton carbon (e.g. detritus; Sathyendranath, Platt and Forget 2007).

Comparing these two examples of model classification it appears that the WRMs of Behrenfeld and Falkowski (1997) are equivalent to the spectral models of Sathyendranath, Platt and Forget (2007), while WIMs, TIMs, DIMs and APMs (Behrenfeld and Falkowski 1997) could be considered ‘non-spectral’ models under the classification of Sathyendranath, Platt and Forget (2007).

In the present study the daily phytoplankton production (see section 6.3 of this chapter) was derived adopting ‘*day_colum_prod4.M*’ that is an ‘available-light’ ‘non spectral’ model (Sathyendranath and Platt 2007) or, according to Behrenfeld and Falkowski (1997), a wavelength-integrated model (WIM). The annual production was derived using an empirical model implementing a truncated Fourier series (*HPLF2d.M*), as described in the method section.

6.2 Methods

6.2.1 Calculation of daily column production

The calculation of the gross daily column production (for the 28 sampling dates for which estimates of α^B and P_{\max}^B were available) was performed using a Matlab script named '*day_colum_prod4.M*'. The script used values of surface irradiance (E_0) and K_d for deriving hourly estimates of irradiance at discrete depths (E_z). Estimates of E_z were used, together with estimates of the photosynthetic parameters and chlorophyll concentration, to derive gross hourly primary production at discrete depth (P_z) expressed in $\text{mg C m}^{-3} \text{ h}^{-1}$. Interpolation of production values at different depths gave a production curve and summing the area under each curve gave gross hourly column production ($\text{mg C m}^{-2} \text{ h}^{-1}$). The sum of the gross hourly column production during a day gave the gross daily column production ($\text{mg C m}^{-2} \text{ d}^{-1}$).

The process for calculating gross daily column production is summarised in Figure 6.3, while Listing 6.1 (in the Appendix 2) shows some of the commands of '*day_colum_prod4.M*'. Hourly surface irradiance for each of the sampling dates was calculated from hourly estimates of surface solar radiation measured at the weather station in Hillsborough (see Chapter 3). The hourly measurements expressed in W m^{-2} were multiplied by 4.15 to convert to $\mu\text{E m}^{-2} \text{ s}^{-1}$ (Morel and Smith 1974) and by 0.45 to account for the PAR component of the electromagnetic spectrum (Kirk 1994). A correction ($\times 0.94$) for reflection at the sea surface was also applied. The amount of light reflected varies with the sun angle (see section 3.1.1); the values of 0.94 is used when the sun is high in the sky.

$$E_0(t) = E_{\text{TOT}}(t) \cdot 4.15 \cdot 0.45 \cdot 0.94 \quad (6.8)$$

Where $E_0(t)$ is the surface irradiance at a given hour t of the day, and $E_{\text{TOT}}(t)$ is the solar irradiance at that given hour of the day t , measured by the weather station.

The 24 estimates of E_0 (derived for a given sampling day) were used, together with estimates of K_d for that given day, to derive the irradiance at discrete depths (E_z), according to the Lambert Beer law (Equation 3.7, Chapter 3). E_z was calculated for every 0.5 m from the surface to 5.5 m depth (the average depth of the water column at the station CLNBuoy). Interpolation of the hourly irradiances along the water column produced the irradiance profiles showed, as example, in the second

plot of Figure 6.3. It was assumed that K_d was constant during the day, therefore the same value was used to derived E_z for the 24 profiles of a given day.

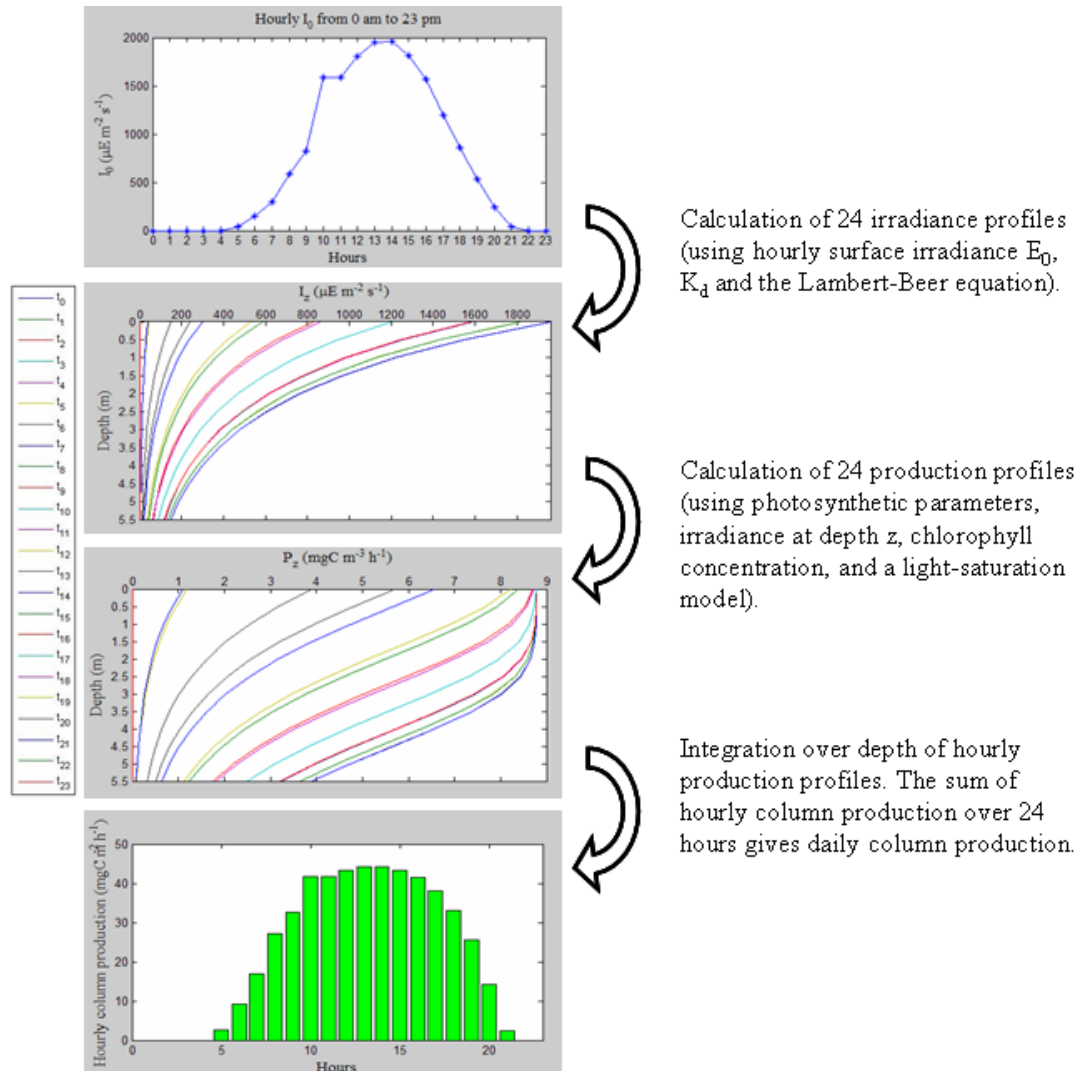


Figure 6.3. A schematic diagram of the process adopted for deriving gross daily column production using the script ‘*day_colum_prod4.M*’.

The next step for calculating production at discrete depths involved the use of the light-saturation models described in Chapter 5. As an example, considering the JasPlatt model (Jassby and Platt 1976), the production at a given depth z and at a given hour of the day t , ($P(z,t)$) was calculated from:

$$P(z, t) = P_{\max}^B \cdot \tanh\left(\frac{\alpha^B \cdot E(z, t)}{P_{\max}^B}\right) \quad (6.9)$$

Where α^B and P_{\max}^B are the photosynthetic parameters (see Chapter 5), and $E(z, t)$ is the irradiance at depth z and hour t . For a given sampling day, the same values of the photosynthetic parameters were used to calculate production during the different hours of the day and at different depths. The photosynthetic parameters that were used in a given model were derived by fitting the same model to the P/E curves derived from ^{14}C experiments with water samples from Carlingford Lough (Chapter 5).

Herman and Platt (1986) normalised gross production $P(z, t)$ to the chlorophyll concentration at that given depth. Chlorophyll concentration was measured at 1 and 4 m, therefore a simple Matlab script named '*interpolatore2.M*' was used to linearly interpolate the two observed estimates of chlorophyll. For each sampling day, the script provided estimates of chlorophyll concentration for every 0.5 m of the water column. The estimates of chlorophyll down the water column were considered constant during the sampling day.

$$P^B(z, t) = P(z, t) \cdot \text{chl}(z) \quad (6.10)$$

Where $P^B(z, t)$ is the normalised gross production at a given depth z and time t , while $\text{chl}(z)$ is the chlorophyll concentration at depth z for that given sampling day.

Considering the average depth of the euphotic zone (8.4 m; see Chapter 3) exceeded the average depth of the water column (5.5 m), gross production was calculated for the whole water column. In reality, on a couple of occasions (5th December 2006 and 13th March 2008) the depth of the 1% light was approximately 4 m depth. However, the light available below 4 m was low and the chlorophyll concentration was $< 1 \text{ mg m}^{-3}$, therefore the contribution of the phytoplankton below 4 m to the daily column production for these two dates was considered negligible.

For each sampling day, the normalised gross production for a given hour of the day was multiplied by the depth step. The productions at discrete depths (now expressed in $\text{mg C m}^{-2} \text{ h}^{-1}$) for a given hour were then summed, giving the gross hourly column production. The repetition of this process for the 24 hours of a given sampling day produced the 24 estimates of column production showed (the bottom plot of Figure 6.3). Sum of gross hourly column production of a given sampling day gave the gross daily column production ($\text{mg C m}^{-2} \text{ d}^{-1}$).

$$GDCP = \sum_{t=1}^{24} P_{column}^B \Delta t \quad (6.11)$$

Where GDCP is the gross daily column production, P_{column}^B is the gross hourly column production, and Δt is the time of the day step (equal to 1 hour).

6.2.2. Relationships between gross daily column production and other environmental variables

The daily estimates of gross column production were regressed against other environmental variables to identify relationships which could be used to predict primary production. As pointed out in the introduction (Chapter 1), primary production is significantly related to the chlorophyll standing stock (Joint and Pomroy 1993; Gowen and Bloomfield 1996). The chlorophyll standing stock was calculated using the script '*interpolatore2.M*', which produced estimates of chlorophyll concentration at discrete depths (0.5 m) which were then summed over the water column.

The other environmental variables used in the regressions were: temperature, salinity, log-transformed river flow, log-transformed phaeopigments/chlorophyll ratio, log-transformed average cell volume (ACV) and average chlorophyll content (ACC), log-transformed chlorophyll standing stock, log-transformed irradiance during the sampling and the previous 24 hours of the sampling (E_{sampling} and E_{24} respectively), K_d of the water column, average water column nutrient concentration (in particular, ammonium, nitrate, nitrite, phosphate, and silicate). The regression analysis was performed using Minitab 15.

Descriptive statistics analysis and plots of estimates of daily column production and microplankton community respiration were performed with Microsoft Excel, while Pearson correlation coefficients were obtained using Minitab 15.

6.2.3 Background information on '*HPLF2d.M*'

The model '*HPLF2d.M*', implementing a truncated Fourier series (TFS), was adopted to derive estimates of gross annual production. As a first step, the model

fitted a seasonal cycle to sparse observations of gross daily primary production to identify the seasonal cycle of gross production. The latter was used, together with the Montecarlo method (meaning the use of random numbers), to generate multiple synthetic data sets from which estimates of gross annual column production were derived (Tett 2008). The analysis of the estimates of annual production from the synthetic data sets produced a median value of production with 90% confidence interval. The model adopted was an empirical model, which means it was based on one or more equations derived from observations. An empirical model was preferred to a mechanistic model (which would be based on scientific knowledge of the physical-biological relationships of the water body and on meteorological time-series) because it is much simpler and robust.

Phytoplankton production is characterised by a repeating annual cycle. Periodical variability can be described by a sum (superposition) of periodic terms such as pairs of sine and cosine waves. This type of analysis is called ‘harmonic analysis’ or ‘Fourier analysis’ (Legendre and Legendre 1998; Zar 1998) and the sum of periodic terms is called ‘Fourier series’. The latter is composed by an infinite sum of sine and cosine waves, however for this study a limited number of waves was used therefore a truncation of the series was applied.

The model adopted in this study considered gross production as a function of the time, in particular:

$$y = f(t) + \varepsilon \quad (6.12)$$

Where y is the variable gross production, $f(t)$ is the deterministic function¹ (in this case the truncated Fourier series) and ε is the error term. In relation to the error term some assumptions were made: the error adds to (or subtracts from) values derived from $f(t)$; it is time-independent and is not related to the expected value of $f(t)$. The error could be related to deterministic factors or unpredictable factors, and the distribution of its values could be unknown, therefore in this case it is assumed that the values of ε were approximately symmetrical around the mean with $\Sigma \varepsilon \rightarrow 0$ as the number of observations increased (Tett 2008).

Assuming the annual pattern of phytoplankton production repeats itself from one year to the next, the simplest model that could be used to capture the annual

¹ Deterministic function is a function that returns the same result when it is used with the same input data.

variability is a single wave with period of 1 year and frequency 1 y^{-1} (Tett 2008). A function of one wave can be described as shown in Equation 6.13.

$$f(t) = \frac{a_0}{2} + a \cdot \sin(\omega t) + b \cdot \cos(\omega t) \quad (6.13)$$

Where $a_0/2$ gives the mean value around which the wave oscillates (the mean value of $f(t)$); and ‘a’ and ‘b’ are the amplitudes of the sine and cosine waves respectively. The function repeats itself after one year/full cycle, therefore $f(t + 2\pi) = f(t)$.

However phytoplankton production may change more often than once a year, therefore more waves with higher frequency ($2, 3 \dots \text{y}^{-1}$) were added to the basic wave. The function $f(t)$ can then be rewritten as a superposition of pairs of sine and cosine waves (Equation 6.14).

$$f(t) = \frac{a_0}{2} + \sum_{n=1}^{n=M} [a_n \sin(\omega_n t) + b_n \cos(\omega_n t)] \quad (6.14)$$

Where M is the maximum number of waves and a_n and b_n are the amplitudes of the sine and cosine of the n -wave respectively.

6.2.4. Estimates of annual production (*HPLF2d.M*)

The script ‘*HPLF2d.M*’ (originally created by Professor Tett in July 2008; Listing 6.2) sorts, collates and arranges data to create time series. It also calls two sub-functions (‘*Mwaves3.M*’ and ‘*TwoWaves.M*’; see Listings 6.3 and 6.4 respectively) which fit and plot the truncated Fourier series (TFS) to the data.

Focusing on the TFS, the first step for capturing the annual cycle of the observed phytoplankton daily production was to estimate the parameters of the function $f(t)$ (the TFS) in the presence of the error ε (Equation 6.12). The script used a step-wise fit of paired sine-cosine waves of increasing frequency starting with a frequency of 1 y^{-1} . For each wave, the mean value of $f(t)$, and the values of the TFS coefficients were shown, together with the sum of square of the residuals, the degree of freedom and the variance. An estimate of the goodness of the fit of the waves was also provided as R^2 (see Equation 5.5, Chapter 5). The best number of waves chosen for fitting the observed data should be the one for which the parameters of the TFS gave the lowest residual sum of square (Equation 6.15).

$$\sum_{j=1}^M \left| y_j - \mu + a \cdot \sin \left(\frac{2\pi}{\tau} (t_j - t_0) \right) + b \cdot \cos \left(\frac{2\pi}{\tau} (t_j - t_0) \right) \right|^2 \rightarrow \min \quad (6.15)$$

Where y_j is the mean value of the function predicted by j -waves, and $\mu = a_0/2$.

Increasing the number of waves fitting the data points reduces the residual sum of square. However the number of waves used to capture the seasonal trend of the observations should be small (e.g. < 3). In fact, increasing the number of waves produced a small increase in the variability explained by the TFS. At the same time, considering the sparse nature of the observations, using a high number of paired sine-cosine waves may give inaccurate predictions for periods with missing data. Primary production is strictly dependent on the light availability and the solar cycle of radiation is usually well fitted by 1 (or 2) waves. Therefore it is seemed likely that the annual cycle of phytoplankton production could also be described by a small set of waves.

Once the appropriate number of waves for fitting the observations was decided, the program was used to plot the observations with the superposition of the waves and the 90% confidence interval of the observations. A simple diagram of how this first part of the program works is given in Figure 6.4, while Figure 6.5 shows an example of a real fit of the TFS to primary production observations.

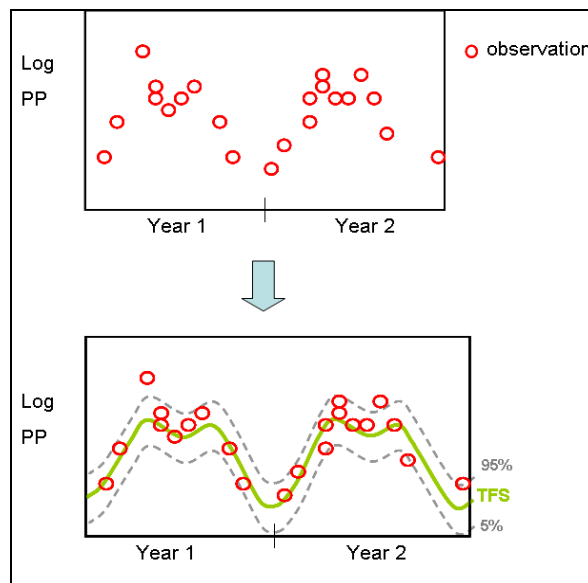


Figure 6.4. Simplification of the fitting of pairs of sine-cosine waves (TFS) to estimates of daily column production (PP) log-transformed, derived from *in situ* experiments over a period of 2 years. The 90% confidence interval is also shown.

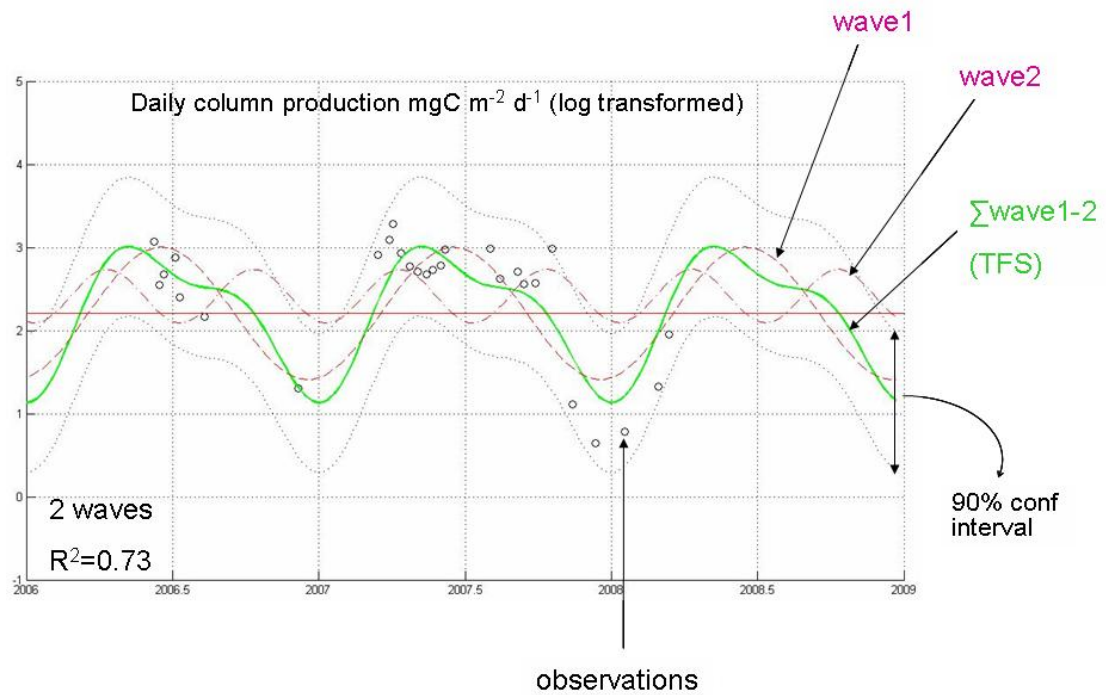


Figure 6.5 The fit of 2 paired sine-cosine waves (with frequency 1 y^{-1} and 2 y^{-1} respectively) to log-transformed daily column production estimates ($\text{mg C m}^{-2} \text{ d}^{-1}$) from June 2006 to March 2008. The waves with frequencies of 1 y^{-1} (wave1) and 2 y^{-1} (wave2) are coloured pink, while their sum (superposition) or TFS is coloured green. The pink straight line is the mean value around which the function is oscillating. The 90% confidence interval is indicated by the dark dotted lines, while the black empty circles represent the observations. In this example, the TFS (sum of the 2 waves) explained 73% of the variability of the observations ($R^2 = 0.73$).

The next step of the process to estimate annual gross production was to generate synthetic data sets, according to Equation 6.16.

$$y^*_j = \bar{y} + \sum_{n=1}^{n=M} \left[a_n \sin(\omega_n t_j) + b_n \cos(\omega_n t_j) \right] + \varepsilon_j \quad (6.16)$$

Where \bar{y} is the mean value of the function. The first and second term of the equation $\left(\bar{y} + \sum_{n=1}^{n=M} \left[a_n \sin(\omega_n t_j) + b_n \cos(\omega_n t_j) \right] \right)$ represent the deterministic part of the function while the error ε_j represents its stochastic part. The error was generated using the Matlab function 'randn' that generates random numbers from a normal distribution

with mean = 0 and standard deviation = 1. The random numbers were then multiply by the residual error from the observations' fit.

The number of synthetic data generated for a standard year reflected the frequency with which the observations were collected (e.g. 21 primary production incubations in a year). The program generated 100 synthetic data sets (with 21 synthetic estimates of production each). For each data set, the 21 synthetic observations were interpolated to derive 365 estimates of daily production which were then summed for estimating the annual production.

The calculation of the descriptive statistics of the 100 estimates of annual production provided a median value of annual production with confidence interval of the estimates. An example of the functioning of this second part of the script is given in Figure 6.6, while a plot of the synthetic data derived from the TFS in Figure 6.5 is shown in Figure 6.7.

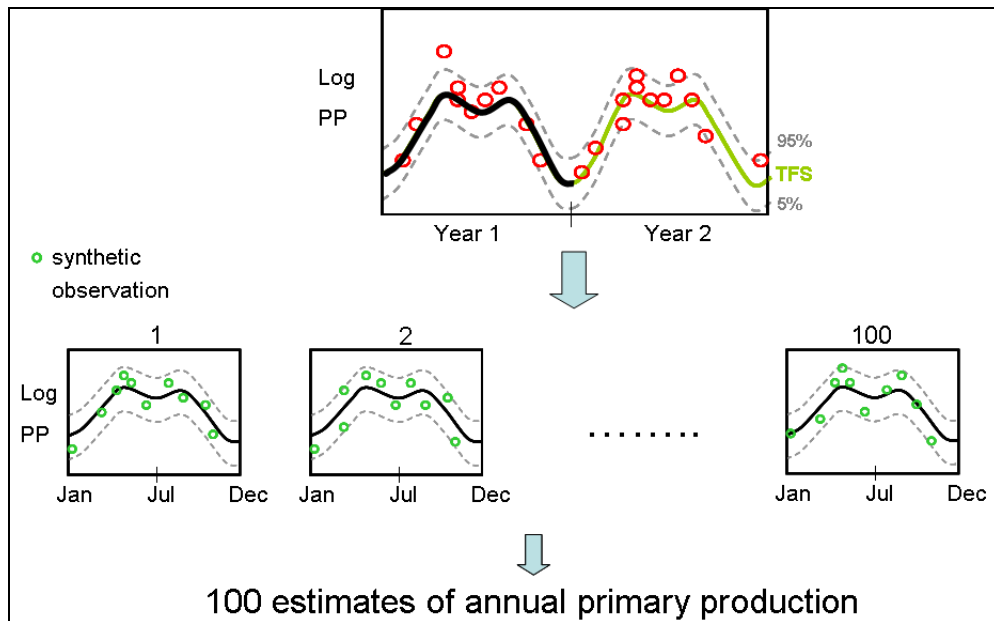


Figure 6.6. The procedure for generating synthetic data sets from real observations using a TFS. In this example, 100 synthetic data sets were produced, each representing a standard year; from these years an estimate of annual production was derived. Using the 100 estimates of annual production it is possible to derive a median and confidence intervals.

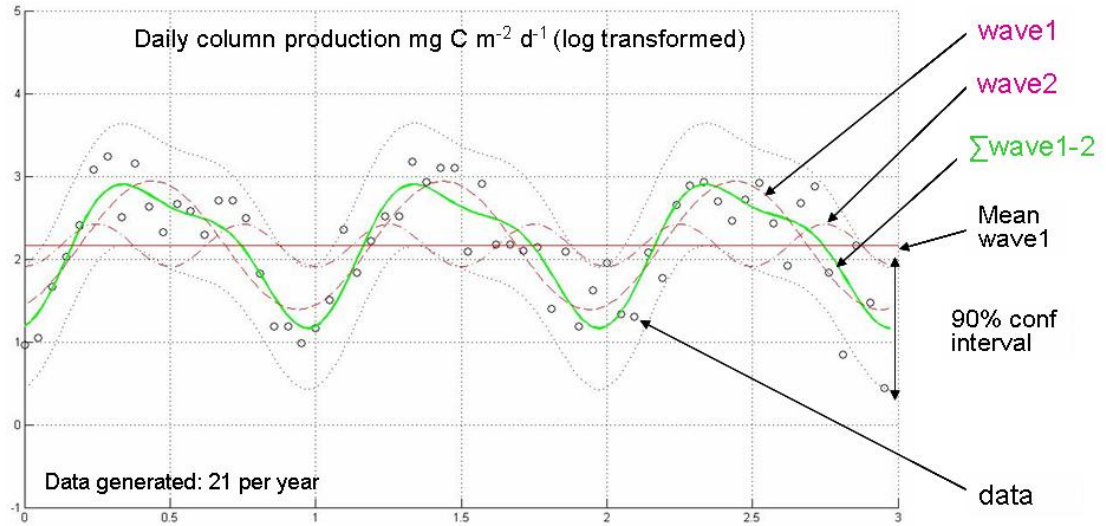


Figure 6.7. Generation of synthetic data (log-transformed daily column production estimates) for a period of 3 years using the TFS of Figure 6.5. The waves with frequencies of 1 y^{-1} (wave1) and 2 y^{-1} (wave2) are coloured pink, while their sum (superposition) or TFS is coloured green. The pink straight line is the mean value around which the function is oscillating. The 90% confidence interval is indicated by the dark dotted lines, while the black empty circles represent the synthetic data.

The final part of the program was used to try and improve the confidence limits of the primary production, by considering relationships between production and environmental variables. The estimate of column production for a given day could be then described by the TFS, by a residual error and by another term ($c_v \cdot x'_{v,j}$) that represents the variability in daily production that can be explained by variation in particular environmental variables (Equation 6.17).

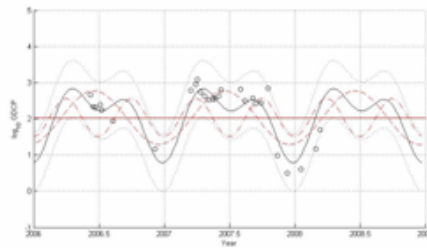
$$Y_j = \bar{Y} + f_M(t_j) + \sum_{v=1}^{v=W} c_v \cdot x'_{v,j} + \varepsilon_j \quad (6.17)$$

Where Y_j is an estimate of column production for a given day j ; \bar{Y} is the mean value of the function; $f_M(t_j)$ is the TFS; v is the number of the environmental variables; and $x'_{v,j}$ is the deviation of the j^{th} value of the environmental variable x_v from its own expected seasonal value (Tett 2008).

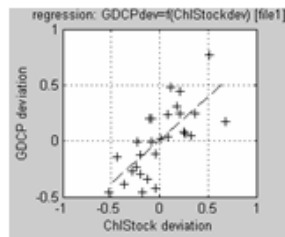
The environmental variables that could explain part of the variability in the production were selected in the following way: 1) all the biological, physical and

chemical variables measured during the sampling period were fitted with the same number of waves that best described the temporal trend in production (in this case 2 waves); 2) the deviations of the fit from the observed data were derived for all variables including production; 3) a correlation matrix was created between the deviations of all variables (included production), and those variables whose deviations were significantly correlated to the deviations in production, were considered in the next step of the analysis.

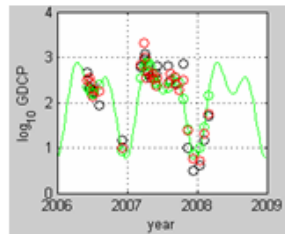
For each environmental variable (whose deviations were significantly correlated to production deviations), 2 files were created and re-analysed with '*HPLF2d.M*': file1 listed estimates of gross daily column production and the corresponding values of environmental variable for that given date (28). File2 listed all available estimates of the environmental variable (46). The script calculated the regression between the deviations of the production versus the deviations of the environmental variable, and added this relationship to the TFS. The environmental variables were sampled more frequently than the primary production experiments were carried out, thus it was possible to increase the number of synthetic observations for each synthetic data set to 46. The rest of the analysis was as described before: 100 synthetic data sets were created from which estimates of annual production were derived. This last part of the analysis is summarised in Figure 6.8.



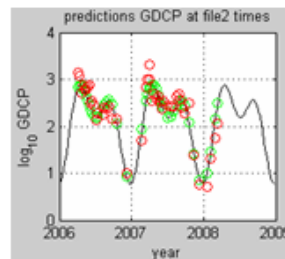
The script fitted the TFS (2 waves) to GDCP from file1, calculating R^2 and plotting the deviations of the modelled values from the observations. Chlorophyll standing stock values were fitted as well by 2 waves function.



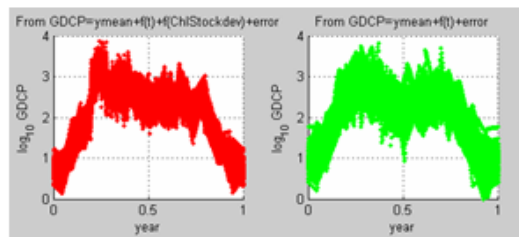
Considering file1 (28 sampling events), deviations of gross daily column production (GDCP) were regressed versus the deviations of chlorophyll standing stock. Deviations of chlorophyll standing stock were significantly correlated to deviations of GDCP.



Considering file1, the predicted values of GDCP by the TFS (green empty circles), and the predicted values of GDCP by the TFS corrected by the relationship with chlorophyll standing stock (red empty circles) were calculated, and plotted together with the observations (black empty circles) and the TFS (green line).



Considering frequency of sampling of file2 (46 sampling events), predicted estimates of GDCP by the TFS (green empty circles) and predicted estimates of GDCP by the TFS corrected by the relationship GDCP/chlstock (red empty circle) were derived and plotted together with the TFS (black line).



Calculation of 100 estimates of gross annual column production, considering the correction of the TFS for the relationship with chlorophyll standing stock.

Figure 6.8. A flow diagram summarising the final steps of the script ‘*HPLF2d.M*’, where gross annual column production estimates were improved by including in the calculations the relationship between deviations of gross daily column production and environmental variables (in this example chlorophyll standing stock).

6.2.5. Microplankton community respiration and net community production

Short term ^{14}C incubations (e.g. 2 hours) give estimates of gross phytoplankton production (see Chapter 4) and for estimating net production it is necessary to derive respiration. As discussed in Chapter 1, respiration derived from samples collected in the field is called microplankton community respiration (MCR) and is the combination of phytoplankton respiration and microheterotrophs (e.g. protozoa, bacteria) respiration. Therefore subtraction of MCR from gross production gives net microplankton production (Tett *et al.* 2007), that is less than net phytoplankton production.

Respiration was estimated from incubation of water samples collected from Carlingford Lough. The water used for these incubations came from the same samples that were used for the primary production incubations (Chapter 4). The water sample in the 5 L container was gently mixed and transferred into 12 glass bottles (~120 mL volume) using a plastic tube to avoid the formation of air bubbles. Six bottles were fixed immediately (t_0) with 1 mL of manganous sulphate and 1 mL of alkaline iodide solution (Strickland and Parsons 1967), while the remaining 6 were wrapped in aluminium foil and incubated in the dark in a controlled temperature bath at *in situ* temperature for 24 hours (t_{24}). At the end of the incubation the 6 t_{24} bottles were fixed as described above.

Oxygen concentrations (mg L^{-1}) in the two sets of bottles were determined by Winkler titration with sodium thiosulphate (Strickland and Parsons 1967) and the difference in average oxygen concentration in the t_0 and t_{24} bottles gave a measure of the microplankton community respiration. A two-sample T-test was used to check that the difference in oxygen concentration between t_0 and t_{24} bottles was statistical significant. The sodium thiosulphate solution was standardised with potassium iodate solution, using the same reagents described above but using deionised water instead of the water from the Lough. The standardisation was performed each time a new thiosulfate solution was made.

From April 2006 until August 2008, a standard Winkler titration was used. However the standard titration was not sensitive enough to detect changes in oxygen concentration between t_0 and t_{24} bottles in winter samples. From August 2008, a microtitrator with photometer (Dissolved Oxygen Analyser, SiS Sensoren

Instrumente Systeme GmbH, Kiel) was used. The greater sensitivity of the microtitrator allowed the measurements of winter microplankton community respiration.

For estimating net community production, the microplankton community respiration was subtracted from the estimates of gross primary production. Respiration, expressed in $\text{mg O}_2 \text{ L}^{-1}$, was first converted to moles $\text{O}_2 \text{ L}^{-1}$ (division by the oxygen atomic mass, 16, multiplied by 2) which, considering a respiratory quotient $\text{RQ} = \text{CO}_2 \text{ produced} / \text{O}_2 \text{ consumed} = 1$, is equivalent to moles C L^{-1} . The moles of C per litre were converted to mg C m^{-3} by multiplying by 12 (carbon atomic mass) and 1000. Assuming that the respiration was constant through the water column, column respiration (mg C m^{-2}) was obtained by multiplying respiration by the average depth (5.5 m).

6.3 Results

6.3.1 A comparison of estimates of daily primary production derived with different light-saturation models

The estimates of gross daily column production derived from the models² (up to 8 although on some occasions a model could not fit the data) are shown in Table 6.1. These estimates were averaged by each sampling day (average of all model estimates) (Table 6.2), and by model (average of all estimates of production derived with a given model for the whole sampling period, Table 6.3). Focusing on the daily estimates of production derived by averaging model estimates for a given day, the highest average production ($1229.3 \text{ mgC m}^{-2} \text{ d}^{-1}$) was observed on the 3rd April 2007, while the lowest ($3.5 \text{ mgC m}^{-2} \text{ d}^{-1}$) on the 11th December 2007 (Table 6.2 and Figure 6.9). The 8th June 2006 was characterised by the highest standard deviation of the mean showing that for this date there were marked differences in model performances. Variability between model estimated values (based on standard deviation) was also observed on the 5th July 2006 (Table 6.2). Excluding the estimates from these two dates (8th June 2006 and 5th July 2006), the standard deviation of the mean was always less than $41 \text{ mgC m}^{-2} \text{ d}^{-1}$.

The estimates of daily column production averaged by model ranged from 348.4 (modPlatt) to 398.7 (Blackman) $\text{mgC m}^{-2} \text{ d}^{-1}$ (Table 6.3). The same table highlights that the minimum estimates of production were similar between models, while the maximum estimates showed a bigger variability. In particular, the maximum estimate derived from Blackman was higher (by approximately $100 \text{ mgC m}^{-2} \text{ d}^{-1}$, equal to an overestimation of approximately 10%) compared to the maximum estimates derived by the other models. In general, the estimates of production by the Blackman model for a given day were higher than the estimate derived using the other models (Table 6.1 and Figure 6.10). Excluding the Blackman model from Figure 6.10, it is possible to observe that the estimates of production from the other models overlapped almost completely (Figure 6.11), except for three sampling events during summer 2006 (8th June 2006, 21st June 2006, and 5th July 2006). The modPlatt model gave the lowest estimates of gross production in these 3 sampling events.

² JasPlatt = Jassby and Platt 1976; Blackman = Blackman 1905; BurkLine = Burk and Lineweaver 1935; STalling = Smith 1936, Talling 1957; Steele = Steele 1962; modSteele = modification of Steele 1962 by Jassby and Platt 1976; Webbexp = Webb, Newton and Star 1974; modPlatt = modification of Platt *et al.* 1975 by Jassby and Platt 1976.

Table 6.1. Estimates of gross daily column production derived for each of the light-saturation models for the 28 sampling days. JasPlatt = Jassby and Platt 1976; Blackm = Blackman 1905; BurkL = Burk and Lineweaver 1935; STallin = Smith 1936, Talling 1957; Steele = Steele 1962; modSte = modification of Steele 1962 by Jassby and Platt 1976; Webb = Webb, Newton and Star 1974; modPlatt = modification of Platt *et al.* 1975 by Jassby and Platt 1976). Production is expressed in mgC m⁻² d⁻¹. Missing values are when a model failed to fit the data.

	JasPlat	Blackm	BurkL	STallin	Steele	modSte	Webb	modPlatt
08/06/06	456.0	792.3	573.7	474.6	528.9	528.9	550.5	428.4
15/06/06	215.3	264.4	227.7	217.3	225.3	225.3	226.3	221.5
21/06/06	207.1		217.1	209.6	203.2	203.2	212.1	157.4
05/07/06	244.6		258.2	248.6	222.5	224.5	248.6	59.6
10/07/06	172.1	186.3	176.1	172.6	175.5	175.5	175.8	174.8
10/08/06	86.5	106.5	89.9	87.2	88.7	88.7	89.3	86.6
05/12/06	14.7	12.9	15.9	14.8	15.4	15.4	15.6	15.0
15/03/07	603.8		603.2	603.8	603.4	603.4	603.3	603.5
29/03/07	890.9	861.2	949.3	895.9	937.8	937.8	941.8	908.8
03/04/07	1209.8	1331.4	1212.1	1208.8	1218.5	1218.5	1216.0	1219.4
12/04/07	551.5	606.5	550.7	551.0	552.8	552.8	551.9	554.3
23/04/07	436.8	400.0	449.1	437.2	452.0	452.0	450.8	451.4
03/05/07	339.0	377.4	341.3	339.3	341.4	341.4	341.4	341.0
15/05/07	351.2	348.0	350.7	350.7	352.4	352.4	351.8	354.1
22/05/07	364.1	411.7	386.7	369.0	374.4	374.4	379.6	365.4
01/06/07	437.3	464.7	440.0	437.7	439.7	439.7	439.8	439.2
07/06/07	641.3	677.6	644.1	641.4	645.1	645.1	644.7	645.5
02/08/07	652.1	657.6	665.9	652.2	666.7	666.7	666.1	665.4
14/08/07	317.7	315.5	316.1	317.5	316.6	316.6	316.4	317.0
05/09/07	373.6	344.8	387.0	373.2	390.3	390.3	388.6	391.1
13/09/07	266.6	253.2	274.1	266.0	276.1	276.1	275.1	277.9
27/09/07	272.6		279.0	273.2	278.1	278.1	278.5	276.9
18/10/07	700.8	671.3	719.2	700.8	720.4	720.4	719.7	720.3
13/11/07	9.7	8.2	12.7	10.1	10.8	10.9	11.5	10.0
11/12/07	3.2	2.4	4.3	3.3	3.9	3.6	3.9	3.2
17/01/08	4.1		4.8		4.9	4.2	4.6	4.0
28/02/08	14.7	14.7	15.6	14.9	15.0	15.0	15.3	14.3
13/03/08	49.8	62.4	53.2	50.8	48.9	49.9	51.7	48.8

Table 6.2. Descriptive statistics (mean, standard deviation, median, maximum, minimum and number of observations) of the estimates of gross daily column production derived from the light-saturation models for a given sampling day. Production is expressed in $\text{mgC m}^{-2} \text{d}^{-1}$.

	Mean	Stan Dev	Median	Min	Max	n
08-Jun-06	541.7	112.7	528.9	428.4	792.3	8
15-Jun-06	227.9	15.4	225.3	215.3	264.4	8
21-Jun-06	201.4	20.0	207.1	157.4	217.1	7
05-Jul-06	215.2	69.9	244.6	59.6	258.2	7
10-Jul-06	176.1	4.4	175.5	172.1	186.3	8
10-Aug-06	90.4	6.6	88.7	86.5	106.5	8
05-Dec-06	15.0	0.9	15.2	12.9	15.9	8
15-Mar-07	603.5	0.2	603.4	603.2	603.8	7
29-Mar-07	915.4	31.2	923.3	861.2	949.3	8
03-Apr-07	1229.3	41.4	1217.2	1208.8	1331.4	8
12-Apr-07	559.0	19.3	552.4	550.7	606.5	8
23-Apr-07	441.2	17.8	449.9	400.0	452.0	8
03-May-07	345.3	13.0	341.3	339.0	377.4	8
15-May-07	351.4	1.8	351.5	348.0	354.1	8
22-May-07	378.2	15.5	374.4	364.1	411.7	8
01-Jun-07	442.2	9.1	439.7	437.3	464.7	8
07-Jun-07	648.1	12.0	644.9	641.3	677.6	8
02-Aug-07	661.6	6.5	665.7	652.1	666.7	8
14-Aug-07	316.7	0.7	316.6	315.5	317.7	8
05-Sep-07	379.8	16.0	387.8	344.8	391.1	8
13-Sep-07	270.7	8.3	274.6	253.2	277.9	8
27-Sep-07	276.6	2.6	278.1	272.6	279.0	7
18-Oct-07	709.1	17.6	719.4	671.3	720.4	8
13-Nov-07	10.5	1.3	10.5	8.2	12.7	8
11-Dec-07	3.5	0.6	3.5	2.4	4.3	8
17-Jan-08	4.4	0.4	4.4	4.0	4.9	6
28-Feb-08	14.9	0.4	14.9	14.3	15.6	8
13-Mar-08	51.9	4.5	50.3	48.8	62.4	8

Table 6.3. Descriptive statistics (mean, standard deviation, median, maximum, minimum and number of observations) of the estimates of gross daily column production derived for each of the 8 light-saturation models for the 28 sampling days. JasPlatt = Jassby and Platt 1976; Blackman = Blackman 1905; BurkLine = Burk and Lineweaver 1935; STalling = Smith 1936, Talling 1957; Steele = Steele 1962; modSteele = modification of Steele 1962 by Jassby and Platt 1976; Webbexp = Webb, Newton and Star 1974; modPlatt = modification of Platt *et al.* 1975 by Jassby and Platt 1976. Production is expressed in $\text{mgC m}^{-2} \text{d}^{-1}$.

	Mean	Stan Dev	Median	Min	Max	n
JasPlatt	353.1	291.8	328.3	3.2	1209.8	28
Blackman	398.7	330.8	348.0	2.4	1331.4	23
BurkLine	364.9	298.7	328.7	4.3	1212.1	28
Stalling	367.5	289.2	339.3	3.3	1208.8	27
Steele	361.0	298.9	329.0	3.9	1218.5	28
modSteele	361.1	298.8	329.0	3.6	1218.5	28
Webbexp	363.2	298.5	328.9	3.9	1216.0	28
modPlatt	348.4	300.9	329.0	3.2	1219.4	28

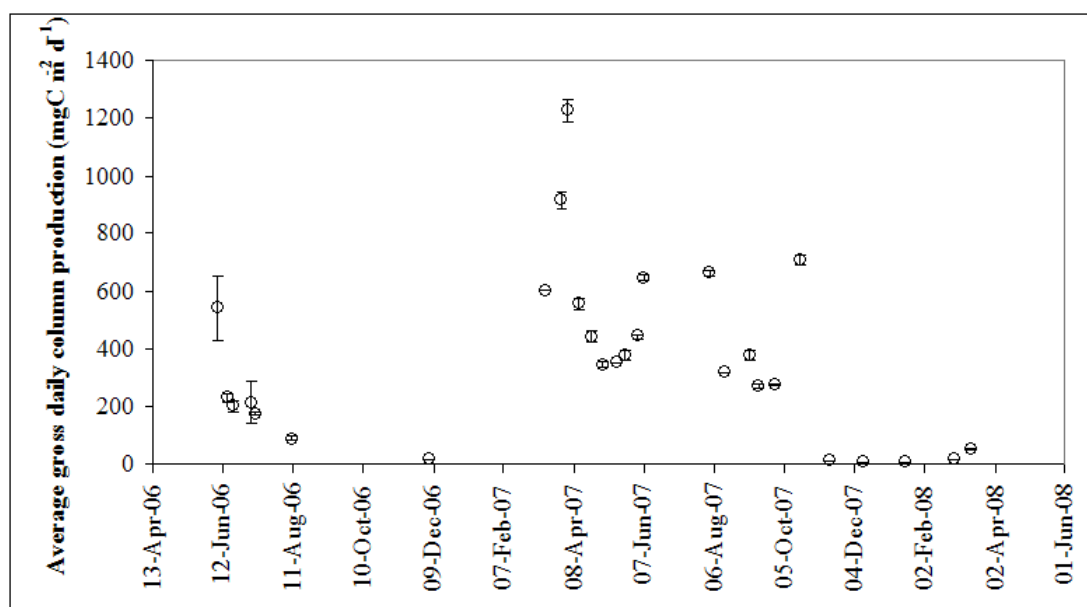


Figure 6.9. The temporal pattern of the gross daily column production ($\text{mgC m}^{-2} \text{d}^{-1}$) derived by averaging estimates of gross daily column production by the 8 light-saturation models for a given sampling day. The error bar is equal to the standard deviation of the mean.

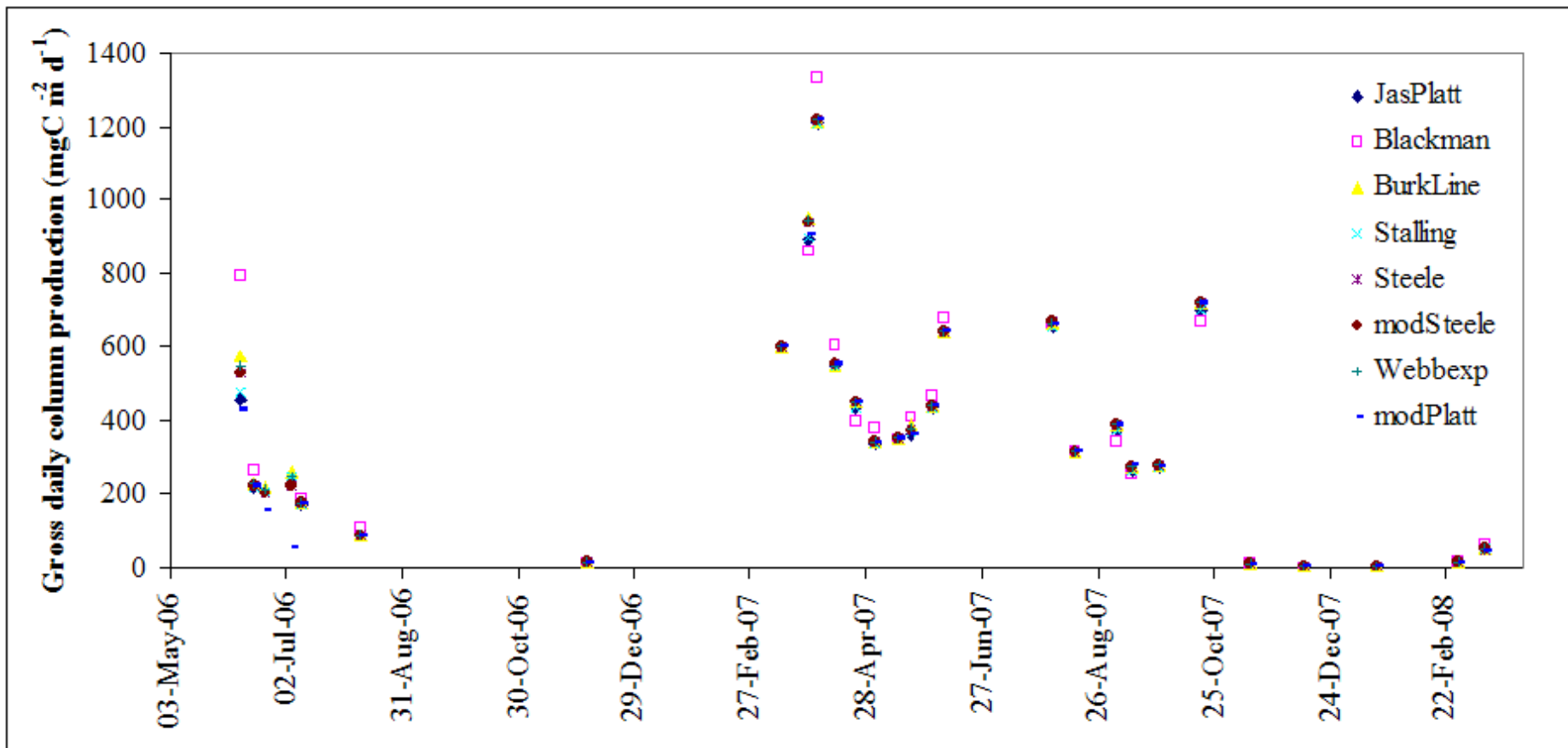


Figure 6.10. The temporal pattern in gross daily column production ($\text{mgC m}^{-2} \text{d}^{-1}$) derived from the 8 light-saturation models (JasPlatt, Blackman, BurkLine, STalling, Steele, modSteele, Webbexp, modPlatt, see text for explanation abbreviations) for a given sampling day.

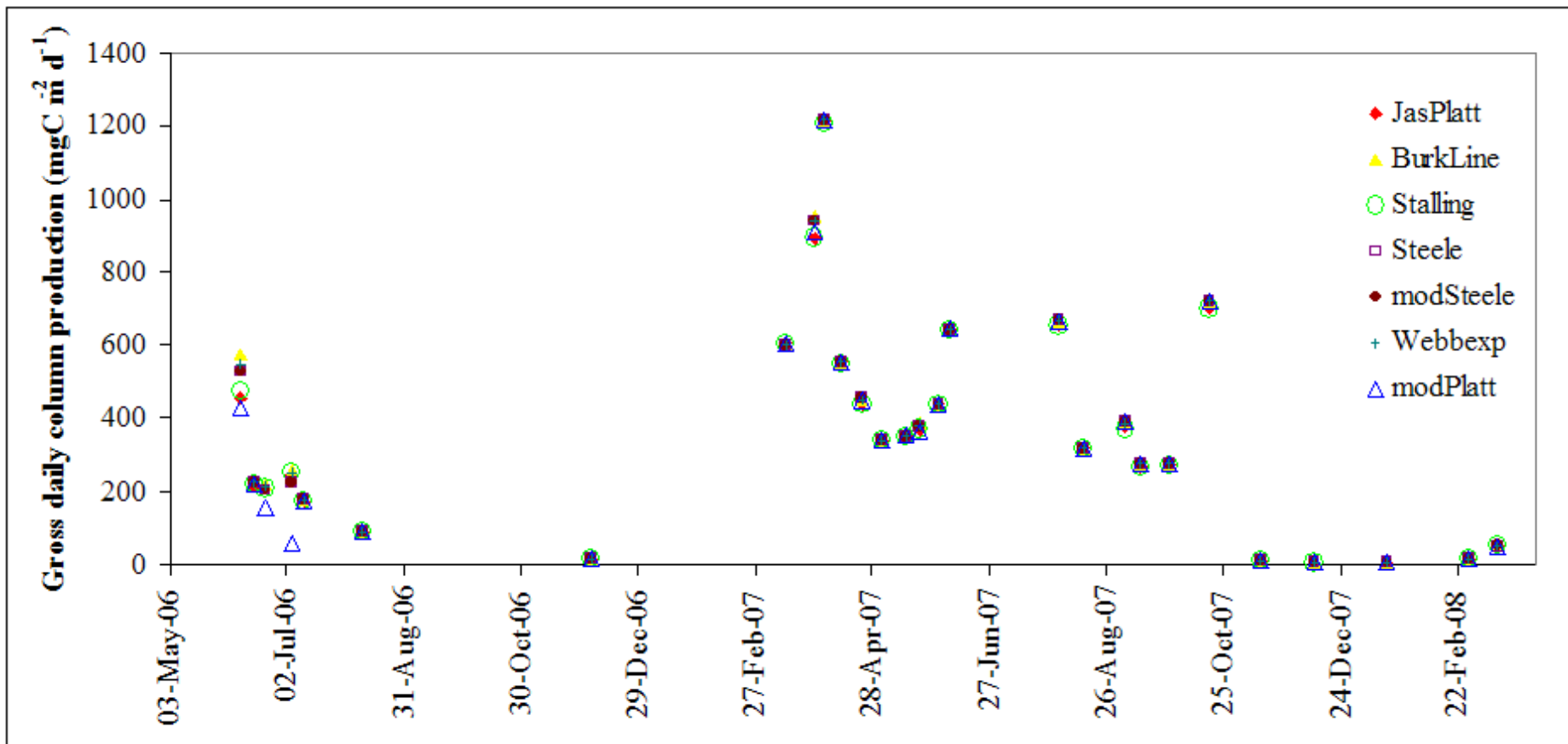


Figure 6.11. The temporal pattern in the gross daily column production (mgC m⁻² d⁻¹) for a given sampling day, derived from the light-saturation models of Figure 6.10 excluding Blackman.

6.3.2 Seasonal variability in production and respiration

Figures 6.9-6.11 provide a graphical representation of the seasonal variability in gross daily column production. Phytoplankton gross daily production showed maxima in June 2006 ($456 \text{ mgC m}^{-2} \text{ d}^{-1}$, JassPlatt model), April 2007 ($1210 \text{ mgC m}^{-2} \text{ d}^{-1}$, JassPlatt model), from June to mid August 2007 ($641\text{-}652 \text{ mgC m}^{-2} \text{ d}^{-1}$, JassPlatt model), and in mid October 2007 ($701 \text{ mgC m}^{-2} \text{ d}^{-1}$, JassPlatt model). Production estimates were low in December 2006 ($15 \text{ mgC m}^{-2} \text{ d}^{-1}$, JassPlatt model) and during winter 2007-08 until mid March 2008 (e.g. $3.2 \text{ mgC m}^{-2} \text{ d}^{-1}$, JassPlatt model). The average of the estimates ($n = 6$) of gross production for summer 2006 (from June to August) was significantly lower (approximately half) than the average of the estimates ($n = 4$) of production for summer 2007 (242 and $517 \text{ mgC m}^{-2} \text{ d}^{-1}$ respectively from JassPlatt model; two-sample T-test, T-value = -2.63 , DF = 6 , p value = 0.039).

Microplankton community respiration (MCR) ranged between $78.8 \text{ mgC m}^{-2} \text{ d}^{-1}$ (13th November 2007) and $919.3 \text{ mgC m}^{-2} \text{ d}^{-1}$ (2nd July 2007), with an average of $396.7 \text{ mgC m}^{-2} \text{ d}^{-1}$ (standard deviation of $206.5 \text{ mgC m}^{-2} \text{ d}^{-1}$, $n = 26$). It is important to note that in 2006, oxygen concentration was measured by a standard Winkler titration while in 2007-08 a microtitrator was used. The latter was more sensitive than the standard Winkler in detecting the oxygen concentration. In fact the lowest respiration derived by the standard titration was $223.8 \text{ mgC m}^{-2} \text{ d}^{-1}$, while the lowest respiration derived by the microtitrator was $78.8 \text{ mgC m}^{-2} \text{ d}^{-1}$, approximately 3 fold smaller. In 2006, MCR showed a peak in April and decreased during the summer. In 2007, MCR increased during spring until reaching a maximum in July, follow by a decrease until winter minimum.

Net microplankton production (NMP) was determined for 20 sampling events by subtracting microplankton community respiration estimates from estimates of gross production calculated using the Jassby and Platt (1976) model. Of these 20 estimates of NMP, only 8 were positive (Figure 6.13). The maximum NMP of $930 \text{ mgC m}^{-2} \text{ d}^{-1}$ was on 3rd April 2007. Positive net microplankton production occurred on the 8th June 2006, and in 2007 during the spring bloom (29th March, 3rd and 12th of April), in June (1st and 7th June), on the 2nd of August and the 18th October.

Focusing on the proportion of gross production used by respiration, and assuming that events with negative net production were equivalent to respiration

using 100% of gross production, on average microplankton community respiration used 83% of gross production. MCR accounted for 23-25% of phytoplankton production during the spring (3rd April) and autumn (18th October) blooms 2007.

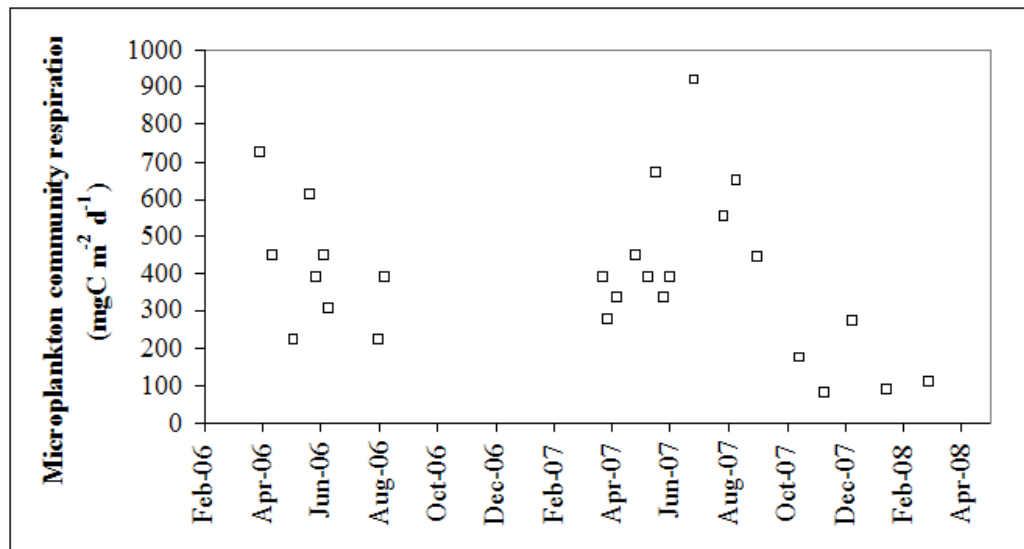


Figure 6.12. Seasonal changes in microplankton community respiration ($\text{mgC m}^{-2} \text{d}^{-1}$), at station CLNBuoy in Carlingford Lough, between April 2006 and March 2008.

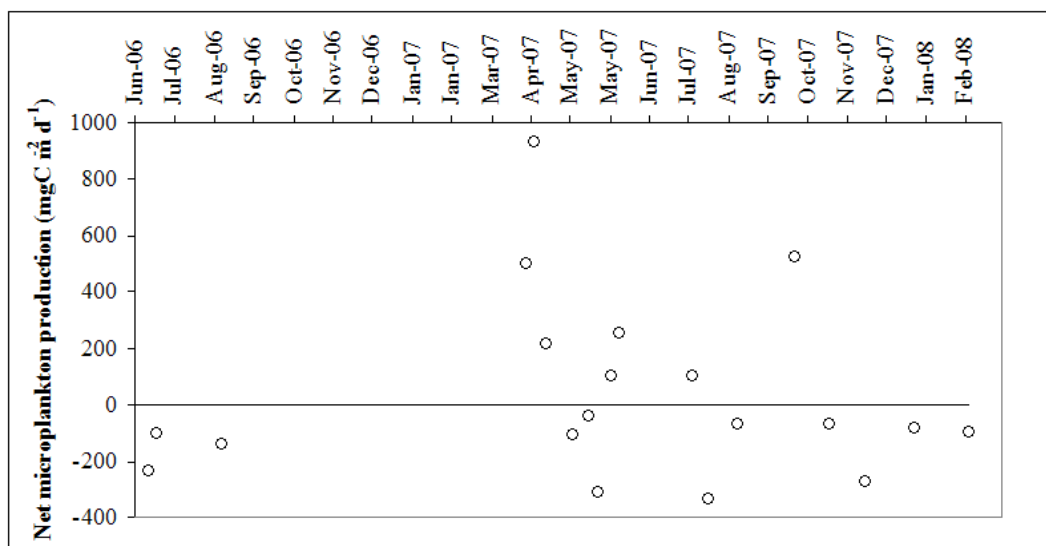


Figure 6.13. Seasonal changes in net microplankton production ($\text{mgC m}^{-2} \text{d}^{-1}$), at station CLNBuoy in Carlingford Lough, between May 2006 and March 2008. The solid line represents zero net microplankton production.

6.3.3 Relationships between gross production, microplankton community respiration and environmental variables

The log-transformed estimates of gross daily column production derived using the Jassby and Platt (1976) model were regressed against the log-transformed chlorophyll standing stock to test the first hypothesis (that chlorophyll standing stock can explain approximately 70% of the variability in primary production). The relationship between the two variables (Equation 6.18) was statistically significant (analysis of variance, $F = 62.48$, $DF = 27$, $n = 28$, $p < 0.001$) and chlorophyll standing stock explained 71% of the variability in gross daily column production (Figure 6.14).

$$\log GDCP = 0.463 + 1.47 \cdot \log Chl_stock \quad (6.18)$$

Where $\log GDCP$ is the log-transformed gross daily column production and $\log Chl_stock$ is the log-transformed chlorophyll standing stock.

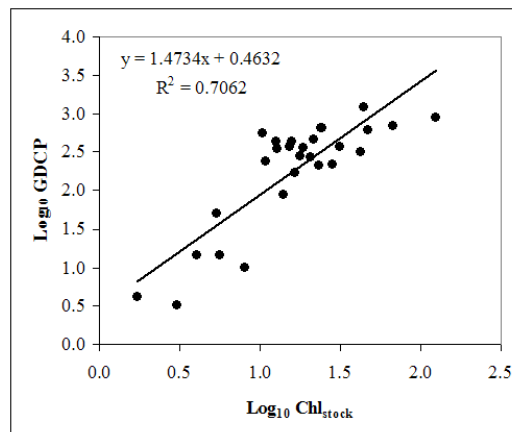


Figure 6.14. Linear regression of log-transformed gross daily column production (GDCP) against log-transformed chlorophyll standing stock.

Considering the other environmental variables (including the photosynthetic parameters), and performing a stepwise multiple regression, log-chlorophyll standing stock ($\log Chl_stock$), log-transformed α^B , K_d (see section 3.3.3) and log-transformed irradiance at the moment of the sampling ($\log I_{samp}$), explained up to 96% of the variability of $\log GDCP$ (Equation 6.19). The regression was statistically significant

(analysis of variance, $F = 137.97$, $DF = 27$, $p < 0.001$) and the intercept was significantly different from zero ($p < 0.001$).

$$\log GDCP = 2.37 + 1.14 \cdot \log \alpha^B + 1.05 \cdot \log Chl_stock + 0.629 \cdot \log I_{samp} - 0.883 \cdot K_d \quad (6.19)$$

LogChl_stock explained 70.6% of the variability in gross daily column production, $\log I_{samp}$ 13.3%, $\log \alpha^B$ 7.2% and K_d the remaining 4.9%.

Table 6.4 shows the Pearson correlation coefficients of log-transformed gross daily column production and other environmental variables. The correlation between gross production and maximum photosynthetic rate, temperature, salinity, chlorophyll standing stock, and irradiance during the sampling and in the previous 24 hours were positive. The correlations with Clanrye River flow, phaeopigments/chlorophyll ratio and dissolved nutrient concentrations were negative.

Table 6.4. Pearson correlation coefficients of log-transformed gross daily column production (logGDCP) and the main physical, chemical and biological variables. Log transformed photosynthetic parameters (α^B and P_{max}^B), temperature (Temp), salinity (Sal), logarithm of Clanrye River flow (logflow), log of phaeopigments/chlorophyll ratio (logPhae/chl), log-transformed average phytoplankton cell volume and chlorophyll content (logACV and logACC), log chlorophyll standing stock, log of irradiance during the sampling and in the previous 24 hours ($\log I_{samp}$, and $\log I_{24}$), vertical attenuation coefficient (K_d), ammonium, nitrate, nitrite, phosphate and silicate concentrations, Dissolved Inorganic Nitrogen concentration (DIN). Two stars (**) indicated p-value ≤ 0.001 , one star (*) indicated p-value < 0.05 . Data collected at station CLNBuoy in Carlingford Lough, between April 2006 and March 2008.

	$\log \alpha^B$	$\log P_{max}^B$	Temp	Sal	logflow	logPhae/chl
logGDCP	0.311	0.547*	0.510*	0.598**	-0.429*	-0.847**
	logACV	logACC	logChl_stoc	$\log I_{samp}$	$\log I_{24}$	K_d
logGDCP	0.300	-0.593**	0.840**	0.558*	0.692**	-0.589**
	NH ₄	Nitrate	Nitrite	DIN	Phosphate	Silicate
logGDCP	-0.893**	-0.705**	-0.781**	-0.737**	-0.847**	-0.812**

Variability in microplankton community respiration (MCR) was explained by salinity and by nitrate concentration (analysis of variance, $R^2 = 55.7\%$, $DF = 25$, $F = 14.44$, $p < 0.001$; Equation 6.20). Nitrate concentration accounted for approximately 35% of variability while salinity for the remaining 20.7%.

$$\log MCR = 8.80 - 0.188 \cdot \text{Salinity} - 0.0333 \cdot \text{Nitrate} \quad (6.20)$$

Based on the Pearson correlation coefficients, log-transformed MCR was positively correlated with temperature, and log-transformed chlorophyll concentration, gross daily column production, phytoplankton abundance and biomass. LogMCR was negatively correlated with nutrient concentrations (Table 6.5).

Table 6.5. Pearson correlation coefficients of log-transformed microplankton community respiration (logMCR) and the main physical, chemical and biological variables. Temperature (Temp), salinity, ammonium, phosphate, nitrate, silicate and nitrite concentrations, logarithm of Clanrye River flow (logflow), log of chlorophyll concentration (logChl) and phaeopigments concentration (logPhaeo), log-transformed phytoplankton abundance and biomass (logAbu and logBio), log-transformed gross daily column production (logGDGP). Two stars (**) indicated p-value ≤ 0.001 , one star (*) indicated p-value < 0.05 . Data collected at station CLNBuoy in Carlingford Lough, between April 2006 and March 2008.

	Temp	Salinity	NH ₄	Phosphate	Nitrate	Silicate
logMCR	0.454*	0.137	-0.661**	-0.686**	-0.591**	-0.641**
	Nitrite	Logflow	logChl	logPhaeo	logAbu	logBio
logMCR	-0.651**	-0.092	-0.522*	0.327	0.566*	0.633*
	logGDGP					
logMCR	0.679*					

6.3.4 Estimates of gross annual production using the TFS

Two pairs of sine-cosine waves gave the best fit (highest R^2) of the observations of gross daily column production ($R^2 = 0.72$, $DF = 23$, $F = 18.45$). The superposition of these 2 waves (Equations 6.21 and 6.22) is shown in Figure 6.15 a, while in Figure 6.15 b the deviations of the modelled values compared to the observations are given.

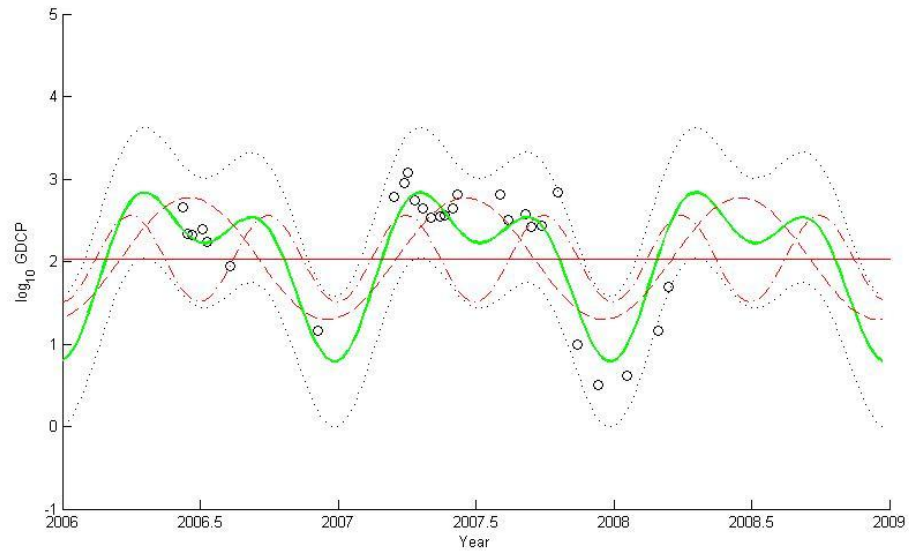
$$f(t) = \frac{a_0}{2} + \sum_{n=1}^{n=M} [a_n \sin(\omega_n t) + b_n \cos(\omega_n t)] \quad (6.21)$$

$$f(t) = \frac{2.03}{2} + [0.177 \cdot \sin(\omega_1 t) - 0.718 \cdot \cos(\omega_1 t) + 0.0253 \cdot \sin(\omega_2 t) - 0.525 \cdot \cos(\omega_2 t)] \quad (6.22)$$

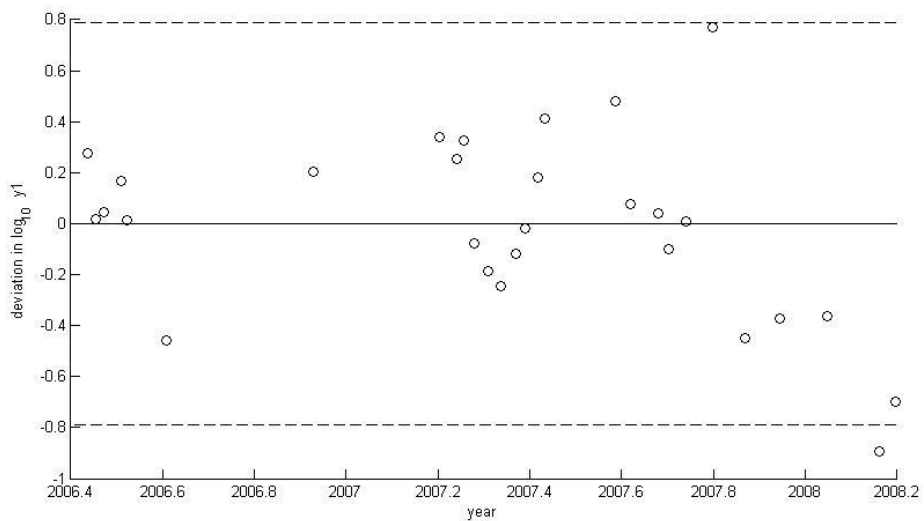
Where $f(t)$ is the function TFS and t is the time in radian.

The annual trend captured by the TFS (Figure 6.15) shows 2 peaks of gross production: a main peak at the end of March/start of April (spring bloom), and a smaller peak at the end of the summer, between August and September. The latter peak was then followed by a decrease in production down to the winter minimum (December-January).

Using the TFS (Equation 6.22), 100 synthetic data sets were generated that plotted together produced Figure 6.16. Descriptive statistics of the estimates of annual production derived from these 100 synthetic data sets gave a median gross annual column production of $101 \text{ gC m}^{-2} \text{ y}^{-1}$ with 90% confidence interval of 72 and $156 \text{ gC m}^{-2} \text{ y}^{-1}$.



a)



b)

Figure 6.15. The TFS time series. a) the fit of 2 paired sine-cosine waves (with frequency 1 y^{-1} and 2 y^{-1} respectively) to log-transformed daily column production estimates ($\text{mgC m}^{-2} \text{ d}^{-1}$) from June 2006 to March 2008; b) deviations of the modelled values from the observed values. In plot a), the wave with frequency 1 y^{-1} (wave1) and the wave with frequency 2 y^{-1} (wave2) are coloured pink and their sum (superposition) or TFS is coloured green. The pink straight line is the mean value around which the function is oscillating. In Figure 6.15 b, the 90% confidence interval is indicated by the dark dotted lines, while the black solid line represents zero. For both graphs the black empty circles represent the observations. In plot a, the TFS (sum of the 2 waves) explained 72% of the variability of the observations.

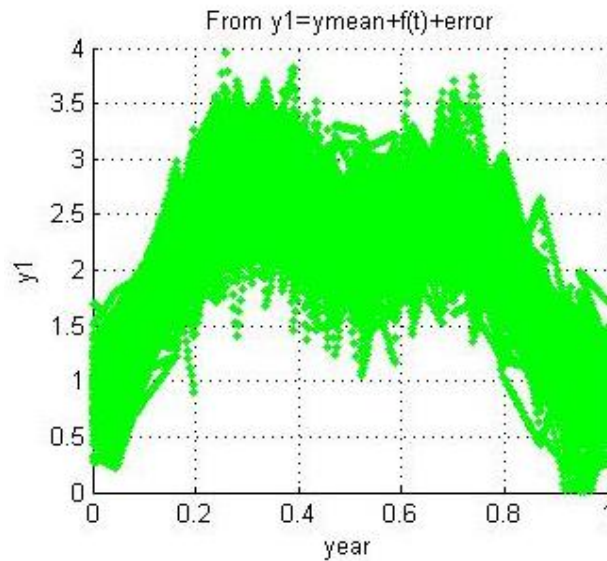


Figure 6.16. Log-transformed synthetic estimates of gross daily column production (y_1) plotted together for a standard year (100 synthetic data sets). Each synthetic data set was created using the TFS (derived by fitting the observed estimates of production with paired sine-cosine waves), summed to the mean value of the TFS, plus the error.

The script was run also with values of the main physical, chemical and biological variables. The best number of waves fitting each variable and the R^2 of the fit was determined as well as the R^2 of the fit of 2 waves (Table 6.6). All variables were best fitted by less than 10 waves except the Clanrye River flow that was best fitted by 32/33 waves. The poorest fit was for SPM_{tot} ($R^2 = 0.20$) while temperature trend was well reproduced by one wave ($R^2 = 0.92$).

As described in section 6.2.4, for improving the confidence interval of the annual gross column production, the environmental variables were fitted by 2 waves and the resulting deviations were tested for correlation to the gross production deviations. The R^2 of the fit of 2 waves to the environmental variables are shown in Table 6.6, while Table 6.7 gives a list of the variables which deviations were significantly correlated to gross production deviations. Except for logACV and logflow, the R^2 of the fit of 2 waves was similar to the R^2 of the fit of the best number of waves for that given variable. Deviations of log-transformed phytoplankton average cell volume, biomass, biovolume, abundance and chlorophyll standing stocks were positively correlated with deviations of gross daily column

production. The deviations of ammonium, phosphate and phaeopigment/chlorophyll ratio were negatively correlated with gross production deviations.

Table 6.6. Application of the truncated Fourier series (TFS) to the main environmental variables. The number of observations (n), the best number of waves fitting the data and the R^2 of the fit are shown for each variable, as well as the R^2 of the fit of 2 waves. The variables are: log- gross daily column production (logGDCP), log- average cell volume and average chlorophyll content (logACV and logACC), log- phytoplankton abundance, biomass and biovolume, log- chlorophyll standing stock (logChl_stock), log- irradiance during the sampling and in the previous 24 hours (logI_{samp} and logI₂₄), nutrient concentrations, log- phaeopigments/chlorophyll ratio, log- flow of the Clanrye River, temperature (Temp), salinity (Sal), Suspended Particulate Matter, inorganic and organic (SPM_{tot}), and log- Microplankton Community Respiration (logMCR). Data collected at station CLNBuoy in Carlingford Lough, between April 2006 and March 2008.

Variable	n	best n. waves	R² best n. waves	R² 2 waves
logGDCP	28	2	0.72	0.72
logACV	69	6	0.39	0.17
logACC	69	6	0.39	0.38
logAbundance	69	9	0.65	0.60
logBiomass	69	6	0.68	0.60
logBiovolume	69	6	0.68	0.59
logChl_stock	46	9	0.52	0.43
logI _{samp}	46	1	0.45	0.43
logI ₂₄	46	2	0.75	0.75
K _d	47	8	0.39	0.37
NH ₄	100	2	0.65	0.65
Nitrate	100	8	0.81	0.81
Nitrite	100	5	0.84	0.82
Phosphate	100	7	0.86	0.80
Silica	100	9	0.86	0.82
logPhaeo/chl	100	7	0.65	0.57
logflow	820	33/34	0.42	0.23
Temp	96	1	0.92	0.91
Sal	96	2	0.34	0.34
SPM _{tot}	72	2	0.20	0.20
logMCR	26	4	0.57	0.54

Table 6.7. Pearson correlation coefficients and p-values of the environmental variables which deviations showed a significant correlation to the deviations of the fit of the gross daily column production. Deviations were derived fitting 2 waves to the variable observations.

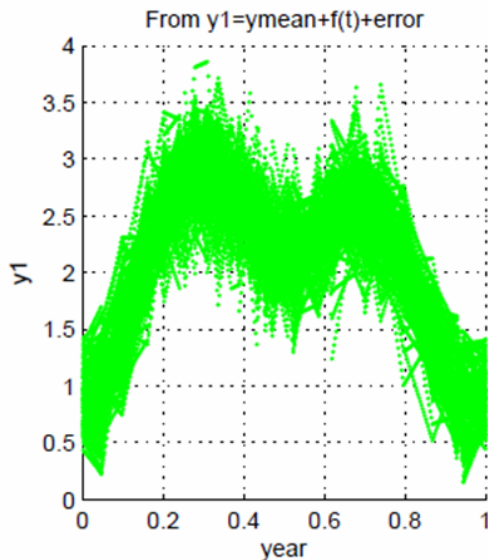
Variable	Pearson coefficient	p-value
logACV	0.412	0.037
logBiovolume	0.755	< 0.001
logAbundance	0.589	0.002
logBiomass	0.737	< 0.001
logChl_stock	0.744	< 0.001
NH ₄	-0.535	0.003
Phosphate	-0.421	0.026
logPhaeo/chl	-0.651	< 0.001

Gross annual column production was then recalculated using the relationship between gross production deviations and the environmental variable deviations into the equation (Equation 6.17) to generate 100 synthetic data sets. The recalculated gross annual column production estimates, confidence interval and R^2 are given for each significant variable in Table 6.8. The recalculated production varied from 93 gC m⁻² y⁻¹ (derived from NH₄) to 116 gC m⁻² y⁻¹ (derived from log-transformed chlorophyll standing stock). For each variable, the recalculated 90% confidence interval was smaller than the one derived from the fit of the GDCP estimates alone, and the R^2 was higher. In particular, the addition of the relationship GDCP deviations/chlorophyll stock deviations to the generation of the synthetic data sets improved the R^2 to 0.92. This last case is presented in Figure 6.17 which clearly shows how the confidence interval was improved after the introduction of the gross production/chlorophyll stock relationship.

Table 6.8. Recalculated estimates of gross daily column production, confidence intervals and R^2 including the relationship between deviations of the gross production and variable into the generation of the 100 synthetic data sets.

Variable	Recalculated GP ($\text{gC m}^{-2} \text{y}^{-1}$)	Recalculated 90% interval	Recalculated R^2
logACV	115	87-156	0.79
logBiovolume	108	91-132	0.91
logAbundance	103	84-133	0.87
logBiomass	108	92-136	0.91
logChl_stock	116	98-141	0.92
NH_4	93	75-124	0.82
Phosphate	114	91-147	0.81
logPhaeo/chl	99	78-124	0.86

Annual PP = $101 \text{ gC m}^{-2} \text{y}^{-1}$
Confidence limits: 72 – 156



Annual PP = $116 \text{ gC m}^{-2} \text{y}^{-1}$
Confidence limits: 98 – 141

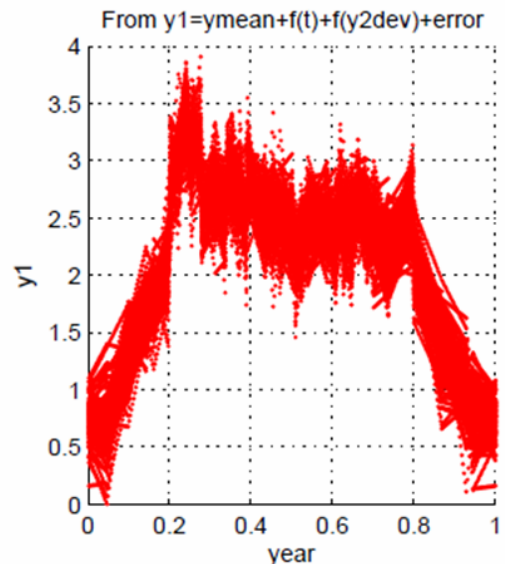


Figure 6.17. An example of how the introduction of the relationship between gross production deviations and variable (in this case chlorophyll standing stock) deviations into the generation of the 100 synthetic data sets improved the confidence interval of the predicted estimate of annual production.

6.3.5 Estimates of annual MCR using the TFS

The approach used in the estimation of gross annual column production was applied to net microplankton production estimates. The best number of waves fitting the observations was 1; however the fit was not good (Figure 6.18) and the resulting R^2 was very low (0.01).

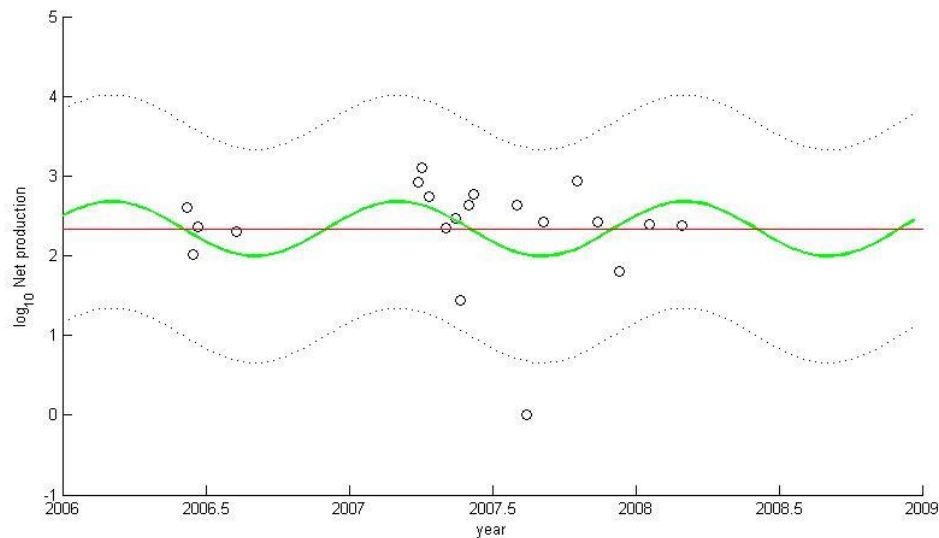


Figure 6.18 Fit of 1 sine-cosine wave (with frequency 1 y^{-1}) to log-transformed net daily microplankton production estimates ($\text{mgC m}^{-2} \text{ d}^{-1}$) from June 2006 to March 2008. The wave with frequency 1 y^{-1} (TFS) is coloured in green. The pink straight line is the mean value around which the function is oscillating. The 90% confidence interval is indicated by the dark dotted lines, while the black empty circles represent the observations. In this plot, the TFS explained 1% of the variability of the observations.

The application of the TFS to daily microplankton community respiration estimates for the water column produced a better R^2 (0.54 for 2 waves, $DF = 21$, $F = 8.24$). The superposition of the 2 waves (Equations 6.23) is shown in Figure 6.19.

$$f(t) = \frac{2.4}{2} + 0.0444 \cdot \sin(\omega t) - 0.304 \cdot \cos(\omega t) + 0.0178 \cdot \sin(2\omega t) - 0.043 \cdot \cos(2\omega t) \quad (6.23)$$

Where $f(t)$ is the function TFS and t is the time in radiant. MCR increased during spring up to summer maximum (end of June, start of July), follow by a decrease to winter minimum. The annual estimates of microplankton community respiration for the water column was calculated in the same way as annual gross phytoplankton production, with generation of 100 synthetic data sets (Figure 6.20). Application of descriptive statistics to annual MCR estimates gave a median value of annual respiration of $113 \text{ gC m}^{-2} \text{ y}^{-1}$ with 90% confidence interval at 97 and $134 \text{ gC m}^{-2} \text{ y}^{-1}$.

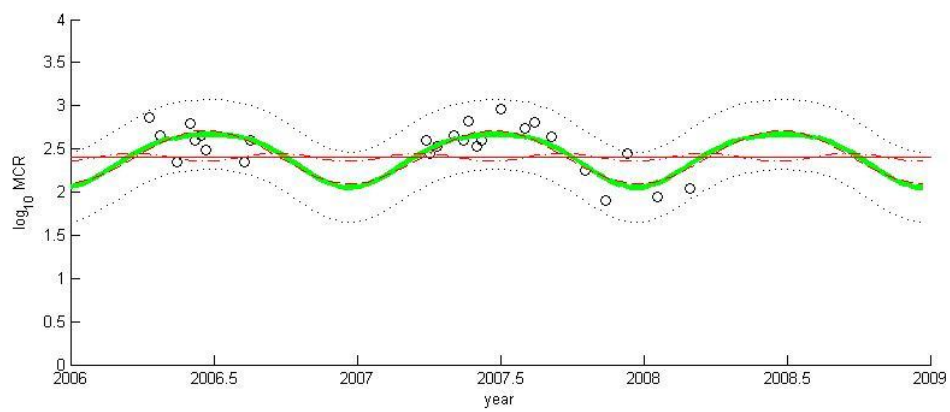


Figure 6.19. The fit of 2 paired sine-cosine waves (with frequency 1 y^{-1} and 2 y^{-1} respectively) to log-transformed microplankton community respiration (MCR) estimates ($\text{mgC m}^{-2} \text{ d}^{-1}$) from June 2006 to March 2008. The wave with frequency 1 y^{-1} (wave1) and the wave with frequency 2 y^{-1} (wave2) are coloured pink, while their sum (superposition) or TFS is coloured green. The pink straight line is the mean value around which the function is oscillating. The 90% confidence interval is indicated by the dark dotted lines, while the black empty circles represent the observations. In this plot, the TFS (sum of the 2 waves) explained 54% of the variability in the observations.

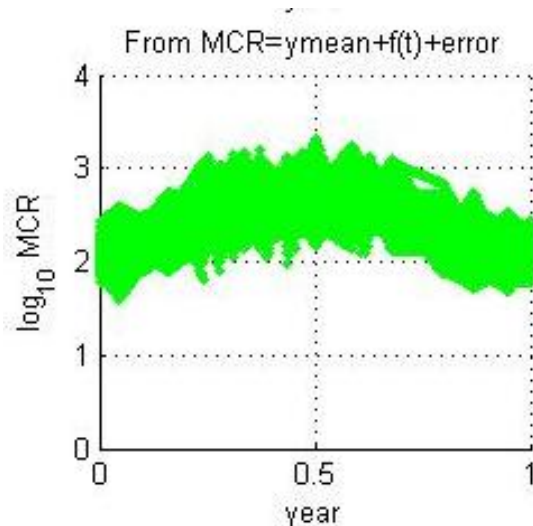


Figure 6.20. Log-transformed synthetic estimates of MCR plotted together for a standard year (100 synthetic data sets). Each synthetic data set was created using the TFS (derived by fitting the observed estimates of respiration with paired sine-cosine waves), summed to the mean value of the TFS, plus the error.

Deviations in phosphate concentration and salinity showed a negative significant correlation with deviations of microplankton community respiration (Table 6.9), therefore they were used to improve the confidence intervals of MCR. The recalculated estimates of annual MCR are given in Table 6.10. The R^2 of these recalculated estimates is higher than the R^2 derived from the fit of the MCR estimates alone.

Table 6.9. Pearson correlation coefficients and p-values of the environmental variables which deviations showed a significant correlation to the deviations of the fit of the microplankton community respiration. Deviations were derived fitting 2 waves to the variable observations.

Variable	Pearson coefficient	p-value
Phosphate	-0.429	0.029
Salinity	-0.407	0.039

Table 6.10. Recalculated estimates of microplankton community respiration, confidence intervals and R^2 including the relationship between deviations of MCR and variable into the generation of the 100 synthetic data sets.

Variable	Recalculated MCR ($\text{gC m}^{-2} \text{y}^{-1}$)	Recalculated 90% interval	Recalculated R^2
Phosphate	111	97-126	0.66
Salinity	117	105-134	0.69

6.4 Discussion

6.4.1 A critical evaluation of the method used to derive daily and annual column production

Estimates of gross daily column production at the sampling station in Carlingford Lough were derived using a ‘non spectral’ photosynthesis-irradiance model (Sathyendranath and Platt 2007) or, according to the classification of Behrenfeld and Falkowski (1997), a wavelength-integrated model (WIM). Photosynthesis-irradiance models describe production as a function of the available light, which in this study was considered to be the whole range of PAR. One of the limitations of using a non spectral model is that there is no information on the spectral response of the photosynthetic process to variability in the light spectra. Phytoplankton organisms belonging to different groups have different capacities to absorb specific wavelength of the PAR domain, due to difference in their size and/or in their pigment composition (see review by Sathyendranath and Platt 2007). In fact, small celled phytoplankters usually have a higher specific absorption due to the reduced packaging effect of the pigments in the cell. In contrast, larger celled species (such as diatoms) have a lower specific absorption coefficient. Differences in absorption can also be related to the taxonomy of the phytoplankton and the pigments contained into the cell. As an example, species of *Prochlorococcus* (Cyanobacteria) out-performs species of the other phytoplankton classes in blue oligotrophic waters, at least under light-limited conditions (Sathyendranath and Platt 2007). Although a spectral photosynthesis-irradiance model may have provided a better representation of the phytoplankton response to light, a non spectral model was easier to apply and used for creating a simple and robust methodology for measuring production in coastal waters.

When calculating phytoplankton production at different depths during the day, the vertical attenuation coefficient of underwater light (K_d) was considered constant for a given sampling day. In reality, K_d can vary during the day due to its dependence on the geometry of the light field (e.g. sun angle) and changes in the concentration of Optically Active Components of the water medium that may occur as a result of tidal exchange and stirring. There is no information available on the daily variability of K_d in Carlingford Lough, and as concluded in Chapter 3, more

work would be needed to fully understand what is controlling the light field in this region of restricted water exchange.

Chlorophyll concentration profiles were used to normalise production profiles, and in calculating column production the chlorophyll concentration was assumed to be constant during a given sampling day. As for K_d , it was not possible to collect multiple data of chlorophyll concentration during the same day, however an independent study (SMILE project) was carried out on the 20th March 2006 to determine the variability in chemical, physical and biological variables during a tidal cycle in Carlingford Lough. An example of daily variability of chlorophyll concentration and salinity at station CL11 (located in front of Greenore; see Figure 2.1) is provided in Figure 6.21. The latter shows that chlorophyll concentration decreased to a minimum at high tide (higher salinity). Chlorophyll concentration was derived using the same method described in section 2.2.5.

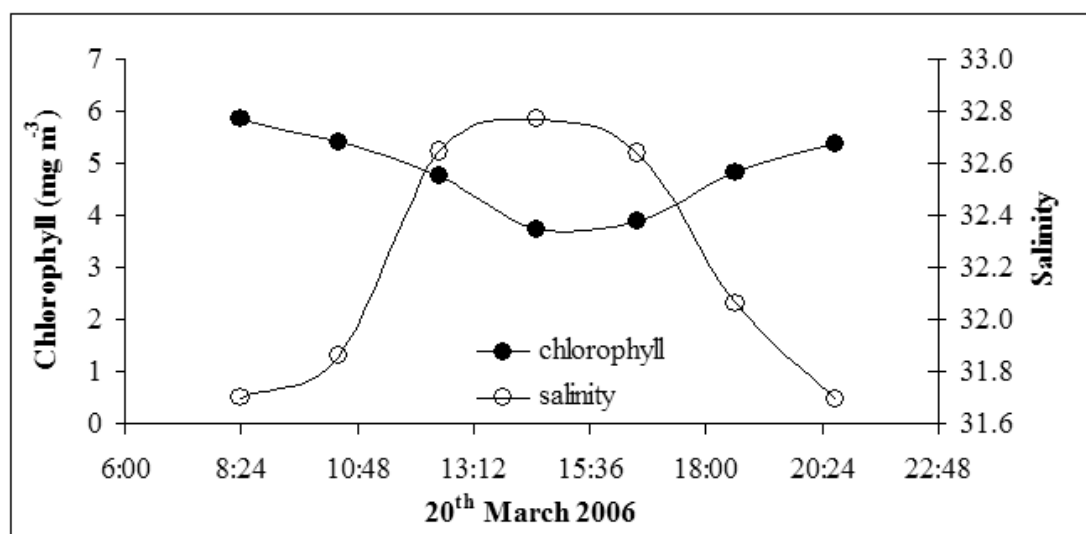


Figure 6.21. Variability in subsurface (1 m) chlorophyll concentration (mg m^{-3}) and salinity on the 20th March 2006, derived from multiple sampling at intervals of 2 hours, at station CL11, of Greenore in Carlingford Lough. Data kindly provided by Dr. H. Moore, AFBI, Belfast.

The variation in chlorophyll concentration due to tidal flow could have been avoided by carrying out the sampling during the same tidal condition. However the

timing of the sampling events was restricted to between 9:00 am and 11:00 am because α^B and P_{\max}^B show diurnal cycle with maximum values around midday (e.g. MacCall and Platt 1977; Côté and Platt 1983; Jouenne *et al.* 2005). Yoshikawa and Furuya (2006) suggested that to calculate production, estimates of the photosynthetic parameters derived from dawn or noon sampling should be used if sampling is only carried out once a day. The same authors measured the daily variability in α^B and P_{\max}^B in Sagami Bay (Japan) and estimated primary production using daily and time varying values of the photosynthetic parameters. They concluded that using daily estimates of α^B and P_{\max}^B derived from dawn or noon incubations gave estimates of primary production similar (on average 3-5% difference) to estimates based on values of α^B and P_{\max}^B that change over the daily cycle. In contrast, using daily values of the photosynthetic parameters derived from incubations carried out at dusk under-estimated production by 43%. The literature on this topic is conflicting. Based on an investigation of primary production in Santa Barbara Channel, Harding *et al.* (1982) suggested that single daily values of the photosynthetic parameters should not be used to estimate production because this could result in under-estimation by up to 10% or over-estimation by up to 20%. Lizon *et al.* (1995) estimated an error of -40% to +33% using single daily values of α^B and P_{\max}^B for a given day for the English Channel. On the other hand, Azevedo, Duarte and Bordalo (2006) did not observe any difference in estimates of production using single daily or time varying values of the photosynthetic parameters during a study of the Douro Estuary in Portugal.

Multiple sampling of biological and physical variables during a tidal cycle as well as repeated primary production experiments would have provided useful information on daily variability. Unfortunately it was not possible to carry out multiple sampling in a day due to the travelling time between the laboratory and study site. Furthermore it was not possible to study the diurnal cycle of photosynthetic parameters in Carlingford Lough because of the impracticality of carrying out the incubations *in situ* due to constraints on using ^{14}C at an unlicensed site.

In Chapter 5 a discussion was included of which model should be used for fitting photosynthesis-irradiance curves and the criteria that could be used for selecting the appropriate model. The Jassby and Platt (1976) model has been shown to provide a consistently good fit to the P/E data from Carlingford Lough. The photosynthesis-irradiance models considered in this study provided similar estimates

of α^B but quite different estimates of P_{\max}^B (Chapter 5). Based on these considerations, it is interesting to notice that the estimates of gross daily column production derived using the models were usually very similar (except for the Blackman model; Tables 6.1-6.3). This result is in agreement with Lederman and Tett (1981) who were of the opinion that the photosynthesis-light models (e.g. Talling 1957; Webb *et al.* 1974; Jassby and Platt 1976) cannot be distinguished based on their ability to describe the photosynthesis/light curve.

Considering the application of the TFS, the daily estimates of gross column production were well fitted by 2 pairs of sine-cosine waves. This might have been expected considering that primary production depends on light availability and the solar radiation cycle was described by 1 wave (see $\log I_{\text{samp}}$ in Table 6.6). The calculation of 100 estimates of annual production, from which a confidence interval was derived, provided information on the variability of the estimate of annual production. The addition of the relationship between deviations in environmental variables and production improved the confidence interval of annual production and also the R^2 of the fit (Table 6.8), increasing the number of sampling events. Between the environmental variables, with deviations that showed a significant correlation with the deviations of production, logarithm of chlorophyll standing stock gave the highest R^2 . The TFS applied to estimates of MCR did not provide as good a fit as the estimates of gross production did, however the generation of the 100 synthetic estimates of annual MCR was helpful for defining the variability in respiration and calculating net annual microplankton production.

6.4.2 A comparison of estimates of gross production between Carlingford Lough and other water bodies

The highest hourly production rates measured in Carlingford Lough (77 mgC $\text{m}^{-3} \text{h}^{-1}$ in October 2007 and 68 mgC $\text{m}^{-3} \text{h}^{-1}$ in April 2007, Jassby and Platt model) were between rates of approximately 50 mgC $\text{m}^{-3} \text{h}^{-1}$ (end of May 1984) and 126 mgC $\text{m}^{-3} \text{h}^{-1}$ (July 1984) derived for the mid and inner regions of Belfast Lough by Parker, Rosell and MacOscar (1988). The maximum hourly rates of production in Carlingford Lough were also similar to the rates (66.6 mgC $\text{m}^{-3} \text{h}^{-1}$ in July 1976 and September 1977) measured by Boney (1986) in the inner Firth of Clyde (Scotland).

Focusing on daily estimates of gross column production, the range at station CLNBuoy (3.2 – 1210 mgC m⁻² d⁻¹, Jassby and Platt model, Table 6.3) was comparable to ranges derived for coastal areas such as the Westerschelde in the Netherlands (< 50 – 2500 mgC m⁻² d⁻¹; Goosen *et al.* 1999), the coastline of the North Frisian Wadden Sea (5 to 2200 mgC m⁻² d⁻¹; Tillmann, Hesse and Coljin 2000), the Douro Estuary in Portugal (4.7 to 1878.5 mgC m⁻² d⁻¹, average 319.9 mgC m⁻² d⁻¹; Azevedo, Duarte and Bordalo 2006), and the Baie de Veys in France (20 - 1430 mgC m⁻² d⁻¹; Jouenne *et al.* 2007). The range in Carlingford Lough was bigger than the range in the Elbe estuary in Germany (< 50 – 600 mgC m⁻² d⁻¹; Goosen *et al.* 1999) and Gironde in France (approximately 2 – 30 mgC m⁻² d⁻¹; Goosen *et al.* 1999), but smaller than the range of the Marennes-Oléron Bay in France (6 – 3600 mgC m⁻² d⁻¹; Struski and Bacher 2006) and of Tokyo Bay (160-7600 mgC m⁻² d⁻¹; Bouman *et al.* 2010).

The maximum rate of daily column production in Carlingford Lough (1210 mgC m⁻² d⁻¹; Jassby and Platt 1976 model) was smaller than the maximum rates of: 5387 mgC m⁻² d⁻¹ in Irish coastal waters of the Irish Sea close to the entrance to Carlingford Lough (Gowen and Bloomfield 1996; Gowen *et al.* 2000); 2968 mgC m⁻² d⁻¹ in Irish Sea coastal waters of Northern Ireland (Gowen and Bloomfield 1996); 3165.8 mgC m⁻² d⁻¹ measured during the 1997 spring bloom in Liverpool Bay by Gowen *et al.* (2000).

The seasonal trend of primary production described for Carlingford Lough (with a main peak in April followed by a secondary peak in September) has been observed in other temperate estuaries such as St Margaret's Bay in Nova Scotia in 1966-69 (Platt 1971), and in the mid region of Belfast Lough in 1988 (Parker, Rosell and MacOscar 1988). Carlingford and mid Belfast Loughs showed nitrate limitation during summer that caused the small reduction in production occurring in June-July. However, in the inner region of Belfast Lough, where concentrations of nitrogen compounds and phosphate were high during summer, production showed a steady increase from April to a maximum in July (Parker, Rosell and MacOscar 1988). Kocum *et al.* (2002) observed a similar trend in production in the Colne Estuary in SE England during 1994-95, although the production season started earlier (in March) and the peak was in August instead of July.

The spring peak in production observed in April in Carlingford Lough was also described by Gowen and Bloomfield (1996) for Irish coastal waters of the Irish

Sea; the North Sea (in 1988-89; Joint and Pomroy 1993) and in the Marsdiep (Dutch Wadden sea, in 1990; Cadée and Hegeman 1991). In the central Irish Sea, the peak in spring production occurred later than it did inshore and Gowen *et al.* (1995) related the timing of the former to the onset of seasonal stratification. An autumn peak in production (mid October) was observed in Carlingford Lough in 2006 and 2007, but no autumn bloom was recorded in the Irish Sea by Gowen and Bloomfield (1996) during 1992-93, but this could have been due to the low (approximately monthly) sampling frequency.

The TSF and the relationship between the deviations in daily production and chlorophyll standing stock gave the highest R^2 (0.92), compared to the other estimates of annual production, derived from considering the relationships between GDCP and the other environmental variables. The estimate of annual production of $116 \text{ gC m}^{-2} \text{ y}^{-1}$ with confidence interval $98\text{-}141 \text{ gC m}^{-2} \text{ y}^{-1}$ (Table 6.8) were used to compare the productivity of Carlingford Lough with that of other water bodies (Figure 6.22 and Table 6.11).

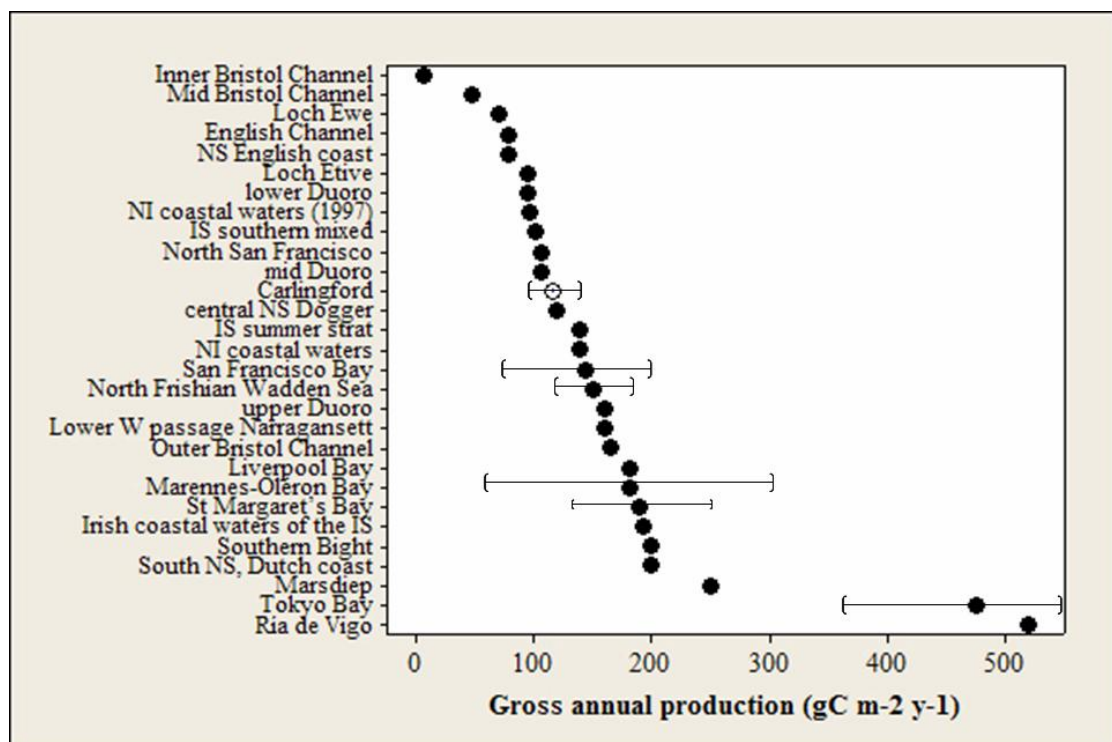


Figure 6.22. Gross annual production ($\text{gC m}^{-2} \text{ y}^{-1}$) of different water bodies. Sources of these estimates of production are given in Table 6.11. Carlingford Lough is indicated by the empty circle, and the brackets indicate range of variability of production (where available). IS = Irish Sea, NS = North Sea, NI = Northern Ireland.

Table 6.11. Estimates of gross annual column production (GACP, $\text{gC m}^{-2} \text{y}^{-1}$) for different water bodies. The year of sampling is also shown. IS = Irish Sea, NS = North Sea, NI = Northern Ireland.

Source	Area	Year	$\text{gC m}^{-2} \text{y}^{-1}$ GACP
Joint and Pomroy 1981	Inner Bristol Channel	1973-77	6.8
Joint and Pomroy 1981	Mid Bristol Channel	1973-77	48.5
Struski and Bacher 2006	Marennes-Oléron Bay	2001-02	64-301
Wood, Tett and Edwards 1973	Loch Etive	1970	70
Howarth <i>et al.</i> 1993	English Channel	1988-89	79
Joint and Pomroy 1993	NS English coast	1988-89	79
Cloern 1987	San Francisco Bay		80-210
Steele and Baird 1968	Loch Ewe		95
Azevedo, Duarte and Bordalo 2006	lower Douro Estuary	2003	95
Gowen <i>et al.</i> 2000	NI coastal waters	1997	97
<i>This study</i>	<i>Carlingford Lough</i>	<i>2006-08</i>	<i>98-141</i>
Gowen and Bloomfield 1996	IS southern mixed	1992-93	101
Alpine and Cloern 1992	Northern San Francisco	1977-90	106
Azevedo, Duarte and Bordalo 2006	mid Douro Estuary	2003	106
Howarth <i>et al.</i> 1993	central NS Dogger	1988-89	119
Tillmann, Hesse and Coljin 2000	North Frisian Wadden Sea	1995-96	124-176
Platt 1971	St Margaret's Bay	1966-69	130-250
Gowen and Bloomfield 1996	IS summer stratified	1992-93	140
Gowen and Bloomfield 1996	IS coastal waters of Northern Ireland	1992-93	140
Azevedo, Duarte and Bordalo 2006	upper Douro Estuary	2003	160
Oviatt, Keller and Reed 2002	Lower W passage Narragansett Bay	1997-98	160
Joint and Pomroy 1981	Outer Bristol Channel	1973-77	164.9
Gowen <i>et al.</i> 2000	Liverpool Bay	1997	182
Gowen and Bloomfield 1996	IS coastal waters of Ireland	1992-93	194
Howarth <i>et al.</i> 1993	Southern Bight	1988-89	199
Howarth <i>et al.</i> 1993	South NS, Dutch coast	1988-89	199
Cadée and Hegeman 1991	Marsdiep	1990	250
Bouman <i>et al.</i> 2010	Tokyo Bay	1997-00	370-580
Cermeño <i>et al.</i> 2006	Ría de Vigo	2001-02	520

According to Figure 6.22 and Table 6.11, annual production in Carlingford Lough was higher than that in the inner and mid regions of the Bristol Channel (Joint and Pomroy 1981); Loch Etive (Scotland; Wood, Tett and Edwards 1973); the English Channel (Howarth *et al.* 1993); the North Sea English Coast (Joint and Pomroy 1993). Estimates of annual production of the Lough were comparable to annual estimates for Loch Ewe (Steele and Baird 1968), the lower and mid Douro estuary (Azevedo, Duarte and Bordalo 2006), Northern San Francisco Bay (Alpine and Cloern 1992), and of the Central North Sea at the Dogger Bank (Howarth *et al.* 1993).

The range in estimates of annual gross production for Carlingford Lough is comparable with estimates of production for different regions of the Irish Sea (Gowen and Bloomfield 1996; Gowen *et al.* 2000), except Irish coastal waters of Ireland (Gowen and Bloomfield 1996) and Liverpool Bay (Gowen *et al.* 2000) which supported higher production than Carlingford Lough (Figure 6.22 and Table 6.11). Gowen *et al.* (2000) attributed elevated production in Liverpool Bay to anthropogenic nutrient enrichment. Although Carlingford Lough was less productive than the nearby Irish coastal waters, it showed a similar length of production season (7 months) and also similar reduction in production during June-July due to nutrient depletion (Gowen and Bloomfield 1996). In contrast, Irish Sea coastal waters of Northern Ireland and the central region of the Irish Sea had a shorter production season (e.g. 2-3 months) with the main part of production (59-79%) occurring in June-July (Gowen and Bloomfield 1996).

Low estimates of annual production from the inner and mid Bristol Channel (Joint and Pomroy 1981), the lower Douro estuary (Azevedo, Duarte and Bordalo 2006), Loch Etive (Wood, Tett and Edwards 1973), and San Francisco Bay (Cloern 1987) were attributed to light limitation. Furthermore, the Gironde in France (Goosen *et al.* 1999) and the Colne estuary in SE England (Kocum *et al.* 2002) are other examples of coastal water bodies in which phytoplankton growth is limited by the light climate. At station CLNBuoy in Carlingford Lough, light availability limited phytoplankton growth during winter (as suggested by z_{eu} value of 3.6 m; see Figure 3.17), and controlled the timing of the spring bloom (see Chapter 3). However phytoplankton growth was not constrained by light during the rest of the year, as suggested by the fact that the average depth of the euphotic zone (8.4 m; Table 3.3) exceeded the average depth of the water column (5.5 m). As argued in Chapter 2, it is

possible that phytoplankton growth in Carlingford Lough was nutrient limited during summer.

6.4.3 Relationships between daily column production and other environmental variables

Joint and Pomroy (1993) and Gowen and Bloomfield (1996) observed that chlorophyll standing stock could explain 69.8% and 71% of the variability in primary production in the North Sea and in the Irish Sea respectively. Furthermore, Bot and Colijn (1996) found that chlorophyll concentration explained 91% of the variation in production in Irish Sea and Dutch coastal waters (Table 6.12). In Chapter 1 it was hypothesised that this empirical relationship should hold for inshore, semi-enclosed water bodies, such as Carlingford Lough, and therefore provide an alternative method of estimating daily production. The data from Carlingford Lough show that chlorophyll standing stock explained 71% of the variability in production (Equation 6.18) and therefore support the first testable hypothesis presented in Chapter 1. The applicability of the production-chlorophyll relationship for estuaries or turbid water bodies is also supported by Joint and Pomroy (1981) who tested the relationship in the Bristol Channel, and found that they could explain up to 86% of the variability in production. Smith (1979) showed that production-chlorophyll relationships are also applicable to a variety of water bodies included fresh waters. In his study, Smith analysed 58 north temperate lakes in the USA and observed that chlorophyll concentration explained 81% of the variability in production (Table 6.12). For San Francisco Bay, Cole and Cloern (1984) derived a similar relationship ($R^2 = 0.88$) based on biomass ($\text{mg chlorophyll m}^{-3}$), surface irradiance and depth of photic zone (as 1% of surface light; Table 6.12).

Table 6.12. Relationships between primary production and chlorophyll derived for different water bodies. P is the photosynthetic rate, Chl is chlorophyll concentration, Chl_{stock} is chlorophyll standing stock, B is biomass (expressed as chlorophyll concentration), Z_p is the depth of the euphotic zone, and I₀ is the subsurface irradiance.

Source	Equation	R ²
Bot and Colijn (1996)	$\ln P \text{ (}\mu\text{gC} \cdot \text{m}^{-3} \cdot \text{h}^{-1}\text{)} = 1.27 \ln \text{Chl} \text{ (}\mu\text{g} \cdot \text{m}^{-3}\text{)} + 1.04$	0.91
Cole and Cloern (1984)	South Bay: $P = 94 + 0.88 \cdot \beta \cdot Z_p \cdot I_0$ North Bay: $P = 63 + 0.67 \cdot \beta \cdot Z_p \cdot I_0$	0.88 0.72
Joint and Pomroy (1981)	$P \text{ (}\mu\text{gC} \cdot \text{m}^{-3} \cdot \text{h}^{-1}\text{)} = 4.93 \cdot \text{Chl} \text{ (}\mu\text{g} \cdot \text{m}^{-3}\text{)} - 0.19$	0.86
This study	$\ln GDCP \text{ (}\mu\text{gC} \cdot \text{m}^{-2} \cdot \text{d}^{-1}\text{)} = 1.47 \ln \text{Chl}_{\text{stock}} \text{ (}\mu\text{g} \cdot \text{m}^{-2}\text{)} + 0.463$	0.71
Smith (1979)	$P \text{ (}\mu\text{gC} \cdot \text{m}^{-3} \cdot \text{d}^{-1}\text{)} = 22.9 \cdot \text{Chl} \text{ (}\mu\text{g} \cdot \text{m}^{-3}\text{)} - 42.6$	0.81
Gowen <i>et al.</i> 2000	$\ln P \text{ (}\mu\text{gC} \cdot \text{m}^{-2} \cdot \text{h}^{-1}\text{)} = 0.974 \ln \text{Chl} \text{ (}\mu\text{g} \cdot \text{m}^{-2}\text{)} + 2.07$	
Joint and Pomroy (1993)	Not given in the paper	0.698
Gowen and Bloomfield (1996)	Not given in the paper	0.71

Equation 6.19 suggests that the contribution of the photosynthetic parameters to the variability in production estimates is small. In fact, approximately 89% of the variability in production was related to chlorophyll standing stock, irradiance during the sampling and K_d, while the contribution of the photosynthetic parameter α^B was only 7.2%. While this result is in agreement with Cole and Cloern (1984) equations for San Francisco Bay, it contrasts with the observations by Bouman *et al.* (2010) for Tokyo Bay (Japan). The latter authors applied a similar equation including biomass (in terms of chlorophyll), irradiance and light attenuation, and they could explain only 52% of the variability in production. Furthermore in their study, α^B accounted for 21% of the variability in production and together with P^B_{max} explained 48% of the variability that was not related to biomass, irradiance and light attenuation.

The importance of chlorophyll, light and K_d values, compared to the photosynthetic parameters values, in determining production could also explain why the production-irradiance models gave similar estimates of production. The modelled production estimates at discrete depths were integrated down the water column and normalised to chlorophyll using the same values of irradiance, K_d and chlorophyll concentration, but changing α^B and P_{\max}^B as derived from that given model. It could be argued that the strong correlation between chlorophyll standing stock, light, K_d and production was merely a consequence of the fact that column production was calculated using these environmental variables. However, results by Joint and Pomroy (1993) for the North Sea showed that the correlation between production and chlorophyll is not a result of the way primary production is calculated. In fact Joint and Pomroy (1993) measured primary production directly using 24 hour incubation of water samples collected at different depth, and they did not normalise the production by chlorophyll. Water column ^{14}C fixation was related to chlorophyll standing stock and the latter explained 69.8% of the variability in production (Joint and Pomroy 1993).

Considering the correlations between GDCP and other environmental variables, the positive correlation between gross daily column production, temperature and salinity was also observed by Azevedo, Duarte and Bordalo (2006) for the Falkowski Estuary, Portugal. The positive correlation with temperature could be explained by considering that the maximum photosynthetic rate is an enzymatic process and temperature explained 43.3% of the variability in P_{\max}^B (when only data from 2007 was considered; see Chapter 5). Jouenne *et al.* (2007) observed a positive correlation between production and temperature in the Baie de Veys in France. On the other hand, the positive correlation with salinity is more difficult to explain considering that the main source of nutrients was the river and, according to Figure 6.21, chlorophyll may have been negatively related to salinity i.e. decreased during high tide at the sampling station.

The positive correlation between production and irradiance (during the sampling and during the 24 hours previous to the sampling) confirmed the strong dependence of production on the light regime. The negative correlation of production with K_d supported this consideration, indicating that when the light attenuation coefficient was low, there was more light available for photosynthesis (chlorophyll concentration $> 10 \text{ mg m}^{-3}$ was observed when $K_d < 0.5 \text{ m}^{-1}$, see discussion Chapter

3). Correlation to light in the water column has been described also for the Baie de Veys (Jouenne *et al.* 2007), while the importance of the light penetration along the water column has been highlighted for the Bristol Channel (Joint and Pomroy, 1981) and the Falkowski Estuary (Azevedo, Duarte and Bordalo 2006). As previously observed, it is also possible that some of the correlations between production and environmental variables (e.g. with light) were an effect of the calculations adopted to derive column production.

The average chlorophyll content per cell was negatively correlated to gross production and α^B (Chapter 5). As already discussed, this could be a consequence of the packaging effect of chlorophyll molecules inside the phytoplankton cell (Platt and Jassby 1976). Gross daily production was negatively correlated with nutrient concentrations and river outflow. The River Clanrye is the major source of nutrients for the Lough and variations in discharge drive ecological and biogeochemical processes in the Lough. Relationships between phytoplankton production and river discharge have been observed in various studies of inshore and coastal water bodies (e.g. Baie de Veys, Jouenne *et al.* 2007; San Francisco Bay, Cloern 1991; Douro Estuary, Azevedo, Duarte and Bordalo 2006).

In relation to the negative correlation with nutrients, Gowen, Tett and Jones (1992) analysed 60 datasets from sea lochs of the West coast of Scotland and observed that 2/3 of the datasets gave significant negative correlations between chlorophyll concentration and nitrate. The authors interpreted these results as the effect of nitrate being assimilated by phytoplankton. Considering the strong correlation between production and chlorophyll standing stock, the explanation provided by Gowen, Tett and Jones (1992) could be used to explain the gross daily column production and nutrients relationship. On the other hand, Dugdale *et al.* (2007) explained the negative relationship between phytoplankton production and ammonium as the effect of inhibition of nitrate-uptake caused by high level of ammonium. During a study of San Francisco Bay (from November 1999 to August 2003), the latter authors, observed that: if NH_4 concentration was $< 1 \mu\text{M}$, NO_3 was taken up by phytoplankton; with concentrations of NH_4 between 1 and $4 \mu\text{M}$ uptake of NO_3 was reduced to about half; with concentrations of $\text{NH}_4 > 4 \mu\text{M}$, NO_3 assimilation by phytoplankton cells was inhibited. It is interesting to observe that in Carlingford Lough, phytoplankton production during summer 2006 was significantly less than production in summer 2007. Ammonium was the only variable to show a

significant difference between 2006 and 2007, and it was higher in spring/summer 2006 compared to spring/summer 2007 (average 1.5 and 0.59 μM respectively). The possible inhibitory role of NH_4 could be an explanation for lower production in 2006 but further work would be required to test this hypothesis.

6.4.4 Respiration and net production

The range of variability in microplankton community respiration in Carlingford Lough (78.8 – 919.3 $\text{mgC m}^{-2} \text{d}^{-1}$) was wider than the range reported for the Ría de Vigo, NW Spain (47 – 588 $\text{mgC m}^{-2} \text{d}^{-1}$, Cermeño *et al.* 2006), but smaller than the range for the Douro Estuary in Portugal (average 1154 $\text{mgC m}^{-2} \text{d}^{-1}$, Azevedo, Duarte and Bordalo 2006).

The temporal trend, with maximum respiration during summer and minimum respiration during winter, has also been observed in the Ría de Vigo (Cermeño *et al.* 2006). This trend could be the direct effect of higher summer temperature on the physiology of microplankton (positive correlation with temperature in Table 6.5). A positive correlation between temperature and MCR has also been observed for the North Sea and English Channel (Iriarte *et al.* 1991), for the Urdaibai estuary in Northern Spain (Iriarte *et al.* 1996) and for Tomales Bay in California (Fourqurean *et al.* 1997). In particular, Iriarte *et al.* (1991) suggested that the increase in temperature in temperate seas was associated with higher solar radiation and stratification of the water column that can lead to higher phytoplankton production. Therefore Iriarte *et al.* (1991) hypothesised that this increase in organic production by phytoplankton could be more important in determining MCR than the direct physiological effect of temperature. The importance of phytoplankton production, abundance and biomass on influencing microplankton community respiration was confirmed by the positive correlation between these variables and MCR. However this was in contradiction with the negative correlation between chlorophyll concentration and MCR (Table 6.5). A correlation between chlorophyll and MCR was also observed in the studies of Iriarte *et al.* (1991 and 1996) and Fourqurean *et al.* (1997) however in all three the relationship derived was positive. It is not clear what was causing the negative correlation between chlorophyll and MCR at station CLNBuoy in Carlingford Lough.

The negative correlation between microplankton respiration and nutrient concentrations could be an effect of the strong correlation between microplankton respiration and gross daily column production or temperature (the latter was negatively correlated to nutrient concentration, see Table 2.11). Similar correlations between microplankton respiration, salinity and nutrients were described for the Douro Estuary by Azevedo, Duarte and Bordalo (2006).

For the Ría de Vigo (NW Spain) Cermeño *et al.* (2006) calculated that respiration accounted for 86% of gross production during winter, 31% during summer and 15% during the upwelling season (when production is highest). In Carlingford Lough, respiration accounted for on average 83% of the gross daily column production. In particular, the Lough exhibited episodes during which gross production exceeded respiration (usually during blooms; Figure 6.13) therefore there was a net production of organic carbon that would be exported to the sea or up the foodweb. However, these episodes were not cyclical as suggested by the inability of the TFS to fit the observations of net production, and in general the microplankton population consumed the organic carbon produced. In fact the median annual microplankton community respiration ($117 \text{ gC m}^{-2} \text{ y}^{-1}$) derived from TFS and the relationship with salinity (Table 6.10), was equivalent to the median value ($116 \text{ gC m}^{-2} \text{ y}^{-1}$) of annual gross column production (Table 6.8). It follows then that on an annual balance, Carlingford Lough was a heterotrophic system.

Combining the confidence interval of microplankton community respiration and gross production, and subtracting the lowest respiration to the highest production, a maximum net microplankton production of $36 \text{ gC m}^{-2} \text{ y}^{-1}$ could be obtained. This estimate is approximately 9-fold lower than the estimate of net production of $312.4 \text{ gC m}^{-2} \text{ y}^{-1}$ derived for Carlingford Lough by Douglas (1992) for the year 1991. Douglas (1992) measured primary production in the Lough using the light and dark bottle oxygen method with 24 hours *in situ* incubations. His estimates (Figure 6.23) of daily net column production seem remarkably high. Assuming that they are estimates of net production, then gross annual production would be similar to that in Tokyo Bay ($370\text{-}580 \text{ mgC m}^{-2}$) and Ría de Vigo (520 mgC m^{-2}), the highest values listed in Table 6.11. An explanation of such high values could be the different methods used for measuring production, and/or the different location of the sampling stations (e.g. closer to the city of Warrenpoint). However, nutrient concentrations measured by Douglas (see Chapter 2, Table 2.2) were similar to concentrations

measured in the Lough during this research project. It is not clear what caused the difference in estimates, but, as already discussed, the values of production derived during this study in 2006-2008 are in the range of values derived for other Northern Irish sea loughs and Scottish sea lochs and also for the adjacent Irish Sea coastal waters.

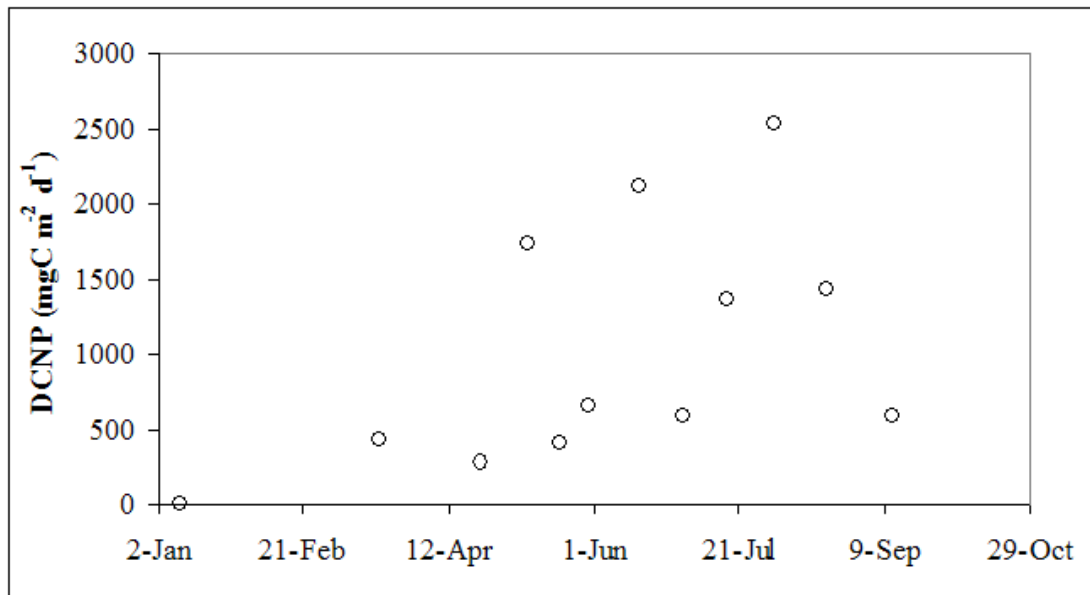


Figure 6.23. Temporal variability of estimates of daily column net production (DCNP) in $\text{mgC m}^{-2} \text{d}^{-1}$, derived by Douglas (1992) in Carlingford Lough during 1991, using the light and dark bottle oxygen method.

The conclusion that Carlingford Lough was a heterotrophic system is supported by the hypothesis of Cloern (1987) that the water column of turbid estuaries (e.g. K_d between 1 and 10 m^{-1}) could be a sink of production (net production < 0). Cloern justified this observation as the effect of light limitation on phytoplankton growth, occurring when the depth of the photic zone was $< 20\%$ of the mixing depth. Observations from the Douro Estuary (Azevedo, Duarte and Bordalo 2006) and the Gironde (France; Goosen *et al.* 1999) are in agreement with Cloern's (1987) hypothesis. In fact, these two heterotrophic estuaries were light limited (e.g. in the Douro estuary the depth of the photic zone was only 23% of the mixing depth).

However, station CLNBuoy in Carlingford Lough only exhibited light limited conditions for phytoplankton growth during winter (as previously discussed in section 6.4.2).

Heip *et al.* (1995) analysed estimates of production and respiration from various temperate estuarine and coastal systems and showed that when annual gross production was less than $160 \text{ gC m}^{-2} \text{ y}^{-1}$ the system was heterotrophic (net production < 0) due to phytoplankton population being light limited. Gross annual production in Carlingford Lough was less than $160 \text{ gC m}^{-2} \text{ y}^{-1}$ but, as argued above, the data show that the phytoplankton in the Lough was not light limited during spring and summer. The types of heterotrophic systems described by Cloern (1987) and Heip *et al.* (1995) were generally enriched in nutrients but phytoplankton was not able to use these nutrients due to high turbidity of the water that results in high attenuation and light limitation of growth. This observation is important in the context of eutrophication. In fact, it implies that nutrient enrichment of a coastal water body does not necessarily lead to an increase in phytoplankton biomass and production, if other factors, such as light availability, are limiting phytoplankton growth. Water bodies such as Carlingford Lough (in which the light climate does not constrain phytoplankton growth) could therefore be more sensitive to changes in nutrient loading (see also Cloern 1999 and Devlin *et al.* 2008).

6.5 Conclusions

- Single daily values of chlorophyll concentration, K_d and photosynthetic parameters were used to derive daily column production for a given sampling event. However, sampling of biological, physical, and chemical variables, and repeated primary production experiments during a tidal cycle, would have provided useful information on the importance of short-term variability on estimates of primary production;
- the TFS described the seasonal cycle of production and the creation of 100 synthetic datasets (including the relationships with deviations of environmental variables) provided information on the variability of the estimates of annual production (in the form of a confidence interval);
- the estimates of gross daily column production derived using the photosynthesis/irradiance models were very similar (except for Blackman model);
- the seasonal trend in gross production in Carlingford Lough showed 2 main peaks (one in spring and one at the end of the summer), and was similar to other temperate estuaries. Annual estimate of production ($116 \text{ gC m}^{-2} \text{ y}^{-1}$ with confidence interval $98\text{-}141 \text{ gC m}^{-2} \text{ y}^{-1}$) was x9 lower than an earlier estimate of annual net production but comparable to estimates of production derived for Scottish sea lochs, temperate estuaries and the Irish Sea;
- the relationship between gross daily column production and chlorophyll standing stock explained 71% of the variability in production and confirmed the first testable hypothesis presented in Chapter 1. Chlorophyll standing stock, irradiance during the sampling and K_d accounted for 89% of the variability in production; while the contribution of the photosynthetic parameter was small (7.2%);
- annual microplankton community respiration ($117 \text{ gC m}^{-2} \text{ y}^{-1}$ with confidence interval $105\text{-}134 \text{ gC m}^{-2} \text{ y}^{-1}$) was positively related to temperature and phytoplankton production, abundance and biomass, and negatively to nutrients concentration and chlorophyll. Annual MCR was comparable to gross annual production. This suggests that annual net microplankton production for Carlingford Lough was approximately zero and the Lough was a heterotrophic system.

CHAPTER 7

General conclusions

7.1 General conclusions and further considerations

The aim of this study was to develop a simple and robust methodology for the routine estimation of primary production in coastal water bodies, such as the sea loughs of Northern Ireland. Primary production estimates are a key element in assessing the trophic status of a water body as well as in defining its carrying capacity. The traditional methods for deriving production, although sensitive and reliable, are time consuming and not suitable as part of a routine monitoring programme. To achieve the aim of this study, high frequency sampling was carried out for two years (April 2006 to March 2008) in Carlingford Lough at station CLNBuoy to characterise the main environmental properties of the Lough (e.g. temperature and nutrients), and derive estimates of phytoplankton photosynthetic parameters from which daily and annual primary production were estimated. Two hypotheses were also tested during this study: 1. Chlorophyll standing stock explains 70% of the variability in primary production for Carlingford Lough 2. Temperature, nutrient concentrations, light availability and phytoplankton community structure are significantly correlated with the photosynthetic parameters of phytoplankton in Carlingford Lough.

From the observations and analysis carried out during this study, it appeared that the run off from the River Clanrye strongly influenced the physical, chemical and biological characteristics of Carlingford Lough at the sampling station CLNBuoy. Fresh water run off was important in the formation of vertical salinity gradients and stratification of the water column. The river was the main source of nutrients for the inner and mid Lough and, with the introduction of riverine suspended particulate material into the Lough, influenced the light extinction coefficient and therefore light availability down the water column.

The flushing rate of 8-26 days provided favourable conditions for the accumulation of phytoplankton biomass resulting from *in situ* growth, when the nutrient and light regimes were suitable. Phytoplankton biomass showed the typical seasonal cycle observed in temperate coastal waters with two peaks, one in spring (March-April) and one at the end of summer (end of August-September). Microalgal growth was limited by light availability during winter, while silicate (diatoms) and nitrogen were considered to be the nutrients that were potentially limiting for phytoplankton growth during spring and summer respectively. The sub-surface light

climate was the main factor controlling the beginning of the spring bloom. High nutrient concentrations and the intermittent mixed and stratified conditions in the Lough favoured the growth of diatoms and species of diatom dominated the phytoplankton during the year.

The estimates of photosynthetic parameters derived from the ^{14}C incubations showed seasonal variability and significant relationships with environmental variables and therefore support the second hypothesis. α^{B} showed a peak between March and May, a decrease during summer and another small peak at the start of the autumn (Figure 5.15). Minimum values of $\text{P}_{\text{max}}^{\text{B}}$ were recorded in winter with a maximum in spring (April/May), followed by a decrease in summer (June/July) and another maximum in late summer (August/September; Figure 5.16). Ammonium and phosphate explained part of the variability in $\text{P}_{\text{max}}^{\text{B}}$ and α^{B} respectively (36.8% and 3% respectively); the incubation temperature was positively related to $\text{P}_{\text{max}}^{\text{B}}$, but only if the summer 2006 estimates were not included in the analysis. Phaeopigments/chlorophyll ratio was a predictor of the variability in α^{B} . The photosynthetic parameters were also negatively correlated with the average chlorophyll content of phytoplankton cells.

Estimates of photosynthetic parameters, E_0 , K_d , and chlorophyll concentration were assumed to be constant during a given day (see section 6.5.1) and single daily values were used to derive gross daily column production. As discussed in section 6.5.1, it would be useful to carry out multiple sampling of biological, chemical and physical variables during a tidal cycle and to undertake repeated short-term (2 hour) primary production experiments over 24 hours, to provide information on daily variability of environmental variables and photosynthetic parameters. The aim would be to determine the importance of short-term variability in these variables on estimates of daily and annual production. A study of the underwater light field during a tidal cycle would also give some more insight on the daily variability of the vertical attenuation coefficient and on how its vertical profile would vary during the phases of the tide and how such variability might affect estimates of daily production.

The range of estimates of daily gross column production of Calingford Lough ($3.2 - 1210 \text{ mgC m}^{-2} \text{ d}^{-1}$, Jassby and Platt model, Table 6.3) was comparable to the ranges derived for other temperate estuaries and coastal areas such as the Westerschelde in the Netherlands (Goosen *et al.* 1999), the coastline of the North Frisian Wadden Sea (Tillmann, Hesse and Coljin 2000), the Douro Estuary in

Portugal (Azevedo, Duarte and Bordalo 2006), and the Baie de Veys in France (Jouenne *et al.* 2007).) Chlorophyll standing stock explained 71% of the variability in phytoplankton daily production (see Equation 6.18) and provides support for the first testable hypothesis that: chlorophyll standing stock can explain $\approx 70\%$ of the variability in primary production in Carlingford Lough. The amount of variability explained increased to 89% when irradiance during the sampling and K_d were included in the relationship as predictors.

The application of the truncated Fourier series (TFS) to daily estimates of production generated an estimate of annual production of $116 \text{ gC m}^{-2} \text{ y}^{-1}$ with 90% confidence interval of 98-141 $\text{gC m}^{-2} \text{ y}^{-1}$. Annual microplankton community respiration was estimated to be in the same range ($117 \text{ gC m}^{-2} \text{ y}^{-1}$ with 90% confidence interval of 105-134 $\text{gC m}^{-2} \text{ y}^{-1}$). The range of estimates of annual gross production of Carlingford Lough was comparable with estimates of production for different regions of the Irish Sea (Gowen and Bloomfield 1996; Gowen *et al.* 2000), except Irish coastal waters of Ireland (Gowen and Bloomfield 1996) and Liverpool Bay (Gowen *et al.* 2000) which supported higher production than Carlingford Lough (Figure 6.22 and Table 6.11). This observation was in agreement with Cloern's (1987) hypothesis that estuaries are less productive than the adjacent coastal water. Cloern (1987) justified this hypothesis by suggesting that phytoplankton production in estuaries is light limited. However, phytoplankton growth at station CLNBuoy was not constrained by light (except during winter) and instead it is possible that phytoplankton growth in Carlingford Lough was nutrient limited during spring and summer.

Within the Lough there were periods of net production (usually during blooms; Figure 6.13) and organic carbon would be exported to the sea or up the foodweb. However, these episodes were not cyclical as suggested by the inability of the TFS to fit the observations of net production. In general, microplankton respiration exceeded the amount of organic carbon produced and on an annual balance Carlingford Lough was a heterotrophic system. This conclusion supports the hypothesis of Cloern (1987) that the water column of turbid estuaries could be a sink of production (net production < 0). However, the assessment of Carlingford Lough being on average heterotrophic was based on measurements at one station in the Lough. It has been observed that in some estuaries (e.g. Bristol Channel; Joint and Pomroy 1981) primary production increased towards the mouth of the estuary, due to

clearer water, while in others (e.g. Falkowski estuary; Azevedo, Duarte and Bordalo 2006) production was higher in the inner part of the estuary. It would be important to quantify the spatial variability in primary production and MCR for Carlingford Lough to derive a better estimate of annual production.

This study confirmed that environmental variables, such as chlorophyll standing stock and irradiance, can be used as a proxy for deriving production in a Northern Ireland sea lough. Chlorophyll concentration, for example, can be measured automatically (e.g. on instrumented moorings) therefore providing high frequency estimates of production. The number of observations could be further improved and increased by using the TFS analysis. The analysis with the TFS was used to create 100 synthetic data sets and provided statistical support for the existence of a seasonal cycle in the lough. The most important aspect of using the TFS and generation of the synthetic data sets was quantification of the error (confidence interval) associated with the estimate of annual production. The 90% confidence interval not only provided information on the range of variability in annual production but could also be used as a reference baseline against which future change could be assessed.

As an example of the applicability of the models, annual primary production of Belfast Lough was estimated in the following way: 1. chlorophyll standing stock was calculated from measurements of chlorophyll concentration at different depths down the water column; 2. estimates of daily gross production were derived using the relationship with chlorophyll standing stock; 3. the daily estimates derived were inputted into the model implementing the TFS to estimate annual production.

Step 1. Chlorophyll data were derived from 2 stations (Pylon 8 and 9) located in the mid part of Belfast Lough. Station Pylon 8 was sampled from January 2006 until June 2007, while station Pylon 9 from July 2007 until November 2008 (approximately monthly frequency at both). The two stations were positioned a short distance apart therefore no differences in physical, chemical and biological variables were expected between the two sites. Chlorophyll concentration was mainly derived from subsurface samples (1 m depth) therefore chlorophyll standing stock was calculated by multiplying the subsurface value by the average depth of the water column (7.2 m). Figure 7.1 shows the seasonal trend in the estimates of chlorophyll standing stock.

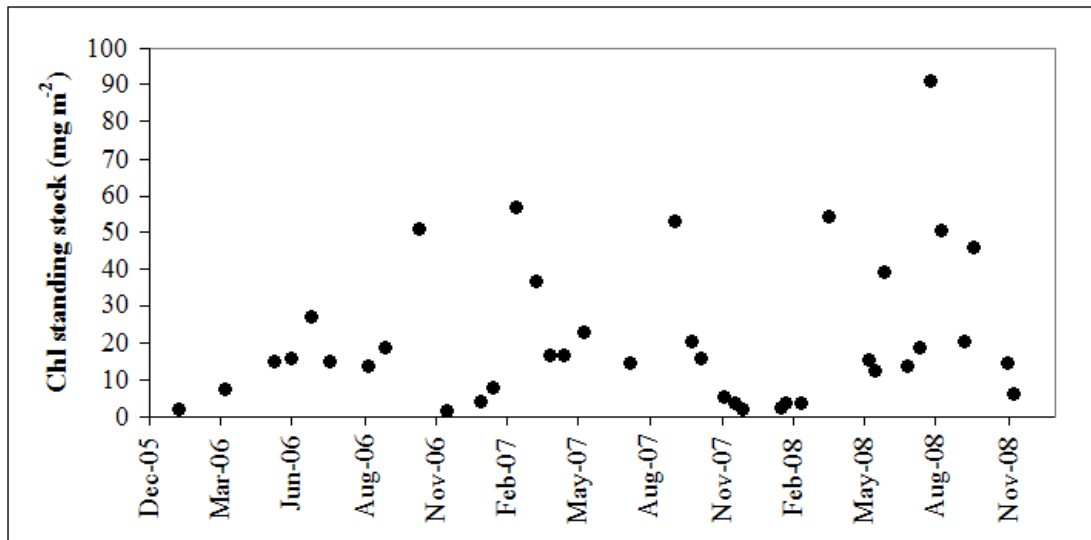


Figure 7.1. Seasonal trend in chlorophyll standing stock (mg m^{-2}) for the stations Pylon 8 and 9 in Belfast Lough from January 2006 until November 2008.

Step 2. Gross daily column production (GDCP) was derived from the estimates of chlorophyll standing stock using Equation 6.18 (see Chapter 6). GDCP varied between 6 and 2204 $\text{mgC m}^{-2} \text{d}^{-1}$, with an average of 329.5 $\text{mgC m}^{-2} \text{d}^{-1}$ (standard deviation 450 $\text{mgC m}^{-2} \text{d}^{-1}$ and median 160 $\text{mgC m}^{-2} \text{d}^{-1}$). The seasonal trend in gross daily column production is given in Figure 7.2.

Step 3. The TFS was applied to the estimates of daily column production. Two waves explained 61% of the variability in production (Figure 7.3) which showed two peaks, one in April and a larger one in September/October. The annual production was estimated as 102 $\text{gC m}^{-2} \text{y}^{-1}$ with confidence interval at 74 and 169 $\text{gC m}^{-2} \text{y}^{-1}$. The estimates of daily production for the 100 synthetic data sets are plotted in Figure 7.4.

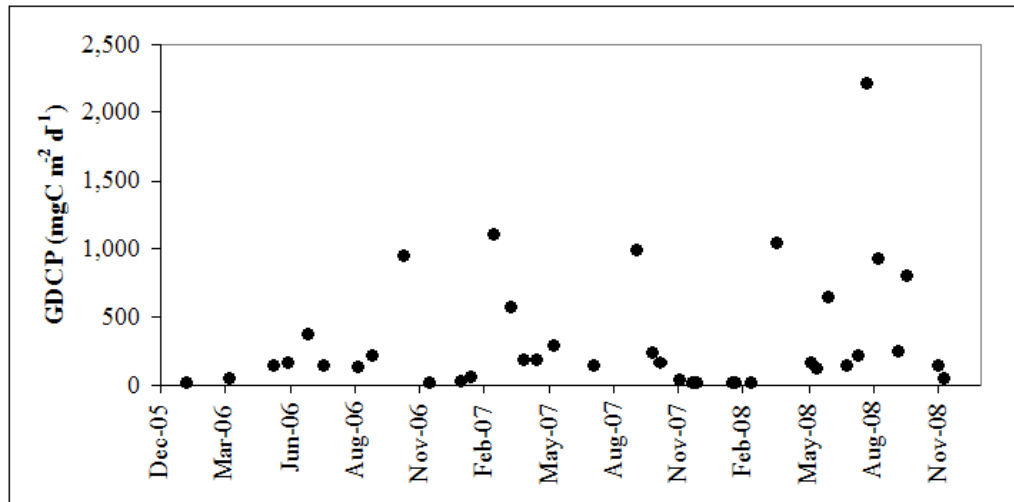


Figure 7.2. Seasonal trend in gross daily column production, GDCCP ($\text{mgC m}^{-2} \text{d}^{-1}$) at stations Pylon 8 and 9 in Belfast Lough from January 2006 until November 2008.

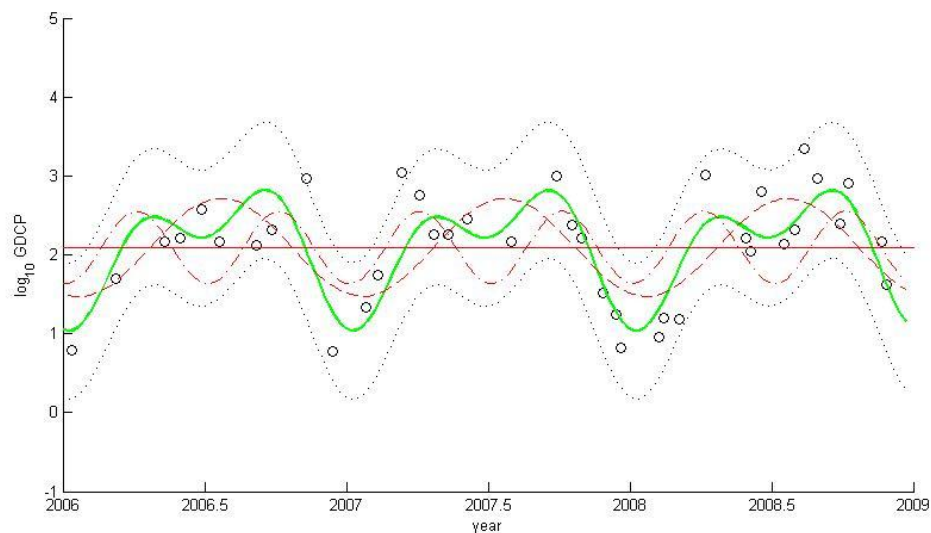


Figure 7.3. A plot of 2 paired sine-cosine waves fitted to log-transformed daily gross column production estimates ($\text{mg C m}^{-2} \text{d}^{-1}$) from January 2006 to November 2008. The waves with frequencies of 1 y^{-1} (wave1) and 2 y^{-1} (wave2) are coloured pink, while their sum (superposition) or TFS is coloured green. The pink straight line is the mean value around which the function is oscillating. The 90% confidence interval is indicated by the dark dotted lines, while the black empty circles represent the observations. In this plot, the TFS explained 61% of the variability of the observations.

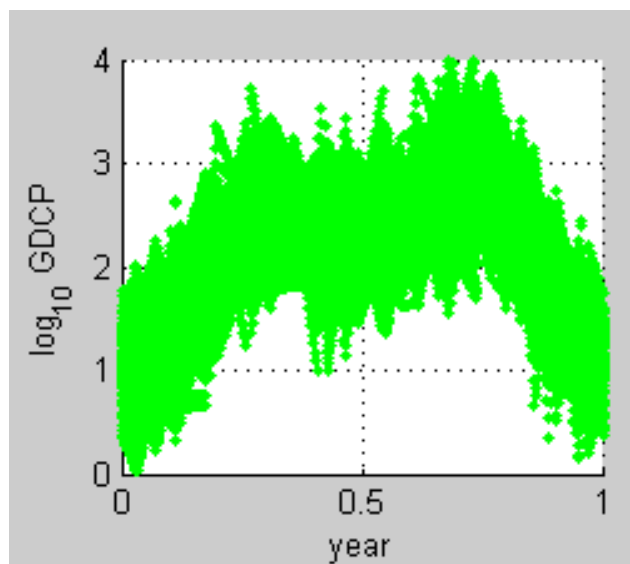


Figure 7.4. Log-transformed synthetic estimates of gross daily column production (\log_{10} GDCP) plotted together for a standard year (100 synthetic data sets). Each synthetic data set was created using the TFS (derived by fitting the observed estimates of production with paired sine-cosine waves), summed to the mean value of the TFS, plus the error.

The observation of two peaks in production is in agreement with the results of the study by Parker, Rosell and MacOscar (1988) on the production cycle in mid Belfast Lough. The only estimates of production available for Belfast Lough were derived from the study by Parker, Rosell and MacOscar (1988). It has already been shown (section 6.4.2) that the highest production rate measured in Carlingford Lough ($77 \text{ mgC m}^{-3} \text{ h}^{-1}$ in October 2007, Jassby and Platt model) was between rates of $\approx 50 \text{ mgC m}^{-3} \text{ h}^{-1}$ (end of May 1984) and $126 \text{ mgC m}^{-3} \text{ h}^{-1}$ (July 1984) derived for the mid and inner regions of Belfast Lough. Therefore the similarity between annual production estimates of mid Belfast Lough and mid Carlingford Lough seemed reasonable. Unfortunately it is not possible to turn the hourly estimates of production determined by Parker, Rosell and MacOscar (1988) into a figure for annual production to provide a direct comparison. The wider range of variability of the estimate of annual production derived for mid Belfast Lough compared to the estimate for Carlingford Lough could be related to the smaller number of observations available for Belfast Lough. Furthermore, it is also important to

remember that the observations for Belfast Lough were collected with a monthly frequency and, as argued in section 2.4.2, this frequency may not be sufficient to characterise short term variability of phytoplankton production especially during the spring bloom.

The column chlorophyll/production relationship has been verified for a variety of water bodies and a preliminary test using Belfast Lough data suggests that it can be used in other Northern Ireland sea loughs. However, it would be necessary to run some primary production experiments in the other sea loughs to test and validate the model. The TFS model also appears to be a useful method of estimating annual production and quantifying the associated error to provide confidence intervals that could be used to assess long-term change. To confirm the value of the TFS modelling approach it would be necessary to apply the TFS to existing production (measured or derived from chlorophyll standing stock) data sets from other water bodies (e.g. the Irish Sea and Scottish sea lochs) to develop a general tool for estimating the annual production in estuarine and coastal waters.

REFERENCES

- AFBI (2010). AFBI - Agri-Food and Biosciences Institute: Carlingford Lough. Available from: <http://www.afbini.gov.uk/index/services/services-specialist-advice/coastal-science/coastal-monitoring/monitored-sites/carlingford-lough-north.htm> [accessed 22 June 2010].
- Aguirre-Hernández, E., Gaxiola-Castro, G., Nájera-Martínez, S., Baumgartner, T., Kahru, M. and Mitchell, B.G. (2004). Phytoplankton absorption, photosynthetic parameters, and primary production off Baja California: summer and autumn 1998. Deep-Sea Research II **51**, pp. 799-816.
- Alpine, A.E. and Cloern, J.E. (1992). Trophic interactions and direct physical effects control phytoplankton biomass and production in a estuary. Limnology and Oceanography **37** (5), pp. 946-955.
- Andersen, J.H., Schlüter, L. and Ærtebjerg, G. (2006). Coastal eutrophication: recent developments in definitions and implications for monitoring strategies. Journal of Plankton Research **28** (7), pp. 621-628.
- Azevedo, I.C., Duarte, P.M. and Bordalo, A.A. (2006). Pelagic metabolism of the Falkowski estuary (Portugal) – Factors controlling primary production. Estuarine, Coastal and Shelf Science **69**, pp. 133-146.
- Babin, M., Morel, A. and Gagnon, R. (1994). An incubator designed for extensive and sensitive measurements of phytoplankton photosynthetic parameters, Limnology and Oceanography **39** (3), pp. 694-702.
- Ball, B., Raine, R. and Douglas, D. (1997). Phytoplankton and particulate matter in Carlingford Lough, Ireland: an assessment of food availability and the impact of bivalve culture. Estuaries **20** (2), pp. 430-440.
- Bambridge/Newry and Mourne Area Plan 2015 (2010). The planning service. Available from: http://www.planningni.gov.uk/index/policy/dev_plans/devplans_az/bnm_2015/bnm_district_proposals/bnm_proposals_newry/bnm_newry_city/bnm_newrycity_background.htm [accessed 27 June 2010].
- Barber, R.T. and Hilting, A.K. (2002). History of the study of plankton productivity. **In:** Williams, P.J.leB., Thomas, D.N. and Reynolds, C.S. (eds) (2002) Phytoplankton productivity. Carbon assimilation in marine and freshwater ecosystems. Oxford: Blackwell Science, pp. 16-43.
- Barnes, H. (1952). The use of transformations in marine biological statistics. Journal Conseil International pour l'Exploration de la Mer **18**, pp. 61-71.

- Bates, S.S. (1976). Effects of light and ammonium on nitrate uptake by two species of estuarine phytoplankton. Limnology and Oceanography **21** (2), pp. 212-218.
- Beardall, J. and Raven, J.A. (2004). The potential effects of global climate change on microalgal photosynthesis, growth and ecology. Phycologia **43** (1), pp. 26-40.
- Beardall, J., Ihnken, S. and Quigg, A. (2009). Gross and net primary production: closing the gap between concepts and measurements. Aquatic Microbial Ecology **56**, pp. 113-122.
- Behrenfeld, M.J. and Falkowski, P.G. (1997). A consumer's guide to phytoplankton primary productivity models. Limnology and Oceanography **42** (7), pp. 1479-1491.
- Behrenfeld, M.J., Esaias, W.E. and Turpie, K.R. (2002). Assessment of primary production at the global scale. **In:** Williams, P.J.leB., Thomas, D.N. and Reynolds, C.S. (eds) (2002) Phytoplankton productivity. Carbon assimilation in marine and freshwater ecosystems. Oxford: Blackwell Science, pp.156-186.
- Behrenfeld, M.J., Marañón, E., Siegel, D.A. and Hooker, S.B. (2002). Photoacclimation and nutrient-based model of light-saturated photosynthesis for quantifying oceanic primary production. Marine Ecology Progress Series **228**, pp. 103-117.
- Behrenfeld, M.J., Prasil, O., Babin, M. and Bruyant, F. (2004). In search of a physiological basis for covariations in light-limited and light-saturated photosynthesis. Journal of Phycology **40**, pp. 4-25.
- Behrenfeld, M.J., Randerson, J.T., McClain, C.R., Feldman, G.C., Los, S.O., Tucker, C.J., Falkowski, P.G., Field, C.B., Frouin, R., Esaias, W.E., Kolber, D.D. and Pollack, N.H. (2001). Biospheric primary production during an ENSO transition. Science **291**, pp. 2594-2597.
- Bender, M., Grande, K., Johnson K., Marra, J., Williams, P.J.leB., Sieburth, J., Pilson, M., Langdon, C., Hitchcock, G., Orchardo, J., Hunt, C., Donaghay, P. and Heinemann, K. (1987). A comparison of four methods for determining planktonic community production. Limnology and Oceanography **32** (5), pp. 1085-1098.
- Blackman, F.F. (1905). Optima and limiting factors. Annals of Botany **19**, pp. 281-295.

- Boney, A.D. 1986. Seasonal studies on the phytoplankton and primary production in the inner Firth of Clyde. Proceedings of the Royal Society of Edinburgh **90B**, pp. 203-222.
- Borkman, D.G. and Smayda, T. (2009). Multidecadal (1959-1997) changes in *Skeletonema* abundance and seasonal bloom patterns in Narragansett Bay, Rhode Island, USA. Journal of Sea Research **61**, pp. 84-94.
- Bot, P.V.M. and Colijn, F. (1996). A method for estimating primary production from chlorophyll concentrations with results showing trends in the Irish Sea and the Dutch coastal zone. ICES Journal of Marine Science **53**, pp. 945-950.
- Bouman, H.A., Nakane, T., Oka, K., Nakata, K., Kurita, K., Sathyendranath, S. and Platt, T. (2010). Environmental controls on phytoplankton production in coastal ecosystems: A case study from Tokyo Bay. Estuarine, Coastal and Shelf Science **87**, pp. 63-72.
- Bowers, D.G. and Mitchelson-Jacob, E.G. (1996). Inherent optical properties of the Irish Sea determined from underwater irradiance measurements. Estuarine, Coastal and Shelf Science **43**, pp. 433-447.
- Bran and Luebbe (1991a). TRAACS 800 Method No. 427 – 91E Bran and Luebbe (GB). Brixworth, Northamptonshire (UK).
- Bran and Luebbe (1991b). TRAACS 800 Method No. 428 – 91E Bran and Luebbe (GB). Brixworth, Northamptonshire (UK).
- Bran and Luebbe (1991c). TRAACS 800 Method No. 429 – 91E Bran and Luebbe (GB). Brixworth, Northamptonshire (UK).
- Bran and Luebbe (1991d). TRAACS 800 Method No. 430 – 91E Bran and Luebbe (GB). Brixworth, Northamptonshire (UK).
- Bran and Luebbe (1992). TRAACS 800 Method No. 431 – 91E Revision A Bran and Luebbe (GB). Brixworth, Northamptonshire (UK).
- Branco, A.B. and Kremer, J.N. (2005). The relative importance of chlorophyll and coloured dissolved organic matter (CDOM) to the prediction of the diffuse attenuation coefficient in shallow estuaries. Estuaries **28** (5), pp. 643-652.
- Brown, P.C. (1982). Phytoplankton production measured *in situ* and under simulated *in situ* conditions in the Southern Benguela upwelling region. Fisheries Bulletin (South Africa) **16**, pp. 31-37.

- Brzezinski, M.A. (1985). The Si:C:N ratio of marine diatoms: interspecific variability and the effect of some environmental variables. Journal of Phycology **21**, pp. 347-357.
- Burk, D. and Lineweaver, H. (1935). The kinetic mechanism of photosynthesis. Cold Spring Harbor Symposia on Quantitative Biology **3**, pp. 165-183.
- Cadée, G.C. (1983). Dark fixation. **In:** Colijn, F., Gieskes, W.W.C. and Zevenboom, W. (eds) (1983) The measurement of primary production: problems and recommendation. Hydrobiological Bulletin **17** (1), pp. 39-40.
- Cadée, G.C. and Hegeman, J. (1991). Phytoplankton primary production, chlorophyll and species composition, organic carbon and turbidity in the Marsdiep in 1990, compared with foregoing years. Hydrobiological Bulletin **25** (1), pp. 29-35.
- Carlingford Lough (2010). Wikipedia the free encyclopedia. Available from: www.en.wikipedia.org/wiki/Carlingford_Lough [accessed 27 June 2010].
- Cermeño, P., Marañón, E., Pérez, V., Serret, P., Fernández, E. and Castro, C.G. (2006). Phytoplankton size structure and primary production in a highly dynamic coastal ecosystem (Ría de Vigo, NW-Spain): Seasonal and short-time scale variability. Estuarine, Coastal and Shelf Science **67**, pp. 251-266.
- Christian, D. and Sheng, Y.P. (2003). Relative influence of various water quality parameters on light attenuation in Indian River Lagoon. Estuarine, Coastal and Shelf Science **57**, pp. 961-971.
- Cloern, J.E. (1987). Turbidity as a control on phytoplankton biomass and productivity in estuaries. Continental Shelf Research **7** (11/12), pp. 1367-1381.
- Cloern, J.E. (1991). Annual variations in river flow and primary production in the South San Francisco Bay Estuary (USA). **In:** M. Elliott and J.-P. Ducrotoy (eds) (1991). Estuaries and coasts: spatial and temporal intercomparisons. ECSA19 Symposium. Olsen and Olsen, pp. 91-96.
- Cloern, J.E. (1999). The relative importance of light and nutrient limitation of phytoplankton growth: a simple index of coastal ecosystem sensitivity to nutrient enrichment. Aquatic Ecology **33**, pp. 3-16.
- Cole, B.E. and Cloern, J.E. (1987). An empirical model for estimating phytoplankton productivity in estuaries. Marine Ecology – Progress Series **36**, pp. 299-305.

- Colijn, F., Cadée, G.C. and Hegeman, J. (1983). Comparison between a laboratory technique and measurements *in situ*. Measurements of marine phytoplankton. **In:** Colijn, F., Gieskes, W.W.C. and Zevenboom, W. (eds) (1983) The measurement of primary production: problems and recommendation. Hydrobiological Bulletin **17** (1), pp. 29-51.
- Costanza, R. (1992). Towards an operational definition of health. **In** Costanza, R., Norton, B. and Haskell, B.D. (Eds.), Ecosystem Health – New goals for environmental management. Inland Press, Washington, DC, pp. 239-256.
- Côté, B. and Platt, T. (1983). Day-to-day variations in the spring-summer photosynthetic parameters of coastal marine phytoplankton. Limnology and Oceanography **28** (2), pp. 320-344.
- DARDNI (2010). Aquaculture Background Information. Available from: www.dardni.gov.uk/index/fisheriesfarmingandfood/fisheries/aquaculture/aqua-info.htm [accessed 22 June 2010].
- Devlin, M.J., Barry, J., Mills, D.K., Gowen, R.J., Foden, J., Sivyer, D. and Tett, P. (2008). Relationships between suspended particulate material, light attenuation and Secchi depth in UK marine waters. Estuarine, Coastal and Shelf Science **79**, pp. 429-439.
- Devlin, M.J., Barry, J., Mills, D.K., Gowen, R.J., Foden, J., Sivyer, D., Greenwood, N., Pearce, D. and Tett, P. (2009). Estimating the diffuse attenuation coefficient from optically active constituents in UK marine waters. Estuarine, Coastal and Shelf Science **82**, pp. 73-83.
- Douglas, D.J. (1992). Environment and mariculture. (A study of Carlingford Lough). Dundalk, Co. Louth: Dundalgan Press (W. Tempest) Ltd, pp. 263.
- Duarte, C.M. (2009). Coastal eutrophication research: a new awareness. Hydrobiologia **629**, pp. 263-269.
- Dugdale, R.C., Wilkerson, F.P., Hogue, V.E. and Marchi, A. (2007). The role of ammonium and nitrate in spring bloom development in San Francisco Bay. Estuarine, Coastal and Shelf Science **73**, pp. 17-29.
- Edler, L. (1979). Recommendations for marine biological studies in the Baltic Sea. Phytoplankton and chlorophyll. Baltic Marine Biologists.
- Falkowski, P.G. (1981). Light-shade adaptation and assimilation numbers. Journal of Plankton Research **3** (2), pp. 203-216.

- Falkowski, P.G. and Raven, J.A. (1997). Aquatic photosynthesis. Oxford: Blackwell Science, pp. 484.
- Falkowski, P.G., Barber, R.T. and Smetacek, V. (1998). Biogeochemical controls and feedbacks on ocean primary production. Science **281**, pp. 200-206.
- Falkowski, P.G., Katz, M.E., Knoll, A.H., Quigg, A., Raven, J.A., Schofield, O. and Taylor, F.J.R. (2004). The evolution of modern eukaryotic phytoplankton. Science **305**, pp. 354-360.
- Fernandes, T.F., Eleftheriou, A., Ackefors, H., Eleftheriou, M., Ervik, A., Sanchez-Mata, A., Scanlon, T., White, P., Cochrane, S., Pearson, T.H. and Read, P.A. (2001). The scientific principles underlying the monitoring of the environmental impacts of aquaculture. Journal of Applied Ichthyology **17**, pp. 181-193.
- Ferreira, J.G., Duarte, P. and Ball, B. (1998). Trophic status of Carlingford Lough for oyster culture – analysis by ecological modelling. Aquatic Ecology **31**, pp. 361-378.
- Ferreira, J.G., Hawkins, A.J.S., Monteiro, P., Moore, H., Service, M., Pascoe, P.L., Ramos, L. and Sequeira, A. (2008). Integrated assessment of ecosystem-scale carrying capacity in shellfish growing areas. Aquaculture **275**, pp. 138-151.
- Ferreira, J.G., Hawkins, A.J.S., Monteiro, P., Service, M., Moore, H., Edwards, A., Gowen, R., Lourenco, P., Mellor, A., Nunes, J.P., Pascoe, P.L., Ramos, L., Sequeira, A., Simas, T., Strong, J. (2007). SMILE – Sustainable Mariculture in northern Irish Lough Ecosystems – Assessment of carrying capacity for environmentally sustainable shellfish culture in Carlingford Lough, Strangford Lough, Belfast Lough, Larne Lough and Lough Foyle. Ed. IMAR – Institute of Marine Research, pp. 100.
- Field, C.B., Behrenfeld, M.J., Randerson, J.T. and Falkowski, P. (1998). Primary production of the biosphere: integrating terrestrial and oceanic components. Science **281**, pp. 237-240.
- Foden, J., Sivyer, D.B., Mills, D.K. and Devlin, M.J. (2008). Spatial and temporal distribution of chromophoric dissolved organic matter (CDOM) fluorescence and its contribution to light attenuation in UK waterbodies. Estuarine, Coastal and Shelf Science **79**, pp. 707-717.
- Fogg, G.E. (1977). Excretion of organic matter by phytoplankton. Limnology and Oceanography **22**, pp. 576-577.

- Fourqurean, J.W., Webb, K.L., Hollibaugh, J.T. and Smith, S.V. (1997). Contribution of the plankton community ecosystem respiration, Tomales Bay, California. Estuarine, Coastal and Shelf Science **44**, pp. 493-505.
- Frenette, J.-J., Demers, S., Legendre, L. and Dodson, J. (1993). Lack of agreement among models for estimating the photosynthetic parameters. Limnology and Oceanography **38** (3), pp. 679-687.
- Gaarder, T. and Gran, H.H. (1927). Investigations of the production of plankton in the Oslo Fjord. Rapports et Proces-Verbaux, Conseil International pour l'Exploration de la Mer **42**, pp. 1-48.
- Gallegos, C.L. (2001). Calculating optical water quality targets to restore and protect submersed aquatic vegetation: overcoming problems in partitioning the diffuse attenuation coefficient for photosynthetically active radiation. Estuaries **24** (3), pp. 381-397.
- Gargas, E., Nielsen, C.S. and Lønholdt, J. (1976). An incubator method for estimating the actual daily planktonalgae primary production. Water Research **10**, pp. 853-860.
- Geider, R.J. and La Roche, J. (2002). Redfield revisited: variability of C:N:P in marine microalgae and its biochemical basis. European Journal of Phycology **37**, pp. 1-17.
- Geider, R.J. and MacIntyre, H.L. (2002). Physiology and biochemistry of photosynthesis and algal carbon acquisition. **In:** Williams, P.J.leB., Thomas, D.N. and Reynolds, C.S. (eds) (2002) Phytoplankton productivity. Carbon assimilation in marine and freshwater ecosystems. Oxford: Blackwell Science, pp. 44-77.
- Geider, R.J. and Osborne, B.A. (1989). Respiration and microalgal growth: a review of the quantitative relationship between dark respiration and growth. New Phytologist **112**, pp. 327-341.
- GESAMP (IMO/FAO/UNESCO-IOC/WMO/IAEA/UN/UNEP Joint Group of Experts on the Scientific Aspects of Marine Environmental Protection) 2001. Planning and management for sustainable coastal aquaculture development. Reports and studies GESAMP **68**, pp. 90.
- Gieskes, W.W.C., and Kraay, G.W. (1975). The phytoplankton spring bloom in Dutch coastal waters of the North Sea. Netherlands Journal of Sea Research **9** (2), pp. 166-196.

- Goosen, N.K., Kromkamp, J., Peene, J., van Rijswijk, P. and van Breugel, P. (1999). Bacterial and phytoplankton production in the maximum turbidity zone of three European estuaries: the Elbe, Westerschelde and Gironde. Journal of Marine Systems **22**, pp. 151-171.
- Gordon, H.R. (1989). Can the Lambert-Beer law be applied to the diffuse attenuation coefficient of ocean water? Limnology and Oceanography **34** (8), pp. 1389-1409.
- Gowen, R.J. and Bloomfield, S.P. (1996). Chlorophyll standing crop and phytoplankton production in the western Irish Sea during 1992 and 1993. Journal of Plankton Research **18** (9), pp. 1735-1751.
- Gowen, R.J., Mills, D.K., Trimmer, M. and Nedwell, D.B. (2000). Production and its fate in two coastal regions of the Irish Sea: the influence of anthropogenic nutrients. Marine Ecology Progress Series **208**, pp. 51-64.
- Gowen, R.J., Stewart, B.M., Mills, D.K. and Elliott, P. (1995). Regional differences in stratification and its effect on phytoplankton production and biomass in the northwestern Irish Sea. Journal of Plankton Research **17** (4), pp. 753-769.
- Gowen, R.J., Tett, P. and Jones, K.J. (1992). Predicting marine eutrophication: the yield of chlorophyll from nitrogen in Scottish coastal waters. Marine Ecology Progress Series **85**, pp.153-161.
- Grande, K.D., Williams, P.J.leB., Marra, J., Purdie, D.A., Heinemann, K., Eppley, R.W. and Bender, M.L. (1989). Primary production in the North Pacific gyre: a comparison of rates determined by the ^{14}C , O_2 concentration and ^{18}O methods. Deep-Sea Research **36** (11), pp. 1621-1634.
- Grangeré, K., Lefebvre, S., Ménesguen, A. and Jouenne, F. (2009). On the interest of using field primary production data to calibrate phytoplankton rate processes in ecosystem models. Estuarine, Coastal and Shelf Science **81**, pp. 169-178.
- Han, B.-P., Virtanen, M., Koponen, J. and Straškraba, M. (2000). Effect of photoinhibition on algal photosynthesis: a dynamic model. Journal of Plankton Research **22** (5), pp. 865-885.
- Harding, L.W. Jr, Meeson, B.W. and Fisher, T.R. Jr (1986). Phytoplankton production in two east coast estuaries: photosynthesis-light functions and patterns of carbon assimilation in Chesapeake and Delaware bays. Estuarine, Coastal and Shelf Science **23**, pp. 773-806.

- Harding, L.W. Jr, Meeson, B.W., Prézelin, B.B. and Sweeney, B.M. (1981). Diel periodicity of photosynthesis in marine phytoplankton. Marine Biology **61**, pp. 95-105.
- Harding, L.W. Jr, Prézelin, B.B., Sweeney, B.M. and Cox, J.L. (1982). Primary production as influenced by diel periodicity of phytoplankton photosynthesis. Marine Biology **67**, pp. 179-186.
- Head, A. (1976). Primary production in an estuarine environment: a comparison of *in situ* and simulated *in situ* ^{14}C techniques. Estuarine, Coastal and Shelf Science **4**, pp. 575-578.
- Heath, R.A. (1973). Flushing of coastal embayments by changes in atmospheric conditions. Limnology and Oceanography **18**, pp. 849-862.
- Heip, C.H.R., Goosen, N.K., Herman, P.M.J., Kromkamp, J., Middelburg, J.J. and Soetaert, K. (1995). Production and consumption of biological particles in temperate tidal estuaries. In: Ansell, A.D., Gibson, R.N. and Barnes, M. Editors (1995). Oceanography and marine biology: an annual review **33**, pp. 1-149.
- Heral, M. (1993). Why carrying capacity models are useful tools for management of bivalve mollusc culture. In: Dame Springer-Verlag, R.F. Editor (1993). Bivalve filter feeders in estuarine and coastal ecosystem processes (NATO ASI series) **33**; pp. 455-477.
- Herman, A.W. and Platt, T. (1986). Primary production profiles in the ocean: estimation from a chlorophyll/light model. Oceanologica Acta **9** (1), pp. 31-40.
- Hillebrand, H., Dürselen, C.-D., Kirschtel, D., Pollinger, U. and Zohary, T. (1999). Biovolume calculation for pelagic and benthic microalgae. Journal of Phycology **35**, pp. 403-424.
- Hilton, J., Lishman, J.P., Mackness, S. and Heaney, S.I. (1986). An automated method for the analysis of particulate carbon and nitrogen in natural waters. Hydrobiologia **141**, pp. 269-271.
- Holmes, R.W. (1970). The Secchi disk in turbid coastal waters. Limnology and Oceanography **15**, pp. 688-694.
- Howarth, M.J., Dyer, K.R., Joint, I.R., Hydes, D.J., Purdie, D.A., Edmunds, H., Jones, J.E., Lowry, R.K., Moffat, T.J., Pomroy, A.J. and Proctor, R. (1993).

- Seasonal cycles and their spatial variability. Phylosophical Transactions of the Royal Society of London A **343**, pp. 383-403.
- IOCCG (2000). Remote sensing of ocean colour in coastal, and other optically-complex, waters. Sathyendranath, S. (Eds.). Reports of the International Ocean-Colour Coordinating Group, No 3, IOCCG, Dartmouth, Canada.
- Iriarte, A. and Purdie, D.A. (2004). Factors controlling the timing of major spring bloom events in an UK south coast estuary. Estuarine, Coastal and Shelf Science **61**, pp. 679-690.
- Iriarte, A., Daneri, G., Garcia, V.M.T., Purdie, D.A. and Crawford, D.W. (1991). Plankton community respiration and its relationship to chlorophyll *a* concentration in marine coastal waters. Oceanologica Acta **14** (4), pp. 379-388.
- Iriarte, A., de Madariaga, I., Diez-Garagarza, F., Revilla, M. and Orive, E. (1996). Primary plankton production, respiration and nitrification in a shallow temperate estuary during summer. Journal of Experimental Marine Biology and Ecology **208**, pp. 127-151.
- Jassby, A.D. and Platt, T. (1976). Mathematical formulation of the relationship between photosynthesis and light for phytoplankton. Limnology and Oceanography **21** (4), pp. 540-547.
- Joint, I.R. and Pomroy, A.J. (1981). Primary production in a turbid estuary. Estuarine, Coastal and Shelf Science **13**, pp. 303-316.
- Joint, I.R. and Pomroy, A.J. (1993). Phytoplankton biomass and production in the southern North Sea. Marine Ecology – Progress Series **99**, pp. 169-182.
- Jones, K.J. and Gowen, R.J. (1990). Influence of stratification and irradiance regime on summer phytoplankton composition in coastal and shelf seas of the British Isles. Estuarine, Coastal and Shelf Science **30**, pp. 557-567.
- Jouenne, F., Lefebvre, S., Véron, B. and Lagadeuc, Y. (2005). Biological and physicochemical factors controlling short-term variability in phytoplankton primary production and photosynthetic parameters in a macrotidal ecosystem (eastern English Channel). Estuarine, Coastal and Shelf Sciences **65**, pp. 421-439.
- Jouenne, F., Lefebvre, S., Véron, B. and Lagadeuc, Y. (2007). Phytoplankton community structure and primary production in small intertidal estuarine-bay

- ecosystem (eastern English Channel, France). Marine Biology **151**, pp. 805-825.
- Kirk, J.T.O. (1994). Light and photosynthesis in aquatic ecosystems. Second Edition. Cambridge: Cambridge University Press, pp. 509.
- Kirk, J.T.O. (2003). The vertical attenuation of irradiance as a function of the optical properties of the water. Limnology and Oceanography **48** (1), pp. 9-17.
- Klausmeier, C.A., Litchman, E., Daufresne, T. and Levin, S.A. (2004). Optimal nitrogen-to-phosphorus stoichiometry of phytoplankton. Nature **429**, pp. 171-174.
- Kocum, E., Underwood, G.J.C. and Nedwell, D.B. (2002). Simultaneous measurement of phytoplanktonic primary production, nutrient and light availability along a turbid, eutrophic UK east coast estuary (the Colne Estuary). Marine Ecology Progress Series **231**, pp. 1-12.
- Kostoglidis, A., Pattiaratchi, C.B., and Hamilton, D.P. (2005). CDOM and its contribution to the underwater light climate of a shallow, microtidal estuary in south-western Australia. Estuarine, Coastal and Shelf Science **63**, pp. 469-477.
- Kremer, B.P. (1981). Dark reactions and photosynthesis. Canadian Bulletin of Fisheries and Aquatic Sciences **210**, pp. 44-54.
- Langdon, C. (1984). Dissolved oxygen monitoring system using a pulsed electrode: design, performance, and evaluation. Deep-Sea Research **31**, pp. 1357-1367.
- Langdon, C. (1987). On the causes of interspecific differences in the growth-irradiance relationship for phytoplankton. Part I. A comparative study of the growth-irradiance relationship of three marine phytoplankton species: *Skeletonema costatum*, *Olisthodiscus luteus* and *Goniaulax tamarensis*. Journal of Plankton Research **9** (3), pp. 459-482.
- Lederman, T.C. and Tett, P. (1981). Problems in modelling the photosynthesis-light relationship for phytoplankton. Botanica Marina **24**, pp. 125-134.
- Lee, Z.-P., Darecki, M., Carder, K.L., Davis, C.O., Stramski, D. and Rhea, W.J. (2005a). Diffuse attenuation coefficient of downwelling irradiance: an evaluation of remote sensing methods. Journal of Geophysical Research **110**, pp. 1-9.

- Lee, Z.-P., Du, K.-P. and Arnone, R. (2005b). A model for the diffuse attenuation coefficient of downwelling irradiance. Journal of Geophysical Research **110**, pp. 1-10.
- Legendre, P. and Legendre, L. (1998). Numerical ecology. Second English edition. Development in Environmental Modelling 20, pp. 853.
- Lewis, M.R. and Smith, J.C. (1983). A small volume, short-incubation-time method for measurement of photosynthesis as a function of incident irradiance. Marine Ecology – Progress Series **13**, pp. 99-102.
- Litchman, E., Klausmeier, C.A. and Bossart, P. (2004). Phytoplankton nutrient competition under dynamic light regimes. Limnology and Oceanography **49** (4, part 2), pp. 1457-1462.
- Livingstone, M.W., Smith, R.V. and Laughlin, R.J. (2000). A spatial study of denitrification potential of sediments in Belfast and Strangford Loughs and its significance. The Science of the Total Environment **251-252**, pp. 369-380.
- Lizon, F., Lagadeuc, Y., Brunet, C., Aelbrecht, D. and Bentley, D. (1995). Primary production and photoadaptation of phytoplankton in relation with tidal mixing in coastal waters. Journal of Plankton Research **17** (5), pp. 1039-1055.
- Lohrenz, S.E. (1992). Estimation of primary production by the simulated *in situ* method. **In: ICES, Primary Production Symposium**, paper 13.
- Lohrenz, S.E., Wiesenburg, D.A., Rein, C.R., Arnone, R.A., Taylor, C.D., Knauer, G.A. and Knap, A.H. (1992). A comparison of *in situ* and simulated *in situ* methods for estimating oceanic primary production. Journal of Plankton Research **14** (2), pp. 201-221.
- Lund-Hansen, L.C. (2004). Diffuse attenuation coefficients $K_d(\text{PAR})$ at the estuarine North Sea-Baltic Sea transition: time-series, partitioning, absorption, and scattering. Estuarine, Coastal and Shelf Science **61**, pp. 251-259.
- Luz, B. and Barkan, E. (2009). Net and gross oxygen production from O_2/Ar , $^{17}\text{O}/^{16}\text{O}$ and $^{18}\text{O}/^{16}\text{O}$ ratios. Aquatic Microbial Ecology **56**, pp. 133-145.
- MacCaull, W.A. and Platt, T. (1977). Diel variations in the photosynthetic parameters of coastal marine phytoplankton. Limnology and Oceanography **22** (4), pp.723-731.
- Macedo, M.F., Duarte, P., Mendes, P. and Ferreira, J.G. (2001). Annual variation of environmental variables, phytoplankton species composition and

- photosynthetic parameters in a coastal lagoon. Journal of Plankton Research **23** (7), pp. 719-732.
- Mangoni, O., Modigh, M., Mozetič, P., Bergamasco, A., Rivaro, P. and Saggiomo, V. (2008). Structure and photosynthetic properties of phytoplankton assemblages in a highly dynamic system, the Northern Adriatic Sea. Estuarine, Coastal and Shelf Science, **77** (4), pp. 633-644.
- Margalef, R. (1978). Life-forms of phytoplankton as survival alternatives in an unstable environment. Oceanologica Acta **1** (4), pp. 493-509.
- Marra, J. (2002). Approaches to the measurement of plankton production. **In:** Williams, P.J.leB., Thomas, D.N. and Reynolds, C.S. (eds) (2002) Phytoplankton productivity. Carbon assimilation in marine and freshwater ecosystems. Oxford: Blackwell Science, pp. 78-108.
- Marra, J. (2009). Net and gross productivity: weighting in with ¹⁴C. Aquatic Microbial Ecology **56**, pp. 123-131.
- Marshall, S.M. and Orr, A.P. (1930). A study of the spring diatom increase in Loch Striven. Journal of Marine Biology Association **16**, pp. 853-878.
- Maske, H. and Garcia-Marquez, E. (1994). Adsorption of dissolved organic matter to the inorganic filter substrate and its implications for ¹⁴C uptake measurements. Applied Environmental Microbiology **60**, pp. 3887-3889.
- McBride, G.B. (1992). Simple calculations of daily photosynthesis by means of five photosynthesis-light equations. Limnology and Oceanography **37** (8), pp. 1796-1808.
- McKinney, E.S.A, Gibson, C.E. and Stewart, B.M. (1997). Planktonic diatoms in the North-West Irish Sea: a study by automatic sampler. Biology and Environment: Proceeding of the Royal Irish Academy **97B** (3), pp. 197-202.
- Menden-Deuer, S. and Lessard, E.J. (2000). Carbon to volume relationship for dinoflagellates, diatoms and other protest plankton. Limnology and Oceanography **45**, pp. 569-579.
- Moll, A. (1998). Regional distribution of primary production in the North Sea simulated by a three-dimensional model. Journal of Marine Systems **16**, pp. 151-170.
- Morán, X.A.G. and Estrada, M. (2005). Winter pelagic photosynthesis in the NW Mediterranean. Deep-Sea Research I **52**, pp. 1806-1822.

- Morel, A. and Smith, R.C. (1974). Relation between total quanta and total energy for aquatic photosynthesis. Limnology and Oceanography **19** (4), pp. 591-600.
- Mousseau, L., Dauchez, S., Legendre, L. and Fortier L. (1995). Photosynthetic carbon uptake by marine phytoplankton: comparison of the stable (^{13}C) and radioactive (^{14}C) isotope methods. Journal of Plankton Research **17** (7), pp. 1449-1460.
- Nixon, S.W. (1995). Coastal marine eutrophication: a definition, social causes, and future concerns. Ophelia **41**, pp. 199-219.
- Nixon, S.W. (2009). Eutrophication and the macroscope. Hydrobiologia **629**, pp. 5-19.
- Nunes, J.P., Ferreira, J.G., Gazeau, F., Lencart-Silva, J., Zhang, X.L., Zhu, M.Y. and Fang, J.G. (2003). A model for sustainable management of shellfish polyculture in coastal bays. Aquaculture **219**, pp. 257-277.
- Obrador, B. and Pretus, J.L. (2008). Light regime and components of turbidity in a Mediterranean coastal lagoon. Estuarine, Coastal and Shelf Science **77**, pp. 123-133.
- Oviatt, C., Keller, A. and Reed, L. (2002). Annual primary production in Narragansett Bay with no bay-wide winter-spring phytoplankton bloom. Estuarine, Coastal and Shelf Science **54**, pp. 1013-1026.
- Parker, J.G., Rosell, R.S. and MacOscar, K.C. (1988). The phytoplankton production cycle in Belfast Lough. Journal of Marine Biology Association UK **68**, pp. 555-564.
- Parsons, T.R., Maita, Y. and Lalli, CM (1984). A manual of chemical and biological methods for seawater analysis. Oxford, Pergamon Press Ltd, pp. 115-120.
- Peeters, J.C.H., Haas, H.A., Peperzak, L. and de-Vries, I. (1993). Nutrients and light as factors controlling phytoplankton biomass on the Dutch continental shelf (North Sea) in 1988-1990. Report DGW-93.004. Dutch Ministry of Transport, Public Works and Water Management, The Hague, The Netherlands.
- Peeters, J.C.H., Haas, H.A., Peperzak, L. and Wetsteyn, L.P.M.J. (1991). Limiting factors for phytoplankton in the North Sea. Water Science Technology **24**, pp. 261-267.

- Peterson, B.J. (1980). Aquatic primary productivity and the ^{14}C - CO_2 method: a history of the productivity problem. Annual Review of Ecology and Systematics **11**, pp. 359-385.
- Piñeiro, G., Perelman, S., Guerschman, J.P. and Paruelo, J.M. (2008). How to evaluate models: observed vs. predicted or predicted vs. observed? Ecological Modelling **216** (3/4), pp. 316-322.
- Platt, T. (1971). The annual production by phytoplankton in St. Margaret's Bay, Nova Scotia. Journal du Conseil International pour l'Exploration de la Mer **33**, pp. 324-333.
- Platt, T. and Jassby, A.D. (1976). The relationship between photosynthesis and light for natural assemblages of coastal marine phytoplankton. Journal of Phycology **12**, pp. 421-430.
- Platt, T., Denman, K.L. and Jassby, A.D. (1975). The mathematical representation and prediction of phytoplankton productivity. Fisheries and Marine Service, Technical Report **523**, pp. 110.
- Platt, T., Gallegos, C.L. and Harrison, W.G. (1980). Photoinhibition of photosynthesis in natural assemblages of marine phytoplankton. Journal of Marine Research **38** (4), pp. 687-701.
- Platt, T., Sathyendranath, S., Forget, M.-H., White III, G.N., Caverhill, C., Bouman, H., Devred, E. and Son, S.H. (2008). Operational estimation of primary production at large geographical scales. Remote Sensing and Environment **112**, pp. 3437-3448.
- Poole, H.H. and Atkins, W.R.G. (1929). Photo-electric measurements of submarine illumination throughout the year. Journal of Marine Biology Association UK **16**, pp. 297-324.
- Preisendorfer, R.W. (1961). Application of radiative transfer theory to light measurements in the sea. Union Geodetic and Geophysical Institute Monography **10**, pp. 11-30. **Cited by** Kirk, J.T.O. (1994). Light and photosynthesis in aquatic ecosystems. Second Edition. Cambridge: Cambridge University Press, pp. 509.
- Preisendorfer, R.W. (1986). Secchi disk science: visual optics of natural waters. Limnology and Oceanography **31** (5), pp. 909-926.

- Raine, R.C.T. and Patching, J.W. (1980). Aspect of carbon and nitrogen cycling in a shallow marine environment. Journal of Experimental Marine Biology and Ecology **47**, pp. 127-139.
- Raven, J.A and Beardall, J. (1981). Respiration and photorespiration. Canadian Bulletin of Fisheries and Aquatic Sciences **210**, pp. 55-82.
- Raven, J.A. (1997). Putting the C in phycoecology. European Journal of Phycology **32**, pp. 319-333.
- Reynolds, C.S. (1996). The plant life of the pelagic. Verhandlungen Internationale Vereinigung für Theoretische und Angewandte Limnologie **26**, pp. 97-113.
- Riegman, R., and Colijn, F. (1991). Evaluation of measurements and calculation of primary production in the Dogger Bank area (North Sea) in summer 1988. Marine Ecology Progress Series **69**, pp. 125-132.
- Roberts, B.J. and Howarth, R.W. (2006). Nutrient and light availability regulate the relative contribution of autotrophs and heterotrophs to respiration in freshwater pelagic ecosystems. Limnology and Oceanography **51** (1), pp. 288-298.
- Ryther, J.H. (1956). The measurement of primary production. Limnology and Oceanography **1**, pp. 72-84.
- Sathyendranath, S. And Platt, T. (2007). Spectral effect in bio-optical control on the ocean system. Oceanologia **49** (1), pp.5-39.
- Sathyendranath, S., Platt, T. And Forget, M.-H. (2007). Oceanic primary production: comparison of models. OCEANS 2007 Europe, pp. 1-3.
- Service, M., Durrant, A.E., Mills, J.A., Taylor, J.E. and Faughey, D. (1996). The trophic status of two northern Irish Sea loughs. Journal of Coastal Conservation **2**, pp. 159-168.
- Shaw, P.J. and Purdie, D.A. (2001). Phytoplankton photosynthesis-irradiance parameters in the near-shore UK coastal waters of the North Sea: temporal variation and environmental control. Marine Ecology Progress Series **216**, pp. 83-94.
- Skogen, M.D., Moll, A., 2000. Interannual variability of the North Sea primary production: comparison from two model studies. Continental Shelf Research **20**, 129-151.

- Slawyk, G., Collos, Y. and Auclair, J.-C. (1977). The use of the ^{13}C and ^{15}N isotopes for the simultaneous measurement of carbon and nitrogen turnover rate in marine phytoplankton. Limnology and Oceanography **22**, pp. 925-932.
- Smaal, A.C., Prins, T.C., Dankers, N. and Ball, B. (1998). Minimum requirements for modelling bivalve carrying capacity. Aquatic Ecology **31**, pp. 423-428.
- Smith, E.L. (1936). Photosynthesis in relation to light and carbon dioxide. Proceeding of the National Academy of Science U.S.A. **22**, pp. 504-511.
- Smith, V.H. (1979). Nutrient dependence of primary productivity in lakes. Limnology and Oceanography **24** (6), pp. 1051-1064.
- Soetaert, K. and Peter, H. (2001). Ecological modelling. Lecture notes. Published by NIOO-CEME, Yerseke, The Netherlands. Available for download at the following link: <http://www.nioo.knaw.nl/users/ksoetaert>.
- Steele, J.H. (1962). Environmental control of photosynthesis in the sea. Limnology and Oceanography **7**, pp. 137-150.
- Steele, J.H. and Baird, I.E. (1968). Production ecology of a sandy beach. Limnology and Oceanography **13** (1), pp. 14-25.
- Stemann Nielsen, E. (1952). The use of radio-active carbon (^{14}C) for measuring organic production in the sea. Journal du Conseil International pour l'Exploration de la Mer **18**, pp. 117-140.
- Stewart, B. (2008a). SOP MARCHEM001v3. The automatic colorimetric determination of ammoniacal nitrogen in seawater. AFBI - Agri-Food and Biosciences Institute.
- Stewart, B. (2008b). SOP MARCHEM003v3. The automatic colorimetric determination of the total oxidized nitrogen in seawater. AFBI - Agri-Food and Biosciences Institute.
- Stewart, B. (2008c). SOP MARCHEM005v3. The automatic colorimetric determination of nitrite in seawater. AFBI - Agri-Food and Biosciences Institute.
- Stewart, B. (2008d). SOP MARCHEM002v3. The automatic colorimetric determination of soluble reactive phosphorous in seawater. AFBI - Agri-Food and Biosciences Institute.
- Stewart, B. (2008e). SOP MARCHEM004v3. The automatic colorimetric determination of soluble silica in seawater. AFBI - Agri-Food and Biosciences Institute.

- Strickland, J.D.H. and Parsons, T.R. (1967). A practical handbook of seawater analysis. Bulletin Fisheries Research Board Canada.
- Struski, C. and Bacher, C. (2006). Preliminary estimate of primary production by phytoplankton in Marennes-Oléron Bay, France. Estuarine, Coastal and Shelf Science **66**, pp. 323-334.
- Suggett, D.J., MacIntyre, H.L., Kana, T.M. and Geider, R.J. (2009). Comparing electron transport with gas exchange: parameterising exchange rates between alternative photosynthetic currencies for eukaryotic phytoplankton. Aquatic Microbial Ecology **56**, pp. 147-162.
- Sverdrup, H.U. (1953). On conditions for the vernal blooming of phytoplankton. Journal du Conseil International pour l'Exploration de la Mer **18**, pp. 287-295.
- Talling, J.F. (1957). Photosynthetic characteristics of some freshwater plankton diatoms in relation to underwater radiation. New Phytologist **56**, pp. 29-50.
- Talling, J.F. (1971). The underwater light climate as a controlling factor in the production ecology of freshwater phytoplankton. Mitteilung Internationale Vereinigung fuer Theoretische und Angewandte Limnologie **19**, pp. 214-243. **As cited by:** Gowen, R.J., Stewart, B.M., Mills, D.K. and Elliott, P. (1995). Regional differences in stratification and its effect on phytoplankton production and biomass in the northwestern Irish Sea. Journal of Plankton Research **17** (4), pp. 753-769.
- Taylor, J., Charlesworth, M. and Service, M. (1999). Nutrient inputs and trophic status of Carlingford Lough. The Queen's University of Belfast and Department of Agriculture (NI).
- Tett, P. (1981). Modelling phytoplankton production at shelf-sea fronts. Philosophical Transactions of the Royal Society of London. Series A. Physical Sciences and Engineering **302**, pp. 605-615.
- Tett, P. (1990). The photic zone. **In:** Herring, P.J., Campbell, A.K., Whitfield, M. and Maddock, L. (eds) (1990) Light and life in the sea. Cambridge: Cambridge University Press, pp. 59-87.
- Tett, P. (2008). Waves (v.2.2). Unpublished notes of the Matlab script HPLF1.
- Tett, P. and Wallis, A. (1978). The general cycle of chlorophyll standing crop in Loch Creran. Journal of Ecology **66**, pp. 227-239.

- Tett, P., Drysdale, M. and Shaw, J. (1981). Phytoplankton in Loch Creran during 1979 and its effect on the rearing of oyster larvae. Oban: Scottish Marine Biological Association, Internal Report 52.
- Tett, P., Edwards, A. and Jones, K. (1986). A model for the growth of shelf-sea phytoplankton in summer. Estuarine, Coastal and Shelf Science **23**, pp. 641-672.
- Tett, P., Ferreira, J.G., Bricker, S., Camo, J., Garcés, E., Heiskanen, A.-S., Humborg, C., Ignatiades, L., Lancelot, C. and Mensguen, A. (2010). The evolving concept of eutrophication. EUTRO2010, Third International Symposium on Research and Management of Eutrophication in Coastal Ecosystems. 15-18 June 2010, Nyborg, Denmark.
- Tett, P., Gilpin, L., Svendsen, H., Erlandsson, C.P., Larsson, U., Kratzer, S., Fouilland, E., Janzen, C., Lee, J.-Y., Grenz, C., Newton, A., Ferreira, J.G., Fernandes, T. and Scory, S. (2003). Eutrophication and some European waters of restricted exchange. Continental Shelf Research **23**, pp. 1635-1671.
- Tett, P., Gowen, R., Granthman, B. and Jones, K. (1986). The phytoplankton ecology of the Firth of Clyde sea-lochs Striven and Fyne. Proceedings of the Royal Society of Edinburgh **90B**, pp. 223-238.
- Tett, P., Gowen, R., Mills, D., Fernandes, T., Gilpin, L., Huxham, M., Kennington, K., Read, P., Service, M., Wilkinson, M., Malcolm, S. (2007). Defining and detecting undesirable disturbance in the context of marine eutrophication. Marine Pollution Bulletin, **55**, pp. 282-297.
- Tett, P., Hydes, D. and Sanders, R. (2003). Influence of nutrient biogeochemistry on the ecology of North-West European shelf seas. **In:** Black, K. and Schimmiel, G. (eds) (2003). Biogeochemistry of marine systems. Sheffield, Blackwell Publishing, pp. 293-333.
- Tett, P.B. (1987). Plankton. **In:** Baker, J.M. and Wolff, W.J. (eds) (1987) Biological surveys of estuaries and coasts. Cambridge: Cambridge University Press.
- Thomsen, H.A. (red.) (1992). Plankton I de indre danske farvande. Analyse af forekomsten af alger og heterotrofe protister (ekskl. ciliater) i Kattegat. Havforskning fra Miljøstyrelsen **11**.
- Tillmann, U., Hesse, K.-J. and Coljin, F. (2000). Planktonic primary production in the German Wadden Sea. Journal of Plankton Research **22** (7), pp. 1253-1276.

- Tilstone, G., Smyth, T., Poulton, A. and Hutson, R. (2009). Measured and remotely sensed estimates of primary production in the Atlantic Ocean from 1998 to 2005. Deep-Sea Research II **56**, pp. 918-930.
- Tomas, C. R. (1996). Identifying marine phytoplankton. San Diego: Academic Press.
- Utermöhl, H. (1958). Zur Vervollkommnung der quantitativen Phytoplankton-Methodik. Mitteilungen Internationale Vereinigung fuer Limnologie **9**, pp. 1-38.
- Varela, R.A., Cruzado, A. and Gabaldón, J.E. (1995). Modelling primary production in the North Sea using the European Regional Sea Ecosystem Model. Netherlands Journal of Sea Research **33** (3/4), pp. 337-361.
- Vegter, F. (1983). Excretion. **In**: Colijn, F., Gieskes W.W.C. and Zevenboom, W. (eds) (1983) The measurement of primary production: problems and recommendation. Hydrobiological Bulletin **17** (1), pp. 40-41.
- Wang, M., Son, S.H. and Harding Jr. L.W. (2009). Retrieval of diffuse attenuation coefficient in the Chesapeake Bay and turbid ocean regions for satellite ocean colour applications. Journal of Geophysical Research **114**, pp. 1-15.
- Webb, W.L., Newton, M. and Starr, D. (1974). Carbon dioxide exchange of *Alnus rubra*: a mathematical model. Oecologia **17**, pp. 281-291.
- Weston, K., Fernand, L., Mills, D.K., Delahunty, R. and Brown, J. (2005). Primary production in the deep chlorophyll maximum of the central North Sea. Journal of Plankton Research **27** (9), pp. 909-922.
- Williams, P.J.leB. (1981). Microbial contribution to overall marine plankton metabolism: direct measurements of respiration. Oceanologica Acta **4** (3), pp. 359-364.
- Williams, P.J.leB., Raine, R.C.T. and Bryan, J.R. (1979). Agreement between the ¹⁴C and oxygen methods of measuring phytoplanktonic primary production: re-assessment of the photosynthetic quotient. Oceanologica Acta **2**, pp. 411-416.
- Wood, B.J.B., Tett, P.B. and Edwards, A. (1973). An introduction to the phytoplankton, primary production and relevant hydrography of Loch Etive. Journal of Ecology **61**, pp. 569-585.
- Yoshikawa, T. and Furuya, K. (2006). Effect of diurnal variations in phytoplankton photosynthesis obtained from natural fluorescence. Marine Biology **150**, pp. 299-311.

Zar, J.H. (1998). Biostatistical Analysis, Fourth Edition. Prentice Hall International, Inc., Pearson Education, New Jersey, pp. 663.

APPENDIX 1

Equations used for calculating phytoplankton cell volumes for each taxon identified in samples. Equations were derived from Edler (1979), except for *Ditylum* cell volume (calculated according to Hillebrand *et al.* 1999) and *Ceratium* volume (according to Thomsen 1992). d = diameter; d1 = major axes (of ellipse); d2 = minor axes (of ellipse); h = height; l = length; w = width; $\pi = \text{pi} \approx 3.14$.

Taxon	Equation
<i>Cerataulina pelagica</i>	$\pi/4*d^2*h$
<i>Chaetoceros affinis</i>	$\pi/4*d1*d2*h$
<i>Chaetoceros brevis</i>	$\pi/4*d1*d2*h$
<i>Chaetoceros compressus</i>	$\pi/4*d1*d2*h$
<i>Chaetoceros curvisetus</i>	$\pi/4*d1*d2*h$
<i>Chaetoceros danicus</i>	$\pi/4*d1*d2*h$
<i>Chaetoceros debilis</i>	$\pi/4*d1*d2*h$
<i>Chaetoceros decipiens</i>	$\pi/4*d1*d2*h$
<i>Chaetoceros densus</i>	$\pi/4*d1*d2*h$
<i>Chaetoceros lacinosus</i>	$\pi/4*d1*d2*h$
<i>Chaetoceros neglectus</i>	$\pi/4*d1*d2*h$
<i>Chaetoceros socialis</i>	$\pi/4*d1*d2*h$
<i>Chaetoceros</i> sp.	$\pi/4*d1*d2*h$
<i>Chaetoceros simplex</i>	$\pi/4*d1*d2*h$
<i>Coscinodiscus granii</i>	$\pi/4*d^2*h$
<i>Coscinodiscus</i> sp.	$\pi/4*d^2*h$
<i>Coscinoscira polychorda</i>	$\pi/4*d^2*h$
<i>Cyclotella</i> sp.	$\pi/4*d^2*h$
<i>Dactyliosolen fragilissimus</i>	$\pi/4*d^2*h$
<i>Ditylum brightwellii</i>	$l*w*h/2$
<i>Eucampia cornuta</i>	$\pi/4*d1*d2*h$
<i>Eucampia zodiacus</i>	$\pi/4*d1*d2*h$
<i>Guinardia delicatula</i>	$\pi/4*d^2*h$
<i>Guinardia flaccida</i>	$\pi/4*d^2*h$
<i>Guinardia striata</i>	$\pi/4*d^2*h$
<i>Lauderia annulata</i>	$\pi/4*d^2*h$
<i>Leptocylindrus danicus</i>	$\pi/4*d^2*h$
<i>Leptocylindrus minimus</i>	$\pi/4*d^2*h$
<i>Lithodesmium undulatum</i>	$l*w*h/2$
<i>Melosira nummuloides</i>	$\pi/4*d^2*h$
<i>Paralia sulcata</i>	$\pi/4*d^2*h$
<i>Proboscia alata</i>	$\pi/4*d^2*h$
<i>Rhizosolenia setigera</i>	$\pi/4*d^2*h$
<i>Rhizosolenia</i> sp.	$\pi/4*d^2*h$
<i>Rhizosolenia styliformis/imbricata</i>	$\pi/4*d^2*h$
<i>Skeletonema costatum</i>	$\pi/4*d^2*h$
<i>Stephanopyxis turris</i>	$\pi/4*d^2*h$
<i>Thalassiosira anguste-lineata</i>	$\pi/4*d^2*h$
<i>Thalassiosira angulata</i>	$\pi/4*d^2*h$
<i>Thalassiosira gravida</i>	$\pi/4*d^2*h$

<i>Thalassiosira nordenskioldii</i>	$\pi/4*d^2*h$
<i>Thalassiosira rotula</i>	$\pi/4*d^2*h$
<i>Thalassiosira</i> sp.	$\pi/4*d^2*h$
<i>Triceratium</i> sp.	$l*w*h/2$
Unidentified centric	$\pi/4*d^2*h$
<i>Amphiprora</i> sp.	$\pi/4*l*d*h$
<i>Amphora laevissima</i>	$\pi/4*l*d*h$
<i>Amphora</i> sp.	$\pi/4*l*d*h$
<i>Asterionellopsis glacialis</i>	$l*w*h/2$
<i>Bacillaria</i> cfr. <i>paxillifera</i>	$l*w*h$
<i>Bacillaria</i> sp.	$l*w*h$
<i>Bellerochea</i> sp.	$l*w*h$
<i>Biddulphia alternans</i>	$\pi/4*d1*d2*h$
<i>Biddulphia</i> sp.	$\pi/4*d1*d2*h$
<i>Cocconeis scutellum</i>	$\pi/4*l*d*h$
<i>Cylindrotheca closterium</i>	$\pi/6*d^2*l$
<i>Cylindrotheca fusiformis</i>	$\pi/6*d^2*l$
<i>Diploneis bombus</i>	$l*w*h$
<i>Diploneis</i> sp.	$l*w*h$
<i>Fragilariopsis</i> sp.	$l*w*h$
<i>Gomphonema</i> sp.	$\pi/4*l*d*h$
<i>Gyrosigma fasciola</i>	$\pi/4*d1*d2*h$
<i>Gyrosigma</i> sp.	$\pi/4*d1*d2*h$
<i>Licmophora</i> sp.	$l*w*h/2$
<i>Navicula cryptocephala</i>	$l*w*h*0.6$
<i>Navicula lira</i>	$l*w*h*0.6$
<i>Navicula</i> sp.	$l*w*h*0.6$
<i>Nitzschia frustulum</i>	$l*w*h*0.6$
<i>Nitzschia longissima</i>	$\pi/12*d^2*l$
<i>Nitzschia lorenziana</i>	$l*w*h*0.6$
<i>Nitzschia panduriformis</i>	$l*w*h*0.6$
<i>Nitzschia</i> sp.	$l*w*h*0.6$
<i>Odontella granulata</i>	$\pi/4*d1*d2*h$
<i>Odontella mobiliensis</i>	$\pi/4*d1*d2*h$
<i>Odontella</i> sp.	$\pi/4*d1*d2*h$
<i>Plagiogramma</i> sp.	$\pi/4*d1*d2*h$
<i>Pleurosigma</i> sp.	$\pi/4*d1*d2*h$
<i>Pseudo-nitzschia delicatissima</i>	$l*w*h*0.9$
<i>Pseudo-nitzschia seriata complex</i>	$l*w*h*0.8$
<i>Pseudo-nitzschia</i> sp.	$l*w*h*0.8$
<i>Striatella unipunctata</i>	$\pi/4*d1*d2*h$
<i>Surirella</i> sp.	$\pi/4*l*d*h$
Unidentified pennate	$l*w*h/2$
<i>Akashiwo sanguinea</i>	$\pi/6*l*d1*d2$
<i>Alexandrium</i> sp.	$\pi/6*d^2*l$
<i>Amphidinium</i> sp.	$\pi/6*l*d1*d2$
<i>Ceratium furca</i>	$2.3038*d^2.532$
<i>Ceratium fusus</i>	$35.198*d^1.9156$
<i>Ceratium lineatum</i>	$1.2375*d^2.5989$
<i>Dinophysis acuminata</i>	$\pi/6*l*d1*d2$

<i>Dinophysis acuta</i>	$\pi/6 * d_1 * d_2$
<i>Dinophysis rotundata</i>	$\pi/6 * d_1 * d_2$
<i>Dinophysis</i> sp.	$\pi/6 * d_1 * d_2$
<i>Diplopsalis lenticula</i>	$\pi/6 * d^3 * 0.7$
<i>Diplopsalis</i> sp.	$\pi/6 * d^3 * 0.7$
<i>Goniaulax</i> sp.	$\pi/6 * d^3 * 0.75$
<i>Gymnodinium</i> sp.	$\pi/6 * d_1 * d_2$
<i>Gyrodinium</i> sp.	$\pi/6 * d_1 * d_2$
<i>Heterocapsa triquetra</i>	$\pi/12 * d^2 * 1$
<i>Oxytoxum</i> sp.	$\pi/12 * d^2 * 1$
<i>Prorocentrum aporum</i>	$\pi/12 * d^2 * h * 0.9$
<i>Prorocentrum compressum</i>	$\pi/12 * d^2 * h * 0.9$
<i>Prorocentrum lima</i>	$\pi/12 * d^2 * h * 0.9$
<i>Prorocentrum micans</i>	$\pi/6 * d_1 * d_2$
<i>Prorocentrum minimum</i>	$\pi/12 * d^2 * h * 0.9$
<i>Prorocentrum</i> sp.	$\pi/12 * d^2 * h * 0.9$
<i>Protoperidinium bipes</i>	$\pi/24 * d^2 * h$
<i>Protoperidinium breve</i>	$\pi/6 * d^3 * 0.9$
<i>Protoperidinium divergens</i>	$\pi/12 * d^2 * (h+d/2) * 0.8$
<i>Protoperidinium</i> sp.	$\pi/12 * d^2 * (h+d/2) * 0.75$
<i>Protoperidinium steinii</i>	$\pi/12 * d^2 * (h+d/2) * 0.75$
<i>Scripsiella</i> sp.	$\pi/6 * d^2 * 1$
<i>Scripsiella trochoidea</i>	$\pi/12 * d^2 * (h+d/2)$
Unidentified naked	$\pi/6 * d^2 * 1$
Unidentified tecate	$\pi/6 * d^2 * 1$
<i>Dictyoca fibula</i>	$\pi/12 * d^3$
<i>Dictyocha speculum</i>	$\pi/12 * d^3$
<i>Emiliana huxleyi</i>	$\pi/6 * d^3$
Unidentified coccolithophorids	$\pi/6 * d^3$
<i>Pyramimonas</i> sp.	$1/2 * h * w * (d_1 + d_2)$
Unidentified prasinophytes	$1/2 * h * w * (d_1 + d_2)$
Unidentified cryptophytes	$\pi/12 * d^2 * (h+d/2)$
Flagellate	$\pi/6 * d^2 * 1$
Nanoflagellate	$\pi/6 * d^2 * 1$
<i>Pediastrum</i> sp.	$\pi/4 * d_1 * d_2 * h$
Unidentified chlorophytes	$\pi/6 * d^3$
Unidentified euglenophytes	$\pi/6 * d^2 * 1$
Unidentified cyanophytes	$\pi/6 * d^3$

APPENDIX 2

biomassa.M

- date of creation: May 2008
- author: E. Capuzzo

```
load fitoab.dat
load biovol.dat
biomass=NaN(128,75);
for n=1:128
    biomass(n,:)=fitoab(n,:).*biovol(n,1)./1000000;
end
```

Where fitoab.dat is a matrix 128x75 containing the abundance of the 128 taxon identified in the 75 samples analysed; and biovol.dat is a vector 128x1 containing the carbon content (pg C cell⁻¹) of one average cell of each taxon.

Listing 2.1. Commands of the Matlab script '*biomassa.M*'.

interpolatore2.M

- date of creation: 19 August 2008
- author: E. Capuzzo

```
fprintf("\n%s\n", '-----New data-----');
load depth.txt;
load all_chl.txt;
x=[0:0.5:5.5];
xi=NaN(47,2);
yi=NaN(47,2);
for j=1:47
    xi(j,:)=depth(:,j);
    yi(j,:)=all_chl(:,j);
    yilog(j,:)=log10(yi(j,:));
end
linear=NaN(length(x),47);
for j=1:47
    linear(:,j)=interp1(xi(j,:),yilog(j,:),x,'linear','extrap');
end
explinear=10.^linear;
explinear2=explinear.*0.5;
standstock_lin=sum(explinear2)
```

Where depth.txt is a 2x47 matrix containing the sampling depths of 47 samples, while all_chl.txt is a 2x47 matrix containing the chlorophyll values measured at the sampling depths in depth.txt.

Listing 2.2. Commands of the Matlab script '*interpolatore2.M*'.

HPLP3A_Elisa.M

- date of creation: 19 August 2006 by P. Tett
- modification: 11 and 15 February 2008 by E. Capuzzo

[...]

```
if replot < 0.5,
    clear LFC
    clear env envb envn ldata cellnod envlab;
    fprintf('%s\n\n', ...
'Choices follow: at prompt, enter integer; <RET> only picks default --');
    fprintf('%s\n', 'Plot envelope?');
    fprintf('%s\n',strcat(['options are: 0 (none), 90 (10-90%ile),'...
        '95 (5-95%ile), 97 (2.5-97.5%ile)']));
    envsw=input(strcat( ...
        [ 'Enter value:  ']));
    fprintf('\n');
    rsno=input(strcat...
(['reference symbol: 1 for circle, 0 for point: ']));
    if rsno<1, rs='k.'; else rs='ko'; end
    fprintf('\n');
end
fprintf('%s\n\n', 'Enter integer data selection parameters; <RET> alone gives default -
-');
fprintf('%s\n', 'Choose tipe of output:  ');
fprintf('%s\n', ' -- for a single taxon type (0)');
fprintf('%s\n', ' -- or for a class (diatoms, dinoflagellate etc) type (1)');
fprintf('%s\n', ' -- or for pennate/centric diatoms type (2)');
fprintf('%s\n', ' -- or for a single genus type (3)');
LFC=input(strcat([' -- enter 0, 1, 2, 3 or [default: ' num2str(default(1)) ' ] :']));
    if isempty(LFC), LFC=default(1);
    end
fprintf('\n');
switch LFC
    case 0
        species=input(strcat(['Enter species code or [default: ' num2str(default(1)) ' ]
:']));
        if isempty(species), species=default(1);
        end
    case 1
        class=input(strcat(['Enter class code [ ' num2str(default(8)) ' ] :']));
        if isempty(class), class=default(8);
        end
```

Listing 2.3. Parts of the commands of the Matlab script ‘*HPLP3A_Elisa.M*’.

```

case 2
    diatom=input(strcat(['Enter pennate or centric diatom code ['
num2str(default(9)) '] :']));
    if isempty(diatom), diatom=default(9);
    end
case 3
    genus=input(strcat(['Enter genus code [' num2str(default(10)) '] :']));
    if isempty(genus), genus=default(10);
    end
end
[...]
switch LFC
case 0
m=1;
for n=1:nmax
[...]
end
    mmax=m-1;
fprintf('\n%s\n\n', strcat(['for species ' num2str(species) ' found ' num2str(mmax) '
rows']));
min_year=min(year);
max_year=max(year);
miny=1;
maxy=9;
minvy=-3;
maxvy=5;
z=10;
zv=0.0227631;
subplot(2,1,1);
plot(dayno,log10(cellno+z), 'ko');
xlabel('day in year');
ylabel('log10 cells/L');
title(strcat(['Abundance and biomass species: ' num2str(species) '; station CLNBuoy ;
years: ' num2str(min_year) ' to ' num2str(max_year)]));
axis([0 365 miny maxy]);
set(gca, 'xtick', mtick);
grid on;
% envelope -----
    if envsw > 88
        ldata(:,1)=dayno;
        ldata(:,2)=log10(cellno+z);
        envn = envf(ldata, envsw);
        hold on;
        plot(envn.min(:,1), envn.min(:,2), 'r--');
        plot(envn.mid(:,1), envn.mid(:,2), 'r--');
        plot(envn.max(:,1), envn.max(:,2), 'r--');
    end
end

```

Listing 2.3. Continued.

```
subplot(2,1,2);
plot(dayno, log10(biono+zv), 'ko');
xlabel('day in year');
ylabel('log10 ugC/L');
axis([0 365 minvy maxvy]);
set(gca, 'xtick', mtick);
grid on;

[...]
```

The script loads a file named fito2.txt containing abundances and biomasses of all the phytoplankton taxa of all the samples. Every taxon is associated to a code number, and the same for every genus and class. fito2.txt has 11 columns containing year, month, day, station, depth, class code, centric/pennate code, genus code, species code, abundance (cell L⁻¹), and biomass (µg C L⁻¹) of each taxon of each sample.

Listing 2.3. Continued.

UWLight0.M

- date of creation: 16 June 2007 by P. Tett
- modification: 8 July 2007 by P. Tett

```
defPontop=1;% normal - PAR1 on top of PAR2
defsepd=0.75;% metres separation between sensors
defP2above=0.5; % second sensor above depth sensor, m
[...]
Idata=load(tfn);
depth=Idata(:,2);
time=Idata(:,8);
btime=max(time(depth==max(depth)));
timedown=time(time<btime);
timeup=time(time>btime);
maxdepth=max(depth);
fprintf('\n\n%s', strcat(['Greatest (raw) depth of CTD was ' num2str(maxdepth) ' m']));
depthdown=depth(time<btime);
depthup=depth(time>btime);
if Pontop<1.5,
PARtopdown=Idata(time<btime,3);
PARbotdown=Idata(time<btime,4);
PARtopup=Idata(time>btime,3);
PARbotup=Idata(time>btime,4);
else
PARtopdown=Idata(time<btime,4);
PARbotdown=Idata(time<btime,3);
PARtopup=Idata(time>btime,4);
PARbotup=Idata(time>btime,3);
end
endtime=max(time);
decktime1=endtime-10;
decktime2=endtime-3;
endtimeindex=time>decktime1 & time<decktime2;
zdeck=mean(depth(endtimeindex));
fprintf('\n%s' strcat(['CTD depth reading in air was ' num2str(zdeck) ' m']));
if zdeck >0, mess='I.e., slightly under the water surface';
else mess='I.e. slightly above the water surface'; end
fprintf('\n%s', mess);
if Pontop<1.5,
PARtopend=mean(Idata(endtimeindex,3));
PARbotend=mean(Idata(endtimeindex,4));
else
PARtopend=mean(Idata(endtimeindex,4));
PARbotend=mean(Idata(endtimeindex,3));
end
P1P2=PARtopend/PARbotend;
fprintf('\n%s' strcat(['PARtop/PARbot in air was ' num2str(P1P2)]));
NS=length(depth(endtimeindex));
```

Listing 3.1. Parts of the commands of the Matlab script ‘UWLight0.M’.

UWLight1.M

- date of creation: 6-15 June 2007 by P. Tett
- modification: 18 July 2008 by E. Capuzzo

```
inwater = zcorrtop + 0.05 * zmax;
depthupwater=depthup(depthup>inwater);
PARtopupwater=PARtopup(depthup>inwater);
PARbotupwater=PARbotup(depthup>inwater);
Kd12down=-log((PARbotdown*P1P2)./PARtopdown)/sepd;
Kd12up=-log((PARbotupwater*P1P2)./PARtopupwater)/sepd;
meanKd=mean([median(Kd12down) median(Kd12up)]);
fprintf('\n%s\n\n', ['N data for: Kd12down: ' ...
    num2str(length(Kd12down)) ' ; Kd12up: ' ...
    num2str(length(Kd12up)) ' ; Mean Kd12 = ' ...
    num2str(meanKd, 3) ' m-1']);
% DEEP VS SHALLOW WATER
odmax=meanKd*zmax;
if inwater*meanKd > defodstart,
    % VERY TURBID WATER
    newodstart = inwater*meanKd; % to ensure top sensor in water
else
    newodstart = defodstart;
end
if odmax > newodstart + defodstep,
    % DEEP WATER OPTION
    odstart=newodstart;
    odstop=odstart;
    odstep=defodstep;
else
    % SHALLOW WATER OPTION
    odstart = inwater*meanKd;% to ensure top sensor in water
    % odstop = (inwater-sepd)*meanKd; % ensures bottom sensor wet
    odstop = odstart;
    odstep = odmax - odstop; % forcing single-layer treatment
    odstep = max(0.05, odstep); % avoid negative or v. small values
end
fprintf('\n%s', 'Processing downcast ...');
rowsdown=ceil((odmax-odstart)/odstep);
bestKddown=zeros(rowsdown,3); % Kd from 2 sensor comparison
regKddown=zeros(rowsdown,4); % Kd from regression (both sensors)
regdowntop=zeros(rowsdown,4); % PAR values to plot regression
regdownbot=zeros(rowsdown,4);
od=odstart;
while od<odmax,
    ztop=od/meanKd; % ztop refers to depth of CTD
    zbot = ztop + odstep/meanKd;
    odi=round((od-odstart)/odstep)+1;
    fprintf('%s', strcat([num2str(odi) ...
```

Listing 3.2. Parts of the commands of the Matlab script ‘UWLight1.M’.

```

    (' num2str(ztop, 2) '-' num2str(zbot, 2) 'm)...']);
whichdepth=depthdown>=ztop & depthdown<=zbot;
Kd12downlocal=Kd12down(whichdepth);
bestKddown(odi,:)= [ztop zbot median(Kd12downlocal)];
depthdownlocal=depthdown(whichdepth); % CTD depth
PARbotdownlocal=PARbotdown(whichdepth);
PARtopdownlocal=PARtopdown(whichdepth);
if (max(depthdownlocal)-min(depthdownlocal))*meanKd>(odstep/3),
    pPb=polyfit(-depthdownlocal, log(PARbotdownlocal), 1);
    pPt=polyfit(-depthdownlocal, log(PARtopdownlocal), 1);
    regKddown(odi,:)= [ztop zbot pPb(1) pPt(1)];% for Kd
    regdowntop(odi,:) = [ztop zbot ...
        exp(pPt(2)-pPt(1)*ztop) exp(pPt(2)-pPt(1)*zbot)];
    regdownbot(odi,:) = [ztop zbot ...
        exp(pPb(2)-pPb(1)*ztop) exp(pPb(2)-pPb(1)*zbot)];
else
    regKddown(odi,:)= [ztop zbot NaN NaN];
    regdowntop(odi,:)= [ztop zbot NaN NaN];
    regdownbot(odi,:)= [ztop zbot NaN NaN];
    fprintf("\n%s\n", ...
['no Kd from regression (depth range too small) for CTDtop = ' ...
    num2str(ztop, 2)]);
end % of regression -----
od=od+odstep;
end

```

Listing 3.2. Continued.

dailySI.M

- date of creation: 14 August 2009 by E. Capuzzo

```

prognum=SIdata(:,1); % progressive number
SI=SIdata(:,5); % solar irradiance data
nummax=max(prognum); % for a standard year of 365 days should be 8760...
numstart=defnumstart;
numstep=defnumstep;
rowsdown=ceil(nummax/numstep); % for a standard year equal to 365.
num=numstart;
while num<nummax,
    numtop=num;
    numbot=numtop + 23;
    numi=round((num-numstart)/numstep)+1;
    interval=prognum>=numtop & prognum<=numbot; % interval of 24 hours
    SIlocal=SI(interval);
    sumSIlocal=sum(SIlocal);
    DSI(numi,:)= [sumSIlocal];
    num=num+numstep;
end

```

Listing 3.3. Parts of the commands of the Matlab script 'dailySI.M'.

PIcurvefit4.R

- date of creation: 12 October 2006 by P. Tett and E. Portilla
- modification: 4-5th June 2008 and 10th June 2008 by E. Capuzzo

```
modelName = c('Blackman2', 'BurkLine2', 'STalling2','Steele2',
             'modSteel2', 'Webbexp2', 'Tettsqrt2', 'JasPlatt2', 'modPlatt2')
W=12000*(((param[2,1]*0.067)-0.05)*0.96)
factors= (W*1.05)/(param[3,1]*param[4,1]*param[5,1])
x0 = c(2.34 ,0.06); # starting guesses for x(1) = pBmax and x(2) = alpha
for(i in 1:9){
  mod=NULL
  iformula=as.formula(paste("y~",modelName[i],"(x,x1,x2)",sep=""))
  fit=try(nls(iformula,start=list(x1=x0[1],x2=x0[2]),trace=FALSE,data=ddata))
  if(inherits(fit, "try-error")){
    print(paste("Model",modelName[i],"did not converge"))
  }
  else{
    mod=nls(iformula,start=list(x1=x0[1],x2=x0[2]),trace=FALSE,data=ddata)
    mod.coef=summary(mod)$parameters
    print(i)
    Rpi[i,2] = mod.coef[1,1];# parameter 1 = pBmax
    Rpi[i,3] = mod.coef[2,1];# parameter 2 = alpha
    Rpi[i,4] = mod.coef[1,2];# se 1 = pBmax
    Rpi[i,5] = mod.coef[2,2];# se 2 = alpha
    Rpi[i,6] = mod.coef[1,1]/mod.coef[2,1];# Ik
    fit=fitted(mod)
    nn=length(fit)
    totalSS=(nn-1)*var(ddata$y)
    dev=deviance(mod)#Residual sum of squares
    r2=1-dev/totalSS#r2-like
    res=residuals(mod)
    RES[i,]=res
    obs=res+fit
    cc=chi2(obs,fit)
    Rpi[i,7] = cc[1];# chi-square
    Rpi[i,8] = r2;# R2 like
    Rpi[i,9] = dev#deviance, or residual sum of squares
    Rpi[i,10] = AIC(mod)#akaike information criteria
    rm(mod)
  }
  [...]
}
```

To perform the analysis the script requires 2 input files: the first is a matrix of 2 columns and 24 rows containing the irradiances and activity in DPM for the 24 incubated vials. The second file contains the values of few parameters necessary for the calculation such as DPM in the vials incubated in the dark, salinity, incubation time (expressed in hour), DPM added to each vial and chlorophyll concentration.

Listing 5.1. Parts of the commands of the R script '*PIcurvefit4.R*'.

day_colum_prod4.M

- date of creation: November 2007 by E. Capuzzo
- last modification: April 2010 by E. Capuzzo

```
C1 = 4.15;
C2 = .94;
C3 = .45;
I0 = NaN(24, 28);
I0 = (((irradiance.* C1).* C2).* C3);

z = [0:.5:5.5]; %Defines the vector depth.
Iz = NaN(length(z), 24, 28);
for x= 1:24
    for n=1:28
        Iz(:,x,n) = I0(x,n).*exp(-(dataprod(n,6))*z);
    end
end

Px = NaN(length(z), 24, 28);
for x=1:24
    for n=1:28
        Px(:,x,n) = dataprod(n,1) * (tanh(dataprod(n,2)) * Iz(:,x,n) ./ dataprod(n,1));
    end
end

Pz = NaN(length(z), 24, 28);
for n=1:28
    for j=1:12
        Pz(j,:,n) = Px(j,:,n).* chl(j,n);
    end
end

Pzm2 = NaN(length(z), 24,28);
deltaz = 0.5;
deltat = 1;
for n=1:28
    Pzm2(:, :,n)=Pz(:, :,n) * deltaz * deltat;
end
hour_colum_prod=NaN(1,24,28);
for n=1:28
    hour_colum_prod(:, :,n)=sum(Pzm2(:, :,n));
end

h_gross_p=NaN(28,24);
for n=1:28
    h_gross_p(n,:)=hour_colum_prod(1,:,n);
end
gross_day_colum_p = sum(h_gross_p');
```

Listing 6.1. Part of the commands of the script ‘*day_colum_prod4.M*’.

HPLF2d.M

- date of creation: July 2008 by P. Tett

- last modification: January 2009 by P. Tett

```
% 2. collate data if there are several sets
% (version c) scalar crflag now a field in structure cp
fprintf('\n%s\n', '-----');
fprintf('%s\n', 'Collation and reduction of data sets:');
fprintf('%s\n', ...
    ' (reduction to 1 mean value for each sampled day));
fprintf('%s\n', ...
    ' (union and intersection made by sampled day));
fprintf('%s\n', ...
    ' 0 = continue with first data set unchanged,');
fprintf('%s\n', ' 1 = reduce and use only first data set,');
defcrf = 1;
if cp.ninfile > 1.5,
    fprintf('%s\n', ...
        ' 2 = use intersection of the two data sets,');
    fprintf('%s\n', ' 3 = use union of the two data sets,');
    defcrf = 2;
end
cp.crflag = input(['Enter your choice [' num2str(defcrf) ']: ']);
if isempty(cp.crflag), cp.crflag=defcrf; end
switch cp.crflag
    case 0,
        fprintf('%s\n', ...
            '---- Continuing with first data set unchanged');
        K = length(datain1);
        data1 = zeros(K,2);
        data1(:,1) = datain1(:,1) + (datain1(:,2)/yearlength);
        data1(:,2) = datain1(:,3); % cellno - need biomass option
    case 1,
        fprintf('%s\n', '---- Reducing first data set');
        D1 = unique(datain1(:,1:2), 'rows');
        K = length(D1);
        data1 = NaN(K,2);
        data1(:,1) = D1(:,1) + (D1(:,2)/yearlength);
        for j=1:K,
            data1(j,2) = mean(...
                datain1(datain1(:,1)==D1(j,1) ...
                    & datain1(:,2)==D1(j,2),3));
        end
    case 2,
        fprintf('%s\n', ...
            '---- Making intersection of both data sets');
```

Listing 6.2. Part of the commands of the script '*HPLF2d.M*'.

```

D1 = unique(datain1(:,1:2), 'rows');
D2 = unique(datain2(:,1:2), 'rows');
C = intersect(D1, D2, 'rows');
K = length(C);
data1 = NaN(K,3);
data1(:,1) = C(:,1) + (C(:,2)/yearlength);
for j = 1:K,
    data1(j,2) = mean(...
        datain1(datain1(:,1)==C(j,1)...
            & datain1(:,2)==C(j,2),3));
    data1(j,3) = mean(...
        datain2(datain2(:,1)==C(j,1)...
            & datain2(:,2)==C(j,2),3));
end
case 3,
fprintf('%s\n', ...
    '---- Making union of both data sets');
D1 = unique(datain1(:,1:2), 'rows');
D2 = unique(datain2(:,1:2), 'rows');
C = union(D1, D2, 'rows');
K = length(C);
data1 = NaN(K,3);
data1(:,1) = C(:,1) + (C(:,2)/yearlength);
warning off % avoid divide by zero messages
for j = 1:K,
    data1(j,2) = mean(...
        datain1(datain1(:,1)==C(j,1)...
            & datain1(:,2)==C(j,2),3));
    data1(j,3) = mean(...
        datain2(datain2(:,1)==C(j,1)...
            & datain2(:,2)==C(j,2),3));
end
warning on
% replace any NaNs with min y value
if cp.ycol < 3.5, subminy = log10(cp.z3);
    else subminy = log10(cp.z4); end
data1(isnan(data1)) = subminy;
otherwise,
fprintf('%s\n', ...
    '---- Bad option! Continuing with null data');
K = length(data1(:,1));
data1 = NaN(K,3);
end % of switch on collate flag
%
```

Listing 6.2. Continued.

```

%3. fit (and plot) the waves for the initial data
fprintf('\n%s\n', '-----');
NF=input(...
    ['Ready to fit waves: how many? [' num2str(defNF) ']: ']);
if isempty(NF), NF=defNF; end
fprintf('\n');
%
cp.currentmessage = 'data as loaded';
cp.figno = cp.figno + 1;
% other cp fields contain identificatory data
[avec1, yft1, reserr1] = Mwaves3(data1, NF, PF, cp);
% where NF is number of waves and PF is printing flag
% repeat if required
morewaves=1;
defNF2=0;
while morewaves,
    fprintf('\n%s\n', '-----');
    fprintf('%s\n', [num2str(NF) ...
        ' waves fitted; enter M = 1 to 99 to refit, or 0 to continue;']);
    fprintf('%s\n', ' (refitting will overwrite data):');
    NF2=input(...
        ['Choose value ( 0, 1-99) [' num2str(defNF2) ']: ']);
    if isempty(NF2), NF2=defNF2; end
    fprintf('\n');
    if NF2 > 0.5,
        NF = NF2;
    [avec1, yft1, reserr1] = Mwaves3(data1, NF2, PF, cp);
    % where NF is number of waves and PF is printing flag
    else
        morewaves=0; % and continue with old value of NF
    end
end % morewaves
continueflag=1;
while continueflag,
    fprintf('\n%s\n', '-----');
    fprintf('%s\n', ...
        'End program (0), sparsify data (1), multiply data (2),');
    fprintf('%s\n', ' call 2waves (3) or SSwaves (4):');
    defaf = 0;
    actionflag=input(['Enter 0, 1, 2, 3 or 4 [' num2str(defaf) ']: ']);
    if isempty(actionflag), actionflag=defaf; end
    fprintf('\n');
    switch actionflag
        case 0
            fprintf('%s\n', 'Ending program ...');
            continueflag = 0;
        case 1

```

Listing 6.2. Continued.

```

%7. CALL 2WAVES AND ESTIMATE EG ANNUAL PRODUCTION
% check that it's possible to call TwoWaves
    if cp.ninfile > 1.5 && exist('datain2','var'),
% *****
    prod = TwoWaves(avec1, NF, reserr1(1), cp, datain2);
    % avec1 contains coefficient vectors (for y1 and y2)
    % NF is number of waves
    % reserr1 contains residual error from wavefit
    % cp is a structure with control variables
    % datain2 contains columns of input data (for y2)
% *****
    else
        fprintf('== Sorry, required 2nd file was not loaded \n\n');
    end
    %
    %
    case 4
% 8. CALL SSWAVES AND PLOT IN STATE SPACE
% -----
    % check that it's possible to call SSWaves
    if cp.ninfile > 1.5 ,
% *****
    SSWaves(yft1, data1, cp, PF);
    % yft1 contains columns of predicted y1, y2 at reg. times
    % no time column, but not needed
    % data1 contains sorted data (cols = date, y1, y2)
    % in both cases, y1 and y2 will remain transformed
    % if transformation was requested
    % cp contains control information
    % PF is flag to control printing
% *****
    else
        fprintf('== Sorry, required 2nd file was not loaded \n\n');
    end
    %
    otherwise
        % allow program to end
        continueflag = 0;
    end % of switch on actionflag
end % of loop on continueflag

```

Listing 6.2. Continued.

Mwave3.M

- date of creation: July 2008 by P. Tett

- last modification: January 2009 by P. Tett

```
function [avec, fts, reserr] = Mwaves3(data, M, printflag, pcp)
global wkf % week as fraction of year
global prog_name
global yd % (export) structure with t, y(s) and ydev(s)
global yr % (export) structure with treg and fts
fname = 'Mwaves3';
years = unique(floor(data(:,1)));% column vector of integer years
treg = (min(years):wkf:max(years)+1-wkf);% col vec of regular time
tregpi = (treg-min(years))*2*pi;% ... in radians
t=data(:,1);% observed time (in years)
tpi = (t - min(years))*2*pi;% observed time in rad
y1 = data(:,2); % observed abundances (or first dependent variable)
ymin = floor(min(y1)) - 1; ymax = ceil(max(y1)) + 1;
K = length(y1); % number of data (same for col 2, if it exists)
twoy=length(data(1,:))>2;
if twoy, % then there are two dependent variables
    v = 2;
    y2 = data(:,3);
    ymin(2) = floor(min(y2)) - 1; ymax(2) = ceil(max(y2)) + 1;
else
    v = 1;
end
if M < 1, M=1; end
greatestM = floor(K/2) - 3; if M > greatestM,
    M = greatestM;
    fprintf('\n%s %4.0f \n', ...
    ['Warning from ' fname ': data set too small; M decreased to:'], M);
end
if M > 99, M = 99; end % to prevent error with diagram legend
totdf = K - 1;
wavdf = 2*M; % new -- original was: wavdf = 2*M + 1
if isfield(pcp, 'trans'),
    if pcp.trans == 0,
        yvartitle = ' ';
    else
        yvartitle = 'log_{10} ';
    end
end
end
yearsofdata=length(years);
count=zeros(yearsofdata, v); av=count; stdev=count;
for yrno=1:yearsofdata,
    thisyear=find(floor(t)==years(yrno));
```

Listing 6.3. Part of the commands of the script '*Mwave3.M*'.

```

count(yrno,1) = length(y1(thisyear));
av(yrno,1) = mean(y1(thisyear));
stdev(yrno,1) = std(y1(thisyear));
if twoy,
    count(yrno,2) = length(y2(thisyear));
    av(yrno,2) = mean(y2(thisyear));
    stdev(yrno,2) = std(y2(thisyear));
end
end
grandmean1 = mean(y1); % NOTE: can differ from wave mean
grandstd1 = std(y1);
grandny1 = length(y1);
if twoy,
    grandmean2 = mean(y2);
    grandstd2 = std(y2);
    grandny2 = length(y2);
end
avec = zeros(3,M);
yresSOS = zeros(1,M);
W1 = [ones(size(tpi)) cos(tpi) sin(tpi)];
if pcp.wmo < 0.5, % calculate wave-mean as grand mean of data
    avec(1,1) = grandmean1;
    y1d = y1 - grandmean1;
    avec(2,1) = (2/K)*sum(cos(tpi).*y1d); % cosine term
    avec(3,1) = (2/K)*sum(sin(tpi).*y1d); % sine term
else % calculate wave-mean by matrix fit of first wave
    % chap 4, Matlab 1998 (for Matlab 5.2) - overdetermined systems
    avec(:,1) = W1\y1;% column vector of the coefficients
end
yhat1 = W1*avec(:,1);
fts = [ones(size(tregpi)) cos(tregpi) sin(tregpi)]*avec(:,1);
fnts(:,1) = fts;
yresSOS(1) = sum((y1 - yhat1).^2);
resdf(1) = K-2-1;
if M>1, % calculate successive waves ----
    for n=2:M,
        y1d = y1 - yhat1; % yhat from previous wave-fit
        avec(1,n) = avec(1,1); % will be reset to zero, later
        avec(2,n) = (2/K)*sum(cos(n*tpi).*y1d); % cosine term
        avec(3,n) = (2/K)*sum(sin(n*tpi).*y1d); % sine term
        yhat1 = yhat1 + ... (previous, plus the new wave terms)
        [zeros(size(tpi)) cos(n*tpi) sin(n*tpi)]*avec(:,n);
        yresSOS(n) = sum((y1 - yhat1).^2);
        resdf(n) = resdf(n-1)-2;
        fnts(:,n) = ... (this wave alone)
        [ones(size(tregpi)) cos(n*tregpi) sin(n*tregpi)]*avec(:,n);
    end
end

```

Listing 6.3. Continued.

```

        fts = fts + ... (add this wave to previous)
        [zeros(size(tregpi)) cos(n*tregpi) sin(n*tregpi)]*avec(:,n);
    end
    avec(1,2:end) = 0;
end
yresSOS=yresSOS';
resdf=resdf';
if twoy, % then repeat for the second data-set
    if pcp.wmo < 0.5, % calculate wave-mean as grand mean of data
        avec(1,:,2) = grandmeany(2);
        y2d = y2 - grandmeany(2);
        avec(2,1,2) = (2/K)*sum(cos(tpi).*y2d); % cosine term
        avec(3,1,2) = (2/K)*sum(sin(tpi).*y2d); % sine term
    else
        avec(:,1,2) = W1\y2;% column vector of the coefficients
    end
    yhat2 = W1*avec(:,1,2);
    fts(:,2) = ...
        [ones(size(tregpi)) cos(tregpi) sin(tregpi)]*avec(:,1,2);
    fnts(:,1,2) = fts(:,2);
    yresSOS(1,2) = sum((y2 - yhat2).^2);
    if M>1, % calculate successive waves ----
        for n=2:M,
            y2d = y2 - yhat2;
            avec(1,n,2) = avec(1,1,2);
            avec(2,n,2) = (2/K)*sum(cos(n*tpi).*y2d); % cosine term
            avec(3,n,2) = (2/K)*sum(sin(n*tpi).*y2d); % sine term
            yhat2 = yhat2 + ... (plus the wave terms)
            [zeros(size(tpi)) cos(n*tpi) sin(n*tpi)]*avec(:,n,2);
            yresSOS(n,2) = sum((y2 - yhat2).^2);
            fnts(:,n,2) = ... ( this wave alone)
            [ones(size(tregpi)) cos(n*tregpi) sin(n*tregpi)]*avec(:,n,2);
            fts(:,2) = fts(:,2) + ... (add this wave to previous)
            [zeros(size(tregpi)) cos(n*tregpi) sin(n*tregpi)]*avec(:,n,2);
        end
        avec(1,2:end,2) = 0;
    end
end % when two Y variables
resVar(:,1) = yresSOS(:,1)./resdf(:);
reserr(:,1) = sqrt(resVar(:,1));
wavemeany(1)=avec(1,1,1); % which could be grand mean, if wmo=0
totSOS = (norm(y1 - wavemeany(1)))^2;
totVar = totSOS/totdf;
wavSOS = totSOS - yresSOS(M,1);
wavVar = wavSOS/wavdf;
r2 = 1 - (resVar(M,1)/totVar);
Fratio = wavVar/resVar(M,1);

```

Listing 6.3. Continued.

```

y1dev = y1-yhat1;
ydevplus = length(y1dev(y1dev > 0));
ydevminus = length(y1dev(y1dev < 0));
yhatmean = mean(yhat1);
yregmean = mean(fts(:,1));
if twoy, % calculate for second variable
    resVar(:,2) = yresSOS(:,2)./resdf(:);
    reserr(:,2) = sqrt(resVar(:,2));
    wavemean(2) = avec(1,1,2);
    totSOS(2) = (norm(y2 - wavemean(2)))^2;
    totVar(2) = totSOS(2)/totdf;
    wavSOS(2) = totSOS(2) - yresSOS(M,2);
    wavVar(2) = wavSOS(2)/wavdf;
    r2(2) = 1 - (resVar(M,2)/totVar(2));
    Fratio(2) = wavVar(2)/resVar(M,2);
    %
    y2dev = y2-yhat2;
    ydevplus(2) = length(y2dev(y2dev > 0));
    ydevminus(2) = length(y2dev(y2dev < 0));
    yhatmean(2) = mean(yhat2);
    yregmean(2) = mean(fts(:,2));
end
yd.t = t;
yd.y1 = y1;
yd.y1hat = yhat1;
yd.y1dev = y1dev;
if twoy,
    yd.y2 = y2;
    yd.y2hat = yhat2;
    yd.y2dev = y2dev;
end
yr.t = treg;
yr.y1f = fts(:,1);
if twoy, yr.y2f = fts(:,2); end
if printflag > 0.5,
    fprintf('\n%s\n', '-----');
    fprintf('%s\n', [fname ' output for ' pcp.currentmessage]);
    zm(1)=0; zm(2) = 0; % for case of no transformation
    if pcp.trans > 0.5,
        fprintf('%s\n', 'Data are transformed log10(x+z).');
        if pcp.ycol < 3.5,
            zm(1) = pcp.z3;
            if twoy,
                if isfield(pcp,'z3y2'), zm(2)=pcp.z3y2;
                else zm(2)=pcp.z3; end
            end
        else zm(1) = pcp.z4;
    end
end

```

Listing 6.3. Continued.

```

        if twoy,
            if isfield(pcp,'z4y2'), zm(2)=pcp.z4y2;
            else zm(2)=pcp.z4; end
        end
    end
end
if pcp.wmo > 0.5,
    wmomess='Wave-mean from matrix fit of wave one';
else
    wmomess='Wave-mean from grand mean';
end
fprintf('%s\n', '-----');
%
for vv = 1:v,
    fprintf('%s\n', ['for variable y' num2str(vv) ' ' ...
                    char(pcp.yname(vv)) ' z=' num2str(zm(vv))]);
    fprintf('%s\n', '-----');
    fprintf('%s\n', ' annual statistics: ');
    fprintf('%s\n', ' year count  mean  semean');
    fprintf('%s\n', '-----');
    for yrno=1:yearsofdata,
        fprintf('%6.0f %6.0f %8.3g %8.3g \n', ...
                years(yrno), count(yrno,vv), av(yrno,vv), ...
                stdev(yrno,vv)/sqrt(count(yrno,vv)));
    end
    fprintf('%s\n', '-----');
    fprintf(' all: %6.0f %8.3g %8.3g \n', grandny(vv), ...
            grandmeany(vv), grandsdy(vv)/sqrt(grandny(vv)));
    fprintf('%s\n', '-----');
    %
    fprintf('%s\n', 'Time t in radians in wave function:')
    fprintf('%s\n', '   y(t) = ');
    fprintf('%s\n', 'sum[n](mean + a*cos(nt) + b*sin(nt)');
    fprintf('%s\n', wmomess);
    fprintf('%s\n', ' wave coefficients: ');
    fprintf('%s\n', ' n  mean  a    b');
    fprintf('%s\n', '-----');
    for n=1:M,
        fprintf('%4.0f %8.3g %8.3g %8.3g \n', ...
                n,avec(1,n,vv),avec(2,n,vv),avec(3,n,vv) );
    end
    fprintf('%s\n', '-----');
    fprintf('%s\n', 'Analysis:')
    fprintf('%s\n', 'component  SOS  df  variance');
    fprintf('%s %8.3g %5.0f %7.3g \n', ' total ', totSOS(vv), ...
            totdf, totVar(vv));
    fprintf('%s\n', 'Residual error after waves:');

```

Listing 6.3. Continued.

```

for n=1:M,
    fprintf('%8.0f %8.3g %5.0f %7.3g \n', n, ...
            yresSOS(n,vv), resdf(n), resVar(n,vv));
end
fprintf('%s %8.3g %5.0f %7.3g \n', 'Waves ', wavSOS(vv), ...
        wavdf, wavVar(vv));

fprintf('%s\n', '-----');
fprintf('-- res std: %6.3g; r2: %5.2f \n', ...
        reserr(M,vv), r2(vv));
fprintf('-- F ratio: %6.2f (%3.0f,%4.0f df)\n', ...
        Fratio(vv), wavdf, resdf(M));
if printflag > 2.5,
    fprintf('-- n>wave: %5.0f; n<wave: %5.0f \n', ...
            ydevplus(vv), ydevminus(vv));
    fprintf('-- avs:yhat: %6.3g; yreg: %6.3g \n', ...
            yhatmean(vv), yregmean(vv));
end
fprintf('%s\n', '-----');
end
fprintf('\n');
end % of (standard) printing to command window
plotstr(1,:) = 'r--';
plotstr(2,:) = 'r-.';
plotstr(3,:) = 'r: ';
legstr = 'data';
legstr(2,:)= 'yhat';
if M > 9,
    legstr(3,:)=['ws' num2str(M)];
else
    legstr(3,:)=['wvs' num2str(M)];
end
legstr(4,:)= '95%.';
legstr(5,:)= '05%.';
legstr(6,:)= 'mnw1';
legstr(7,:)= 'wav1';
legstr(8,:)= 'wav2';
legstr(9,:)= 'wav3';
%
figure(1);
clf;
if twoy,
    subplot(2,1,1);
end % (else single plot)
grid on
hold on
plot(t, y1, 'ko');
plot(t, yhat1, 'g-', 'Linewidth', 2); % the predicted y (actual t)

```

Listing 6.3. Continued.

```

plot(treg, fts(:,1), 'k-'); % the total compound wave (regular t)
plot(treg, fts(:,1)+2*reserr(M,1), 'k:'); % upper 95%ile
plot(treg, fts(:,1)-2*reserr(M,1), 'k:'); % lower 95%ile
plot(xlim, [avec(1,1,1) avec(1,1,1)], 'r-'); % mean of wave 1
if M > 1,
    for n=1:min(M,3),
        plot(treg, fnts(:,n,1), plotstr(n,:));
    end
end
warning off; % to avoid warnings when fewer lines to label
legend(legstr, 'Location', 'EastOutside');
warning on;
ylim([ymin(1) ymax(1)]);
xtextloc = min(t) + 0.05 * (max(t)-min(t));
ytextloc = ymax(1) - 0.1 * (ymax(1) - ymin(1));
message1 = ['y1 = ' char(pcp.yname(1)) ' in '];
if pcp.ycol < 3.5,
    message1 = [message1 pcp.col3name];
else
    message1 = [message1 pcp.col4name];
end
if pcp.infiletype < 1.5,
    message1 = [message1 ' from ' pcp.mf1name];
else
    message1 = [message1 ' from ' pcp.tf1name];
end
text(xtextloc, ytextloc, message1);
xlabel('year');
ylabel([yvaritle 'y1']);
title(['Annual and subannual waves fitted to ' pcp.currentmessage ...
    ' by ' prog_name ' on ' date]);
if twoy, subplot(2,1,2); % start plot for y2
    grid on
    hold on
    plot(t, y2, 'ko');
    plot(t, yhat2, 'g-', 'Linewidth', 2); plot(treg, fts(:,2), 'k-'); % the total compound
wave
    plot(treg, fts(:,2)+2*reserr(M,2), 'k:'); % upper 95%ile
    plot(treg, fts(:,2)-2*reserr(M,2), 'k:'); % lower 95%ile
    plot(xlim, [avec(1,1,2) avec(1,1,2)], 'r-'); % mean of wave 1
    if M > 1,
        for n=1:min(M,3),
            plot(treg, fnts(:,n,2), plotstr(n,:));
        end
    end
    % add the legend and set the scale
    warning off;

```

Listing 6.3. Continued.

```

legend(legstr, 'Location', 'EastOutside');
ylim([ymin(2) ymax(2)]);
warning on;
ytextloc2 = ymax(2) - 0.1 * (ymax(2) - ymin(2));
message2 = ['y2 = ' char(pcp.yname(2)) ' in '];
if pcp.ycol < 3.5,
    message2 = [message2 pcp.col3name];
else
    message2 = [message2 pcp.col4name];
end
if pcp.infiletype < 1.5,
    message2 = [message2 ' from ' pcp.mf2name];
else
    message2 = [message2 ' from ' pcp.tf2name];
end
text(xtextloc, ytextloc2, message2);
xlabel('year');
ylabel(['yvar' title ' y2']);
end % (of y2 plot plot)
if printflag > 1.5,
    ptype=pcp.figfiletype; % pdf, ai or ps
    orient portrait; % or landscape or tall
    ofn=[pcp.uname prog_name 'fig' num2str(pcp.figno) '.' ptype];
    switch ptype
        case 'ai'
            print('-dill', ofn);
        case 'pdf'
            print('-dpdf', ofn);
        case 'ps'
            print('-dpsc2', ofn);
    end
    fprintf('\n%s\n', ['=== Graph (data, waves) saved as ' ofn]);
end
[...]%
% 9. Optionally show component variance analysis in command window
% for y1 only. totVar = totSOS/(K-1)
% totSOS = sum of squares of (y - wave mean of y)
if printflag > 2.5,
    wavdfmod = K - 2*M;
    wavVarmod = wavSOS(1)/wavdfmod;
    % propwavVar = wavVarmod/totVar(1);
    if pcp.crflag < 1,
        % using unprocessed single data set, and so able to
        % calculate within-day component
        D1 = unique(t); % list of unique dates
        L = length(D1);
        dvf = K > (L+1); % 'true' if at least 1 df for component
    else

```

Listing 6.3. Continued.

```

    dvf = false;
end
if dvf,
    y1daymean = NaN(K,1);
    for j = 1:L,
        y1daymean(t==D1(j)) = mean(y1(t==D1(j)));
    end
    daySOS = sum((y1 - y1daymean).^2);
    daydf = K - L;
    dayVar = daySOS/daydf;
    % propdayVar = dayVar/totVar(1);
    resSOS = yresSOS(M,1) - daySOS;
else
    daySOS = 0;
    dayVar = 0;
    % propdayVar = 0;
    resSOS = yresSOS(M,1);
end
resdfmod = K - 2*M - 1;
resVarmod = resSOS/resdfmod;
sumVar = wavVarmod + dayVar + resVarmod;
propwavVar = wavVarmod/sumVar;
propdayVar = dayVar/sumVar;
propresVar = resVarmod/sumVar;
sumSOS = wavSOS(1) + daySOS + resSOS;
% sumpropVar = propwavVar + propdayVar + propresVar;
%
fprintf('\n%s\n', ...
'-----');
fprintf('%s\n', ...
[fname ' extended output: component analysis of variance for --']);
fprintf('%s\n', message1);
if pcp.trans > 0.5,
    fprintf('%s\n', ' data are transformed log10(x+z).');
end
fprintf('%s\n', wmomess);
fprintf('%s\n', ...
'-----');
fprintf('%s\n', ...
'Component   SOS   df variance var/totY   df   MS MS/allY');
fprintf('%s\n', ...
'-----');
fs = '%s %8.4g %6.0f %8.4g %6.3f %6.0f %8.4g %7.3f \n';
fprintf(fs, '---- waves', ...
        wavSOS(1), wavdfmod, wavVarmod, propwavVar, ...
        K, wavSOS(1)/K, wavSOS(1)/totSOS(1));
if dvf, % -----

```

Listing 6.3. Continued.

```

    fprintf(fs, 'within day', ...
           daySOS, daydf, dayVar, propdayVar, ...
           K, daySOS/K, daySOS/totSOS(1));
end % - - - - -
fprintf(fs, '- residual',...
       resSOS, resdfmod, resVarmod, propresVar, ...
       K, resSOS/K, resSOS/totSOS(1));
fprintf(...
       '%s %8.4g %s %8.4g %6.3f %s %8.4g %7.3f\n', ...
       '--- totals', sumSOS, ' ', sumVar, 1.00, ...
       ' ', sumSOS/K, sumSOS/totSOS(1) );
fprintf('%s\n', '( ... from components)');
fprintf(fs, '---- all Y', ...
       totSOS(1), totdf, totVar(1), totVar(1)/sumVar, ...
       K, totSOS(1)/K, 1.00);
fprintf('%s\n', ...
       '( ... directly calculated, from sum(Y - wave mean Y)^2)');
fprintf('%s\n', ...
       '-----');
fprintf('%s\n', ...
       'Waves SOS = all Y SOS - residual SOS;');
fprintf('%s\n', ...
       'Residual SOS = sum(Y - Yhat)^2');
if dvf
    fprintf('%s\n', ' ... then subtract within day SOS;')
    fprintf('%s\n', 'Within day SOS = sum(Y - day mean Y)^2;');
end
fprintf('%s\n', ...
       '-----');
end
if twoy,
    reserr = [reserr(M,1) reserr(M,2)];
else
    reserr = reserr(M,1);
end

```

Listing 6.3. Continued.

TwoWaves.M

- date of creation: July 2008 by P. Tett

- last modification: January 2009 by P. Tett

```
function annprod = TwoWaves(AVEC, M, reserry1, CP, y2data)
global yearlength wkf prog_name% defined in main script
global yd % an implicit input -- see comments above
global yr % an implicit input -- see comments above
fprintf('\n%s\n', 'TwoWaves has started .....');
fprintf('%s\n', ['y1 is ' char(CP.yname(1)) ]);
fprintf('%s\n', ['y2 is ' char(CP.yname(2)) ]);
if CP.trans > 0.5,
    fprintf('data transformed log10(x+z) \n');
    if CP.ycol < 3.5,
        fprintf(' z(y1) = %6.2g, z(y2) = %6.2g \n', CP.z3, CP.z3y2);
        zy1=CP.z3;
    else
        fprintf(' z(y1) = %6.2g, z(y2) = %6.2g \n', CP.z4, CP.z4y2);
        zy1=CP.z4;
    end
end
end
```

figure (3)

clf;

```
% 1. Calculate y1dev = f2(y2dev)
% -----
% [p, S] = polyfit(x,y,n)
[p,S] = polyfit(yd.y2dev, yd.y1dev, 1);
a=p(2); b=p(1); % why can't I write [a b] = polyfit ... ?
fprintf('%s\n', '-----');
fprintf('%s\n', '--- using (consolidated) data from file 1');
fprintf('%s\n', 'Coefficients in y1dev = f2(y2dev) = a + b*y2dev:');
fprintf(' a = %8.4g, b = %8.4g \n', a, b);
subplot(2,3,1);
% title('regression: y1=f(y2) [file 1]'); % won't write this!
y2plot = [min(yd.y2dev) max(yd.y2dev)];
y1plot = a + b.*y2plot;
plot(yd.y2dev, yd.y1dev, 'k+');
hold on
plot(y2plot, y1plot, 'k--');
grid on
xlabel('y2 deviation');
ylabel('y1 deviation');
title('regression: y1dev=f(y2dev) [file 1]');
% 2. Calculate y1hatf2 = y1mean + f(t) + f2(y2dev)
% -----
```

Listing 6.4. Part of the commands of the script ‘*TwoWaves.M*’.

```

y1hatf2 = yd.y1hat + a + b.*yd.y2dev;
subplot(2,3,2);
% title('Better y1 using f(y2dev) [file 1]');
plot(yd.t, yd.y1, 'ko');
hold on
plot(yr.t, yr.y1f, 'g-');
plot(yd.t, yd.y1hat, 'go');
plot(yd.t, y1hatf2, 'ro');
grid on
legend('obsv', 'f(t)', 'f(t)', '+f(y2)');
xlabel('year');
ylabel('y1');
title('Better y1 using f(y2) [file 1]');
% 3. Calculate the statistics
K = length(yd.y1);
% old (i.e. before taking f(y2) into account
SOSy1dev = sum(yd.y1dev.^2);
dfy1dev = K - 2*M - 1;
reserrold = sqrt(SOSy1dev/dfy1dev);
% residual deviations after taking f(y2) into account
y1fy2dev = y1hatf2 - yd.y1;
SOSy1fy2 = sum(y1fy2dev.^2);
dfy1fy2 = K - 2*M - 1 - 2;
reserry1fy2 = sqrt(SOSy1fy2/dfy1fy2);% *****
% total SOS
y1meanhat = AVEC(1,1,1);
y1dev = yd.y1 - y1meanhat;
SOSy1total = sum(y1dev.^2);
dfy1total = K - 1;
% explained SOS, by difference
SOSy1explf2 = SOSy1total - SOSy1fy2;
dfy1explf2 = M + 1 + 2;
r2SOS = SOSy1explf2/SOSy1total;
% r2var = SOSy1explf2*dfy1total/(SOSy1total*dfy1explf2);
% print statistics in command window
fprintf('%s\n', ...
        'Statistical analysis for y1hat = ymean + f(t) + f(y2)');
fprintf(' SOS (y1-y1hat)      = %8.4g, df = %6.0f \n', ...
        SOSy1fy2, dfy1fy2);
fprintf(' SOS (y1hat - y1mean) = %8.4g, df = %6.0f \n', ...
        SOSy1explf2, dfy1explf2);
fprintf(' SOS (y1 - y1mean)   = %8.4g, df = %6.0f \n', ...
        SOSy1total, dfy1total);
fprintf(' r^2 (from SOS) = %6.3f \n', r2SOS);
fprintf(' res err = %8.4g (cf. old = %8.4g)\n', reserry1fy2, reserrold);
fprintf('%s\n', '-----');

```

Listing 6.4. Continued.

```

% 4. Calculate y2 deviations
fprintf('%s\n', '---- Now using (and reducing) data from file 2');
D1 = unique(y2data(:,1:2), 'rows');
K2 = length(D1);
y2dd = NaN(K2,2);
y2dd(:,1) = D1(:,1) + (D1(:,2)/yearlength);
for j = 1:K2,
    y2dd(j,2) = mean(...
        y2data(y2data(:,1)==D1(j,1) & y2data(:,2)==D1(j,2),3));
end

years = unique(floor(y2dd(:,1)));% column vector of integer years
tpiy2 = (y2dd(:,1)-min(years))*2*pi;
y2ftsfull = [ones(size(tpiy2)) cos(tpiy2) sin(tpiy2)]*AVEC(:,1,2);
if M > 1, % add contribution of extra waves
    for n = 2:M,
        y2ftsfull = y2ftsfull + ...
            [ones(size(tpiy2)) cos(n*tpiy2) sin(n*tpiy2)]*AVEC(:,n,2);
    end
end
subplot(2,3,3);
plot(y2dd(:,1), y2dd(:,2), 'k*'); % day-meaned data from file 2
hold on
plot(yr.t, yr.y2f, 'g-');% wave fitted to y2 data from file 1
plot(y2dd(:,1), y2ftsfull, 'g*');% estimated y2 from f(t) file 1
    % but on file 2 obs days
xlabel('year');
ylabel('y2');
grid on
legend('obsv[file 2]', 'f(t)[file 1]', ...
    'f(t)[file 2 sample times]');
title('y2 from file 2 also');
y2devfull = y2dd(:,2) - y2ftsfull; % y2hatfull = y2(tj)
% 5. [Repeatedly] Calculate annual production
y1ftsfull = [ones(size(tpiy2)) cos(tpiy2) sin(tpiy2)]*AVEC(:,1,1);
if M > 1, % add contribution of extra waves
    for n = 2:M,
        y1ftsfull = y1ftsfull + ...
            [ones(size(tpiy2)) cos(n*tpiy2) sin(n*tpiy2)]*AVEC(:,n,1);
    end
end
y1ftsfully2 = y1ftsfull + a + b.*y2devfull;
treg = (min(years):wkf:max(years)+1-wkf);% col vec of regular time
tregpi = (treg-min(years))*2*pi;% ... in radians
y1fts = [ones(size(tregpi)) cos(tregpi) sin(tregpi)]*AVEC(:,1,1);
if M > 1, % add contribution of extra waves
    for n = 2:M,

```

Listing 6.4. Continued.

```

    y1fts = y1fts + ...
        [ones(size(tregpi)) cos(n*tregpi) sin(n*tregpi)]*AVEC(:,n,1);
    end
end
subplot(2,3,4);
plot(treg, y1fts, 'k-');
hold on
plot(y2dd(:,1), y1ftsfull, 'go');
plot(y2dd(:,1), y1ftsfully2, 'ro');
grid on
xlabel('year');
ylabel('y1');
legend('f(t)[1]', 'f(t)[1]', '+ f(y2dev)[2]')
title('predictions y1 at file 2 times');
    rand('state', sum(100*clock));
nr = 100; % loops (number of realizations)
tsdata(:,1) = y2dd(:,1) - min(years);% year.day (day as decimal)
tsdata(:,2) = mod(tsdata(:,1),1); % .day (as decimal)
utsdata(:,1) = unique(tsdata(:,2)); % unique also sorts
ii=length(utsdata(:,1));
ayear = (1:yearlength)/yearlength;
annprod1 = zeros(nr,1);
subplot(2,3,5);
title('From y1=ymean+f(t)+f(y2dev)+error');
% *****
ylim([0 4]);
grid on
hold on
xlabel('year');
ylabel('y1');
fprintf('-- making %5.0f estimates of annual y1 \n', nr);
fprintf('    from (sum) y1 = y1mean + f(t) + f(y2dev) + error; \n');
fprintf('    for all days on which y2 sampled, sorted to 1 year:\n');
fprintf('    %5.0f unique days.\n', ii);
% start looping
for r = 1:nr,
    % add the error to y1
    tsdata(:,3) = y1ftsfully2 + randn(size(y1ftsfully2))*reserry1fy2;
    % average any values for the same day
    for i=1:ii,
        utsdata(i,2) = mean(tsdata(tsdata(:,2)==utsdata(i,1),3));
    end
    % add after-the-end row and before-the-start row
    utsdata(ii+1,1) = utsdata(1,1)+1.0;
    utsdata(ii+1,2) = utsdata(1,2);
    for i = 1:ii+1, utsdata2(i+1,:) = utsdata(i,:); end
    utsdata2(1,1) = utsdata(ii,1)-1.0;
    utsdata2(1,2) = utsdata(ii,2);

```

Listing 6.4. Continued.

```

% interpolate the y1 to a daily basis
logdailyGP = interp1(utsdata2(:,1), utsdata2(:,2), ayear);
plot(ayear,logdailyGP, 'r. ');
% back-transform, add up, and change units
dailyGP = iotransform(logdailyGP, 1, zy1, 0);
annprod1(r) = sum(dailyGP)/1000;% from mg C to g C
end
annprod = sort(annprod1);
% the vector, annprod, is returned by the function
avannprod = median(annprod);
limits = [annprod(floor(0.05*nr)) annprod(floor(0.95*nr))];
if CP.ycol < 3.5, y1unit = CP.col3name; else y1unit = CP.col4name; end
fprintf('-----\n');
fprintf(' best estimate of annual y1: %9.0f \n', avannprod);
fprintf(' with limits at 5%% and 95%%: %6.0f, %6.0f \n', limits);
fprintf(' units are %s /1000 \n', y1unit);
fprintf('-----\n');
% 6. repeat 5 without f(y2dev) correction
yearsyl = unique(floor(yd.t));% new column vector of integer years
tsdatay1(:,1) = yd.t - min(yearsy1);% year.day (day as decimal)
tsdatay1(:,2) = mod(tsdatay1(:,1),1); % .day (as decimal)
utsdatay1(:,1) = unique(tsdatay1(:,2)); % unique also sorts
iii=length(utsdatay1(:,1));
annprod2 = zeros(nr,1);
% *****
% plot all the annual series of production
subplot(2,3,6);
title('From y1=ymean+f(t)+error');
% *****
ylim([0 4]);
grid on
hold on
xlabel('year');
ylabel('y1');
fprintf('%s\n', '--- Returning to file 1;');
fprintf('%s %8.4f \n', ' using original residual error: ', reserry1);
fprintf('-- making %5.0f estimates of annual y1 \n', nr);
fprintf(' from (sum) y1 = y1mean + f(t) + error; \n');
fprintf(' for all days on which y1 sampled, sorted to 1 year:\n');
fprintf(' %5.0f unique days\n', iii);
% start looping
for r = 1:nr,
    % add the error to y1
    tsdatay1(:,3) = yd.y1hat + randn(size(yd.y1hat))*reserry1;
    % average any values for the same day
    for i=1:iii,
        utsdatay1(i,2) = mean(tsdatay1(tsdatay1(:,2)==utsdatay1(i,1),3));
    end
end

```

Listing 6.4. Continued.

```

end
% add after-the-end row and before-the-start row
utsdatay1(iii+1,1) = utsdatay1(1,1)+1.0;
utsdatay1(iii+1,2) = utsdatay1(1,2);
for i = 1:iii+1, utsdatay12(i+1,:) = utsdatay1(i,:); end
utsdatay12(1,1) = utsdatay1(iii,1)-1.0;
utsdatay12(1,2) = utsdatay1(iii,2);
% interpolate the y1 to a daily basis
logdailyGPy1 = interp1(utsdatay12(:,1), utsdatay12(:,2), ayear);
plot(ayear,logdailyGPy1, 'g. ');
% back-transform, add up, and change units
dailyGPy1 = iotransform(logdailyGPy1, 1, zy1, 0);
annprod2(r) = sum(dailyGPy1)/1000;% from mg C to g C
end
annprod(:,2) = sort(annprod2);
% the vector, annprod, is returned by the function
avannprod2 = median(annprod2);
limits2 = [annprod(floor(0.05*nr),2) annprod(floor(0.95*nr),2)];
if CP.ycol < 3.5, y1unit = CP.col3name; else y1unit = CP.col4name; end
fprintf('-----\n');
fprintf(' best estimate of annual y1: %9.0f \n', avannprod2);
fprintf(' with limits at 5%% and 95%%: %6.0f, %6.0f \n', limits2);
fprintf(' units are %s /1000 \n', y1unit);
fprintf('-----\n');
%
% 7. save the diagram
% -----
orient landscape; % or portrait or tall
ofn=[CP.uname prog_name 'fig3.' CP.figfiletype];
switch CP.figfiletype
case 'ai'
print('-dill', ofn);
case 'pdf'
print('-dpdf', ofn);
case 'ps'
print('-dpsc2', ofn);
end
fprintf('\n%s\n', ['=== Graph (deviations) saved as ' ofn]);
end

```

Listing 6.4. Continued.